Lappeenranta
University of Technology

Sara-Maaria Alatalo

HYDROTHERMAL CARBONIZATION IN THE SYNTHESIS OF SUSTAINABLE POROUS CARBON MATERIALS

Thesis for the degree of Doctor of Science (Technology) to be presented with due permission for public examination and criticism in the MUC, Mikkeli University Consortium, Mikkeli, Finland on the 6.7.2016 at noon.

Acta Universitatis
Lappeenrantaensis 701

Supervisor Professor Mika Sillanpää
LUT School of Engineering Science
Lappeenranta University of Technology
Finland

Reviewers Assistant professor Amit Bhatnagar
Department of Environmental and Biological Sciences
University of Eastern Finland
Finland

Professor Niklas Hedin
Avdelninger för materialkemi
Stockholms universitetet
Sweden

Opponent Professor Niklas Hedin
Avdelninger för materialkemi
Stockholms universitetet
Sweden

ISBN 978-952-265-963-7
ISBN 978-952-265-964-4 (PDF)
ISSN-L 1456-4491
ISSN 1456-4491

Lappeenrannan teknillinen yliopisto
Yliopistopaino 2016

Abstract

Sara-Maaria Alatalo
Hydrothermal carbonization in the synthesis of sustainable porous carbon materials
Lappeenranta 2016
81 pages
Acta Universitatis Lappeenrantaensis 701
Diss. Lappeenranta University of Technology
ISBN 978-952-265-963-7, ISBN 978-952-265-964-4 (PDF), ISSN-L 1456-4491, ISSN 1456-4491

Carbon materials are found versatile and applicable in wide range of applications. During the recent years research of carbon materials has focussed on the search of environmentally friendly, sustainable, renewable and low-cost starting material sources as well as simple cost-efficient synthesis techniques. As an alternative synthesis technique in the production of carbon materials hydrothermal carbonization (HTC) has shown a great potential. Depending on the application HTC can be performed as such or as a pre-treatment technique. This technique allows synthesis of carbon materials *i.e.* hydrochars in closed vessel in the presence of water and self-generated pressure at relatively low temperatures (180-250 ˚C). As in many applications well developed porosity and heteroatom distribution are in a key role. Therefore in this study different techniques *e.g.* varying feedstock, templating and post-treatment in order to introduce these properties to the hydrochars structure were performed. Simple monosaccharides *i.e.* fructose or glucose and more complex compounds such as cellulose and sludge were performed as starting materials. Addition of secondary precursor *e.g.* thiophenecarboxaldehyde and ovalbumin was successfully exploited in order to alter heteroatom content. It was shown that well-developed porosity (S_{BET} 550 m^2/g) can be achieved *via* one-pot approach (*i.e.* exploitation of salt mixture) without conventionally used post-carbonization step. Nitrogen-enriched hydrochars indicated significant Pb(II) and Cr(VI) removal efficiency of 240 mg/g and 68 mg/g respectively. Sulphur addition into carbon network was not found to have enhancing effect on the adsorption of methylene blue or change acidity of the carbon material. However, these hydrochars were found to remove 99.9 % methylene blue and adsorption efficiency of these hydrochars remained over 90 % even after regeneration. In addition to water treatment application N-rich high temperature treated carbon materials were proven applicable as electrocatalyst and electrocatalyst support. Hydrothermal carbonization was shown to be workable technique for the production of carbon materials with variable physico-chemical properties and therefore hydrochars could be applied in several different applications *e.g.* as alternative low-cost adsorbent for pollutant removal from water.

Keywords: Hydrothermal carbonization, porous carbon, templating, metal removal, dye removal, water treatment, oxygen reduction reaction, electrocatalyst

Abstrakti

Sara-Maaria Alatalo
Märkäpyrolyysin hyödyntäminen huokoisten ympäristöystävällisten hiilimateriaalien valmistuksessa
Lappeenranta 2016
81 pages
Acta Universitatis Lappeenrantaensis 701
Diss. Lappeenranta University of Technology
ISBN 978-952-265-963-7, ISBN 978-952-265-964-4 (PDF), ISSN-L 1456-4491, ISSN 1456-4491

Hiilimateriaalit ovat monipuolinen ja useissa sovelluksissa hyödynnettävä materiaaliryhmä. Viime vuosina hiilimateriaalien tutkimus on keskittynyt ympäristöystävällisten, uusiutuvista ja edullisista lähtömateriaaleista tuotettujen materiaalien tuottamiseen ja lisäksi yksinkertaisten sekä kustannustehokkaiden tekniikoiden luomiseen. Märkäpyrolyysi on tavallisista hiilimateriaalien valmistustekniikoista poikkeava menetelmä, jossa synteesi tapahtuu suljetussa astiassa vesiliuoksessa suhteellisen alhaisessa lämpötilassa (180-250 ˚C) ja korkeassa paineessa. Useissa sovelluksissa materiaalin huokoisuus ja heteroatomien jakautuminen ovat avainasemassa. Märkäpyrolyysissä erityisesti huokoisuuden tuottaminen on haasteellista tekniikan asettamien rajoitteiden vuoksi. Hiilimateriaalien ominaisuuksia muokattiin erilaisilla lähestymistavoilla joita ovat lähtöaineen valinta, templaatin hyödyntäminen ja jälkimodifiointi. Märkähiiltä tuotettiin yksinkertaisista monosakkarideista, kuten fruktoosista ja glukoosista, sekä monimutkaisemmista rakenteista, kuten selluloosasta ja lietteestä. Hiilimateriaaleihin onnistuttiin lisäämään typen sekä rikin toiminnallisia ryhmiä hyödyntäen toissijaisia lähtöaineita, kuten ovalbumiinia ja tiofeenikarboksaldehydiä. Huokoisuutta (S_{BET} 550 m^2/g) onnistuttiin lisäämään ilman tavanomaista korkealämpötilakäsittelyä. Märkähiilien haitta-aineiden poistokyky vesiliuoksista oli korkea, erityisesti runsaasti typpeä sisältävien hiilimateriaalien havaittiin poistavan tehokkaasti lyijyä (Pb(II) q_e=240 mg/g) ja kromia (Cr(VI) q_e=68 mg/g). Rikin funktionaalisuuksien lisäämisellä ei havaittu olevan merkittävää vaikutusta metyleeninsinisen poistossa. Metyleenin sininen onnistuttiin poistamaan 99.9 % vesiliuoksesta ja näiden hiilimateriaalien adsorptiotehokkuus oli suuri regeneroinnin jälkeenkin. Vedenkäsittely sovelluksen lisäksi märkähiili materiaalit osoittivat elektrokatalyyttistä aktiivisuutta. Korkealämpötilakäsitelty typpeä sisältävä hiilimateriaali antoi positiivisen vasteen hapetus-pelkistysreaktiossa polttokennosovelluksia silmälläpitäen. Märkäpyrolyysi osoittautui toimivaksi menetelmäksi fysikaalis-kemiallisilta ominaisuuksiltaan vaihtelevien hiilimateriaalien valmistamisessa. Nämä märkähiilet olivat erityisen tehokkaita haitta-aineiden poistamisessa vedestä.

Avainsanat: Märkäpyrolyysi, huokoinen hiili, synteesi sapluunaa hyödyntäen, metallin poistaminen, värin poistaminen, veden käsittely, hapetus-pelkistys reaktio, elektrokatalyytti

Acknowledgements

Research work for this PhD was conducted at the Lappeenranta University of Technology Laboratory of Green Chemistry September 2011- February 2016. Studies were financially supported by the Finnish Funding Agency for Technology and Innovation (Tekes) – project Biomassan märkäpyrolyysin uudet sovellutukset, Tekniikan edistämissäätiö (TES) and Maa- ja vesitekniikan tuki (MVTT).

I express my gratitude for my supervisor professor Mika Sillanpää for providing me the opportunity to perform this study under his guidance. I am grateful for Dr. Eveliina Repo for the scientific discussions and guidance in the design of the experimental studies.

I am sincerely grateful for assistant professor Amit Bhatnagar for reviewing my thesis and Professor Niklas Hedin for reviewing my thesis and acting as an opponent.

Professor Maria-Magdalena Titirici is gratefully acknowledged for her guidance into the world of HTC, valuable advice and comments during the writing process. Ermei Mäkilä is thanked for the discussions and experiments related to gas sorption studies during these years. I am also very grateful to my friends and colleagues Dr. Anne Vuorema, Marina Shestakova, Tarja Seppänen, Dr. Jean-Marie Fontmorin and Dr. Yunfan Zhang for the friendship during these years. You have truly lightened up my days!

I am deeply grateful to my family for all encouragement along these years whatever challenges I have faced. You have had more faith in me than myself. I am grateful to have you all in my life. You are the best!

Sara-Maaria Alatalo
May 2016
Mikkeli, Finland

Contents

List of publications

This thesis is based on the following papers. The rights have been granted by publishers to include the papers in dissertation.

I. Alatalo, S-M., Repo, E., Mäkilä, E., Salonen, J., Vakkilainen, E., Sillanpää, M. (2013). Adsorption behavior of Hydrothermally Treated Municipal Sludge & Pulp and Paper Industry Sludge. Bioresource Technology, 147, pp. 71-76.

II. Alatalo, S-M., Repo, E., Mäkilä, E., Salonen, J., Sillanpää, M. Hydrothermal conversion of sludge into effective adsorbents for the removal of lead from aqueous media. Submitted.

III. Alatalo, S-M., Pileidis, F., Mäkilä, E., Sevilla, M., Repo, E., Salonen, J., Sillanpää, M., Titirici, M-M (2015). Versatile cellulose based carbon aerogel for the removal of both cationic and anionic metal contaminants from water. ACS applied materials and interfaces, 7, pp. 25875-25883.

IV. Alatalo, S-M., Mäkilä, E., Repo, E., Heinonen, M., Salonen, J., Kukk, E., Sillanpää, M., Titirici, M-M (2016). Meso- and microporous soft templated hydrothermal carbons for dye removal from water. Green Chemistry, 18, pp. 1137-1146.

V. Alatalo, S-M., Qiu, K., Preuss, K., Marinovic, A., Sevilla, M., Sillanpää, M., Guo, X., Titirici, M-M (2016). Soy protein directed hydrothermal synthesis of porous carbon aerogels for electrocatalytic oxygen reduction. Carbon, 96, pp.622-630.

Author's contribution

I. Author carried out all the experimental work, analysed data and prepared the first draft, of the manuscript.

II. Author carried out all the experimental work, analysed data and prepared the first draft of the manuscript.

III. Author carried out all the experimental work, analysed data and prepared the first draft of the manuscript.

IV. Author carried out all the experimental work, analysed data and prepared the first draft of the manuscript.

V. Author carried out most of the experimental data, analysed most of the data and prepared the first draft of the manuscript. Kaipei Qui wrote application part related to electrocatalytic activity.

Nomenclature

List of Symbols

S_{BET}	Surface area determined with Brunauer-Emmet-Teller tehcnique	m^2/g
V_p	Pore volume	cm^3/g
C_e	equilibrium concentration	mmol/l or mg/l
C_i	Initial concentration	mmol/l or mg/l
C	Intaparticle diffusion constant	
k_{dif}	Diffusion rate constant	
k_1	Pseudo-first-order rate constant	
k_2	Pseudo-second-order rate constant	
K_L	Langmuir affinity constant	
K_F	Freundlich affinity constant	
n_F	Freundlich heterogeneity factor	
n_S	Sips heterogeneity factor	
p/p_0	Relative Pressure	
q_e	Equilibrium adsorption capacity	mmol/g or mg/g
q_m	Theoretical maximum adsorption capacity	mmol/g or mg/g
q_t	Adsorption capacity at time t	mmol/g or mg/g
R^2	Correlation coefficient	

T	Temperature	K or ˚C
V	Volume	mL or L
J	Measured current density	
J_K	Kinetic current density	
J_L	Diffusion current density	
ω	Angular velocity	
F	Faraday constant	sA/mol
D_0	Diffusion coefficient	cm^2/s
C_0	Bulk concentration	mol/L
v	Kinematic viscosity	m^2/s
I_d	Disc current	
I	Ionic strength	
I_r	Ring Current	
N	Current collection efficiency of the Pt ring	
n	Electron transfer number	
pH_{IEP}	Isoelectric point	

Abbreviations

AP	Acidification
ATR	Attenuated total reflectance
BET	Brunauer-Emmet-Teller
COD	Chemical oxygen demand
^{13}C SS MAS NMR	^{13}C solid state magic angle spinning nuclear magnetic resonace
CP	Cross polarization
CV	Cyclic voltammetry
DCDTO	4,5-dicyano-1,3-dithiol-2-one
EDX	Energy dispersive X-ray
ESEM	Environmental scanning electron microscope
FTIR	Fourier transform infrared spectroscopy
GWP	Green warming potential
HF	Hydrofluoric acid
HMF	5-(hydroxymethyl)furfural
HTC	Hydrothermal Carbonization
HHV	Higher heating value
HTT	High temperature treatment
ICP-OES	Inductively coupled plasma - optical emission spectrometry
LCA	Life cycle assessment
MB	Methylene blue
MSW	Municipal Solid Waste
NLDFT	non-local density functional theory
ORR	Oxygen reduction reaction
PCA	2-pyrrolcarboxaldehyde
PSD	Pore size distribution
RRDE	Rotating disc electrode
SEM	Scanning Electron Microscopy
STDEV	Standard deviation
TCA	2-thiophenecarboxaldehyde
TEM	Transmission electron microscopy
TMS	Tetramethylsilane
XPS	X-ray Photoelectron spectroscopy
XRD	X-ray diffraction
ZP	Zeta potential

1 Introduction

Carbon is an extremely fascinating element since it can form bonds with almost every element resulting in wide range of compounds and allotropic forms from crystalline diamond to graphite or amorphous carbon (*e.g.* carbon black and activated carbon). Researchers have managed to synthesis and characterize a large number of new carbon materials in variable shapes and sizes. For example graphite is a good example of a very flexible layered material which has been found in forms such as fullerenes, cones, toroids and wide range of different 1-, 2-, and 3-dimensional structures (*e.g.* nanotubes, antidote graphene and Schwarzite crystals).[1]

Carbon materials and especially porous carbon materials are interesting because of their versatile properties and wide range of suitable applications such as gas separation, water- and air purification, catalyst supports and electrodes for electrochemical double layer capacitors, chromatography, drug delivery, sensing and fuel cells.[2, 3, 4, 5, 6, 7] Many advances in the carbon technology have been made during the recent years through improvement of existing techniques as well as introduction of new synthetic techniques. Carbon materials can be synthesized *via* techniques such as pyrolysis, high-voltage-arc discharge, chemical vapour deposition, hydrothermal carbonization and laser ablation approach in order to prepare amorphous or crystalline nanostructured carbon materials with different sizes, shapes and chemical compositions.[8, 9, 10, 11, 12, 13]

The exhaustion of fossil fuel resources and the requirement for carbon-neutral alternatives due to environmental concern has boosted researchers to find optional feedstock and process techniques in the material production for various applications.[14] From this point of view biomass is an advantageous raw material in the synthesis of carbon materials because of its high availability, environmentally friendly renewable nature and high quality (*e.g.* pure saccharose).[15] During the past few decades hydrothermal carbonization (HTC) has shown its high potential among the other techniques in order to produce tailored carbon structures for a wide range of applications providing simple straightforward and environmentally friendly approach with modifiable final products. Advantages of this technique are the mild reaction conditions, one-pot approach and unnecessary pre-treatment before synthesis. HTC technique allows production of carbon materials with well-developed porosity and surface functional features from wide range of starting materials. Applicability of hydrochars has been tested in several fields such as soil improvement in agriculture, adsorption in liquid and gas phase (*e.g.* metal ion removal, CO_2 capture and methane storage), heterogeneous catalysis, photocatalysis, energy storage (*e.g.* Li/Na ion batteries, supercapacitors, fuel cells) and bioimaging.[16, 17]

1.1 Activated Carbon

The most conventional application of activated carbon is use in adsorption in which it can be considered as one of the oldest adsorbents.[18] The first known use of activated carbon is mentioned in an old Egyptian papyrus dated from 1550 B.C. Egyptians used activated carbon for medical purposes and purifying agent.[19] Until 18th century carbon was made from wood or animal bones for the purification of liquids. In the 19th century English sugar industry started to use bone char for the decolourisation of sugarcane leading to the several patent on the field in the United Kingdom and in the beginning of the 20th century first patents for the industrial processes for the production of activated carbon appeared.[20] Nowadays activated carbon is largely commercially available with almost 1 million tons per years of activated carbons produced in different forms/properties depending on the target application. In addition to use as adsorbent in water treatment it has proven applicability in CO_2 capture, energy storage and heterogeneous catalysis.[21]

1.1.1 Structural properties

Activated carbons have microcrystalline structure which begins to develop during the carbonization process. However, crystalline structure of activated carbon differs from graphite in terms of interlayer spacing. Additionally orientation of microcrystalline layers in activated carbons depends on the embedded heteroatoms like oxygen and hydrogen.[19] Due to impregnated heteroatoms activated carbons can be considered as amphoteric solids. Furthermore heteroatoms are also responsible for the development of surface charge.[8] Disturbance in the basic microcrystalline structure is caused by the presence of imperfect or partially burnt graphitic layers in the crystallites. This results variation in the arrangement of electron clouds in the carbon network and furthermore allows formation of unpaired electrons and incompletely saturated valences as well as on the adsorption behaviour of activated carbon especially in the case of polar and polarizable compounds.[19]

1.1.2 Synthesis/Activation process

Synthesis of activated carbon is a multistep process. Raw materials are pre-treated in the absence of oxygen at low temperatures. Pyrolytic temperature, heating rate, nitrogen flow rate and time of pyrolysis are main parameters controlling this step.[22] Final step is the physical or chemical activation which is used to create pores with desired pore size and distribution. Physical activation involves the use of an oxidizing gas such as CO_2, steam O_2 or mixture of them at elevated temperatures (>800 ˚C).[22] In chemical activation, pre-treated char is in contact with chemical agent such as H_2SO_4, H_3PO_4, $ZnCl_2$ or KOH in which naturally the choice of an activation agent effects on the final properties of the activated carbon. Conventionally, chemical activation operational temperatures are lower than required in physical activation and final carbon yields are higher compared to

physical activation.[23] Choice of activation agent depends strongly on the desired final properties of the activated carbon as it effects on the textural properties and/or improves heteroatom content.[7] Inorganic matter content in the activated carbons are generally 2-10 %.[21]

In the production of activated carbons micropores are predominantly formed (pore size ≤2 nm).[24] Often meso- and macropores coexist in the carbon materials with micropores and they existence may be important in order to receive larger microporosity. As mesopores are considered pore sizes 2-50 nm and macropores > 50 nm. Carbon from biomasses (*e.g.* coconut shells) are abundant in macropores already formed during the carbonization process further on easing the formation of micropores in the activation process. Disadvantageous aspects in the activation process includes the fact that: mesopores are usually created as enlargement of micropores and some of the carbon atoms are gasified to CO and/or CO_2 during activation process and therefore final yields are rather low.[25]

During the carbonization of the raw material, final carbon material is reached by condensation of polynuclear aromatic compounds and expulsion of side chain groups.[26] In the meantime, cross-linking reaction occur inhibiting the formation of a pre-graphite structure. This type of activated carbon is considered as non-graphitizing. The graphitizing type of activated carbons apply to pitches derived from petroleum, coal tar and aromatic hydrocarbons, which form an intermediate liquid crystal phase known as mesophase. Typically these carbon materials have well-developed porosity and large internal surface area. These features depend on the features of raw material and carbonization technique. Range of utilized raw materials in the production of activated carbon are wide: bituminous coal, wood, petroleum coke, coconut shell, peat, pitch, polymers, apricot stone.[27] Anthracite and bituminous coal have been the mainly applied feedstock types.[21]

1.2 Hydrothermal carbonization

1.2.1 Fundamentals

Hydrothermal carbonization (HTC) was discovered by German chemist Friedrich Bergius in 1911 as a consequence when investigating production of H_2 *via* coal oxidation using "Water Gas Shift Reaction".[28] He managed to produce CO and H_2 at temperatures <600 ˚C in the presence of transition metals. Bergius observed that when peat was used as carbon source in the reaction, exceptionally large amounts of CO formed, and that the carbonaceous residues in the reaction vessel resembled natural coal. It was noticed that biomass when applied as a feedstock has to be in close contact with water which at mild temperatures (180-250 ˚C) at high-pressure vessel cannot decompose into gases but favour the formation of solid product. Bergius continued this work and later in 1931 won

the Nobel Prize in chemistry for invention and development of high pressure techniques.[28] Number of researchers continued the work initially started by Bergius. After being somewhat forgotten hydrothermal carbonization or so called "synthetic coalification" was rediscovered at the beginning of 21th century, starting with reports on the low temperature hydrothermal carbonization of carbon spheres from monosaccharide glucose.[29, 30]

Hydrothermal carbonization has been considered as energy- and atom-economical process because only one-third of the combustion energy is released *via* dehydration, pre-drying process is unnecessary due to the aqueous reaction media and the carbon efficiency is close to one after suitable operational conditions.[31] According to life cycle assessment (LCA) of HTC and the processed food waste followed by electricity generation would result negative environmental impact when associated with the global warming potential (GWP) and acidification (AP) categories. This was examined by systems level analysis of environmental effect of different HTC process parameters. It was found that liquid phase and combustion conditions have major effect on the environmental impact of the system. However, knowledge about the environmental impacts of hydrochar is still limited.[32]

Hydrochar differs significantly from the classical activated carbons. They result amorphous polyfuranic/aromatic carbon network with increased surface functional properties.[31] Hydrochars especially from the carbohydrate based materials tend to appear as spherically shaped particles. Shape and size of these particles can be altered by varying operational condition, which is impossible in the case of activated carbons. Simple monosaccharides *i.e.* glucose or fructose are often applied starting materials but successful HTC synthesis has been performed with starting materials such as cellulose, rye straw, sunflower stems and walnut shells as well.[33, 34, 35] Typically, hydrochar is brown/dark brown powderous solid product with ~60-70 wt.% carbon content. These hydrochars resemble natural coal and are typically rich in oxygen surface functionalities (*e.g.* –OH, -C=O and -COOH) unlike coal.[36] Due to high amount of oxygen functionalities hydrochars are not prone to autoignition and unlike pyrolysis hydrothermal carbonization does not generate large amount of harmful gases.[37] Heating value for the hydrochars has been found between 28.9-29.3 MJ/kg indicating strong potential in the energetic use.[38]

1.2.2 Reaction mechanism and the role of feedstock

Hydrothermal carbonization takes place in H_2O at lower temperatures (180-250 ˚C) in a closed vessel (Figure 1.). Water is kept on the liquid state by letting the pressure to rise with the steam pressure in high pressure reactors. Pressure and increased temperature alter properties of water *e.g.* density, dielectric constant as well as viscosity change.[39, 40]At these conditions water becomes excellent reaction environment, reactant and solvent. By altering the operation conditions major HTC product can be either gas (gasification), liquid (liquefaction) or solid.[15, 40, 41]

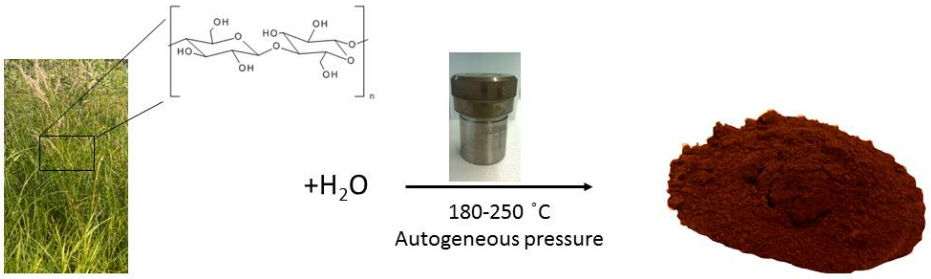

Figure 1. Schematic presentation of the hydrothermal carbonization process from the plant-derived starting material to final carbon product. Reaction takes place in the presence of water in the closed vessel at relatively mild reaction conditions.

Reaction mechanism of the HTC process has been studied with simple carbohydrate glucose. Reaction mechanism is assumed to include several different consecutive and simultaneous reaction stages. Decomposition of carbohydrates under subcritical conditions begins *via* dehydration and retro-aldol condensation. At temperatures below 300 ˚C dehydration is favoured. Hydroxymethylfurfural (HMF) and furfural are typical dehydration products of hexoses (*e.g.* glucose and fructose) whereas pentoses like xylose result generation of furfural. It is commonly accepted that prior to the dehydration of glucose it first isomerizes to fructose *via* the Lobry de Bruyn-Alberda van Ekenstein isomerization. As fructose is formed, this intermediate then dehydrates forming 5-(hydroxymethyl)furfural (HMF) and releasing three H_2O molecules. HMF acts as primary monomer undergoing series of polymerization-polycondensation reactions leading to the formation of polyfuranic type of aromatic carbon network.[42] Simplified schematic illustration of the formation of final carbon structure is presented in the Figure 2. However, it should be recognized that some of the HMF degrades to levulinic acid and formic acid instead of solid product.[43] Furthermore, it has been found that final degree of aromatization of the carbon network depends on the HTC processing temperature differing between applied starting materials.[42]

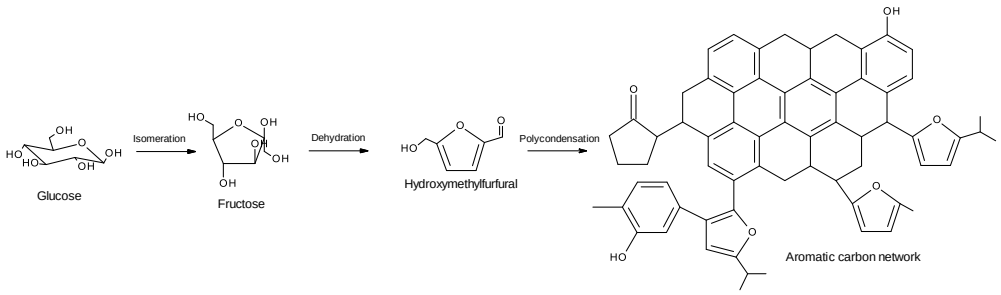

Figure 2. Simplified schematic illustration of the formation of aromatic carbon network *via* hydrothermal carbonization at temperatures 180-250 ˚C beginning with isomeration of Glucose to Fructose followed by dehydration to Hydroxymethylfurfural (HMF). HMF acts as a primary compound/monomer in the formation of final carbon network.

In the case of polysaccharides first step in hydrolysis is degradation to monosaccharides. Monosaccharides can further on decompose and form organic acids such as acetic, lactic, propenoic, levulinic and formic acids instead of HMF. These acids can on further reaction stages act as catalysts in the degradation of polysaccharides and therefore HTC process can be considered autocatalytic.[44] However in the case of lignocellulosic biomass or organic municipal waste, because of the strong resistance to hydrolysis, catalyst has to be used in order to enhance reaction rate. For example hydrolysis of cellulose and further dehydration of sugars to HMF can be promoted by utilizing acidic conditions. Basic conditions can be applied if depolymerisation of lignin is desired.[16] However, in the pure water dehydration of glucose in to HMF is non-selective.[45] Glucose is the most abundant compound in biomass and the major decomposing product of acidic hydrolysis of lignocellulosic biomass. It has been suggested that degradation mechanisms of aminosugar glucosamine would lead to the formation of HMF similar to glucose under similar conditions and release of ammonia. Further on ammonia would react with HMF forming different nitrogen containing compounds.[46]

Biomass can be defined as "a renewable energy source, living or recently living." Besides plant based materials it comprises both animal- and vegetable derived materials as well.[47] It is qualified as a raw material for the production of carbon materials due to availability in high quality, abundancy as well as environmental friendliness. The use of some biomasses in processes like pyrolysis are restricted due to their high natural water content, but in here HTC process is a positive exception. Typical lignocellulosic biomasses consist approximately of 50 % cellulose, 25 % hemicellulose, 20 % lignin and some percentages of other substances such as minerals, organic extractives and other plant components (*e.g.* sugars, starch).[39, 48] Choice of feedstock has an effect on the chemical process and the final product. Water soluble monosaccharides Glucose and Fructose are easily convertible materials choices already at low process temperatures (Glucose 180-200 ˚C and Fructose 120-140 ˚C).[49] Fructose is an isomerization product of Glucose. Glucose

has found to have a very stable ring structure and therefore the fraction of the open chain forms in the solution and the enolisation rate are consequently low, unlike in the case of Fructose which has less stable ring structure.[50]

Conversion/degradation of more complex structures such as cellulose, lignin or lignocellulosic biomasses *via* HTC is more challenging. This kind of material does not undergo any structural disruption at low temperatures (T=180 ˚C).[42] Cellulose is a skeletal polysaccharide composed of β-1,4 glycoside linked glucose units[51] in which two glucose anhydride units are known as cellobiose unit. Similarly to starch it can be considered as a condensation polymer of glucose, but however differing from the links between the glucose monomers. Insolubility is attributed to low-surface area semicrystalline form of two allomorphs (I_α; metastabile low-density form and I_β; thermodynamically more stable high density form) connected with hydrogen bonds.[52] The level of crystallinity depends on the origin and treatment of cellulose.[39] Depolymerization of cellulose depends on the operational conditions which in general takes place by dehydration of reducing end glucose *via* pyrolytic cleavage of glycosidic bond or hydrolysis of the glycosidic bond *via* swelling and dissolution of cellulose. The former takes place when reaction temperature increases but pressure decreases, while the latter is predominant at high-density regions in near critical and supercritical water. At subcritical state crystallite is hydrolyzed.[39] Concentrated acid (*e.g.* H_2SO_4) hydrolysis can be used to enhance decomposition of cellulose as it disrupts hydrogen bonding between cellulose chains. In addition to cellulose other major components in lignocellulosic biomasses are hemicellulose and lignin. Hemicellulose is randomly ordered amorphous compound degradable *via* HTC. Lignin is highly branched polyphenolic compound which can be only partially degraded at low temperature conditions giving negative impact on the effective conversion of cellulose and hemicellulose. This problem can be solved for example by removing lignin from the reaction matrix prior to HTC.[53] It has been observed that in acidic conditions carbon content is higher than in alkaline conditions.[54] Variation of alkalinity and basicity of process water did not appear to have effect on the solid product yield, gas yield or filtrated chemical oxygen demand (COD).[55]

Algae in the HTC synthesis is an interesting starting material choice from the sustainability and green point of view as it is very fast growing biomass doubling its biomass volume within a 24 h growth window.[56] Aquatic microalgae like *spirulina platensis* composes of proteins (66 wt.%), carbohydrates (19 wt.%), lipids (7 wt.%) and minerals (8 wt.%). Algae as well as glucosamine and chitosan are naturally rich in nitrogen which remain in the final material after HTC treatment.[46, 57] In addition to the above described potential feedstock, some non-conventional feedstocks such as wet animal manure, human waste, municipal solid waste and sewage sludge can be used to be processed *via* HTC.[58, 59, 60]

1.3 Modification of hydrochar features

There are several techniques available for the modification of plain hydrothermal carbons. Naturally, suitable technique depends on the desired outcome for the product. Perhaps, the most conventional techniques for the introduction of porosity into carbon materials are exploitation of physical/chemical activation. Another approach is a simple high temperature treatment. Furthermore, porosity can be introduced by utilizing structure directing agent also defined as a template. Depending on the template synthesis, product is an inverse copy of the exploited template structure. As opposite to nanostructured inorganic materials, the introduction of nanostructure into organic, "soft" materials is much more restricted and therefore dispose strict requirements on the resulting framework.[61] Besides modification of the porosity these above mentioned techniques can be used to alter heteroatom content and type in the carbon materials. For instance when considering HTC process induction of heteroatoms can be performed *in situ* during HTC or by additional post-treatment *i.e.* chemical reaction.

1.3.1 Post-functionalization:

Properties of surface functionalities can be improved with careful selection of feedstock, addition of secondary precursor or post functionalization techniques such as high temperature treatment, physical/chemical activation procedure, cycloaddition or nucleophilic substitution. As it is known hydrochars present limited pore texture when synthesized as such which can be overcome for example by the use of high temperature (HT) treatment resulting alteration of surface properties *i.e.* polarity and acidity *via* choice of the temperature (T=350-500 ˚C) and increase carbon content in the solid product. HT-treatment at T >500 ˚C leads to the turbostratic-like disordered carbon structure with increased aromatic character, hydrophobic properties and electrocatalytic activity whereas majority of oxygen groups are eliminated.[16]

Introduction of physical/chemical activation for the modification of hydrothermal carbon can be performed as well. Research of these activated hydrochars has concentrated on the effects of KOH activation. Introduction of chemical activation with KOH for the hydrochars prepared from glucose, cellulose, sawdust and glucosamine was found to result carbon materials with high surface areas (1200-2250 m^2/g) and high microporosity.[62, 63] Despite the differences in the morphology due to hydrochars precursors, after chemical activation morphology of activated hydrochars were found similar, indicating that chemical activation has a strong altering effect on the hydrochars precursor.[63] Romero-Anaya *et al.* studied chemical activation of spherically shaped hydrochars with different activation agents (H_3PO_4, NaOH, KOH and CO_2). [64] They found that spherical hydrochars maintained their morphology over the activation process. Yields after H_3PO_4 activation were 30%, being clearly higher compared to yields after other activation agents.

Oxygen surface functional groups of hydrochars can be exploited to alter surface functionality. Titirici *et al.* presented research in which oxygen functional groups on the surface of hydrochar were chemically transformed into amino groups *via* nucleophilic substitution reaction with chloropropylamine.[65] Successful amino functionalisation has been reached by silylation of hollow HTC-derived carbon spheres as well.[66] Use of Diel-Alder cycloaddition in the modification of hydrochar surface functionality has been reported by Ukarami *et al.* who added masked maleimide terminated PEG2000 (pMI-PEG2K) onto diene groups of the surface of hydrochars in which pMI-PEG2K acted as a dienophile.[67] Later on, they managed to modify carbon surface by introduction of maimide, tetracyanoethylene and 4,5-dicyano-1,3-dithiol-2-one (DCDTO). DCDTO-functionalized hydrochar was further hydrolysed in order to obtain thiol functionalized final product.[68] On the other hand, surface functionality can be altered simply by treatment with a strong acid such as H_2SO_4 resulting sulfonic group containing ([S] 5.1 - 6.4 wt.%) hydrochars.[69, 70]

1.3.2 **Templating**

Utilization of templating offers opportunity to control morphologies and pore systems of the hydrochars. Typically, templating techniques can be classified as hard- and soft templating. Utilization of hard- and soft template involve three main steps: 1. Formation of template, 2. The casting step with target precursor, including the conversion of the precursor and 3. Removal of the template.[71] Templating technique is illustrated in the Figure 3 in which HTC has been exploited as a conversation technique. Traditionally, one of the most used approaches to design porous materials has been the nanocasting or impregnation of premade sacrificial hard-templates. A hard-template could be defined as follows: rigid/semirigid solid or colloidal sol, bearing an organic, inorganic or hybrid three dimensional cross-linked framework such as zeolites, alumina membranes and ordered mesoporous silica.[72] Since template structure in the hard template is fixed, syntheses are rather easy to control.

Mesoporous silicate template is a great example of the hard template in which precursor is incorporated into channels by sorption, phase transition, ion exchange, complex or covalent grafting. In the use of silica templates mesopores are commonly in the range of 2-10 nm and may express variable topologies with highly ordered replicas. Additionally, silicate templates can be prepared with different macroscopic morphologies allowing further control over the morphology of the replica. Silicate templates are rather stable both chemically and thermally.[71] Template has to be removed by NaOH or HF. For this reason template can be considered as a single-use. Templating technique has been applied for the synthesis of hydrochars as well. In HTC it is critical to make sure that liquid organic intermediates can penetrate the pores of the template and further carbonization takes place in or on, the silica template not in the surrounding aqueous media. By control over the degree of the surface polarity of the template impregnation level can be determined.[73] Some non silica-based hard templates such as anodic alumina membranes

and tellurium nanowires have been introduced in the HTC synthesis as well.[74, 75] Core-Shell strategy was implied in the synthesis of tellurium rich nanowires in which the first step was preparation of wires and further on coating with carbon material. Additionally, similar pre-existing hard templates as described above has been utilized in HTC in which hard templates has been formed *in situ* during HTC synthesis like in the synthesis of metal carbon nanocables.[76]

Soft templates are often more flexible compared to hard templates being for example dependent on the temperature, solvent and ionic strength.[77] They perform weaker electrochemical interactions *e.g.* van der Waals forces ad hydrogen bonding unlike hard templates which form covalent ionic or metallic bonding in templating process. In these soft templated processes reaction leading to the solid product happens *via* chemical reaction, such as a sol-gel reaction or a reductive coupling, thus leading to a mesostructured product. However, successful exploitation inorganic precursor and organic template requires carefully controlled and stable conditions *e.g.* pH, solvents and temperature as well as conformation about the compability.[78]

In soft templating can be used materials such as classical amphiphiles, amphiphilic block copolymers, single polymers a latex particles or microgels.[72, 79, 80] Use of soft, polymeric templates of specified size and shape can also be performed in the synthesis of HTC-derived carbon materials. The use of aqueous dispersion of latex nanoparticles is a fine example about soft templating approach in which nanostructured hollow carbon materials were received. Beneficial in the use of latex nanoparticles is that they can be produced at selectable size and shape with narrow size distribution. After HTC synthesis carbon layer on the spherical latex nanoparticle is formed. Latex can be removed by heating at elevated temperatures (>500 ˚C) in which hollow carbon sphere is reached as a final product.[66] Furthermore, Kubo *et al.* presented HTC synthesis (130 ˚C) of fructose based carbon materials which structure formation was controlled *via* block copolymer (Pluronic® F127 triblock polymer).[81] Applied soft templated is unstable at temperature ~180 ˚C and therefore lower temperature and fructose as a starting carbon source was chosen. Received carbon material indicated cuboctahedron-like particles of 1-10 μm diameter in size with faceted edge/layered morphology. Like latex, also block copolymer has to be removed by thermal treatment.

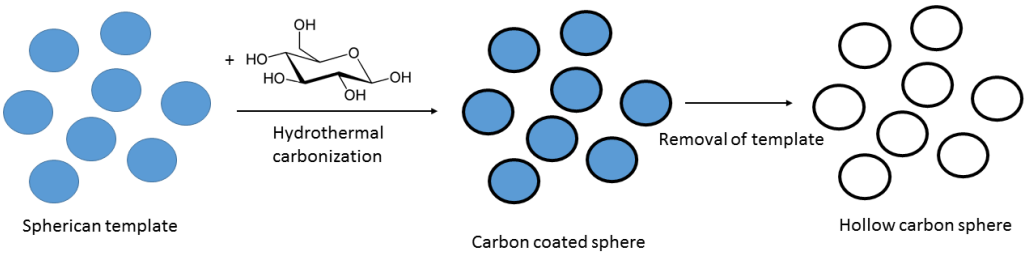

Figure 3. Schematic representation of the hydrothermal carbonization process in the presence of spherical template leading to the formation carbon coated carbon@composite. Removal of template results formation of hollow carbon sphere.

Alternative approach to replace sacrificial templates has been investigated in order to decrease the number of synthetic steps, reduce the amount of wastes and avoid harsh chemical etching. Design of alternative porous networks was first developed for silica-based materials, *via* a fine control over both the sol-gel transition and the drying of the as-synthesised wet hydrogel.[52] From this point of view salt mediated hydrothermal processes have shown potential over the control of hydrothermal process in the production of fine structured carbon materials. Fechler *et al.* reported that the HTC of carbohydrate *in situ* with different salt mixtures enable different pore size distributions. [82] Introduction of LiCl-$ZnCl_2$ salt mixture resulted mainly microporous materials whereas KCl-$ZnCl_2$ large mesopores. These binary $ZnCl_2$ based hypersaline salt mixtures with *e.g.* NaCl, KCl and LiCl) are known to form low melting eutectics.[83] The introduction of these very hydrophilic ions in to the reaction media causes decrease in the partial pressure of water and changes its structure so that reactions can be performed under less extreme conditions.[84] Additionally, they were found to regulate the formation of pore diameters and stabilize the surface of the forming primary particles during HTC process as well as acting as a molecular template. Further on salts do not bound onto final product material and can be removed by washing with water.[85, 86]

Effect of borax as catalyst and structure directing agent in HTC process (180 ˚C/8 h) and structure directing agent has been studied as well. Use of borax resulted monolithic carbon materials with improved textural properties. Borax was removed simply by washing with water. Additional post-carbonization improved porosity and specific conductivity of the carbon monolith.[87] Borax was proposed to catalyze isomerization of glucose to fructose *via* interaction with sugar diols forming of negatively charged complexes.[85] Xie *et al.* presented HTC study of several carbohydrates *i.e.* glucose, fructose, xylose and starch in the presence of molten salt 1-butyl-3-methylimidazoliumtetrachloroferrate(III), [Bmim][$FeCl_4$] resulting high 80 % yields.[88] [Bmim][$FeCl_4$] was claimed to have triple role in the synthesis: 1. Soft template, 2.

Effective catalyst for the carbonization and 3. Safe, recyclable solvent for the carbonization reaction. After synthesis it can be removed by washing with H_2O. Surface area and pore volume of obtained amorphous hydrochars varied between S_{N2} 44-155 m^2/g, S_{CO2} 60-420 m^2/g, $V_{p,N2}$ 0.10-0.16 cm^3/g and $V_{p,CO2}$ 0.02-0.13 cm^3/g. Sustainability of the used salts and ionic liquids may be questioned but irrelevant if they can be recovered and reused. Chieffi *et al.* reported the HTC treatment of rye straw in the presence salt BaOH in order to receive lactic acid as a product.[89] However, synthesis route resulted lignin-derived oligomers as a by-product. This "lignin waste" was recovered together with BaOH and then HTC treated. Interestingly carbon content of these materials was rather low and even further carbonization did not improve it.

1.3.3 **Organic aerogels - Carbogels**

Synthesis using organic precursors can result organic polymers in which chemical bonding bases on strong covalent C-C linkage. This allows production of monolithic aerogels *via* the sol-gel technique.[90] The first organic carbon gels were performed by Pekala *et al. via* recorcinol-formaldehyde (RF) condensation in the presence of acid or base catalyst.[91, 92] RF-aerogels together with melamine-formaldehyde (MF) aerogels are most extensively studied aerogels. This sol-gel processing is a versatile method for synthesising these solid organic gels in a liquid solution at low temperatures.[93] Synthesis begins with the preparation of sol mixture, its gelation and drying of the wet gel and in some cases activation of the carbonized derivative.[94] Carbonaceous aerogels are lightweight nanostructured materials monoliths or powders. Density of these organic aerogels varies according to applied synthesis conditions.[90] Synthesis of carbogel is an attractive approach in the synthesise of carbon materials with properties such as lightweight, high surface area and controllable pore structure.[95]

In hydrothermal carbonization this sol-gel type of approach has been exploited in the use of globular proteins such as ovalbumin as a porosity and structure directing agent as well as natural nitrogen source. These proteins form thermally induced aqueous gels when heated above the denaturation temperature. Furthermore, such proteins undergo Maillard reaction *via* co-condensation with the carbohydrate dehydration products leading to the formation of nitrogen doped carbon scaffolds. This produced HTC-derived aerogel indicated low density $\rho \sim 0.07$ g/cm^3.[96] Their surface chemistry was further modified by thermal treatment or post functionalization.[18, 97] Moreover, in situ "one-step" functionalizing is a practical solution, implying the use of precursors or co-reactants containing desired functionalities.[8] Similar approach was used in the HTC of carbohydrate and phenolic compound phloroglucinol in which phloroglucinol was assumed to act as a crosslinking agent, promoting the nucleation mechanism.[98] Drying procedure of synthesized carbon materials may have crucial effect on the material morphology. When sol-gel type of synthesis is performed and synthesis product supercritical CO_2 dried, gel structure is maintained. Supercritical CO_2 drying is the most significant technique in order to minimize effects of the capillary collapse of the material

during the drying. In the study of phenol derived carbon monoliths significant difference in surface area was noticed when drying technique was changed (supercritical CO_2 drying S_{BET} 607 m^2/g and freeze drying S_{BET} 409 m^2/g). Therefore, the use of supercritical drying would be preferable however, rather expensive.[99] Introduction of freeze-drying would be more economical way to avoid liquid-vapour interfaces and therefore may be used as optional drying technique for supercritical CO_2 drying.[91] Another study exploited amphiphilic di-block co-polymer P4VP-PEG as a structure directing agent in the formation of carbogel in water/alcohol solution. Alteration of synthesis parameters such as concentration, pH of the reaction system and water/ethanol ratio allowed control over the textural properties such as particle size, pore volume and mechanical stability.[79]

1.3.4 **Addition of heteroatoms**

Besides porosity of carbon materials significant changes in the materials properties can be made by introduction of heteroatom in the carbon network. Addition of oxygen, nitrogen, phosphorus, sulphur and boron can improve electrical conductivity, material stability and catalytic performance because of increased number of active sites, acidity/basicity and hydrophobicity/hydrophilicity.[100, 101] Heteroatom doping in HTC can be performed by *in situ* using certain heteroatom containing starting materials or post-modification techniques. Significant difference between *in situ* functionalization and post-modification is that former results modification of the whole bulk material whereas post-modification allows alteration of the surface. However, post-modification of HTC derived materials allow further control of hydrochars with desired properties.

Oxygen is the most common heteroatom in the carbon network. It is very abundant in the hydrochars which is due to biomass related starting materials containing significant amounts of oxygen functionalities. These oxygen functional groups remain in the carbon structure upon the HTC treatment.[102, 103, 104] The water adsorption tendency of carbon materials depends on their surface chemistry and polarity. Oxygen containing functional groups are fundamental part of the surface chemistry and perhaps most conventional on the carbon surface.[1] Furthermore incorporation of carboxylic, lactonic and phenolic surface functionalities enhance surface acidity whereas contribution of carbonyl, quinone and ether type of functionalities are considered neutral and chromene and pyrone basic.[105] Besides by choice of starting materials and additional HT-treatment appearance of oxygen functionalities can be controlled with acid treatment *e.g.* HTC in the presence of acrylic acid enhanced surface acidic properties of the produced carbon, which then showed high heavy metal removal potential.[106]

Nitrogen modifies the electronic structure leading to the localized charge accumulation. Localized charge density induced by defects has a significant role in electron transfer reactions facilitating the adsorption and/or dissociation of molecules. These properties have particular importance in catalysis and sensor applications. Also, addition of nitrogen provides a way to introduce basic surface properties.[107] In HTC, nitrogen doping has been

implemented by using nitrogen rich precursor *i.e* chitin,[108] glucosamine[46] or secondary precursor *i.e.* ovalbumin[96], phloroglucinol. Nitrogen functionalities were further modified by post treatment at high temperature.[109] Pyridine and Pyrrole-like functionalities contribute to the π system donating ρ-electrons whereas quaternary nitrogen forms three σ-bonds and contributes two electrons to the system.[107, 110] Among the different nitrogen functionalities only pyridinic nitrogen and amine can provide basicity into carbon network while pyrrolic structures, nitrogen oxides show acidic character. Quaternary nitrogen has shown no effect on the enhancement of basicity.[111] Addition of nitrogen functionalities can be reached by ammonia treatment as well. XPS studies of these hydrochars indicated to appear in pyridinic and neutral amine structural motifs.[112]

Compared to nitrogen doping sulphur doping is less investigated but gaining more attention in current carbon materials research. Potentially it can contribute basicity into carbon network. Sulphur is a large molecule and therefore often used to alter physical properties by inducing structural defects or increase interlayer spacing of graphitic lattices.[113] Further on it has easily polarizable lone pairs. In the synthesis of sulphur doped activated carbons conventionally introduction of sulphur is reached by the use of sulfurization agents such as H_2S, SO_2, CS_2 or dimetmylsulfide.[114] Only few studies have been published about sulphur doped hydrochars. Fraile *et al.* reported sulfonation of the hydrochar which was accomplished by the treatment with concentrated H_2SO_4 upon HTC.[115] Catalytic activity of these sulfonated carbon materials was tested in the esterification of palmitic acid. Bulk elemental analysis after sulfonation revealed sulphur contents up to 4.3 wt.%.[116] Few HTC based articles has been published related to *in situ* dual heteroatom doped, *i.e.* nitrogen and sulphur. As a starting material were used compounds like cysteine, thiophenecarboxaldehyde and ovalbumin.[117, 118] Thiophenic sulphur is considered neutral whereas oxygen containing sulphur functionalities provide acidic character to the carbon network.[115, 119] However, clarification is needed about the role of C-S portions in acid-base interaction. Figure 4. summarizes potential oxygen, nitrogen and sulphur functional groups on the surface of carbon network.

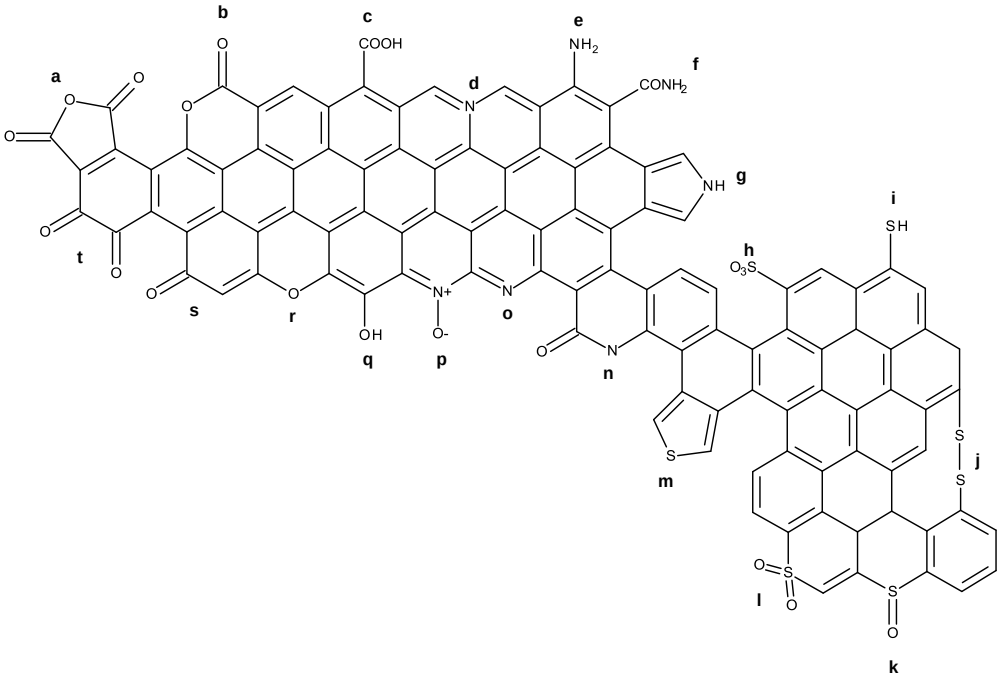

Figure 4. Potential N, O and S functionalities in the carbon materials. a. Anhydrine, b. Lactone, c. Carboxyl, d. Quaternary nitrogen, e. Amine, f. Amide, g. Pyrrole, h. Sulfonic, i. Thiophene, j. Disulfide, k. Sulfoxide, l. Sulfone, m. Thiophene, o. Pyridine p. Nitrogen oxide, q. Phenol, r. Pyrone, s. Ketone and t. Quinone.

1.4 Adsorption in water treatment

Adsorption can be considered as a phase transfer process in which components are removed from fluid phases *i.e.* gases or liquids on the surface of the adsorbent (solid phase). In water treatment adsorption has been proved to be an efficient removal process for several unwanted components. Here, molecules or ions are removed from the aqueous media onto solid surfaces. In natural systems binding of substances by some materials with complexed structure can happen on both external and internal surfaces.[24] In the water treatment processes adsorption is largely used in the application fields like surface water, ground water and wastewater treatment for the removal of organic and inorganic pollutants. Additionally it has been applied in the fields like remediation of contaminated soil and flue gases.[120] In the water treatment applications activated carbon is conventionally applied adsorbent. Its advantages are well developed textural properties such as high internal surface area, porosity and surface chemical properties.[121] In the

synthesis of activated carbons disadvantages come mostly from the rather harsh multistep synthesis and low yields. In the industrial applications adsorption from liquid phases could be used in the fields like food processing, decolourization of oils and fats, purification in textile, pharmaceutical, chemical and petrochemical industries.[120]

1.4.1 **Metal ion Removal**

Metal pollution in the environment is the result of the direct or indirect release of metal containing waste waters from industries such as metal plating facilities, mining operations, fertilizer and pesticide production, tanneries, and battery and paper industries. The origin of heavy metals in natural waters is frequently attributed to improper disposal of industrial wastes. Due to mobility and toxicity, they have been classified as priority pollutants. For example, lead (Pb(II)) is known to cause encephalopathy, cognitive impairment, behavioural disturbances, kidney damage, anaemia, and toxicity to the reproductive system for humans[122] whereas chromium, particularly Cr(VI), is known to be carcinogenic and mutagenic.[123] There are several techniques available for metals removal from waste effluents with varying degree of efficiency. These include adsorption, coagulation, foam flotation, filtration, ion exchange, aerobic and anaerobic treatment, advanced oxidation process (AOP), solvent extraction, electrolysis, and microbial reduction.[124, 125] Compared to other processes, the adsorption process is considered better due to its convenience, ease of operation, and simple design. Activated carbons have been the most popular and widely used adsorbents in waste water treatment with good performance for the removal of organic pollutants, whereas their applicability for the removal of inorganics is limited.

Adsorption is a complex phenomenon for which several factors have effect on. Amongst them the textural properties of the adsorbent (*e.g.* surface area, porosity, surface functional groups and their acidity/basicity as well as quantity), solution properties (*e.g.* temperature, pH and ionic strength) and pollutant features. Adsorption mechanisms may involve ion-exchange, complex formation, redox reaction and non-electrostatic attractions such as van der Waals forces or hydrogen bonding.[126,127, 128, 129, 130] Hydrochars prepared for the metal removal purposes vary greatly from the HTC treated biomasses with variable morphologies to magnetic nanoparticles or other carbon-composite materials as clay@carbon (Table 1.).[106, 131, 132, 133] Interestingly, several research papers have been published related to Uranium removal by different hydrochars during last years.[134, 135, 136, 137, 138] Phosphoric acid (H_3PO_4) treated hydrochars indicated highest affinity on U(VI) removal ($q_{e,max}$=260 mg/g) whereas removal efficiencies for pristine hydrochars and chitosan based hydrochars were 60 mg/g and 230 mg/g respectively. Adsorption of U(VI) by H_3PO_4 treated hydrochars indicated increased selectivity in the presence of competing ions Mn(II), Na(I), Zn(II), Mg(II), Ni(II) and Sr(II).[135, 136, 137] Increase in the amount of carboxylic groups enhanced U(VI) removal efficiency significantly from 62 mg/g to 200 mg/g. Addition of –COOH groups by HNO_3 treatment decreased porosity of the material dramatically which however appeared to be

compensated by high amount of –COOH groups.[134] Similar behaviour was observed by Demir-Cakan *et al.* who prepared hydrochars from glucose in the presence of acrylic acid (190 ˚C/16 h) and tested them towards Pb(II) removal.[106] This hydrochar showed low surface area but instead large amount of oxygen surface functionalities. Despite the minor porosity (<50 m^2/g and PSD 1-10 nm) hydrochar showed significant adsorption efficiency towards lead, Pb(II) (351.4 mg/g). Thus the lack of porosity may have been compensated by abundancy of oxygen surface functional groups. Moreover, low pH_{IEP} indicated strong acidity of the functional groups on the surface of biochar. In another study type and distribution of oxygen surface functional groups of hydrochar was controlled *via* HT-treatment (100-350 ˚C). Increased carboxyl, lactonic and phenolic features indicated to favour both Pb(II) and Cd(II) adsorption.[139] These studies support the idea of important role of surface chemistry in the removal of metallic contaminants besides porosity which importance cannot be completely diregarded.[140] On the other hand metal ions may behave differently in the similar conditions. Sanhez-Polo *et al.* reported that Cd(II) removal increased together with number of oxygen surface functional groups whereas removal of Hg(II) was found to decrease.[141] On the other hand solution pH may have significant impact on the adsorption performance. In the Cr(VI) and Pb(II) removal studies by HTC produced attapulgite clay@carbon composite (ATP@C) solution pH changed adsorption capacity of the adsorbent dramatically *e.g.* in the Pb(III removal at pH 4 q_e ~25 mg/g, pH 5 q_e ~100 mg/g and pH 6 q_e ~200 mg/g.[131] Magnetic carbon microspheres indicated reduced Cd(II) removal capacity at pH below 4. Removal efficiency remained constant from pH 4 to 7. Maximum adsorption capacity (q_e=124 mg/g) was reached at 15 ˚C. Adsorption capacity of magnetic microspheres decreased at higher temperatures (25 ˚C q_e=98 mg/g and 35 ˚C q_e=94 mg/g).[142] Cu(II) adsorption by graphene@hydrochar composite enhanced at higher ionic strength (in the presence of $NaNO_3$ and $NaClO_4$) solution. Furthermore higher temperature (25, 40 and 55 ˚C) had a slight positive impact on the adsorption capacity. The effect of natural organic matter and 1-butyl-3-methylimidazolium chloride ([Bmim][Cl]) on the adsorption performance was studied in which both humic and fulvic acid were found to enhance removal of Cu(II).[143] Adsorption remains a complex phenomenon and therefore careful characterization of adsorbent and detailed explanation of applied experimental conditions would be needed in order to understand adsorption behaviour of certain exploited materials.

HTC-derived Tellurium templated nanowires indicated high adsorption capacity for the removal of Pb(II) and Cr(VI). Adsorbent indicated highly negative surface charge over the whole studied pH range favouring adsorption of Pb(II) *via* electrostatic interaction. However, efficient removal of primarily anionic Cr(VI) (chromate or dichromate in acidic solution) is an interesting phenomenon when surface charge of adsorbent was determined negative.[144] This may be possible by synergetic effect of surface complexation, redox reaction and cation exchange.[145, 146] Reduction of Cr(VI) to Cr(III) has been supported by XPS studies in which higher amount of Cr(III) after exposure of adsorbent towards Cr(VI) was found.[144, 147] In the Table 1 are presented metal adsorption studies performed with different HTC-derived carbon materials together with selected properties of carbon materials.

Table 1. Metal removal efficiencies of different hydrothermally treated carbons and their textural properties.

Materials	Metal	S_{BET} (m^2/g)	V_p (cm^3/g)	$pH_{solution}$	Acidity (meq/g)	q_e (mg/g)	REF
H 300	Cu(II)	21	0.05	6.2	0.84	4	[148]
Mt-spC	Cr(VI)	34	-	2	-	90	[149]
DAWC	Pb(II)	161	0.15	-	-	52	[150]
DWSBC	Pb(II)	49	0.03	-	-	44	
P300	Pb(II)	-	-	5	0.84	4	[151]
R300	Pb(II)	-	-	5	0.42	3	
10AcA-C	Pb(II)	< 50	-	6	-	351	[106]
	Cd(II)					89	
HTC *prosporis africana*	Pb(II)	6.05	-	-	-	45	[152]
	Cd(II)		-	-	-	38	
Graphene@hydrochar (GA3)	Cu(II)	-	-	5	7.6	146	[143]
FMAs	Pb(II)	72	0.21			70	[132]
	Cr(VI)					75	
Te-templated carbon	Pb(II)	43.8	-	6	-	380	[144]
	Cr(VI)		-	2	-	175	
CNM nanowires	Cd(II)	29	-	-	-	85	[153]
Attapulgite clay@Carbon	Cr(VI)	62	0.208	2		138	[131]
	Pb(II)			6		180	
HTC-COOH	U(VI)	1.2	0.01	6	2.3	200	[134]

1.4.2 Organic Removal

Adsorption studies of organic compounds by HTC-derived carbon materials have concentrated mostly on the removal of organic dyes such as methylene blue. Dyes are under environmental concern due to their absorption and reflection of sunlight entering the water which interferes the growth of bacteria and inhibiting the photosynthesis in aquatic plants.[154] Additionally, they are visible already at very low concentration levels. Mainly, dyes originate from industrial waste waters. Removal of organic substances is different from the removal of metal ions. Three different mechanisms have been proposed to exist by carbon based adsorbents which are π-π interactions, hydrogen bonding and electron donor-acceptor complex formation.[155, 156] There has also been discussion about parallel adsorption mechanism between electrostatic interactions and dispersive interactions.[156, 157] As it is very well known, carbon materials have amphoteric nature and this directly influences on the sorption mechanism.[158] Amphoteric nature depends strongly on the heteroatom content which determine charge of the surface, hydrophobicity and electronic density.[130]

In the study of palm date seed (PDS) activated carbon, hydrothermal carbonization was used as a pre-treatment technique. Further improvement on the textural properties was performed by NaOH chemical activation. Final HTC-derived activated carbon had high surface area S_{BET} 1283 m^2/g with high microporosity S_{micro} 770 m^2/g with 2 nm average pore size. Presence of surface functionalities was examined with FTIR. Abundance or the type of acidic surface functionalities were not examined. However, chemical activation and pHpzc 7.06 refer to the decreased amount of acidic oxygen functionalities. Effect of solution pH on the adsorption performance for the removal of methylene blue (MB) appeared to be minor, Δq_e=2 mg/g at tested pH range (3-11) whereas change in temperature resulted dramatic change on the adsorption capacity. The highest MB removal capacity (612.1 mg/g) took place at 30 ˚C decreasing to 410 mg/g at 50 ˚C.[159] MB adsorption on HTC-derived KOH activated carbon material resulted 524 mg/g maximum adsorption capacity. Despite of high porosity (S_{BET} 1700 m^2/g, V_p=0.03 cm^3/g with 1 nm average pore size) adsorption performance was weaker compared to PDS activated carbon adsorption performance was weaker. Bulk oxygen content in the material was 31 wt.% and FTIR indicated presence of C-O vibrations in the activated carbon. Adsorption efficiency of KOH activated carbon was 10 times higher than corresponding hydrothermally treated carbon material (q_e=52 mg/g).[160] Dramatic difference in the adsorption efficiency towards tetracycline (antibiotic) by HTC-derived *salix psammophila* (P700) was observed when abundance of acidic groups on the adsorbent decreased and number of basic groups increased correspondingly.[161] Tetracycline removal studies by HTC-derived magnetic (MPC) carbon materials as well. However, adsorption efficiency compared to metal-free adsorbent as P700 was found similar. Adsorption of tetracycline appeared to be favoured in acidic conditions in which MPC indicated positive surface charge.[162]

Methylene blue removal was studied by magnetic-graphene-Fe_3O_4@carbon nanoparticles. These hybrid materials indicated rather good performance (q_e=70 mg/g) for MB removal considering the porosity of the materials (S_{BET}=94 m^2/g). Graphene-Fe_3O_4 hybrid was regenerated by washing with ethanol after adsorption in which adsorption performance of adsorbent remained over 90 % during five cycles after ethanol washing from H_2O solution. Adsorption experiments under acidic (0.1 M HCl) conditions indicated that after some time hybrid begins to dissolve.[163] Clay mineral composite structures produced *via* HTC has also been employed in the adsorption studies of dyes. Unlike in the MB adsorption studies of palm date seed activated carbon attapulgite@carbon composite indicated strong dependence on the solution pH in which variation of adsorption capacity was Δq_e=82 mg/g between the studied pH range (3-10). Additionally increase of the KCl (0-300 mmol/L) in the solution decreased adsorption efficiency (Δq_e=27 mg/g) and higher temperature (298.15 K, 308.15 K and 318.17 K) during the adsorption resulted higher MB removal efficiency. Temperature dependence has been referred to the endothermic or exothermic adsorption process. Determined maximum adsorption capacity was rather high q_e=216 mg/g despite the lower porosity (S_{BET}=81 m^2/g, S_{micro}=11 m^2/g and V_p=0.24 cm^3/g with 24.5 nm average pore size). Role of the surface functionalities was not discussed in detail. However, pH_{IEP} was determined as 3.2.[164]

Table 2. Adsorption performances of different carbon based materials for the removal of organic substances and textural properties of adsorbents.

Material	Compound	S_{BET} (m^2/g)	V_p (cm^3/g)	pH	q_e (mg/g)	REF
Palm date seed AC	Methylene Blue	1283	0.66	7	612	[159]
Graphene/Fe_3O_4@carbon	Methylene Blue	94		-	65	[163]
Polygorskite@carbon	Methylene Blue	15		-	45	[165]
	Orange II	259		-	12	
FMAs	Methylene Blue	72	0.21	-	39	[132]
	Malachite Green				40	
ATP@CCS	Methylene Blue	81	0.24	-	226	[164]
CAl-10	Orange II	182	0.21	5-6	190	[166]
Hazelnut shell hydrochar	Methylene Blue	60	0.05	7	52	[160]
Sucroce der. hydrochar	Paracetamol	2431	1.14	-	514	[167]
	iopamidol				1050	
P700 (*salix psammophila*)	Tetracycline	316	0.24	-	30	[161]
FCM	[BMIM][Cl]	20	0.09	7	30[a]	[168]

[a] estimated from the reported mmol/g value

Drug residues ending up into natural waters are growing environmental problem due to toxic effects in aquatic organisms. Mestre *et al.* synthesised of ultramicroporous sucrose-derived hydrochars and tested their applicability in the removal of pharmaceutical

compounds ibuprofen, paracetamol, clofibric acid caffeine and iopamidol from aqueous solutions.[167] Deeper insight on the adsorption behaviour was conducted with iopamidol (q_e=1050 mg/g) and paracetamol (q_e=514 mg/g). These sucrose-derived hydrochars showed increased removal potential compared to corresponding commercially available activated carbon(iopamidol q_e=472 mg/g and paracetamol q_e=267 mg/g) supplied by Norit.[167] HTC-derived activated carbons from orange peels were used as adsorbents for the removal of diclofenac, sodium, salicylic acid and flurbiprofen. H_3PO_4 activated hydrochar (HC-PN) indicated best adsorption performance compared to other activated carbon prepared with different activation techniques towards diclofenac sodium (q_e=0.21 mmol/g) and salisylic acid (q_e=0.6 mmol/g) at pH 7 and pH 2 respectively. HC-A (hydrochars activated by thermal treatment under air) resulted slightly better adsorption capacity towards flurbiprofen (q_e=0.6 mmol/g) at pH 2. It was reported that at acidic condition diclofenac sodium is mainly in neutral form and undergoes reaction cascade leading to the inactivation which also decrease its solubility and therefore adsorption studies we performed at pH 7. In the case of flurbiprofen and salisylic acid pH 2 was found as optimal for the adsorption studied.[169] Qi *et al.* studied removal of rather unconventional pollutant 1-butyl-3-methylimidazolium chloride, [Bmim][Cl] by hydrothermally produced functional carbon microspheres (FCM).[168] Adsorption performance of FCM was compared with commercial activated carbon (supplied by Hengtai Co., Ltd.) in which activated carbon indicated slightly higher adsorption capacity. However, adsorption capacity of FCM (q_e=0.17 mmol/g) was comparable with adsorption capacity of activated carbon (q_e= 0.21 mmol/g). Summary of the adsorption capability of hydrochars towards different organic pollutants are presented in the Table 2.

1.5 Hydrochar as an electrocatalyst

Production of sustainable energy is an important global challenge.[1] Among various energy production techniques, fuel cells offer are very efficient and attractive choices because they do not generate pollution. Operation principle of the fuel cell is presented in the Figure 5. Utilized fuel in the fuel cell vary according to the type of the cell. Proton exchange fuel cells and phosphoric acid fuel cells conventionally utilize hydrogen as a fuel, while methanol and ethanol are typically used in the direct methanol/ethanol fuel cells. These fuel cells are known as low-temperature fuel cells due to their practical operational temperatures are below 200 ˚C.[170] The high-temperature (600-1000 ˚C) fuel cells such as solid oxide fuel cells and molten carbonate fuel cells use hydrogen, natural gas, hydrocarbon or coals as a fuel.[171]

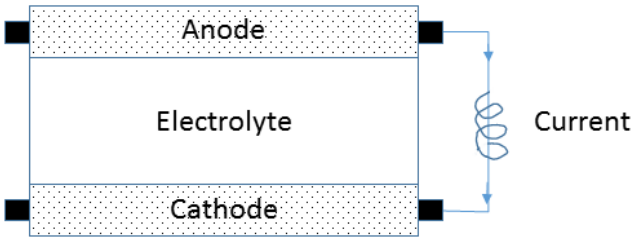

Figure 5. Schematic illustration of operation principle of the alkali fuel cell. At the anode, used fuel is oxidized to protons and electrons, whereas at the cathode reduction of oxidized agent takes place.

Fuel cell is defined as a electrochemical device which converts chemical energy, this is, *e.g.* hydrogen or methanol molecules into electric energy *via* electrochemical redox reactions.[172] In the general concept fuel cell involves the electrocatalytic oxidation of a fuel at the anode and the electrocatalytic reduction of an oxidizing agent at the cathode. This oxygen reduction reaction (ORR) at cathode plays a key role in controlling the performance of a fuel cell.[109] In the proton-exchange fuel cells the ORR can proceed either through 1. four electron process in which reaction of oxygen with electrons and protons produce water as the end product or 2. a less efficient two-electron pathway involves reduction to hydrogen peroxide (H_2O_2).[173, 174] Sluggish cathodic oxygen reduction reaction (ORR) is one of the key challenges for fuel cells and metal-air batteries.[175]

On the other hand morphology, structure and activity of the catalyst depends strongly on the catalyst support. Catalyst support does not only act as a suitable base for even dispersion of metal particles but also impacts on its electronic structure and further on its catalytic activity. The most important features for catalyst support involve high surface area allowing high catalyst loadings with even dispersion. Furthermore, adequate pore sizes enabling smooth mass transfer of the fuel and its oxidized form whilst efficient electrical conductivity is required for the powerful electron transport through electrode as well as electrochemical corrosion resistance in harsh fuel cell environments.[176] Noble-metal *e.g.* Pt-based materials are favoured as catalysts because of their attractive properties such as low operating temperatures, high power densities and relatively easy up-scaling.[172] Alkaline fuel cells utilizing Pt-loaded carbon as an electrocatalyst and in which reaction happens *via* the four-electron ORR process were developed for the Apollo lunar mission in the 1960s. However, their large scale commercial application has been

hindered due to the high cost of the noble metals.[3, 177, 178] Additionally, Pt-based electrodes suffer from the sensitivity to time dependent drift and CO deactivation.[177] However, resistance of Pt loaded materials towards poisoning can be avoided by alloying with materials less sensitive to CO and CO_2 blockage.[172]

Intensive research effort has been done in the reduction and/or replacement of noble metal based such as Pt-based electrodes in the fuel cells.[179] This has resulted development of wide range of ORR electrocatalysts such as Pt-based alloys, transition metal oxides, chalcogenides, carbon nanotube-supported metal particles, enzymatic electrocatalytic systems and conducting poly(3,4-ethylenedioxythiophene)(PEDOT)-coated membranes.[177, 179] Heteroatom doped carbons have been demonstrated as the promising ORR catalysts in which sulphur, nitrogen, boron and phosphorus doped carbon materials has been shown potential.[101, 180, 181, 182] Among these heteroatom doped carbon materials nitrogen has received great interest. Nitrogen groups are known to change the electrochemical properties *e.g.* electron-donating character, conductivity and capacitance behaviour of carbon materials.[62] However, researchers are still discussing what are the active sites in the ORR of the nitrogen doped carbon materials. Main focus in the discussion is on the chemical bonding states of nitrogen *i.e.* pyridinic, pyrrolic and quaternary N. Pyridinic and pyrrolic nitrogen structures have a lone electron pair in the plane of the carbon matrix. It has been assumed that especially pyridinic nitrogen can enhance the electron-donating ability to promoting ORR electrocatalytic activity *via* $4e^-$ pathway.[183]

Besides alternatives for noble metal loading and properties of electrocatalysts attention has been paid for the materials synthesis routes. In the production of nitrogen doped carbon materials metal catalysts are often employed in order to obtain carbon nanomaterials. In order to avoid presence of residual metal catalysts techniques such as reactive magnetron sputtering has been performed.[183] HTC technique as a primary process in order to receive potential metal-free electrocatalysts or electrocatalyst supports in the oxygen reaction reactions has been studied rather extensively.[62, 184, 185, 186, 187] Wohlgemuth *et al.* has examined potential of HTC in the production of carbon aerogels and their applicability as electrocatalyst.[188] In this study high surface area and nitrogen rich aerogel was received by borax mediated HTC reaction with glucose and 2-pyrrolcarboxaldehyde (PCA) as nitrogen source. Further HT- treatment at 900 ˚C was performed to enhance conductivity and alter the binding states of nitrogen. Nitrogen doped carbon aerogel was observed to have a rather good long term stability and great methanol tolerance in comparison to Pt-catalyst which was poised after methanol addition. Further on these carbon aerogels were found to favour 4 electron process rather than 2 electron process. Performance of dual nitrogen-sulphur doped hydrochar in oxygen reduction reaction has been studied as well. Dual doping was achieved by addition of suitable secondary precursor *e.g.* Thienyl-cysteine. Catalytic activity was tested in the acidic and basic reaction medium in which comparable overall performance was found when compared to commercially available Vulcan. Furthermore, typical to carbon materials better performance in the basic reaction medium was observed. Electron

transfer processes were found to favour 4 electron process in the basic (0.1 M KOH) reaction medium and 2 electron process in the acidic (0.1 M $HClO_4$) reaction medium.[117]

2 Research Objective

In this thesis suitability of hydrothermal carbonization technique for the production of hydrochars in different applications was examined. In addition to reaction technique itself use of the sustainable and readily available feedstock was under interest. In wide range of applications textural and structural properties play a key role. Therefore, in this research modification of properties such as porosity, *i.e.* micro- and mesoporous carbon materials, heteroatom content and type in the material network was studied (Papers I-V).

In order to modify morphological and structural features of carbonaceous materials different synthesis procedures were used *i.e.* HTC as such, secondary precursor as natural heteroatom source and structure directing agent, HT-treatment and templating techniques (Papers III, IV and V). These techniques allow control of porosity as well as distribution of heteroatoms in the carbon network. Obtained carbon materials were carefully characterized to understand the formation of carbon network and type of functional groups.

Suitability of these hydrochars as alternative adsorbents over the traditional activated carbons in the pollutant removal from waters was tested for both organic and inorganic contaminants. Effect of pH, temperature, ionic strength, presence of competing ions and contact time were examined. Moreover, adsorption behaviour and correspondence to the experimental data was estimated with different theoretical models such as Langmuir, Freundlich and Sips.

Utilization of waste streams in the material production would be beneficial. Therefore, applicability of hydrothermally treated sludge (pulp and paper industry and municipal sludge) for the removal of several metal ions (Pb(II), Cr(III), Cr(VI), As(III) and As(V)) was examined in Paper I. Effect of the operational conditions on the properties of sludge based hydrochars and its effect on the adsorption efficiency towards Pb(II) was studied in Paper II. Moreover, alteration of heteroatom distribution on carbon surface was examined by introduction of secondary precursor ovalbumin in Paper III. Adsorption efficiency of this nitrogen-enriched carbon material was studied towards Pb(II) and Cr(VI). In Paper IV applicability of salt templated hydrochars was examined towards methylene blue removal.

Nitrogen rich carbon materials have shown potential as a metal-free catalyst in oxygen reduction reactions this was examined in Paper V. Textural properties of hydrochars was modified by post-high temperature treatment and suitability of these nitrogen rich carbon aerogels were tested as metal free electrocatalyst as well as electrocatalyst support. Testing as an electrocatalyst support was conducted with impregnation of noble metal platinum on the carbon surface.

3 Materials and Methods

3.1 Synthesis of hydrochars

3.1.1 Carbon aerogels

In the synthesis of carbon aerogels two carbohydrates were introduced as main carbon source (detailed synthesis presented in Papers III-IV), *i.e.* D-Glucose (wasserfrei p.a., Carl Roth) and Cellulose (microcrystalline powder, Sigma-Aldrich), together with Soya bean flour (Sigma-Aldrich) or Ovalbumin (from chicken egg white, grade II, Sigma-Aldrich).

Typical synthesis of carbon aerogel carbohydrate, soy bean flour and deionized H_2O was weighted in a glass inlet and mixed. Precisely, dry chemicals were well mixed and then followed by H_2O addition. When using cellulose as a starting material, acidic conditions were used in order to catalyse the reaction (concentrated H_2SO_4 1 mL) and the soy bean flour amount was 0.5 g. A glass inlet was introduced inside the PTFE-lined autoclave, sealed and placed into a preheated oven. After synthesis autoclaves were allowed to cool down, carbon materials were vacuum filtrated and washed extensively with deionized water and finally freeze dried.

To prepare thermally treated carbon material, the original freeze dried sample carbon material was placed in a crucible and introduced in a carbonization oven and then heated up to 1000 ˚C under inert atmosphere (N_2 flow of 25 mL/min) using a heating rate of 5.0 ˚C and 4 h dwell time. Platinum impregnation was conducted for the HT-treated carbon materials. Carbon material was suspended in H_2PtCl_6 (Sigma-Aldrich) solution and an excessive amount of $NaBH_4$ (Sigma-Aldrich) solution was added in order to reduce platinum on the carbon surface. Carbon suspension was centrifuged and washed with water several times and dried under vacuum at elevated temperature.

3.1.2 Salt mixture templated carbon materials

The carbon materials were synthesized from D-Fructose (Alfa Aesar) via hydrothermal carbonization in which 2-thiophenecarboxyaldehyde (TCA) (Sigma-Aldrich) was added as a sulphur source. LiCl-$ZnCl_2$ eutectic salt mixture was used as a template controlling the formation of carbon network. In a typical synthesis, the monosaccharide Fructose was mixed with water, TCA and LiCl-$ZnCl_2$ salt mixture. The reaction mixture was placed in glass inlet, sealed in a Teflon lined autoclave and placed in an oven, which was preheated to 180 ˚C. The autoclave was kept in the oven for 16 h. The obtained carbon material was removed from the glass inlet, placed in water and stirred overnight in order to remove the salt from the carbon material. Finally, the carbon material was vacuum filtrated, washed extensively with water and dried in the oven under vacuum at 80 ˚C overnight.

3.1.3 HTC treated sludge

Pulp and paper industry sludge and anaerobically digested sludge were used as received. HTC treated carbonaceous materials were produced in a stainless steel high-pressure reactor. Reactor was loaded with 70 wt.% of sludge and 30 wt.% of water. Reaction temperatures were 160 ˚C, 200 ˚C and 240 ˚C and the reaction time was 12 h. The reactor was allowed to cool down after the reaction. The reaction mixture was vacuum filtrated and the solid carbonaceous material washed repeatedly with deionized water. Eventually, the carbonaceous material was dried at 80 ˚C overnight and ground to finer powder for the further experiments.

3.2 Characterization

Nitrogen adsorption isotherms at -196 ˚C were determined with TriStar 3000 (Micromeritics Inc.) or Quantachrome instrument consisting of high speed surface area and pore size analyser Nova 4000e. The specific surface areas were calculated from the adsorption branch of the isotherm using Brunauer-Emmett-Teller theory (BET) or t-plot and pore size distribution (PSD) was determined with non-local density functional theory (NLDFT) assuming slit shaped pores. CO_2 sorption isotherms were performed at 0 ˚C with Quantachrome autosorb-iQ C automated gas sorption analyser. The surface area of the carbon materials were calculated by applying the BET model. Pore size distribution and pore volume were determined using NLDFT, similar to N_2 sorption studies. Before sorption the samples were degassed under vacuum at 150 ˚C for 20 h. Fourier transform infrared spectroscopy (FTIR) was conducted with Bruker Tensor 27 equipped with an attenuated total reflectance unit for the analysis of the surface functionalities. The surface morphology was surveyed with FEI Quanta 3D environmental scanning electron microscope (ESEM) and JEOL JEM-2010 transmission electron microscope (TEM) operating at 200 kV. Elemental amounts of C, H, N and S present in the carbon materials composition were determined with Vario EL elemental analyser. X-ray photoelectron spectroscopy (XPS) analysis was performed with PHI 5400 ESCA spectrometer (PerkinElmer Co.,) using a Mg Kα X-ray source (hv = 1253.6 eV). The background pressure during the measurements was < 10-8 mbar. The peak fitting process was done with Casa XPS (Casa Software Ltd.). Shirley-type background was subtracted from the spectra and the binding energy values were referenced to the hydrocarbon C(1s) peak at 285 eV. ^{13}C solid-state magic angle spinning (MAS) nuclear magnetic resonance studies (NMR) were acquired on Bruker Advance 300 MHz (7T) spectrometer using 4 mm zirconia rotors sipping at a MAS frequency of vMAS= 14 kHz. Chemical shifts were referenced relative to tetramethylsilane (TMS; δ=0 ppm). Zeta potential was determined by pH titration utilizing Zetasizer Nano ZS (Malvern Instruments Ltd.). The total acidity of the carbon materials was estimated by mixing 50 mg of each carbon material with 30 ml of 0.1 M NaOH. The suspension was mixed for one hour at ambient temperature and separated using a 0.45 µm polypropylene syringe filter. The supernatant was titrated with 0.1 M HCl solution. The solution was sparged with N_2 for 10 min before titration and

continued throughout titration in order to prevent interfering effect of dissolved CO_2. The equivalent point was observed using phenolphthalein indicator. X-ray röntgen diffraction (XRD) patterns were recorded with a Panalytical Xpert Pro diffractometer over the 2 theta range of 10 - 70 ˚, using Cu kα-radiation reflection mode, divergence slit and Ni-filter.

3.3 Adsorption and desorption experiments

Adsorption experiments are described in detail in Papers I-IV. In brief dye removal efficiency (methylene blue) was determined with UV-VIS spectrophotometry maximum wavelength (λ_{max}) 664 nm for methylene blue. Metal solutions were analysed with inductively coupled plasma optical atomic emission spectrometry (ICP-OES) model iCAP 6300 (Thermo Electron Corporation, USA). The used wavelengths for different metals were: 283.5 nm (Cr(IV)), 220.353 nm (Pb(II)), 189.042 (As(V)) and 324.7 nm (Cu(II)).

In the adsorption test solution containing organic/inorganic pollutant (10 ml) was mixed with carbon material (20 mg) and allowed to reach equilibrium state after which the carbon material was removed from the solution by filtration. Adsorption capacity *i.e.* amount of pollutant adsorbed per unit mass of adsorbent was calculated as follows:

$$q_e = \frac{(C_i - C_e)}{m} V \quad (1)$$

Where q_e (mg/g) is equilibrium adsorption capacity, C_i and C_e (mmol/l) are the initial and equilibrium dye or metals concentrations, respectively, m (g) represents the weight of the adsorbent, and V (l) is the volume of the solution.

In adsorption modelling of experimental data following equations were used:

Langmuir

$$q_e = q_m \left(\frac{K_L C_e}{1 + K_L C_e} \right) \quad (2)$$

In which K_L is the affinity constant and q_m describes the maximum adsorption capacity of adsorbents.

Freundlich

$$q_e = K_F C_e^{\frac{1}{n_F}} \quad (3)$$

In which K_F is the affinity constant and n_F describes the system heterogeneity.

Sips adsorption isotherm:

$$q_e = q_m \frac{(K_S C_e)^{n_S}}{1+(K_S C_e)^{n_S}} \quad (4)$$

In which K_S (lmg^{-1}) is the affinity constant, C_e ($mmoll^{-1}$) is the dye or metals concentration at the equilibrium state and n_S describes the surface heterogeneity.

Below are listed equations used in the kinetic modelling in which pore diffusion as a controlling step in the adsorption was considered by intraparticle diffusion model as follows:

$$q_e = k_{dif} t^{\frac{1}{2}} + (C) \quad (5)$$

where k_{dif} mg (g $min^{1/2})^{-1}$ is the rate constant of intraparticle diffusion and C represents the thickness of the boundary layer.

Pseudo-first-order non-linear (PS1) kinetic model:

$$q_t = q_e(1 - exp^{-k_1 t}) \quad (6)$$

In which k_1 is the PS1 rate constant (g/mmol min).

Pseudo-second-order non-linear (PS2) kinetic model:

$$q_t = \frac{q_e^2 k_2 t}{1+q_e k_2 t} \quad (7)$$

In which k_2 is the PS2 rate constant (g/mmol min) and $k_2 qe^2$ represents the initial sorption rate.

3.4 Oxygen reduction reaction

Electrocatalytic activities were measured in O_2- or N_2-saturated 0.1 M KOH using three-electrode configuration. Oxygen or nitrogen was purged for 30 min before measurement, and continuously bubbled though the electrolyte during the tests, in order to ensure the saturation of the electrolyte with O_2 or N_2. Rotating ring disk electrode (Pt-ring / glassy carbon disk, Gamry) was used as working electrode, Ag/AgCl (sat. KCl, Sigma-Aldrich) as reference electrode and platinum sheet (Metrohm) as counter electrode. The scan rates for cyclic and rotating voltammetry were 100 mV/s and 10 mV/s respectively, and ring potential was constant at 0.4 V vs. Ag/AgCl for rotating voltammetry. All the results were recorded using Metrohm Autolab 302N.

For electrode preparation, 4 mg catalyst was added to a mixture of nafion, absolute ethanol and 750 µl distilled water, followed by ultrasonication in order to achieve uniform dispersion of the sample in the solvent. Catalyst suspensions were then drop casted on a rotating ring disk electrode (5 mm diameter) and dried at 60 ˚C.

The electron transfer number (n) and the ratio of peroxide formation (% HO_2^-) were determined by the followed equations respectively:

$$n = 4 \times \frac{I_d}{I_d + \frac{I_r}{N}} \tag{8}$$

$$\%HO_2^- = 200 \times \frac{\frac{I_r}{N}}{I_d + \frac{I_r}{N}} \tag{9}$$

where I_d is disk current, I_r is ring current and N is current collection efficiency of the Pt ring (0.37).

For Tafel plot, the kinetic current density (J_K) is calculated on the basis of Koutecky-Levich equation:

$$\frac{1}{J} = \frac{1}{J_L} + \frac{1}{J_K} = \frac{1}{B\omega^{\frac{1}{2}}} + \frac{1}{J_K} \tag{10}$$

$$J_K = \frac{J \times J_L}{J_L - J} \tag{11}$$

$$B = 0.2nFC_0(D_0)^{-\frac{2}{3}}v^{-\frac{1}{6}} \tag{12}$$

where J is the measured current density, J_K and J_L are the kinetic- and diffusion limiting current densities, ω is the angular velocity (in RPM), n is a number of electrons transferred, F is the Faraday constant (96485 sA/mol), C_0 is the bulk concentration of dissolved O_2 in 0.1 M KOH (1.2×10^{-3} mol/L), D_0 is the diffusion coefficient of O_2 in 0.1 M KOH (1.9×10^{-5} cm^2/s), and v is the kinematic viscosity of the electrolyte (0.01 m^2/s).

4 Results and Discussion

4.1 Characterization of hydrochars

Characteristic properties directs the potential application of carbon materials and can be modified during the synthesis process by choice of feedstock, operation conditions and/or use of secondary precursor. Hydrochars synthesized in Papers I-V were produced with different approach particularly taking consideration of heteroatom distribution and porosity. Plain HTC processed hydrochars (Papers I and II) with variable operation temperatures were applied to produce carbon materials. In Papers III and V secondary precursor was added together with actual carbon source. This secondary precursor was assumed to act as natural nitrogen source and structure directing agent. Furthermore, in Paper V post-modification in order to enhance conductivity and textural properties was applied. In the Paper IV salt mixture template was introduced in order to control the development of porosity. All the materials presented in the chapter Results and Discussion are summarized in the Table 3.

Table 3. Summary of the carbon based materials presented in results and discussion section and

Abbreviation	Material	Paper
ADS[a]	Anaerobically digested sludge HTC treated	I,II
INS[a]	Industrial sludge HTC treated	I,II
GluOva	Glucose+Ovalbumin HTC treated	unpublished data
CeOvaS	Cellulose+Ovalbumin HTC treated	III
FruLi	Fructose salt templated ($LiCl$-$ZnCl_2$) HTC treated	IV
FruLi+TCA	Fructose + TCA salt templated ($LiCl$-$ZnCl_2$) HTC treated	IV
CeLi	Cellulose salt templated ($LiCl$-$ZnCl_2$) HTC treated	unpublished data
GluSo	Glucose + Soy bean flour HTC treated	V
CeSoS	Cellulose + Soy bean flour HTC treated	V
GluSo_1000	HT-treated GluSo	V
CeSoS_1000	HT-treated CeSoS	V
GluSo_1000_Pt	Platinum impregnated GluSo_1000	V
CeSoS_1000_Pt	Platinum impregnated CeSoS_1000	V

[a] In the Paper II these materials indexed *e.g.* ADS_1, ADS_2, ADS_3 referring to the treatment temperature during HTC process.

4.1.1 Morphological properties

Morphological properties of hydrochars depend strongly on the experimental setup. In Paper III ovalbumin protein was introduced as natural nitrogen source and structure directing agent. Obtained hydrochars, CeOvaS showed greatly branched long interconnected fibrous spacious network, in which the average diameter for single fiber was ≤ 50 nm. This can be seen from both SEM and TEM images provided in Figure 6 and Figure 7. These fibrous long filaments appeared to be formed from single spherical particles, which may be due to the tendency of globular proteins to grow from single monomers to longer chains. Morphological structure of CeOvaS was found to differ from glucose-based carbon aerogels which were found to form sponge-like structure from individual nanosized spherically shaped particles synthesized *via* a similar approach (unpublished data). The difference is most probably related to solution pH which determines the type of aggregates in the gelation of ovalbumin. Similar morphological features were observed when soy bean flour was used as secondary precursor instead of ovalbumin (Paper V). Further HT-treatment of soy based carbon aerogels (GluSo and CeSoS) upon HTC showed that carbon network was not disrupted by HT-treatment and therefore continuous morphology was maintained.

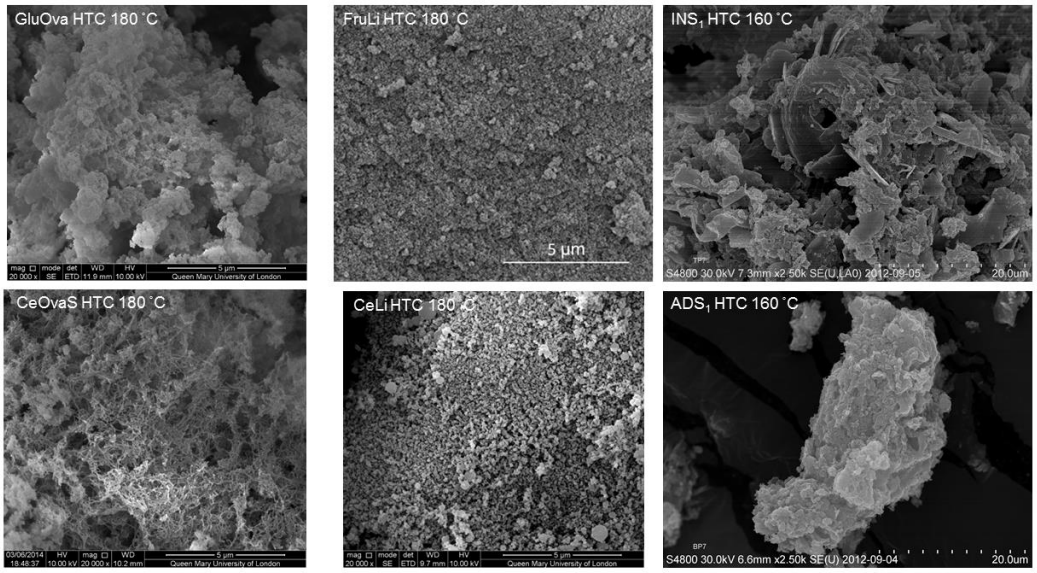

Figure 6. SEM images of hydrochars produced from different precursors at variable operational conditions (Paper II, Paper III, Paper IV and unpublished data). GluOva and CeOvaS refer to the glucose and cellulose based hydrochars in the presence of Ovalbumin respectively whereas FruLi and CeLi are fructose and cellulose based salt templated hydrochars and INS_1 and ADS_1 are HTC treated sludge derived hydrochars.

HTC of carbohydrates in the presence of salt mixture resulted carbon monoliths. These fructose based hydrochars were found to consist of spherically shaped primary particles (Paper IV). Diameters of these individual particles were determined as both ~20 nm and ~50 nm in size. Further aggregation of these spherical particles lead to the formation of final amorphous carbon network. Similar structural features were observed when cellulose and rye straw were used as a precursor at similar experimental conditions to fructose (see chapter 3.1.2). However, particle sizes of cellulose and rye straw based carbon materials were found somewhat larger compared to corresponding fructose based materials. Different operation temperatures (160-240 ˚C) in the synthesis of sludge based (ADS and INS) hydrochars were not observed to have significant effect on the formation of the morphology (Paper I and Paper II). These sludge based hydrochars revealed rather heterogeneous structural features in which individual particles were observed micrometres in size. Variable morphological features may be mostly due to the nature of starting material.

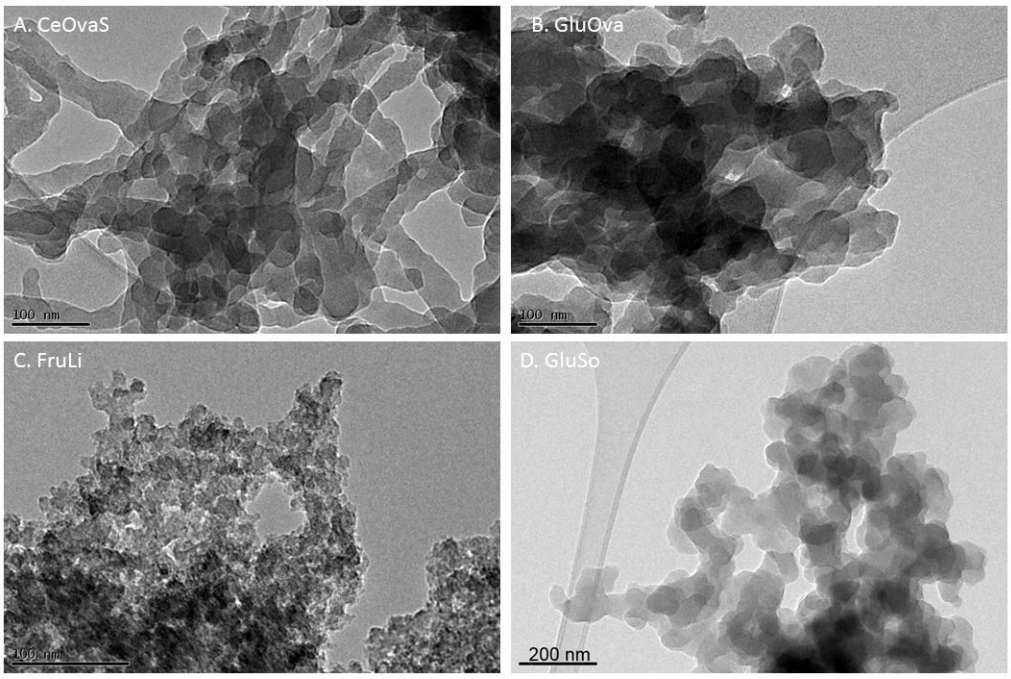

Figure 7. TEM images of hydrothermally produced carbon materials in the presence of ovalbumin A. CeOvaS and B. GluOva whereas image C. FruLi was produced in the presence of salt mixture and image in the presence of soy protein D. GluSo (Paper III, Paper IV, Paper V and unpublished data).

4.1.2 Physico-chemical properties of hydrochars

Hydrochars are typically amorphous which can be seen as brown to dark brown colour after HTC synthesis. Darker colour gives an indication about the higher degree of aromatization. Bulk carbon content for the carbon materials after HTC is approximately 60-70 wt.% (wt.% refers to weight percent) which naturally depends on the feedstock and operation temperature. Amount of oxygen can be estimated by subtraction (*e.g.* 100 wt.%-[C]-[H]-[N]). Oxygen content of hydrochars in our studies was 22-30 wt.%. Additionally further HT-treatment increases the carbon content (*e.g.* CeSoS [C]=65.7 wt.% and CeSoS_1000 [C]=82.6 wt.%) whereas amount of other heteroatoms such as nitrogen or hydrogen decrease. Elemental composition, surface area, pore volume, acidity/ and pH_{IEP} data are summarized in the Table 4. Information was gathered from Papers III-V.

Table 4. Properties HTC produced hydrochars (Papers III, IV, V and unpublished data).

	N_2 sorption			Elemental composition				Acidity	
Material	S_{BET} (m^2/g)	V_p (cm^3/g)	S_{micro} (m^2/g)	C (wt.%)	H (wt.%)	N (wt.%)	S (wt.%)	(mmol/g)	pH_{IEP}
GluSo	22	0.14		63.0	5.2	3.7			
GluSo_1000	449	0.25		72.2	2.3	1.9			
CeSoS	24	0.19		65.7	4.9	1.0			
CeSoS_1000	697	0.38		82.6	1.7	0.5			
CeOvaS	38	0.18	13[a]	61.0	4.8	2.1		0.7	3.0
GluOva[a]	35[b]	0.15[b]	8[a,b]	63.4[b]	5.4[b]	5.2[b]		0.4[b]	3.4[b]
FruLi	431	0.4	415[c]	70.2	4.7			0.87	
Fruli+TCA	554	1.2	441[c]	66.6	4.3		7.2	0.77	

[a] determined with t-plot, [b] unpublished data and [c] determined from CO_2 sorption data at 0 ˚C

Surface functionality and structural features were studied with FTIR, XPS and ^{13}C ss-NMR techniques. FTIR and XPS give information about surface functional groups whilst ^{13}C ss-NMR give deeper insight into the structural arrangement. In the study of CeOvaS, C 1(s) photoelectron envelopes indicated sp^2 C=C/C-C/C-H carbon, hydroxyl, ether and amide structural motifs (Paper III). These findings are similar with XPS studies performed with GluSo and CeSoS (Paper V) prepared under similar conditions. High temperature treatment conducted for GluSo and CeSoS was found to change the type of surface species so that two new binding energies referring to carbonyl and carboxyl/lactone/ester structural motifs were observed. Furthermore, N 1(s) envelope analysis of HTC treated GluSo indicated nitrogen to occur as amide, amide lactam and imine. However further HT-treatment of GluSo indicated transformation of nitrogen into quaternary, pyridinic and pyridine oxide form. These type of nitrogen functionalities has been observed rather typical outcome upon HT-treatment. Interestingly in the case of CeSoS nitrogen was found to appear in quaternary form already after HTC and further HT-treatment was found to increase the amount of quaternary nitrogen. Similarities in the

distribution of nitrogen functionalities in HTC-derived CeOvaS and GluOva (glucose +ovalbumin, unpublished data) was found when comparing to carbon materials CeSoS and GluSo (Figure 8.). In GluOva nitrogen was found mostly as an amine, hydrogen bonded amine and amide/lactam type of structure and minority in pyridinic form in GluOva whereas in the CeOvaS nitrogen indicated to occur mostly as quaternary nitrogen and some in pyrrolic, amine and amide/lactam type of nitrogen. FTIR analysis of GluSo, CeSoS, GluOva and CeOvaS supported findings from XPS. FTIR spectras indicated presence of aromaticity (*e.g.* furan type of structure v(C=C-O) ~1518 cm^{-1}), carbonyl (*e.g.* v(C=O) ~1700 cm^{-1}) features, nitrogen functionalities (*e.g.* amines v(C-N) ~1164 cm^{-1} and pyridinic/pyrrolic/pyrrolic structures ~1570 cm^{-1}).

In carbon material FruLi+TCA type of sulphur in the carbon network was determined with XPS in which S 2(p) spectra indicated presence of thiophenic structural (Paper IV). In the C 1(s) deconvolution spectra presence of sulphur cannot be recognized because close binding energies between different bonding types *e.g.* C-S and C-O, which is problematic in XPS studies. Besides, FruLi and FruLi+TCA indicated peak at 289.9 eV referring to the carboxylate (-COO) group. This was not detected in the XPS studies of nitrogen doped hydrochars.

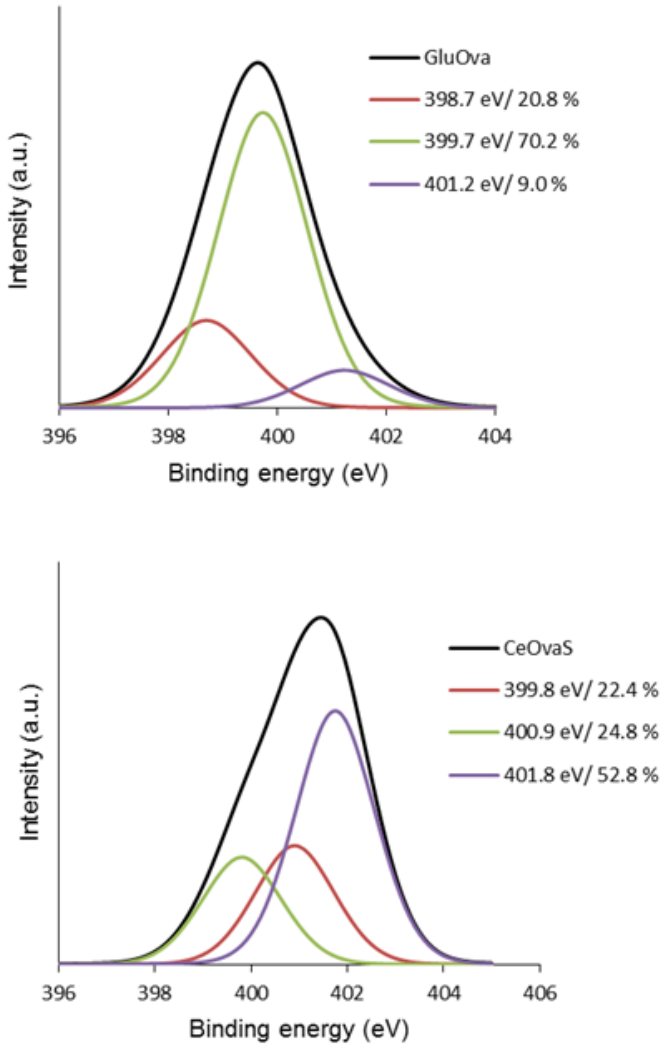

Figure 8. XPS deconvolution spectras of GluOva and CeOvaS N 1(s) photoelectron envelopes in which binding energy at 398.7 eV refers to Pyridinic-N, 399.7 eV Amines, amides/lactam, 400.9 eV pyrrolic-N, 401.2 eV hydrogen protonated amine and 401.8 eV quaternary-N (Paper III and unpublished data).

^{13}C solid-state cross polarization mafic angle spinning nuclear magnetic resonance(CP MAS NMR) analysis of hydrochars produced in this study (GluSo, CeSoS, CeOvaS, FruLi and FruLi+TCA) indicated typical structural features for hydrochars presented earlier in the literature (Papers III-V). ^{13}C ss-NMR studies of CeOvaS indicated presence

of delocalized aromatic sp^2 carbons (δ=90-160 ppm (in which δ refers to the chemical shift)), aliphatic sp^3-carbons (δ=0-60 ppm) and carbonyl structural motifs in the carbonaceous material (Figure 9.). Within the aromatic carbon region, a strong resonance is identified at ~130 ppm, indicating a high abundance of all-carbon aromatic structures, accompanied by a smaller proportion of furan-type structural motifs (~150 ppm and ~110 ppm). Carboxylate/amide structural motifs are responsible for the resonance at ~175 ppm and further on resonance at ~210 ppm is indicative for ketone/aldehyde-type of groups. Addition of sulphur in the carbon network may increase the degree of aromatization. ^{13}C ss-NMR spectra of FruLi+TCA in which thiophenic sulphur was added into the carbon network. Relative intensity of aromatic sp^2 carbon appeared to be more pronounced compared to carbon network without added sulphur (*i.e.* FruLi).

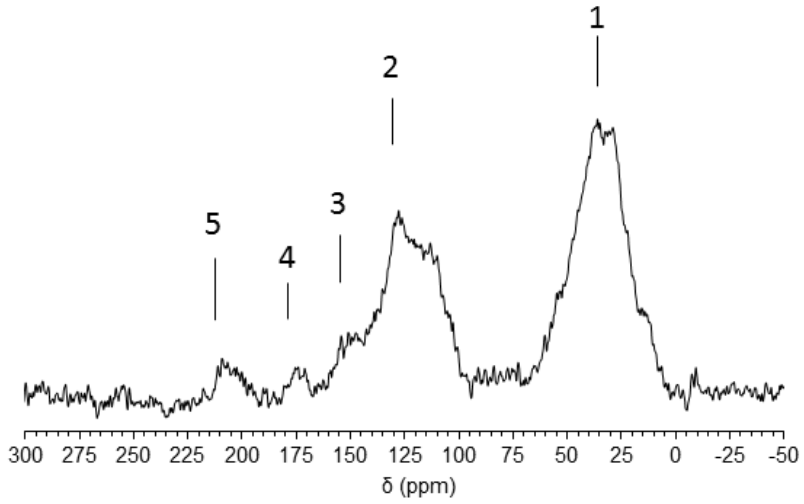

Figure 9. ^{13}C solid-state CP MAS NMR spectra of CeOvaS in which 1. Aliphatic sp^3 carbon, 2. Delocalized sp^2 carbon, 3. Furan type, 4. Carboxylic acids, 5. Ketones/Aldehydes from Paper III.

Determination of pH_{IEP} gives information about the change in the surface charge and furthermore the nature of surface functional groups. Hydrochars tend to have negative surface charge over the studied pH range indicating presence of large number of oxygen surface functional groups. This was observed in the case of FruLi and FruLi+TCA, which presented negative surface over the studied pH range (pH 1-8) (Paper IV). Nitrogen enriched hydrochar CeOvaS (Paper III) showed positively shifted surface charge at acidic

pH. This indicated existence of some basic surface functionalities in otherwise rather strongly acidic material (pH_{IEP} ~3) CeOvaS.

4.1.3 **Porosity studies**

Conventionally, plain HTC treatment results micrometer sized nonporous carbon materials. This can be overcome with different methodologies as discussed earlier. In our study introduction of secondary precursor globular protein ovalbumin was used to control formation of carbon structure (Paper III). N_2 sorption isotherms of the studied carbon material are type IV with H3 hysteresis loop, suggesting mesoporosity. However, sharp knee at the lower relative pressure of the sorption isotherm indicates the presence of microporosity in the material structure as well. The determination of pore size distribution (PSD) indicated pores over the whole mesoporous range in which high intensity peak was observed at 1-2 nm. The S_{BET} surface area of the CeOvaS was determined 38 m^2/g and estimated S_{micro} portion was determined 13.0 m^2/g. In overall, the surface area of CeOvaS is higher than that of hydrochars in general, but lower than determined for protein-controlled carbogels reported earlier. This may be due to applied drying technique which in some cases can have significant effect on the development of porosity. In our study freeze drying was applied for the studied materials and due to the crossing of the boundary layer it may have disturbed the structure of carbon network resulting lower surface areas than in the case of corresponding supercritical CO_2 dried carbon materials.

In Paper V textural properties of hydrochars GluSo and CeSoS were further modified by HT-treatment under inert atmosphere (*i.e.* N_2 gas) and *e.g.* surface area and pore volume of GluSo improved from 22 m^2/g to 449 m^2/g and from 0.14 cm^3/g to 0.25 cm^3/g respectively. Since HT-treatment increase amount of micropores CO_2 sorption studies were performed. HT-treated carbon materials (GluSo_1000 and CeSoS_1000) indicated micropores 0.3-0.9 nm in size. In general, pore sizes concentrated on the lower mesoporous range which was observed by the N_2 sorption analysis of GluSo_1000 and CeSoS_1000 as well. On the other hand development of micro- and mesoporosity can be controlled by introduction of salt mixture. Use of LiCl-$ZnCl_2$ salt mixture *in situ* was found to improve specific surface area significantly (400-550 m^2/g). Pore size distribution of FruLi focused on the lower mesoporous range (2-10 nm) whereas FruLi+TCA indicated pores at wider range 2-60 nm. Presence of microporosity was pronounced in the N_2 sorption isotherms of salt templated hydrochars which can be seen as a knee at low relative pressure (p/p_0) (Figure 10.). Further CO_2 analysis revealed micropores 0.3-1.0 nm in size and estimated surface area S_{micro} was 415-441 cm^3/g.

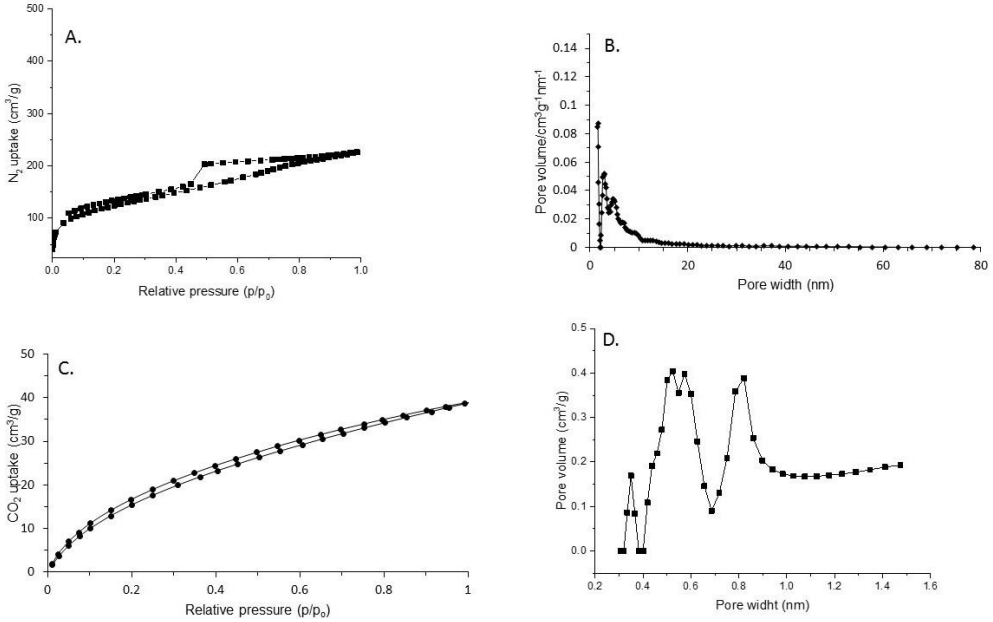

Figure 10. Salt templated hydrochar FruLi A. N_2 sorption isotherm, B. pore size distribution (PSD), C. CO_2 sorption isotherm and D. PSD distribution determined from the CO_2 sorption data (Paper IV).

4.1.4 Crystallinity analysis of HT-treated Pt impregnated carbon

X-ray diffraction (XRD) is a very useful tool for the study of atomic and molecular structure of crystalline materials. XRD studies were applied for calcined and platinum (Pt) impregnated carbon materials (GluSo_1000_Pt and CeSoS_1000_Pt) in which crystalline state of Pt was particularly under the interest (Paper V). Pt impregnated carbon materials indicated diffraction peak at 22.0˚referring to the (002) plane of the graphite. Diffraction peaks at 40.0˚, 46.6˚ and 68.0˚are associated with (111), (200) and (220) planes of the face-centered-cubic (fcc) structure of Pt (Figure 11.). This suggested that Pt on the carbon surface is on the crystalline state.

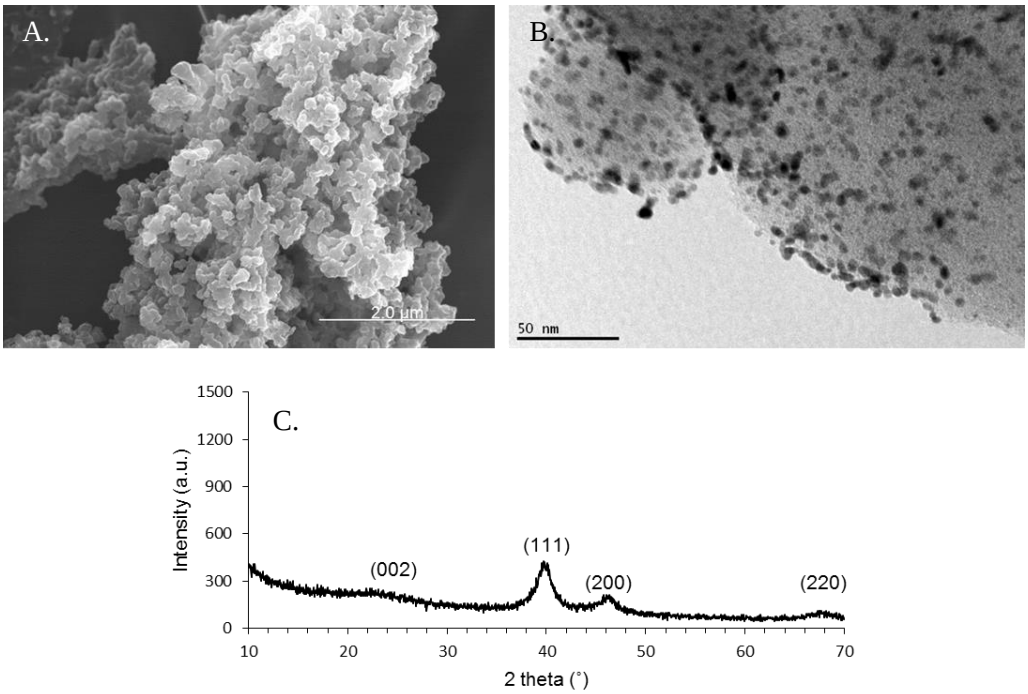

Figure 11. Morphological, structural and crystal analysis of platinum impregnated GluSo_1000_Pt carbon material A. SEM image 20 k magnification, B. TEM image 80 k magnification revealing well dispersed platinum nanoparticles on the carbon material and C. XRD pattern indicating crystalline structure of Pt on GluSo_1000 carbon material (Paper V).

4.2 Adsorption of metals and dyes

4.2.1 Effect of pH, ionic strength and temperature

In addition of the adsorbent-adsorbate properties, several other factors related to the adsorption conditions such as solution pH, ionic strength, contact time or temperature have effect on the adsorption performance of the adsorbent. In several studies solution pH has been found as crucial parameter whereas significance of other parameters has been minor. In our studies pH showed moderate or minor effect on the adsorption efficiency (Figure 12. and Figure 13.). Adsorption behaviour related to solution pH gives an indication about adsorption mechanism. Strongly pH dependent adsorption performance is assumed to indicate electrostatic interactions as an adsorption mechanism whereas pH independent adsorption refers to the non-electrostatic interactions. In our studies adsorption dependency of pH was under major interest. Adsorbents such as sludge based (ADS and INS materials) adsorbents were found to be pH dependent to some extent in which adsorption efficiency indicated to increase along with solution pH whereas increased ionic strength seemed to hinder adsorption capacity of the adsorbent. Adsorption efficiency of CeOvaS towards Pb(II) and Cr(VI) remain rather constant over the studied pH range.

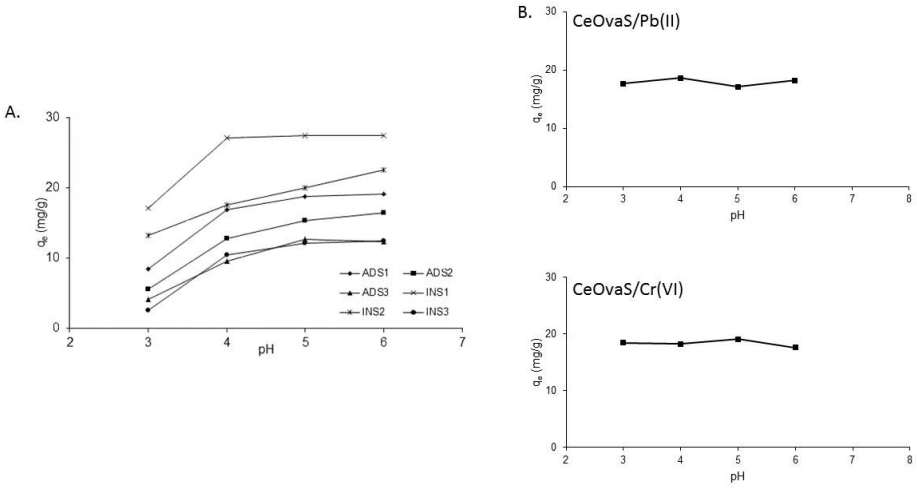

Figure 12. Effect of solution pH to the adsorption performance of A. ADS and INS based adsorbents for Pb(II) removal (Paper II) and B. CeOvaS for Pb(II) and Cr(VI) removal (Paper III).

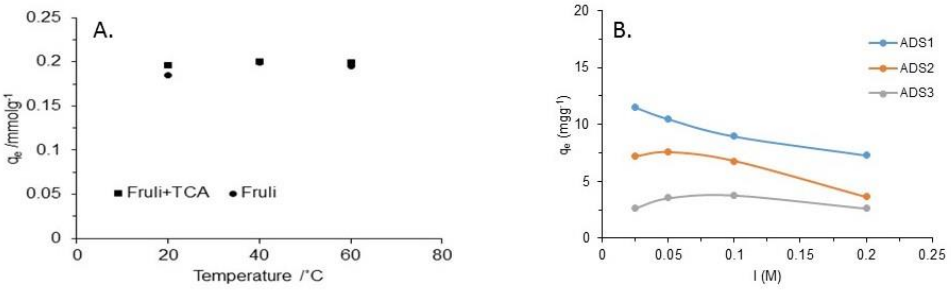

Figure 13. A. Effect of temperature on the removal of methylene blue by FruLi and FruLi+TCA (Paper IV) and B. effect of ionic strength for the removal of Pb(II) by sludge based adsorbents (ADS_1, ADS_2 and ADS_3) (unpublished data).

4.2.2 **Multicomponent solutions**

Conventionally single solutions are utilized in the study of adsorption capacity of target contaminant. However, this is rarely the situation in the real cases. Study of competing contaminants for the adsorption capacity can be implemented several ways in order to simulate real systems if not using real one. In the study of the adsorption behaviour of Pb(II) and Cr(VI) by CeOvaS the effect of the co-existing ion on the adsorption performance was examined. As(V) and Cu(II) were selected as competing ions in order to examine adsorption efficiency of Cr(VI) and Pb(II) respectively (Paper III). The presence of other species with a similar charge showed a minor to moderate interfering effect on the targeted metal adsorption, causing lower maximum adsorption capacities for aimed metals compared to one-component systems. A somewhat different approach was used in the adsorption studies of methylene blue. In addition to single solution experiments, adsorption performance of methylene blue from synthetic sewage was studied. Methylene blue adsorption efficiency by both adsorbents FruLi and FruLi+TCA indicated to enhance from the synthetic sewage.

4.2.3 **Regenerability**

Regeneration studies were conducted for the FruLi and Fruli+TCA which were used to adsorb methylene blue. Chemical extraction with ethanol was chosen for the removal of Methylene blue (Paper IV). Ethanol was found as efficient in desorption of methylene

blue. FruLi was found to maintain its adsorption capacity well over 99 % through all three adsorption/desorption cycles, whereas the adsorption efficiency of FruLi+TCA decreased after regeneration and was found to be 90 % after the third cycle (Figure 14.). Methylene blue could be recovered from the ethanol solution.

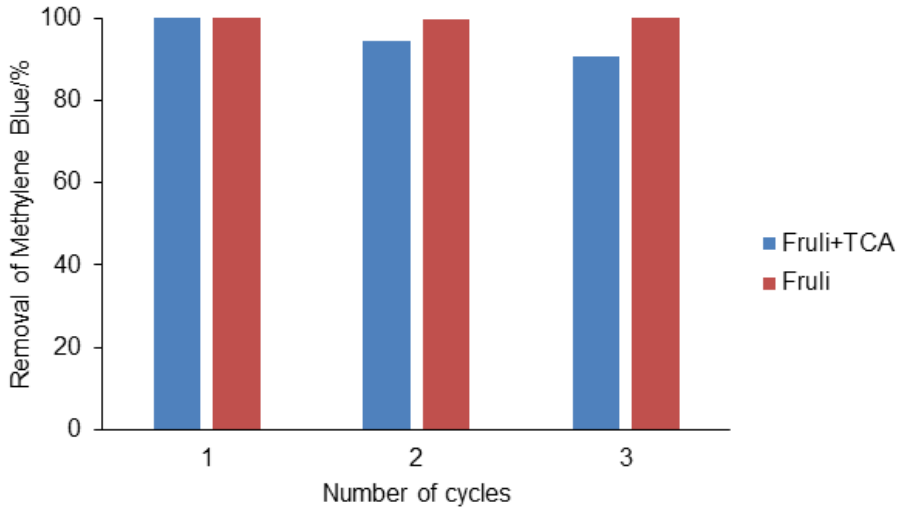

Figure 14. Desorption of methylene blue by chemical extraction with ethanol (Paper IV).

4.2.4 Adsorption kinetics and modelling

Optimum time to reach the adsorption equilibrium was examined in the case of all studied adsorbents (Papers II-IV). From the practical point of view shortly reached adsorption equilibrium is favoured. This depends on the textural properties of the adsorbent. Among the studied adsorbents equilibrium was reached within 60-150 min. Removal of Pb(II) removal by CeOvaS was extremely fast in which equilibrium was reached in few minutes (Paper III). In addition to fast adsorption equilibrium ability for complete adsorbate removal is advantageous adsorbent feature. INS_1 appeared to remove 99.9 % of Pb(II) from the solution phase (Paper II) whereas both FruLi and FruLi+TCA indicated to remove 99.9 % of Methylene Blue (Paper IV). Removal efficiency of CeOvaS was weaker with approximately 70% removal efficiency in the studied pollutant concentration (Pb(II) and Cr(VI)).

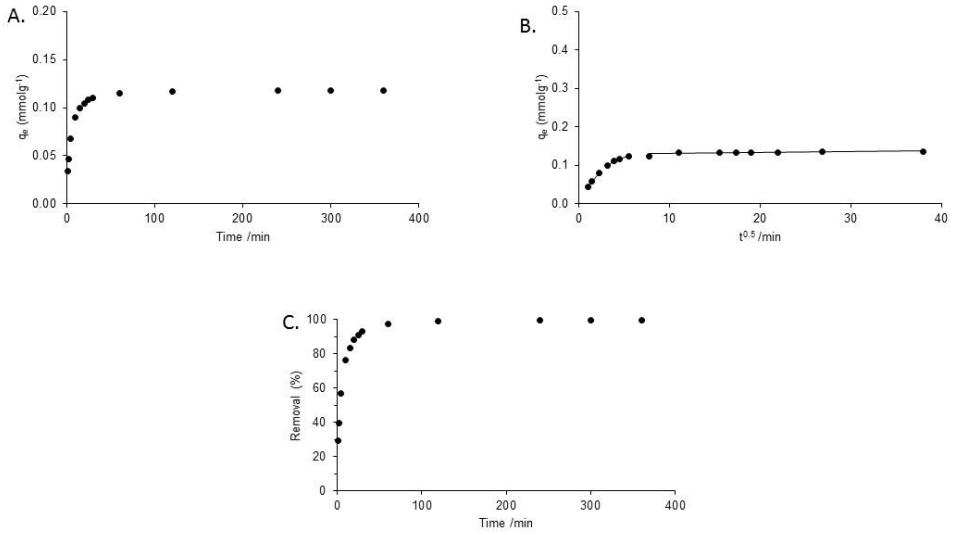

Figure 15. Adsorption of Methylene Blue by FruLi A. Experimental kinetic data, B. Intraparticle diffusion model and C. Maximum adsorption removal (Paper IV and unpublished data).

There are different kinetic models available which can be applied to explain speed of adsorption. In the study of adsorption kinetics non-linear regressions of pseudo-second-order and intraparticle diffusion models were used. In the Papers I and II both PS1 and PS2 model were applied to study role of the ion exchange in the rate of adsorption. PS2 model indicated to give better fitting over the PS1 model suggesting that chemical reaction (*i.e.* ion-exchange) is a rate determining step in the adsorption kinetics. In addition to chemical reaction mass transfer may be responsible for the speed of adsorption. This was examined by performing intraparticle diffusion model. Detailed results can be found from the Papers I-IV. Materials with higher micro- and mesoporosity *e.g.* FruLi indicated multilinearity, when plotting $t^{0.5}$ against q_t. This suggested that more than one process would be responsible for the control of the adsorption kinetics (Paper IV). There has been some discussion that results received from the kinetic models may strongly depend on the experimental setup and may describe only phenomenon at those specific conditions and therefore caution should be taken in the evaluation of results.

4.2.5 Adsorption equilibrium studies, modelling of adsorption isotherms

Adsorption equilibrium studies were performed by changing pollutant concentrations and keeping other parameters constant. In this way maximum adsorption capacity ($q_{e,max}$) for the tested adsorbent could be determined. Experimentally determined maximum adsorption capacities for the studied adsorbents are presented in the Table 5. Furthermore, to understand adsorption mechanism adsorption modelling can be applied. In the Papers I-IV following adsorption isotherms were applied: Langmuir, Freundlich, Sips and Extended Sips model.

Table 5. Experimentally determined maximum adsorption capacities ($q_{e,max}$) of studied pollutants and applied adsorption isotherms in the modelling.

Adsorbent	Pollutant	$q_{e,max}$ (mgg^{-1})	Applied isotherms
ADS	Pb(II)	11	Langmuir, Freundlich and Sips
INS	Pb(II)	11	Langmuir, Freundlich and Sips
INS_1	Pb(II)	40	Langmuir, Freundlich and Sips
INS_2	Pb(II)	22	Langmuir, Freundlich and Sips
INS_3	Pb(II)	15	Langmuir, Freundlich and Sips
ADS_1	Pb(II)	27	Langmuir, Freundlich and Sips
ADS_2	Pb(II)	15	Langmuir, Freundlich and Sips
ADS_3	Pb(II)	12	Langmuir, Freundlich and Sips
CeOvaS	Pb(II)	240	Sips, Extended Sips
CeOvaS	Cr(VI)	68	Sips, Extended Sips
FruLi	Methylene Blue	83	Sips
FruLi+TCA	Methylene Blue	57	Sips
Norit Hydrocarbo[a]	Pb(II)	200[b]	-

[a] Commercial activated carbon and [b] unpublished data

Fittings of the modelled adsorption isotherms were examined by comparing predicted q_e values with experimentally received data as well as magnitudes of error functions. In Papers I and II several adsorption isotherms were applied. Freundlich adsorption isotherm was observed to give the poorest fit in the all cases (Figure 16.). Clear deviation between Langmuir and Sips adsorption isotherm was in some cases rather difficult to observe as can be seen from the results presented in the Table 6. However, by comparing the obtained data and properties of adsorbent Sips adsorption isotherm appeared to give better fit. Use of Langmuir adsorption isotherm is not often suitable to describe the experimental data in aqueous solutions. This may be due to the fact that all theoretical assumptions related to this theory are not often fulfilled, in particular monolayer coverage of the adsorbent surface and energetic homogeneity of the adsorption sites. On the other hand, Langmuir

isotherm equation was also found to be applicable in the cases where the underlying assumptions were obviously not fulfilled. Generally, it should be noticed that the fitting of adsorption isotherm is also related to the amount and quality of experimental point measured and suitability of the particular model should be finally evaluated by throughout comparison of the theoretical background of the model and the adsorbent characteristics.

Table 6. Fitting results of different adsorption isotherms calculated from ADS and INS based adsorbents adsorption equilibrium studies towards Pb(II).

	Langmuir			Freundlich			Sips			
Adsorbent	q_m (mg/g)	K_L (l/mg)	R^2	K_F (l/mg)	n_F	R^2	q_m (mg/g)	n_s	K_S (l/mg)	R^2
INS_1	38.9	2.16	0.982	17.8	6.58	0.922	39.4	0.77	1.77	0.985
INS_2	20.9	2.06	0.930	10.8	7.92	0.956	21.2	0.84	1.79	0.933
INS_3	14	0.49	0.806	6.6	7.04	0.782	15.5	0.49	0.44	0.838
ADS_1	26.4	0.76	0.928	11.7	6.62	0.936	28.4	0.53	0.61	0.965
ADS_2	14.6	0.45	0.839	7.1	7.38	0.777	15.5	0.58	0.51	0.857
ADS_3	11.9	0.56	0.844	5.8	7.31	0.892	14.9	0.35	0.26	0.928

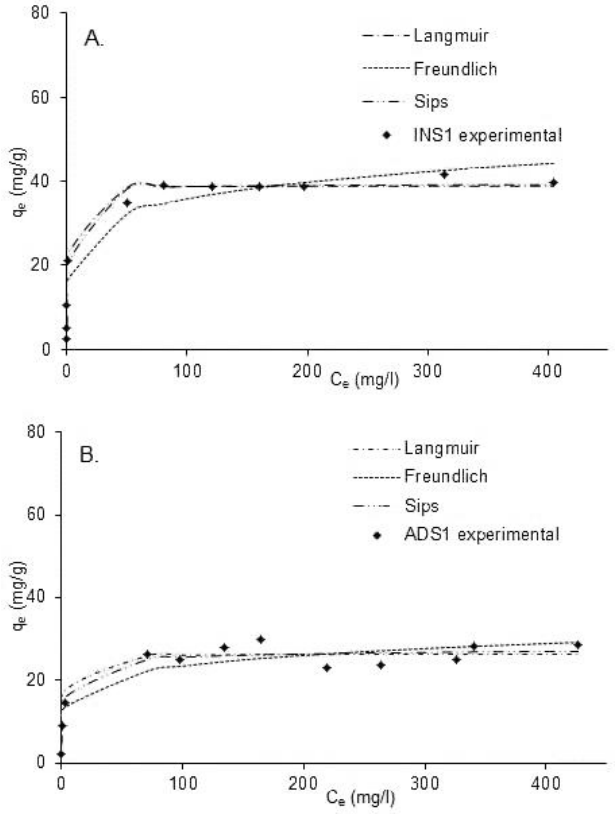

Figure 16. Adsorption equilibrium data of INS_1 and ADS_1 and fitting results of modelled adsorption isotherms from the Paper II.

In the study of Pb(II) and Cr(VI) by CeOvaS, the effect of the competing ion was examined (Paper III) and extended Sips adsorption isotherm was applied. Model was noticed to result reasonable fit. However, model tended to overestimate the maximum adsorption capacities unlike modelling of Sips adsorption isotherm for one-component solution which gave very good correlation.

4.3 Electrocatalytic activity

Hydrothermally produced carbon materials especially after further improvement of electrical conductivity by HT-treatment may act as a metal free electrocatalyst or potential electrocatalyst support. Applicability can be enhanced by doping with nitrogen functionalities into carbon network. Electrocatalytical activity for oxygen reduction reaction (ORR) was tested in alkaline solution (0.1 M KOH) in which peak reduction potential at - 0.3 V vs. Ag/AgCl was observed (Paper V) (Figure 17.). Electron transfer number of GluSo_1000 was observed 3.3-3.7 with 10-30 % peroxide formation and CeOvaS 3-3.2 with 35-50 % peroxide formation. For the corresponding Pt impregnated samples electron transfer number was determined 3.8-4.0 with peroxide formation lower than 10 % indicating four electron process as a favoured reaction mechanism.

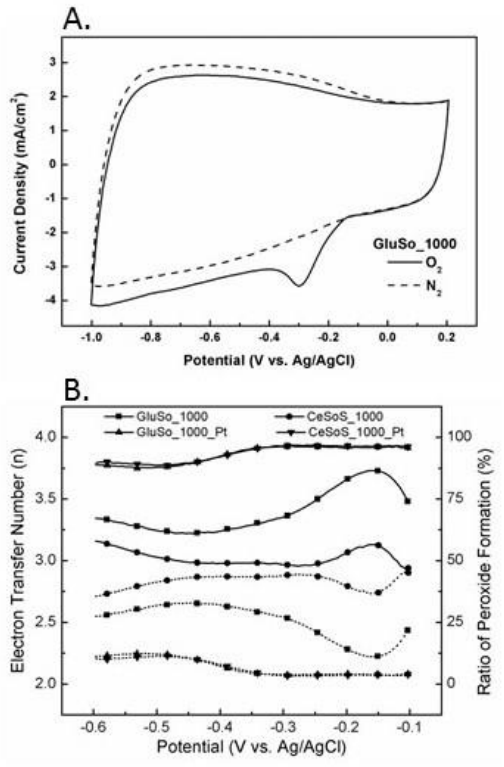

Figure 17. A. Cyclic voltammetry of GluSo_1000 in O_2 saturated (solid line) and N_2-saturated (dashed line) 0.1 M KOH with scan rate 100 mV/s. B. Electron transfer number (solid line) and ratio of peroxide(HO_2^-) formation (dashed line) from Paper V.

5 Conclusion and Further research

In this study hydrochars from different starting materials and synthesis techniques were studied. Successful conversion of more complex structures like cellulose and rye straw into hydrochars widens the range of available starting materials. It was found that besides rich oxygen functionalities in the hydrochars other functional groups *i.e.* N-doped and S-doped can be easily added. These heteroatoms changes the properties of hydrochars opening doors for new applications. Addition of alternative heteroatoms was reached by introduction of secondary precursor ovalbumin, soy bean flour and thiophenecarboxaldehyde (TCA).

The clear benefit in the use of HTC technique is the simple one-pot approach through which advanced materials properties can be reached *in situ* at relatively mild operation conditions *e.g.* temperature. However, one should notice that well developed porosity cannot be reached *via* HTC as such. Additional actions such as the use of templates and catalysts has to be performed however still allowing one-step approach. With specific choice of technique and compounds, detailed features *i.e.* designed porosity, functionality and morphology for certain applications can be reached. However, there is a danger that these additional actions decrease the idea of sustainable and environmentally friendly technique which is often emphasized when referring to benefits of HTC. This may be avoided if reuse/recycling of chemicals can be performed. Hydrochars have shown a great flexibility allowing modification of surface functionality and porosity *via* additional steps without disrupting effect on the morphology like was observed in the post-carbonization of nitrogen enriched carbon materials (GluSo and CeSoS). Introduction of salt mixture in the reaction mixture during HTC of fructose showed that high surface area of 550 m^2/g and pore volume of 1.2 cm^3/g can be reached even *via* one-pot approach.

Certainly, more research is needed to reach deeper understanding related to reaction mechanism which further would allow production of better controlled and designed carbon materials for the specific applications. HTC process is very complex due to the several simultaneous reactions taking place. Research to understand importance and dependence of these aspects on each other has been performed by using simple monosaccharide glucose. Little by little more complex biomasses are used and knowledge about their behaviour in the HTC process widens. However, their full potential cannot be utilized without complete basic understanding of the reaction mechanism with the simplest materials available. This is important because it effects on the design of the desired target materials. In several applications surface functionality and porosity are in a key role. In the control of materials porosity it would be important to develop materials with well-designed porosity with ideal distribution of macro-, meso- and micropores. In the study of surface functionalities it would be important to control the formation of certain functionalities by minimum amount of reaction steps. Contribution of acidity/basicity of certain functional groups such as nitrogen functionalities on the carbon network is missing or the acidic/basic nature of these materials is under debate. Besides most studied oxygen functionalities more research is needed in the study of other heteroatoms (*e.g.* N, S, P or B).

In the water treatment hydrochars showed remarkable potential for the metal and dye removal from the liquid phases in which complete removal from relatively low pollutant concentrations was achieved. CeOvaS indicated large metal ion removal ability against Pb(II) (q_e ~240 mg/g) and Cr(VI) (q_e ~68 mg/g) despite of relatively low porosity compared to general activated carbons. However, deeper investigation about the adsorbent-adsorbate interactions is needed. This is crucial for the design and synthesis of more efficient materials for the water treatment applications especially emphasizing the role of the acidic/basic surface functional groups. There is a good agreement about the significance of surface functional groups but research related to the importance of their acid/basic distribution is lacking. Reuse of adsorbent is beneficial from the green chemistry point of view. FruLi and FruLi+TCA were found reusable after simple washing with ethanol maintaining their adsorption capacity over 90 % after three cycles. Also upscaling studies in the HTC synthesis as well as applications are needed. Most of the hydrochars has been produced in the small reactor with few grams yield. Along the upscaling studies production cost for the high-value carbon materials should be estimated. Besides application studies in the laboratory conditions are small scale studies. Depending on the experimental set up of HTC higher amounts of process water may be produced after synthesis. Investigation related to the chemical content as well as discard of this water is needed. Further steps in water treatment studies would be real effluents and extension to pilot scale experiments.

In addition to potential application in the water purification, versatility of hydrochars was confirmed in the study of potential as electrocatalyst in ORR and electrocatalyst support. It was observed that N-doped HTC-derived carbon materials indicated good electrocatalytic activity for oxygen reduction reaction and potentiality as electrocatalyst support as was showed in the successful Pt-impregnation.

In this study we have investigated applicability of HTC in the production of porous carbon materials in the applications like water treatment and energy storage. It was found that designed carbon materials with well-developed porosity and variable heteroatom content can be reached simply by utilization of HTC. These carbon materials showed potential as adsorbents for the removal of both inorganic and organic pollutants as well as electrocatalyst in ORR and electrocatalyst support.

References

1. Tascon, J. M. D. Novel carbon adsorbents. **2012**.
2. Lee, J.; Kim, J.; Hyeon, T. Recent Progress in the Synthesis of Porous Carbon Materials. *Advanced Materials* **2006,** *18* (16), 2073-2094.
3. Wu, T. X.; Wang, G. Z.; Zhang, X.; Chen, C.; Zhang, Y. X.; Zhao, H. J. Transforming chitosan into N-doped graphitic carbon electrocatalysts. *Chemical Communications* **2015,** *51* (7), 1334-1337.
4. Sircar, S.; Golden, T. C.; Rao, M. B. Activated carbon for gas separation and storage. *Carbon* **1996,** *34* (1), 1-12.
5. Sun, X.; Liu, Z.; Welsher, K.; Robinson, J. T.; Goodwin, A.; Zaric, S.; Dai, H. Nano-graphene oxide for cellular imaging and drug delivery. *Nano research* **2008,** *1* (3), 203-212.
6. Wang, X.; Li, W.; Chen, Z.; Waje, M.; Yan, Y. Durability investigation of carbon nanotube as catalyst support for proton exchange membrane fuel cell. *Journal of Power Sources* **2006,** *158* (1), 154-159.
7. Rivera-Utrilla, J.; Sánchez-Polo, M.; Gómez-Serrano, V.; Alvarez, P.; Alvim-Ferraz, M.; Dias, J. Activated carbon modifications to enhance its water treatment applications. An overview. *Journal of Hazardous Materials* **2011,** *187* (1), 1-23.
8. Tascon, J. M. D. *Novel carbon adsorbents* 2012.
9. Eftekhari, A.; Jafarkhani, P.; Moztarzadeh, F. High-yield synthesis of carbon nanotubes using a water-soluble catalyst support in catalytic chemical vapor deposition. *Carbon* **2006,** *44* (7), 1343-1345.
10. Thess, A.; Lee, R.; Nikolaev, P.; Dai, H.; Petit, P.; Robert, J.; Xu, C.; Lee, Y. H.; Kim, S. G.; Rinzler, A. G. Crystalline ropes of metallic carbon nanotubes. *Science-AAAS-Weekly Paper Edition* **1996,** *273* (5274), 483-487.
11. Lua, A. C.; Yang, T. Effect of activation temperature on the textural and chemical properties of potassium hydroxide activated carbon prepared from pistachio-nut shell. *Journal of Colloid and Interface Science* **2004,** *274* (2), 594-601.
12. Satishkumar, B. C.; Govindaraj, A.; Rao, C. N. R. Bundles of aligned carbon nanotubes obtained by the pyrolysis of ferrocene–hydrocarbon mixtures: role of the metal nanoparticles produced in situ. *Chemical Physics Letters* **1999,** *307* (3–4), 158-162.

13. Szabó, A.; Perri, C.; Csató, A.; Giordano, G.; Vuono, D.; Nagy, J. B. Synthesis methods of carbon nanotubes and related materials. *Materials* **2010,** *3* (5), 3092-3140.
14. Falco, C.; Sieben, J. M.; Brun, N.; Sevilla, M.; Van der Mauelen, T.; Morallón, E.; Cazorla-Amorós, D.; Titirici, M. M. Hydrothermal Carbons from Hemicellulose-Derived Aqueous Hydrolysis Products as Electrode Materials for Supercapacitors. *ChemSusChem* **2013,** *6* (2), 374-382.
15. Hu, B.; Wang, K.; Wu, L.; Yu, S.-H.; Antonietti, M.; Titirici, M.-M. Engineering Carbon Materials from the Hydrothermal Carbonization Process of Biomass. *Advanced Materials* **2010,** *22* (7), 813-828.
16. Titirici, M.-M.; White, R. J.; Falco, C.; Sevilla, M. Black perspectives for a green future: hydrothermal carbons for environment protection and energy storage. *Energy & Environmental Science* **2012,** *5* (5), 6796-6822.
17. Steinbeiss, S.; Gleixner, G.; Antonietti, M. Effect of biochar amendment on soil carbon balance and soil microbial activity. *Soil Biology and Biochemistry* **2009,** *41* (6), 1301-1310.
18. Titirici, M.-M. *Sustainable Carbon Materials from Hydrothermal Processes*; Wiley2013.
19. Bansal, R. C.; Goyal, M. *Activated carbon adsorption*; CRC press2005.
20. Carabineiro, S. A.; Pereira, M. F.; Órfão, J. J.; Figueiredo, J. L. SURFACE CHEMISTRY OF ACTIVATED CARBONS. *Chemical Physics Research Journal* **2011,** *4* (3/4), 291.
21. Yang, R. T. Adsorbents: fundamentals and applications. *John Wiley & Sons Inc* **2003**.
22. Mohamed, A. R.; Mohammadi, M.; Darzi, G. N. Preparation of carbon molecular sieve from lignocellulosic biomass: A review. *Renewable and Sustainable Energy Reviews* **2010,** *14* (6), 1591-1599.
23. Maciá-Agulló, J. A.; Moore, B. C.; Cazorla-Amorós, D.; Linares-Solano, A. Activation of coal tar pitch carbon fibres: Physical activation vs. chemical activation. *Carbon* **2004,** *42* (7), 1367-1370.
24. Worch, E. *Adsorption technology in water treatment: fundamentals, processes, and modeling*; Walter de Gruyter2012.
25. Inagaki, M. Pores in carbon materials-importance of their control. *New Carbon Materials* **2009,** *24* (3), 193-232.

26. Barton, T. J.; Bull, L. M.; Klemperer, W. G.; Loy, D. A.; McEnaney, B.; Misono, M.; Monson, P. A.; Pez, G.; Scherer, G. W.; Vartuli, J. C.; Yaghi, O. M. Tailored Porous Materials. *Chemistry of Materials* **1999,** *11* (10), 2633-2656.

27. Chen, Y.; Zhu, Y.; Wang, Z.; Li, Y.; Wang, L.; Ding, L.; Gao, X.; Ma, Y.; Guo, Y. Application studies of activated carbon derived from rice husks produced by chemical-thermal process—A review. *Advances in Colloid and Interface Science* **2011,** *163* (1), 39-52.

28. Titirici, M.-M.; White, R. J.; Brun, N.; Budarin, V. L.; Su, D. S.; del Monte, F.; Clark, J. H.; MacLachlan, M. J. Sustainable carbon materials. *Chemical Society Reviews* **2015,** *44* (1), 250-290.

29. Wang, Q.; Li, H.; Chen, L.; Huang, X. Monodispersed hard carbon spherules with uniform nanopores. *Carbon* **2001,** *39* (14), 2211-2214.

30. Sun, X.; Li, Y. Colloidal Carbon Spheres and Their Core/Shell Structures with Noble-Metal Nanoparticles. *Angewandte Chemie International Edition* **2004,** *43* (5), 597-601.

31. Kubo, S.; Demir-Cakan, R.; Zhao, L.; White, R. J.; Titirici, M. M. Porous Carbohydrate-Based Materials via Hard Templating. *ChemSusChem* **2010,** *3* (2), 188-194.

32. Berge, N. D.; Li, L.; Flora, J. R. V.; Ro, K. S. Assessing the environmental impact of energy production from hydrochar generated via hydrothermal carbonization of food wastes. *Waste Management* **2015,** *43*, 203-217.

33. Falco, C.; Titirici, M.-M.; Antonietti, M. HYDROTHERMAL CARBONISATION OF AGRICULTURAL WASTES. *6th Tnt Con f on Renew Resour & Biorefineries, Dusseldorf, Germany* **2010**, 300-301.

34. Roman, S.; Nabais, J. V.; Ledesma, B.; González, J.; Laginhas, C.; Titirici, M. Production of low-cost adsorbents with tunable surface chemistry by conjunction of hydrothermal carbonization and activation processes. *Microporous and Mesoporous Materials* **2013,** *165*, 127-133.

35. Falco, C.; Marco-Lozar, J. P.; Salinas-Torres, D.; Morallón, E.; Cazorla-Amorós, D.; Titirici, M.-M.; Lozano-Castelló, D. Tailoring the porosity of chemically activated hydrothermal carbons: influence of the precursor and hydrothermal carbonization temperature. *Carbon* **2013,** *62*, 346-355.

36. M. M. Titirici, M. A., N. Baccile. Hydrothermal carbon from biomass: Comparison of the local structure from the poly- to monosaccharide and pentoses/hexoses. *Green Chemistry* **2008,** (10).

37. Sevilla, M.; Maciá-Agulló, J. A.; Fuertes, A. B. Hydrothermal carbonization of biomass as a route for the sequestration of CO2: Chemical and structural properties of the carbonized products. *Biomass and Bioenergy* **2011,** *35* (7), 3152-3159.

38. Basso, D.; Castello, D.; Baratieri, M.; Fiori, L. In *Hydrothermal carbonization of waste biomass: Progress report and prospects*, Proceedings of the 21th European Biomass Conference and Exhibition, Copenhagen, 2013, pp 3-7.

39. Yu, Y.; Lou, X.; Wu, H. Some Recent Advances in Hydrolysis of Biomass in Hot-Compressed Water and Its Comparisons with Other Hydrolysis Methods†. *Energy & Fuels* **2008,** *22* (1), 46-60.

40. Kruse, A.; Funke, A.; Titirici, M.-M. Hydrothermal conversion of biomass to fuels and energetic materials. *Current opinion in chemical biology* **2013,** *17* (3), 515-521.

41. Patil, P. T.; Armbruster, U.; Martin, A. Hydrothermal liquefaction of wheat straw in hot compressed water and subcritical water–alcohol mixtures. *The Journal of Supercritical Fluids* **2014,** *93*, 121-129.

42. Falco, C.; Baccile, N.; Titirici, M.-M. Morphological and structural differences between glucose, cellulose and lignocellulosic biomass derived hydrothermal carbons. *Green Chemistry* **2011,** *13* (11), 3273-3281.

43. Patil, S. K. R.; Heltzel, J.; Lund, C. R. F. Comparison of Structural Features of Humins Formed Catalytically from Glucose, Fructose, and 5-Hydroxymethylfurfuraldehyde. *Energy & Fuels* **2012,** *26* (8), 5281-5293.

44. Sevilla, M.; Fuertes, A. B. Chemical and structural properties of carbonaceous products obtained by hydrothermal carbonization of saccharides. *Chemistry-A European Journal* **2009,** *15* (16), 4195-4203.

45. Chheda, J. N.; Roman-Leshkov, Y.; Dumesic, J. A. Production of 5-hydroxymethylfurfural and furfural by dehydration of biomass-derived mono- and poly-saccharides. *Green Chemistry* **2007,** *9* (4), 342-350.

46. Zhao, L.; Baccile, N.; Gross, S.; Zhang, Y.; Wei, W.; Sun, Y.; Antonietti, M.; Titirici, M.-M. Sustainable nitrogen-doped carbonaceous materials from biomass derivatives. *Carbon* **2010,** *48* (13), 3778-3787.

47. Marteel-Parrish, A. E.; Abraham, M. A. *Green chemistry and engineering: A pathway to sustainability*; John Wiley & Sons2013.

48. Bobleter, O. Hydrothermal degradation of polymers derived from plants. *Progress in polymer science* **1994,** *19* (5), 797-841.

49. White, R. J.; Budarin, V.; Luque, R.; Clark, J. H.; Macquarrie, D. J. Tuneable porous carbonaceous materials from renewable resources. *Chemical Society Reviews* **2009,** *38* (12), 3401-3418.

50. Kuster, B. 5-Hydroxymethylfurfural (HMF). A review focussing on its manufacture. *Starch-Stärke* **1990,** *42* (8), 314-321.

51. Onda, A.; Ochi, T.; Yanagisawa, K. Selective hydrolysis of cellulose into glucose over solid acid catalysts. *Green Chemistry* **2008,** *10* (10), 1033-1037.

52. White, R. J. *Porous Carbon Materials from Sustainable Precursors*; Royal Society of Chemistry2015.

53. Liu, F.; Guo, M. Comparison of the characteristics of hydrothermal carbons derived from holocellulose and crude biomass. *J Mater Sci* **2015,** *50* (4), 1624-1631.

54. Reza, M. T.; Rottler, E.; Herklotz, L.; Wirth, B. Hydrothermal carbonization (HTC) of wheat straw: Influence of feedwater pH prepared by acetic acid and potassium hydroxide. *Bioresource technology* **2015,** *182*, 336-344.

55. Flora, J. F.; Lu, X.; Li, L.; Flora, J. R.; Berge, N. D. The effects of alkalinity and acidity of process water and hydrochar washing on the adsorption of atrazine on hydrothermally produced hydrochar. *Chemosphere* **2013,** *93* (9), 1989-1996.

56. Falco, C.; Sevilla, M.; White, R. J.; Rothe, R.; Titirici, M. M. Renewable Nitrogen-Doped Hydrothermal Carbons Derived from Microalgae. *ChemSusChem* **2012,** *5* (9), 1834-1840.

57. Zhao, L.; Fan, L. Z.; Zhou, M. Q.; Guan, H.; Qiao, S.; Antonietti, M.; Titirici, M. M. Nitrogen-Containing Hydrothermal Carbons with Superior Performance in Supercapacitors. *Advanced Materials* **2010,** *22* (45), 5202-5206.

58. Berge, N. D.; Ro, K. S.; Mao, J.; Flora, J. R.; Chappell, M. A.; Bae, S. Hydrothermal carbonization of municipal waste streams. *Environmental science & technology* **2011,** *45* (13), 5696-5703.

59. Oliveira, I.; Blöhse, D.; Ramke, H.-G. Hydrothermal carbonization of agricultural residues. *Bioresource technology* **2013,** *142*, 138-146.

60. Hao, W.; Björkman, E.; Lilliestråle, M.; Hedin, N. Activated carbons prepared from hydrothermally carbonized waste biomass used as adsorbents for CO 2. *Applied Energy* **2013,** *112*, 526-532.

61. Thomas, A.; Goettmann, F.; Antonietti, M. Hard templates for soft materials: Creating nanostructured organic materials†. *Chemistry of Materials* **2008,** *20* (3), 738-755.
62. Salinas-Torres, D.; Lozano-Castello, D.; Titirici, M. M.; Zhao, L.; Yu, L.; Morallon, E.; Cazorla-Amoros, D. Electrochemical behaviour of activated carbons obtained via hydrothermal carbonization. *Journal of Materials Chemistry A* **2015,** *3* (30), 15558-15567.
63. Sevilla, M.; Fuertes, A. B. Sustainable porous carbons with a superior performance for CO2 capture. *Energy & Environmental Science* **2011,** *4* (5), 1765-1771.
64. Romero-Anaya, A. J.; Ouzzine, M.; Lillo-Ródenas, M.; Linares-Solano, A. Spherical carbons: Synthesis, characterization and activation processes. *Carbon* **2014,** *68*, 296-307.
65. Maria-Magdalena Titirici, A. T. a. M. A. Aminated hydrophilic ordered mesoporous carbons. *Journals of Materials Chemistry* **2007,** *17*, 3412-3418.
66. White, R. J.; Tauer, K.; Antonietti, M.; Titirici, M.-M. Functional hollow carbon nanospheres by latex templating. *Journal of the American Chemical Society* **2010,** *132* (49), 17360-17363.
67. Urakami, H.; Yilmaz, A. G.; Osiceanu, P.; Yagci, Y.; Vilela, F.; Titirici, M. M. Facile Polymer Functionalization of Hydrothermal-Carbonization-Derived Carbons. *Macromolecular rapid communications* **2013,** *34* (13), 1080-1084.
68. Urakami, H.; Antonietti, M.; Vilela, F. Facile functionalization of HTC-derived carbon microspheres. *Chemical Communications* **2012,** *48* (89), 10984-10986.
69. Maciá-Agulló, J. A.; Sevilla, M.; Diez, M. A.; Fuertes, A. B. Synthesis of Carbon-based Solid Acid Microspheres and Their Application to the Production of Biodiesel. *ChemSusChem* **2010,** *3* (12), 1352-1354.
70. Pileidis, F. D.; Tabassum, M.; Coutts, S.; Ttitirici, M.-M. Esterification of levulinic acid into ethyl levulinate catalysed by sulfonated hydrothermal carbons. *Chinese Journal of Catalysis* **2014,** *35* (6), 929-936.
71. Yang, H.; Zhao, D. Synthesis of replica mesostructures by the nanocasting strategy. *Journal of Materials Chemistry* **2005,** *15* (12), 1217-1231.
72. Polarz, S.; Antonietti, M. Porous materials via nanocasting procedures: innovative materials and learning about soft-matter organization. *Chemical Communications* **2002,** (22), 2593-2604.

73. Titirici, M. M.; Thomas, A.; Antonietti, M. Replication and Coating of Silica Templates by Hydrothermal Carbonization. *Advanced Functional Materials* **2007,** *17* (6), 1010-1018.

74. Qian, H.-S.; Yu, S.-H.; Luo, L.-B.; Gong, J.-Y.; Fei, L.-F.; Liu, X.-M. Synthesis of uniform Te@ carbon-rich composite nanocables with photoluminescence properties and carbonaceous nanofibers by the hydrothermal carbonization of glucose. *Chemistry of Materials* **2006,** *18* (8), 2102-2108.

75. Kubo, S.; Tan, I.; White, R. J.; Antonietti, M.; Titirici, M.-M. Template synthesis of carbonaceous tubular nanostructures with tunable surface properties. *Chemistry of Materials* **2010,** *22* (24), 6590-6597.

76. Yu, S.-H.; Cui, X.; Li, L.; Li, K.; Yu, B.; Antonietti, M.; Cölfen, H. From starch to metal/carbon hybrid nanostructures: hydrothermal metal-catalyzed carbonization. *Advanced Materials* **2004,** *16* (18), 1636-1640.

77. Lu, A. H.; Schüth, F. Nanocasting: a versatile strategy for creating nanostructured porous materials. *Advanced Materials* **2006,** *18* (14), 1793-1805.

78. Lu, A.-H.; Schüth, F. Nanocasting pathways to create ordered mesoporous solids. *Comptes Rendus Chimie* **2005,** *8* (3), 609-620.

79. Wang, S.; Liu, R.; Han, C.; Wang, J.; Li, M.; Yao, J.; Li, H.; Wang, Y. A novel strategy to synthesize hierarchical, porous carbohydrate-derived carbon with tunable properties. *Nanoscale* **2014**.

80. Kubo, S.; White, R. J.; Tauer, K.; Titirici, M.-M. Flexible coral-like carbon nanoarchitectures via a dual block copolymer–latex templating approach. *Chemistry of Materials* **2013,** *25* (23), 4781-4790.

81. Kubo, S.; White, R. J.; Yoshizawa, N.; Antonietti, M.; Titirici, M.-M. Ordered Carbohydrate-Derived Porous Carbons. *Chemistry of Materials* **2011,** *23* (22), 4882-4885.

82. Fechler, N.; Wohlgemuth, S.-A.; Jaker, P.; Antonietti, M. Salt and sugar: direct synthesis of high surface area carbon materials at low temperatures via hydrothermal carbonization of glucose under hypersaline conditions. *Journal of Materials Chemistry A* **2013,** *1* (33), 9418-9421.

83. Janz, G. *Thermodynamic and Transport Properties for Molten Salts: Correlation Equations for Critically Evaluated Density, Surface Tension, Electrical Conductance and Viscosity Data*; American Chemical Society1988.

84. Fechler, N.; Fellinger, T. P.; Antonietti, M. “Salt templating”: a simple and sustainable pathway toward highly porous functional carbons from ionic liquids. *Advanced Materials* **2013,** *25* (1), 75-79.
85. Queen, W. L.; Hwu, S.-J.; Reighard, S. Salt-Templated Mesoporous Solids Comprised of Interlinked Polyoxovanadate Clusters. *Inorganic Chemistry* **2010,** *49* (4), 1316-1318.
86. Nina Fechler, T.-P. F. a. M. A. "Salt Templating": A Simple and Sustainable Patway toward Highly Porous Functional Carbon from Ionic Liquids. *Material Views* **2012**.
87. Fellinger, T. P.; White, R. J.; Titirici, M. M.; Antonietti, M. Borax-Mediated Formation of Carbon Aerogels from Glucose. *Advanced Functional Materials* **2012,** *22* (15), 3254-3260.
88. Xie, Z.-L.; White, R. J.; Weber, J.; Taubert, A.; Titirici, M. M. Hierarchical porous carbonaceous materials via ionothermal carbonization of carbohydrates. *Journal of Materials Chemistry* **2011,** *21* (20), 7434-7442.
89. Chieffi, G.; Fechler, N.; Esposito, D. Valorization of lignin waste from hydrothermal treatment of biomass: towards porous carbonaceous composites for continuous hydrogenation. *RSC Advances* **2015,** *5* (78), 63691-63696.
90. Pierre, A. C.; Pajonk, G. M. Chemistry of Aerogels and Their Applications. *Chemical Reviews* **2002,** *102* (11), 4243-4266.
91. ElKhatat, A. M.; Al-Muhtaseb, S. A. Advances in Tailoring Resorcinol-Formaldehyde Organic and Carbon Gels. *Advanced materials* **2011,** *23* (26), 2887-2903.
92. Antonietti, M.; Fechler, N.; Fellinger, T.-P. Carbon Aerogels and Monoliths: Control of Porosity and Nanoarchitecture via Sol–Gel routes. *Chemistry of Materials* **2014,** *26* (1), 196-210.
93. White, R. J.; Brun, N.; Budarin, V. L.; Clark, J. H.; Titirici, M.-M. Always Look on the “Light” Side of Life: Sustainable Carbon Aerogels. *ChemSusChem* **2014,** *7* (3), 670-689.
94. Moreno-Castilla, C.; Maldonado-Hódar, F. J. Carbon aerogels for catalysis applications: An overview. *Carbon* **2005,** *43* (3), 455-465.
95. Kiciński, W.; Norek, M.; Jankiewicz, B. J. Heterogeneous Carbon Gels: N-Doped Carbon Xerogels from Resorcinol and N-Containing Heterocyclic Aldehydes. *Langmuir* **2014,** *30* (47), 14276-14285.
96. White, R. J.; Yoshizawa, N.; Antonietti, M.; Titirici, M.-M. A sustainable synthesis of nitrogen-doped carbon aerogels. *Green Chemistry* **2011,** *13* (9), 2428-2434.

97. Titirici, M.-M.; Antonietti, M. Chemistry and materials options of sustainable carbon materials made by hydrothermal carbonization. *Chemical Society Reviews* **2010,** *39* (1), 103-116.
98. Brun, N.; García-González, C. A.; Smirnova, I.; Titirici, M. M. Hydrothermal synthesis of highly porous carbon monoliths from carbohydrates and phloroglucinol. *RSC Advances* **2013,** *3* (38), 17088-17096.
99. Tamon, H.; Ishizaka, H.; Yamamoto, T.; Suzuki, T. Influence of freeze-drying conditions on the mesoporosity of organic gels as carbon precursors. *Carbon* **2000,** *38* (7), 1099-1105.
100. Pietrzak, R.; Wachowska, H.; Nowicki, P. Preparation of nitrogen-enriched activated carbons from brown coal. *Energy & fuels* **2006,** *20* (3), 1275-1280.
101. Paraknowitsch, J. P.; Thomas, A. Doping carbons beyond nitrogen: an overview of advanced heteroatom doped carbons with boron, sulphur and phosphorus for energy applications. *Energy & Environmental Science* **2013,** *6* (10), 2839-2855.
102. Ryu, J.; Suh, Y.-W.; Suh, D. J.; Ahn, D. J. Hydrothermal preparation of carbon microspheres from mono-saccharides and phenolic compounds. *Carbon* **2010,** *48* (7), 1990-1998.
103. Fuertes, A.; Arbestain, M. C.; Sevilla, M.; Maciá-Agulló, J.; Fiol, S.; López, R.; Smernik, R.; Aitkenhead, W.; Arce, F.; Macias, F. Chemical and structural properties of carbonaceous products obtained by pyrolysis and hydrothermal carbonisation of corn stover. *Soil Research* **2010,** *48* (7), 618-626.
104. Cao, X.; Ro, K. S.; Libra, J. A.; Kammann, C. I.; Lima, I.; Berge, N.; Li, L.; Li, Y.; Chen, N.; Yang, J.; Deng, B.; Mao, J. Effects of Biomass Types and Carbonization Conditions on the Chemical Characteristics of Hydrochars. *Journal of Agricultural and Food Chemistry* **2013,** *61* (39), 9401-9411.
105. Machnikowski, J.; Grzyb, B.; Machnikowska, H.; Weber, J. Surface chemistry of porous carbons from N-polymers and their blends with pitch. *Microporous and mesoporous materials* **2005,** *82* (1), 113-120.
106. Demir-Cakan, R.; Baccile, N.; Antonietti, M.; Titirici, M. M. Carboxylate-Rich Carbonaceous Materials via One-Step Hydrothermal Carbonization of Glucose in the Presence of Acrylic Acid. *Chemistry of Materials* **2009,** *21* (3), 484-490.
107. Arrigo, R.; Hävecker, M.; Wrabetz, S.; Blume, R.; Lerch, M.; McGregor, J.; Parrott, E. P. J.; Zeitler, J. A.; Gladden, L. F.; Knop-Gericke, A.; Schlögl, R.; Su, D. S. Tuning

the Acid/Base Properties of Nanocarbons by Functionalization via Amination. *Journal of the American Chemical Society* **2010,** *132* (28), 9616-9630.

108. White, R. J.; Antonietti, M.; Titirici, M.-M. Naturally inspired nitrogen doped porous carbon. *Journal of Materials Chemistry* **2009,** *19* (45), 8645-8650.

109. Brun, N.; Wohlgemuth, S. A.; Osiceanu, P.; Titirici, M. M. Original design of nitrogen-doped carbon aerogels from sustainable precursors: application as metal-free oxygen reduction catalysts. *Green Chemistry* **2013,** *15* (9), 2514-2524.

110. Lahaye, J.; Nanse, G.; Bagreev, A.; Strelko, V. Porous structure and surface chemistry of nitrogen containing carbons from polymers. *Carbon* **1999,** *37* (4), 585-590.

111. Bitter, J. H.; van Dommele, S.; de Jong, K. P. On the virtue of acid–base titrations for the determination of basic sites in nitrogen doped carbon nanotubes. *Catalysis Today* **2010,** *150* (1–2), 61-66.

112. Braghiroli, F.; Fierro, V.; Izquierdo, M.; Parmentier, J.; Pizzi, A.; Celzard, A. Nitrogen-doped carbon materials produced from hydrothermally treated tannin. *Carbon* **2012,** *50* (15), 5411-5420.

113. Titirici, M.-M. Sustainable Carbon Materials from Hydrothermal Processes. *Wiley* **2013**.

114. Kiciński, W.; Szala, M.; Bystrzejewski, M. Sulfur-doped porous carbons: synthesis and applications. *Carbon* **2014,** *68*, 1-32.

115. Fraile, J. M.; García-Bordejé, E.; Pires, E.; Roldán, L. New insights into the strength and accessibility of acid sites of sulfonated hydrothermal carbon. *Carbon* **2014,** *77*, 1157-1167.

116. Roldán, L.; Pires, E.; Fraile, J. M.; García-Bordejé, E. Impact of sulfonated hydrothermal carbon texture and surface chemistry on its catalytic performance in esterification reaction. *Catalysis Today* **2015,** *249*, 153-160.

117. Wohlgemuth, S.-A.; White, R. J.; Willinger, M.-G.; Titirici, M.-M.; Antonietti, M. A one-pot hydrothermal synthesis of sulfur and nitrogen doped carbon aerogels with enhanced electrocatalytic activity in the oxygen reduction reaction. *Green Chemistry* **2012,** *14* (5), 1515-1523.

118. Wohlgemuth, S.-A.; Vilela, F.; Titirici, M.-M.; Antonietti, M. A one-pot hydrothermal synthesis of tunable dual heteroatom-doped carbon microspheres. *Green Chemistry* **2012,** *14* (3), 741-749.

119. Seema, H.; Kemp, K. C.; Le, N. H.; Park, S.-W.; Chandra, V.; Lee, J. W.; Kim, K. S. Highly selective CO2 capture by S-doped microporous carbon materials. *Carbon* **2014,** *66* (0), 320-326.

120. Çeçen, F.; Aktaş, Ö. Water and wastewater treatment: Historical Perspective of Activated Carbon adsorption and its Integration with biological processes. *Activated Carbon for Water and Wastewater Treatment: Integration of Adsorption and Biological Treatment* **2011**, 1-11.

121. Galán, J.; Rodríguez, A.; Gómez, J. M.; Allen, S. J.; Walker, G. M. Reactive dye adsorption onto a novel mesoporous carbon. *Chemical Engineering Journal* **2013,** *219* (0), 62-68.

122. O'Connell, D. W.; Birkinshaw, C.; O'Dwyer, T. F. Heavy metal adsorbents prepared from the modification of cellulose: A review. *Bioresource Technology* **2008,** *99* (15), 6709-6724.

123. Singh, K. K.; Rastogi, R.; Hasan, S. H. Removal of Cr(VI) from wastewater using rice bran. *Journal of Colloid and Interface Science* **2005,** *290* (1), 61-68.

124. Bhatnagar, A.; Sillanpää, M. Utilization of agro-industrial and municipal waste materials as potential adsorbents for water treatment—A review. *Chemical Engineering Journal* **2010,** *157* (2–3), 277-296.

125. Kurniawan, T. A.; Chan, G. Y. S.; Lo, W.-h.; Babel, S. Comparisons of low-cost adsorbents for treating wastewaters laden with heavy metals. *Science of The Total Environment* **2006,** *366* (2–3), 409-426.

126. Cao, C.-Y.; Qu, J.; Yan, W.-S.; Zhu, J.-F.; Wu, Z.-Y.; Song, W.-G. Low-Cost Synthesis of Flowerlike α-Fe2O3 Nanostructures for Heavy Metal Ion Removal: Adsorption Property and Mechanism. *Langmuir* **2012,** *28* (9), 4573-4579.

127. Swiatkowski, A.; Pakula, M.; Biniak, S.; Walczyk, M. Influence of the surface chemistry of modified activated carbon on its electrochemical behaviour in the presence of lead(II) ions. *Carbon* **2004,** *42* (15), 3057-3069.

128. Corapcioglu, M.; Huang, C. The adsorption of heavy metals onto hydrous activated carbon. *Water Research* **1987,** *21* (9), 1031-1044.

129. Bhaumik, M.; Maity, A.; Srinivasu, V.; Onyango, M. S. Enhanced removal of Cr (VI) from aqueous solution using polypyrrole/Fe 3 O 4 magnetic nanocomposite. *Journal of hazardous materials* **2011,** *190* (1), 381-390.

130. Moreno-Castilla, C. Adsorption of organic molecules from aqueous solutions on carbon materials. *Carbon* **2004,** *42* (1), 83-94.
131. Chen, L.-F.; Liang, H.-W.; Lu, Y.; Cui, C.-H.; Yu, S.-H. Synthesis of an Attapulgite Clay@Carbon Nanocomposite Adsorbent by a Hydrothermal Carbonization Process and Their Application in the Removal of Toxic Metal Ions from Water. *Langmuir* **2011,** *27* (14), 8998-9004.
132. Wang, J.; Zhao, G.; Li, Y.; Zhu, H.; Peng, X.; Gao, X. One-step fabrication of functionalized magnetic adsorbents with large surface area and their adsorption for dye and heavy metal ions. *Dalton Transactions* **2014,** *43* (30), 11637-11645.
133. Wu, Q.; Li, W.; Liu, S. Carboxyl-rich carbon microspheres prepared from pentosan with high adsorption capacity for heavy metal ions. *Materials Research Bulletin* **2014,** *60*, 516-523.
134. Liu, Y.-H.; Wang, Y.-Q.; Zhang, Z.-B.; Cao, X.-H.; Nie, W.-B.; Li, Q.; Hua, R. Removal of uranium from aqueous solution by a low cost and high-efficient adsorbent. *Applied Surface Science* **2013,** *273*, 68-74.
135. Zhang, W.-L.; Zhang, Z.-B.; Cao, X.-H.; Ma, R.-C.; Liu, Y.-H. Uranium adsorption studies on hydrothermal carbon produced by chitosan using statistical design method. *J Radioanal Nucl Chem* **2014,** *301* (1), 197-205.
136. Zhang, Z.-b.; Liu, Y.-h.; Cao, X.-h.; Liang, P. Sorption study of uranium on carbon spheres hydrothermal synthesized with glucose from aqueous solution. *J Radioanal Nucl Chem* **2013,** *295* (3), 1775-1782.
137. Zhang, Z.-b.; Zhou, Z.-w.; Cao, X.-h.; Liu, Y.-h.; Xiong, G.-x.; Liang, P. Removal of uranium(VI) from aqueous solutions by new phosphorus-containing carbon spheres synthesized via one-step hydrothermal carbonization of glucose in the presence of phosphoric acid. *J Radioanal Nucl Chem* **2014,** *299* (3), 1479-1487.
138. Cheng, W.; Ding, C.; Sun, Y.; Wang, X. Fabrication of fungus/attapulgite composites and their removal of U(VI) from aqueous solution. *Chemical Engineering Journal* **2015,** *269*, 1-8.
139. Chen, Z.; Ma, L.; Li, S.; Geng, J.; Song, Q.; Liu, J.; Wang, C.; Wang, H.; Li, J.; Qin, Z. Simple approach to carboxyl-rich materials through low-temperature heat treatment of hydrothermal carbon in air. *Applied Surface Science* **2011,** *257* (20), 8686-8691.

140. Rivera-Utrilla, J.; Sánchez-Polo, M. Adsorbent-adsorbate interactions in the adsorption of organic and inorganic species on ozonized activated carbons: a short review. *Adsorption* **2011,** *17* (3), 611-620.
141. Sánchez-Polo, M.; Rivera-Utrilla, J. Adsorbent−Adsorbate Interactions in the Adsorption of Cd(II) and Hg(II) on Ozonized Activated Carbons. *Environmental Science & Technology* **2002,** *36* (17), 3850-3854.
142. Zhou, X.; You, S. J.; Wang, X. H.; Gan, Y.; Zhong, Y. J.; Ren, N. Q. Hydrothermal synthesis of magnetic carbon microspheres for effective adsorption of Cd (II) in water. *Journal of Chemical Technology and Biotechnology* **2014,** *89* (7), 1051-1059.
143. Longlong, T.; Dan, L.; Lingxin, H.; Shiwei, C.; Wei, Q.; Jing, L.; Qiang, W.; Zhan, L.; Wangsuo, W. One-pot hydrothermal synthesis of carbonaceous nanocomposites for efficient decontamination of copper. *RSC Advances* **2015,** *5* (119), 98041-98049.
144. Liang, H.-W.; Cao, X.; Zhang, W.-J.; Lin, H.-T.; Zhou, F.; Chen, L.-F.; Yu, S.-H. Robust and Highly Efficient Free-Standing Carbonaceous Nanofiber Membranes for Water Purification. *Advanced Functional Materials* **2011,** *21* (20), 3851-3858.
145. Aggarwal, D.; Goyal, M.; Bansal, R. C. Adsorption of chromium by activated carbon from aqueous solution. *Carbon* **1999,** *37* (12), 1989-1997.
146. Selvi, K.; Pattabhi, S.; Kadirvelu, K. Removal of Cr (VI) from aqueous solution by adsorption onto activated carbon. *Bioresource Technology* **2001,** *80* (1), 87-89.
147. Wang, X.; Liu, J.; Xu, W. One-step hydrothermal preparation of amino-functionalized carbon spheres at low temperature and their enhanced adsorption performance towards Cr(VI) for water purification. *Colloids and Surfaces A: Physicochemical and Engineering Aspects* **2012,** *415*, 288-294.
148. Liu, Z.; Zhang, F.-S.; Wu, J. Characterization and application of chars produced from pinewood pyrolysis and hydrothermal treatment. *Fuel* **2010,** *89* (2), 510-514.
149. Li, T.; Shen, J.; Huang, S.; Li, N.; Ye, M. Hydrothermal carbonization synthesis of a novel montmorillonite supported carbon nanosphere adsorbent for removal of Cr (VI) from waste water. *Applied Clay Science* **2014,** *93*, 48-55.
150. Inyang, M.; Gao, B.; Yao, Y.; Xue, Y.; Zimmerman, A. R.; Pullammanappallil, P.; Cao, X. Removal of heavy metals from aqueous solution by biochars derived from anaerobically digested biomass. *Bioresource Technology* **2012,** *110*, 50-56.
151. Liu, Z.; Zhang, F.-S. Removal of lead from water using biochars prepared from hydrothermal liquefaction of biomass. *Journal of Hazardous Materials* **2009,** *167* (1), 933-939.

152. Elaigwu, S. E.; Rocher, V.; Kyriakou, G.; Greenway, G. M. Removal of Pb2+ and Cd2+ from aqueous solution using chars from pyrolysis and microwave-assisted hydrothermal carbonization of Prosopis africana shell. *Journal of Industrial and Engineering Chemistry* **2014,** *20* (5), 3467-3473.
153. Zhong, Y.-J.; You, S.-J.; Wang, X.-H.; Zhou, X.; Gan, Y.; Ren, N.-Q. Synthesis of carbonaceous nanowire membrane for removing heavy metal ions and high water flux. *Chemical Engineering Journal* **2013,** *226*, 217-226.
154. Allen, S. J.; McKay, G.; Porter, J. F. Adsorption isotherm models for basic dye adsorption by peat in single and binary component systems. *Journal of Colloid and Interface Science* **2004,** *280* (2), 322-333.
155. Terzyk, A. P. Molecular properties and intermolecular forces—factors balancing the effect of carbon surface chemistry in adsorption of organics from dilute aqueous solutions. *Journal of colloid and interface science* **2004,** *275* (1), 9-29.
156. Radovic, L. R.; Silva, I. F.; Ume, J. I.; Menéndez, J. A.; Leon, C. A. L. Y.; Scaroni, A. W. An experimental and theoretical study of the adsorption of aromatics possessing electron-withdrawing and electron-donating functional groups by chemically modified activated carbons. *Carbon* **1997,** *35* (9), 1339-1348.
157. Faria, P. C. C.; Órfão, J. J. M.; Pereira, M. F. R. Adsorption of anionic and cationic dyes on activated carbons with different surface chemistries. *Water Research* **2004,** *38* (8), 2043-2052.
158. Órfão, J. J. M.; Silva, A. I. M.; Pereira, J. C. V.; Barata, S. A.; Fonseca, I. M.; Faria, P. C. C.; Pereira, M. F. R. Adsorption of a reactive dye on chemically modified activated carbons—Influence of pH. *Journal of Colloid and Interface Science* **2006,** *296* (2), 480-489.
159. Islam, M. A.; Tan, I.; Benhouria, A.; Asif, M.; Hameed, B. Mesoporous and adsorptive properties of palm date seed activated carbon prepared via sequential hydrothermal carbonization and sodium hydroxide activation. *Chemical Engineering Journal* **2015,** *270*, 187-195.
160. Unur, E. Functional nanoporous carbons from hydrothermally treated biomass for environmental purification. *Microporous and Mesoporous Materials* **2013,** *168*, 92-101.
161. Zhu, X.; Liu, Y.; Zhou, C.; Luo, G.; Zhang, S.; Chen, J. A novel porous carbon derived from hydrothermal carbon for efficient adsorption of tetracycline. *Carbon* **2014,** *77*, 627-636.

162. Zhu, X.; Liu, Y.; Qian, F.; Zhou, C.; Zhang, S.; Chen, J. Preparation of magnetic porous carbon from waste hydrochar by simultaneous activation and magnetization for tetracycline removal. *Bioresource Technology* **2014,** *154*, 209-214.

163. Fan, W.; Gao, W.; Zhang, C.; Tjiu, W. W.; Pan, J.; Liu, T. Hybridization of graphene sheets and carbon-coated Fe3O4 nanoparticles as a synergistic adsorbent of organic dyes. *Journal of Materials Chemistry* **2012,** *22* (48), 25108-25115.

164. Zhou, Q.; Gao, Q.; Luo, W.; Yan, C.; Ji, Z.; Duan, P. One-step synthesis of amino-functionalized attapulgite clay nanoparticles adsorbent by hydrothermal carbonization of chitosan for removal of methylene blue from wastewater. *Colloids and Surfaces A: Physicochemical and Engineering Aspects* **2015,** *470*, 248-257.

165. Sarkar, B.; Liu, E.; McClure, S.; Sundaramurthy, J.; Srinivasan, M.; Naidu, R. Biomass derived palygorskite–carbon nanocomposites: Synthesis, characterisation and affinity to dye compounds. *Applied Clay Science* **2015,** *114*, 617-626.

166. Zhou, J.; Tang, C.; Cheng, B.; Yu, J.; Jaroniec, M. Rattle-type carbon–alumina core–shell spheres: synthesis and application for adsorption of organic dyes. *ACS applied materials & interfaces* **2012,** *4* (4), 2174-2179.

167. Mestre, A. S.; Tyszko, E.; Andrade, M. A.; Galhetas, M.; Freire, C.; Carvalho, A. P. Sustainable activated carbons prepared from a sucrose-derived hydrochar: remarkable adsorbents for pharmaceutical compounds. *RSC Advances* **2015,** *5* (25), 19696-19707.

168. Qi, X.; Li, L.; Tan, T.; Chen, W.; Smith, R. L. Adsorption of 1-Butyl-3-Methylimidazolium Chloride Ionic Liquid by Functional Carbon Microspheres from Hydrothermal Carbonization of Cellulose. *Environmental Science & Technology* **2013,** *47* (6), 2792-2798.

169. Fernandez, M. E.; Ledesma, B.; Román, S.; Bonelli, P. R.; Cukierman, A. L. Development and characterization of activated hydrochars from orange peels as potential adsorbents for emerging organic contaminants. *Bioresource Technology* **2015,** *183*, 221-228.

170. Gattia, D. M.; Antisari, M. V.; Giorgi, L.; Marazzi, R.; Piscopiello, E.; Montone, A.; Bellitto, S.; Licoccia, S.; Traversa, E. Study of different nanostructured carbon supports for fuel cell catalysts. *Journal of Power Sources* **2009,** *194* (1), 243-251.

171. Ormerod, R. M. Solid oxide fuel cells. *Chemical Society Reviews* **2003,** *32* (1), 17-28.

172. Seselj, N.; Engelbrekt, C.; Zhang, J. Graphene-supported platinum catalysts for fuel cells. *Science Bulletin* **2015,** *60* (9), 864-876.

173. Matter, P. H.; Zhang, L.; Ozkan, U. S. The role of nanostructure in nitrogen-containing carbon catalysts for the oxygen reduction reaction. *Journal of Catalysis* **2006,** *239* (1), 83-96.

174. Shao, Y.; Sui, J.; Yin, G.; Gao, Y. Nitrogen-doped carbon nanostructures and their composites as catalytic materials for proton exchange membrane fuel cell. *Applied Catalysis B: Environmental* **2008,** *79* (1), 89-99.

175. Sevilla, M.; Yu, L.; Fellinger, T. P.; Fuertes, A. B.; Titirici, M.-M. Polypyrrole-derived mesoporous nitrogen-doped carbons with intrinsic catalytic activity in the oxygen reduction reaction. *RSC Advances* **2013,** *3* (25), 9904-9910.

176. Li, W.; Liang, C.; Zhou, W.; Qiu, J.; Zhou, Z.; Sun, G.; Xin, Q. Preparation and characterization of multiwalled carbon nanotube-supported platinum for cathode catalysts of direct methanol fuel cells. *The Journal of Physical Chemistry B* **2003,** *107* (26), 6292-6299.

177. Gong, K.; Du, F.; Xia, Z.; Durstock, M.; Dai, L. Nitrogen-Doped Carbon Nanotube Arrays with High Electrocatalytic Activity for Oxygen Reduction. *Science* **2009,** *323* (5915), 760-764.

178. Qiu, K.; Guo, Z. X. Hierarchically porous graphene sheets and graphitic carbon nitride intercalated composites for enhanced oxygen reduction reaction. *Journal of Materials Chemistry A* **2014,** *2* (9), 3209-3215.

179. Jin, H.; Zhang, H.; Zhong, H.; Zhang, J. Nitrogen-doped carbon xerogel: A novel carbon-based electrocatalyst for oxygen reduction reaction in proton exchange membrane (PEM) fuel cells. *Energy & Environmental Science* **2011,** *4* (9), 3389-3394.

180. Frackowiak, E. Carbon materials for supercapacitor application. *Physical chemistry chemical physics* **2007,** *9* (15), 1774-1785.

181. Zhu, B.; Qiu, K.; Shang, C.; Guo, Z. Naturally derived porous carbon with selective metal- and/or nitrogen-doping for efficient CO2 capture and oxygen reduction. *Journal of Materials Chemistry A* **2015,** *3* (9), 5212-5222.

182. Choi, C. H.; Park, S. H.; Woo, S. I. Binary and ternary doping of nitrogen, boron, and phosphorus into carbon for enhancing electrochemical oxygen reduction activity. *ACS nano* **2012,** *6* (8), 7084-7091.

183. Chen, J.; Wang, X.; Cui, X.; Yang, G.; Zheng, W. Amorphous carbon enriched with pyridinic nitrogen as an efficient metal-free electrocatalyst for oxygen reduction reaction. *Chemical Communications* **2014,** *50* (5), 557-559.

184. Zhu, C.; Zhai, J.; Dong, S. Bifunctional fluorescent carbon nanodots: green synthesis via soy milk and application as metal-free electrocatalysts for oxygen reduction. *Chemical Communications* **2012,** *48* (75), 9367-9369.

185. Liu, Z.-Q.; Xu, Q.-Z.; Wang, J.-Y.; Li, N.; Guo, S.-H.; Su, Y.-Z.; Wang, H.-J.; Zhang, J.-H.; Chen, S. Facile hydrothermal synthesis of urchin-like NiCo 2 O 4 spheres as efficient electrocatalysts for oxygen reduction reaction. *International Journal of Hydrogen Energy* **2013,** *38* (16), 6657-6662.

186. Hu, F. P.; Wang, Z.; Li, Y.; Li, C.; Zhang, X.; Shen, P. K. Improved performance of Pd electrocatalyst supported on ultrahigh surface area hollow carbon spheres for direct alcohol fuel cells. *Journal of Power Sources* **2008,** *177* (1), 61-66.

187. Su, Y.; Zhang, Y.; Zhuang, X.; Li, S.; Wu, D.; Zhang, F.; Feng, X. Low-temperature synthesis of nitrogen/sulfur co-doped three-dimensional graphene frameworks as efficient metal-free electrocatalyst for oxygen reduction reaction. *Carbon* **2013,** *62*, 296-301.

188. Wohlgemuth, S.-A.; Fellinger, T.-P.; Jaker, P.; Antonietti, M. Tunable nitrogen-doped carbon aerogels as sustainable electrocatalysts in the oxygen reduction reaction. *Journal of Materials Chemistry A* **2013,** *1* (12), 4002-4009.

Publication I

S-M. Alatalo, E. Repo, E. Mäkilä, J. Salonen, E. Vakkilainen and M. Sillanpää
Adsorption behaviour of hydrothermally treated municipal sludge & pulp and paper industry sludge

Reprinted with permission from
Journal Bioresource Technology
Vol. 147, 2013
© 2013, Elsevier

Provided for non-commercial research and education use.
Not for reproduction, distribution or commercial use.

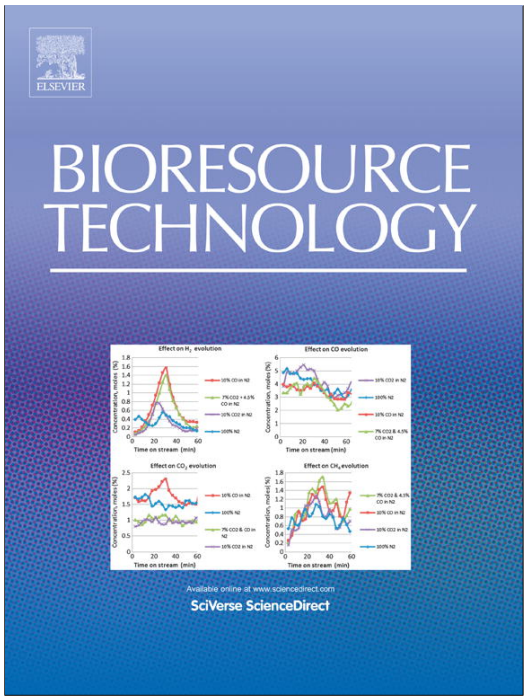

This article appeared in a journal published by Elsevier. The attached copy is furnished to the author for internal non-commercial research and education use, including for instruction at the authors institution and sharing with colleagues.

Other uses, including reproduction and distribution, or selling or licensing copies, or posting to personal, institutional or third party websites are prohibited.

In most cases authors are permitted to post their version of the article (e.g. in Word or Tex form) to their personal website or institutional repository. Authors requiring further information regarding Elsevier's archiving and manuscript policies are encouraged to visit:

http://www.elsevier.com/authorsrights

Author's personal copy

Bioresource Technology 147 (2013) 71–76

Contents lists available at ScienceDirect

Bioresource Technology

journal homepage: www.elsevier.com/locate/biortech

Adsorption behavior of hydrothermally treated municipal sludge & pulp and paper industry sludge

Sara-Maaria Alatalo [a,*], Eveliina Repo [a], Ermei Mäkilä [b], Jarno Salonen [b], Esa Vakkilainen [c], Mika Sillanpää [a]

[a] Laboratory of Green Chemistry, Department of Chemistry, Lappeenranta University of Technology, Sammonkatu 12, FI-50130 Mikkeli, Finland
[b] Laboratory of Industrial Physics, Department of Physics and Astronomy, University of Turku, FI-20014 Turku, Finland
[c] Laboratory of sustainable energy systems, LUT Energy, Lappeenranta University of technology, Skinnarilankatu 34, FI-53850 Lappeenranta, Finland

HIGHLIGHTS

- Hydrothermally produced adsorbents were effective adsorbents for positively charged Pb(II) metal ions.
- Hydrothermal carbonization showed potential for the production of carbonaceous material and waste materials can be used as feedstock of low-cost adsorbents.
- Pb(II) had the highest adsorption efficiency from tested metals and adsorption followed Sips adsorption isotherm.
- Adsorption kinetics followed non-linear pseudo-second order kinetic model.

ARTICLE INFO

Article history:
Received 11 June 2013
Received in revised form 3 August 2013
Accepted 5 August 2013
Available online 14 August 2013

Keywords:
Adsorption
Sludge
Metals
Hydrothermal carbonization
Modeling

ABSTRACT

Aim of the study was to investigate how hydrothermal carbonization changes adsorption efficiency toward metal ions of typical sludges. Hydrothermal carbonization is a novel and green method of treating biomasses. Reactions take place in an aqueous environment at relatively mild temperature and high pressure resulting a different end biomass structure than obtained from traditional pyrolysis. Anaerobically digested sludge (ADS) and pulp and paper industry sludge (INS) were utilized as a feedstock. Adsorption behavior of ADS and INS was examined towards Pb(II), Cr(III), Cr(VI), As(III) and As(V). Both ADS and INS were found to remove Pb(II) effectively and followed Sips adsorption isotherm. Adsorption kinetics was fast and followed pseudo-second order model. Furthermore, intraparticle diffusion was observed to be partly responsible in the adsorption process. Hydrothermal carbonization indicated high potential for the production of novel carbonaceous materials for metal removal from waters.

© 2013 Elsevier Ltd. All rights reserved.

1. Introduction

In wastewater and drinking water treatment activated carbon has widely been used as an adsorbent because of its efficiency to remove organic compounds, metals and other inorganic pollutants. Activated carbon refers to carbon-based materials with characteristics such as highly developed porosity, large surface area, variable surface chemistry, and high degree of surface reactivity (Bhatnagar et al., 2012).

Despite of wide use of activated carbon its exploitation is sometimes restricted due to high cost, which depends on availability of the raw material, processing requirement, treatment conditions, and both recycle and lifetime issues (Gupta et al., 2009). Therefore, researchers are looking for new low-cost alternatives for activated carbon where raw materials comprise of natural materials (wood, peat, lignite, clay etc.), as industrial, agricultural or domestic wastes and byproducts. Replacement of activated carbon by low-cost adsorbent would reduce the production cost of adsorbents. In addition exploitation of waste materials as feedstock would reduce partly the cost of waste disposal. In the view of low production cost, regeneration of the material would not be necessary (Babel and Kurniawan, 2003; Bhatnagar and Sillanpää, 2010; Dias et al., 2007).

Hydrothermal carbonization (HTC) is an unconventional method for the production of carbonaceous material. Process is attractive due to its green aspect, simplicity, low-cost, and energy and CO_2 efficiency (Titirici et al., 2012). Major advantage of HTC over other methods for the production of carbonaceous material is converting wet input material into solids without the need for energy-intensive drying before and during the process. This expands the feedstock choice to high water content raw materials such as wet animal manures, human waste, sewage sludge, municipal solid waste (MSW), aqua culture and algal residues (Libra et al., 2011).

* Corresponding author. Tel.: +358 406843958.
E-mail address: sara-maaria.alatalo@lut.fi (S.-M. Alatalo).

0960-8524/$ - see front matter © 2013 Elsevier Ltd. All rights reserved.
http://dx.doi.org/10.1016/j.biortech.2013.08.034

Author's personal copy

Reaction takes place in an aqueous environment at the moderate temperature (180–250 °C) and pressure in a closed system. Pressure formation is self-generated and mostly related to water steam but also raw material and design of vessel. At process temperature around 220 °C corresponding pressure has been reported to be approximately 20 bar. Overall HTC reaction is a combination of several simultaneous reactions. Reaction mechanism includes dehydration, decarboxylation, condensation polymerization and aromatization. However, the reaction mechanism is not understood in detail (Funke and Ziegler, 2010). HTC process results higher solid yields, more water soluble organics, and fewer gases compared to dry pyrolysis, which is the most commonly used method for the production of adsorbents.

Hydrochar resembles natural coal with respect to the type of chemical bonds, their relative quantity, and chemical composition. It has also higher hydrogen/carbon and oxygen/carbon ratios than carbonaceous material from dry pyrolysis (Libra et al., 2011). Significant differences in structural studies of hydrochars produced from small pure carbohydrates and complex biomass was not noticed. These hydrochars showed similarities with respect to morphology and local structural connectivity (Titirici and Antonietti, 2010).

In this study suitability of hydrochar produced by hydrothermal carbonization for adsorption of various metals was investigated. Adsorption behaviors of these carbonaceous materials were examined towards both cationic and anionic metal ions. Furthermore equilibrium behavior and adsorption kinetics of prepared hydrochars were investigated.

2. Methods

2.1. Materials and physicochemical characterization

Anaerobically digested municipal sludge (total solids 3.5 wt.%) (Mikkeli wastewater treatment plant, Finland) and pulp and paper industrial sludge (Dry solids (total solids 38 wt.%) Ekokem) were used as a starting material. Pulp and paper industry sludge consisted of both fiber rich primary sludge and biological secondary sludge.

Heavy metals Pb(II), As(III), As(V), Cr(III) and Cr(VI) were used for the adsorption studies. All metals were of analytical grade. 1000 mg l^{-1} stock solutions were prepared from corresponding salts ($Pb(NO_3)_2$ (Merck), $CrN_3O_9{\cdot}H_2O$ (Acros Organic), $K_2Cr_2O_7$ (Sigma Aldrich), As_2O_3 (Fluka) and As_2O_5 (Alfa Aesar)). Metal salts were dissolved in deionized water except As_2O_3 and As_2O_5 which were dissolved in 25% NaOH and neutralized with 37% HCl. pH adjustments were performed by 0.1 M NaOH and 0.1 M HNO_3 (As(III) and As(V) 0.1 M HCl).

Agitation of the adsorption system under investigation was performed in Rotary shaker Ika KS 4000i at ambient temperature. Changes in the metal concentrations due the adsorption were analyzed at wavelengths of 189.042 nm (As), 298.919 nm (Cr) and 220.353 nm (Pb) by inductively coupled plasma optical emission spectrometry (ICP-OES) model iCAP 6300 (Thermo Electron Corp., USA). The amount of metal ions adsorbed per unit mass of hydrochar was calculated as follows:

$$q_e = \frac{(C_i - C_e)}{m} V \quad (1)$$

where q_e (mg g^{-1}) is equilibrium adsorption capacity, C_i and C_e (mg l^{-1}) are initial and equilibrium ion concentrations, respectively, m (g) represent the weight of the adsorbent, and V (l) is the volume of the solution.

Equilibrium isotherms were calculated according to the following equations.

Langmuir isotherm equation non-linear form:

$$q_e = q_m \frac{K_L C_e}{1 + K_L C_e} \quad (2)$$

where q_e is the equilibrium adsorption capacity. q_m is a theoretical maximum adsorption capacity and K_L (L mg^{-1}) affinity constant.

Freundlich isotherm equation non-linear form:

$$q_e = k_F C_e^{\frac{1}{n_F}} \quad (3)$$

in which k_F (L mg^{-1}) and n_F (mg g^{-1}) are Freundlich adsorption constants.

Sips isotherm (Langmuir–Freundlich) equation:

$$q_e = q_m \frac{(K_S C_e)^{n_S}}{1 + (K_S C_e)^{n_S}} \quad (4)$$

in which K_S (L mg^{-1}) is an affinity constant and n_S (mg g^{-1}) describes surface heterogeneity. When n_S equals unity, Sips isotherms returns to the Langmuir isotherm and predicts homogeneous adsorption. On the other hand, deviation of n_S from the unity indicates heterogeneous surface. At high concentrations Sips approaches to a constant value and at low concentrations Freundlich type equation.

Modeling of adsorption kinetics was conducted by using the pseudo-first-order and pseudo-second-order models. The non-linear pseudo-first order model is expressed as:

$$q_t = q_e(1 - e^{-k_1 t}) \quad (5)$$

The pseudo-second-order model equation is:

$$q_t = \frac{q_e^2 k_2 t}{1 + q_e k_2 t} \quad (6)$$

where q_t and q_e (mg g^{-1}) are the adsorption capacity at time t (min) and at equilibrium, respectively, while k_1 (min^{-1}) and k_2 (g mg^{-1} · min^{-1}) are the pseudo-first-order and pseudo-second-order rate constants. Furthermore, pore diffusion as a controlling step in the adsorption was tested by intraparticle diffusion model as follows:

$$q = k_{dif} t^{\frac{1}{2}} (+C) \quad (7)$$

where k_{id} (mg g^{-1} $min^{-1/2}$) is the rate constant of intraparticle diffusion and C (mg g^{-1}) represents the thickness of the boundary layer.

Field-emission scanning electron microscopy (FE-SEM, Hitachi S-4800) was used for surface morphology examination. Surface groups of the hydrochar were observed by Fourier transform infrared spectroscopy (FTIR Vertex 70 Bruker Corp.) with integrated Diffuse Reflectance Accessory EasiDiff™ unit. Nitrogen sorption isotherms at −196 °C were determined using TriStar 3000 (Micromeritics Inc.). The specific surface area was calculated from the adsorption branch of the isotherm using Brunauer–Emmett–Teller theory, and the total pore volume was taken from the adsorbed amount at a relative pressure of $p/p_0 = 0.97$. Ash content was defined by applying SFS-standard 3008. The amount of elements C, H, N and O were analyzed by Organic Elemental Analyzer Flash 2000 (Thermo Scientific). Surface charge and isoelectric point (IEP) charge were determined by pH titration utilizing by Zetasizer Nano ZS (Malvern Instruments Ltd.). The pH where zeta potential equals to zero is called isoelectric point (IEP). Determination of pH_{IEP} is used to evaluate surface charge of the adsorbent (Li et al., 2003). FinnSonic m08 (Hersteller) was used to disperse hydrochars in the water phase.

2.2. Synthesis of carbonaceous material

Carbonaceous material was produced in stainless steel batch reactors with inner polytetrafluoroethylene (PTFE) vessel, which

Author's personal copy

total volume was 200 ml. Both anaerobically digested sludge (ADS) and industrial sludge (INS) based hydrochars were prepared in the same way. The batch reactor was loaded with mixture of 70 wt.% (105 g) of the sludge and 30 wt.% deionized water when total sludge–water mixture load was 150 g. Batch reactor was closed and placed into oven TS8000 (Termaks) in which temperature was set at 200 °C. Reactor was kept in the oven for 24 h. Batch reactor was allowed to cool down naturally until room temperature. Reaction mixture was then filtrated by using vacuum filtration technique through a quantitative filter paper (Munktell) in a Buchner funnel. Formed hydrochars were washed several times with deionized water. Hydrochar was dried at 80 °C overnight and finally ground to fine powder for further experiments.

2.3. Adsorption studies

Adsorption behavior of ADS and INS in different pH solutions was studied towards As(III), As(V), Cr(III), Cr(VI) and Pb(II). Solution of each metal with a concentration of 50 mg l^{-1} was prepared from 1000 mg l^{-1} stock solution. pH values varied between 3 and 7 and were adjusted with 0.1 M NaOH or 0.1 M HNO_3. Cr(III) solution was prepared only at pH 3 due to precipitation as hydroxide at higher pH values. The same phenomenon was noticed in the preparation of Pb(II) solutions at pH higher than 6. Hydrochar dosage was 10 mg and volume of the metal solution 5 ml. Agitation time was 24 h and rotation speed 300 rpm. Adsorbent and metal solutions were separated by 0.45 μm polypropylene syringe filter.

Metal total removal test was performed for the Pb(II). Adsorbent amounts were 10, 20, 30 and 40 mg. Metal concentration was kept constant (50 mg l^{-1}). Equilibrium studies were performed at ambient temperature in varied Pb(II) concentrations 4–800 mg l^{-1}. Adsorbent dose in these experiments was 50 mg and addition of Pb(II) solution was 25 ml. In adsorption kinetic studies reaction pH was adjusted to 5, adsorbent dose was 2 gl^{-1}, agitation speed 100 rpm and the experiment was conducted at ambient temperature. Pb(II) concentration was the same than in total removal test (50 mg l^{-1}). Adsorbents were found hydrophobic. Therefore, ultrasound treatment was used to disperse adsorbent into water phase.

3. Results and discussion

3.1. Characterization

Adsorption process is adsorbent specific and depends strongly on the characteristics of the adsorbent. In this study the structural properties of the adsorbent were examined by determining surface area, pore volume, isoelectric point (pH_{IEP}) and organic elemental composition of adsorbents. Surface morphology was imaged by using SEM and structural composition of hydrochars was examined by using FTIR.

Both hydrochars presented weakly developed surface area and pore volume, which is common for hydrothermally treated materials (Table 1) (Román et al., 2013). Comparison of ADS and INS indicated higher surface area and internal volume for ADS. Surface morphology imaging by SEM indicated similar results. Significant differences between ADS and INS could not be observed. However, ADS indicated slightly rougher surface structure whereas INS showed smoother surfaces and lower morphology.

Elemental composition analysis of ADS and INS revealed rather high ash contents and low carbon contents typical for sludge based materials (Table 1) (Gu et al., 2012). Besides the composition of the feedstock, reaction conditions, especially the reaction temperature, has influence on the final ash content of the material (Park and Jang, 2011). Behavior of inorganic matter during the HTC reaction is unknown. Major parts of inorganics remain within hydrochars but there is still little evidence on how this ash content is dependent on process parameters (Funke and Ziegler, 2010). Rather high oxygen content in the hydrochars indicated acidic properties, which was supported by pH_{IEP} around pH 3 for both hydrochars (Fig. 1). Nevertheless, it is likely that a significant part of the oxygen derives from inorganic compounds. Small quantities of nitrogen and hydrogen were also found in both ADS and INS.

Structural composition of hydrochars was examined by FTIR. Especially, presence of oxygen functional groups was under of interest. The FTIR spectras of both ADS and INS presented severe overlapping between different wave numbers especially below 1800 cm^{-1} which made interpretation rather difficult. Most likely this was related to the heterogeneity of the hydrochars. However, some indications could be made. Bands typically related to aromatic structure were detected at 1450–1600 cm^{-1}. Also, carbonyl (C=O) stretching between 1640 and 1870 cm^{-1} could be observed in both hydrochars ADS and INS, as well as the CH_x stretching bands at 2800–3000 cm^{-1} (Kumar et al., 2011). The broad absorbance above 3000 cm^{-1} referred to –OH stretching and further onto the presence of hydroxyl functionalities.

3.2. Adsorption studies

In adsorption behavior of ADS and INS effect of pH, complete metal removal capacity and modeling of adsorption isotherms were investigated. Adsorption of metal ions depends strongly on solution pH, which has significant effect on surface charge of the adsorbent and the degree of ionization and speciation of the adsorbate (Kula et al., 2008). The adsorption efficiency of ADS and INS was studied for As(III), As(V), Cr(III), Cr(VI), and Pb(II).

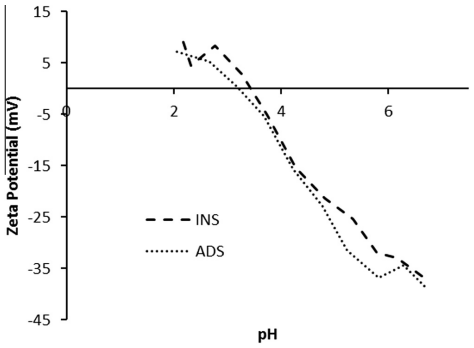

Fig. 1. Determination of isoelectric point by acid–base titration of hydrochars ADS and INS.

Table 1
Properties of ADS and INS.

Adsorbent	Ash (mg g^{-1})	Surface area (m^2 g^{-1})	Pore volume (cm^3 g^{-1})	C (%)	H (%)	N (%)	O (%)	pH_{IEP}
ADS	639.18	18.0	0.090	23.21	2.70	1.45	24.10	3.20
INS	475.04	9.1	0.040	34.68	3.78	1.67	15.50	3.40

Author's personal copy

ADS was observed to remove small quantities of Cr(VI), As(V) and As(III) anions whereas INS removed only Cr(VI) (Fig. 2). Adsorption of these anions decreased at higher pH values. Removal of Cr(VI), As(V) and As(III) was most efficient at pH 3 for both ADS and INS. Neither ADS or INS was able to remove Cr(III) even though it existed as positive ion form in the pH range covered in this study. This may be related to repulsion between Cr(III) and adsorbent surface because at pH 3 adsorbent surface indicated to be positively charged (Fig. 1). Both hydrochars indicated significant removal efficiency towards Pb(II). In the case of ADS, the Pb(II) removal was observed to be most efficient at pH 5 whereas INS favored pH 4. Weak Pb(II) adsorption at more acidic pH is caused by the surface charge of the adsorbent. At low pH, the binding sites are protonated, resulting in competition between H^+ and Pb(II) ions for occupancy of the binding sites decreasing the adsorption of Pb(II) (Singha and Kumar Das, 2012). Adsorption of inorganic species in addition of solution pH depends on the characteristics of the adsorbent. In addition to surface area and pore volume, metal removal efficiency depends on certain surface heteroatom functionalities such as oxygen, nitrogen, halogen and sulfur. However, influence of carbon–oxygen groups remains most important. Presence of polar acidic groups enhances ion-exchange properties and thereby increases the adsorption of cations (Bansal and Goyal, 2005). Therefore better adsorption performance for Pb(II) removal was expectable compared to anionic metal ions studied. In addition, technical applicability of adsorbent was estimated by determining the amount of adsorbent required for the complete removal of Pb(II) where total removal of Pb(II) was reached when INS dosage was 20 mg. ADS required 30 mg adsorbent dosage for Pb(II) total removal. This finding suggested that tested adsorbents were relatively potential for the water treatment applications.

3.2.1. Adsorption equilibrium and adsorption isotherms

Based on the specific surface area and pore volume data (Table 1), ADS can be expected to show better adsorption behavior than INS. Even though the specific surface area and pore volume of INS are lower compared to ADS it shows higher C, H, N and O composition than ADS. Especially higher oxygen content indicates to larger amount of functional groups on the surface of INS, which has been reported to have important role in metal cation adsorption as discussed earlier. Experimental equilibrium adsorption capacity experiments and adsorption isotherms for INS and ADS for the removal of Pb(II) are presented in Fig. 3. Clear maximum adsorption capacity is difficult to determine due to slightly ascending trend of the curve and scattering of the data points. Most likely heterogeneous nature of the feedstock is the reason for the scattering because less scattered equilibrium curves were reached by increasing the amount of adsorbent and metal solution (adsorbent-metal solution ratio was kept constant). Experimental adsorption equilibrium for ADS and INS was found to be on the same level, around 11 mg g^{-1}. The pH was observed to increase after adsorption process in the case of both hydrochar types. This phenomenon may be related to the liberation of Ca^{2+} ions from the adsorbent into the reaction solution, which was observed by ICP measurements (Bansal and Goyal, 2005).

The adsorption isotherm defines the relationship between the amount of adsorbate adsorbed per unit mass of adsorbent and adsorbate concentration in solution phase at equilibrium condition and at constant temperature. Metal uptake of adsorbents was simulated by the Langmuir, Freundlich, and Sips adsorption isotherms. The Langmuir and Freundlich isotherms are the most frequently used models to represent the equilibrium data of adsorption from aqueous solution. The Langmuir isotherm assumes that adsorption occurs at specific homogenous sites within the adsorbent without any interactions between the adsorbed substances (Kadirvelu et al., 2001). The Freundlich adsorption isotherm is an empirical model, which can be used for the heterogeneous surfaces and multilayer adsorption (Allen et al., 2004). The Sips isotherm is a combination of the Langmuir and Freundlich isotherms. Its behavior is similar to Freundlich isotherm with the exception of possessing a finite saturation limit when the concentration is sufficiently high. This isotherm is usually applicable where both the Langmuir and Freundlich model fail (Do, 1998; Ho et al., 2002).

Examination of the results indicated similar correlation of the Langmuir and Sips adsorption isotherms with experimental ADS adsorption equilibrium data (Fig. 3). Parameters of these adsorption isotherms are presented in Table 2. Sips resulted slightly higher theoretical maximum adsorption capacity (q_m) than Langmuir. Theoretical maximum adsorption values from both isotherms correlate reasonably well with the experimental adsorption capacity (q_e). Standard deviations (σ) of Langmuir and Sips isotherms do not differ from each other. Based on the correlation coefficient

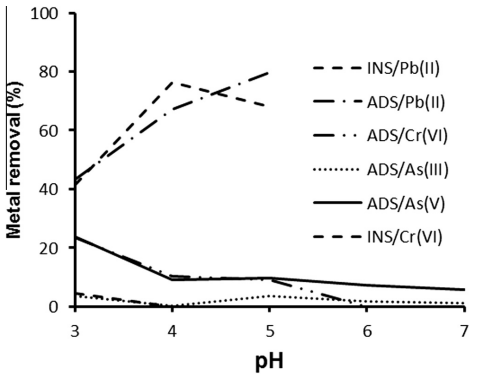

Fig. 2. Percentual removal of Cr(VI), As(III) and As(V) and Pb(II) ions by hydrochars ADS and INS.

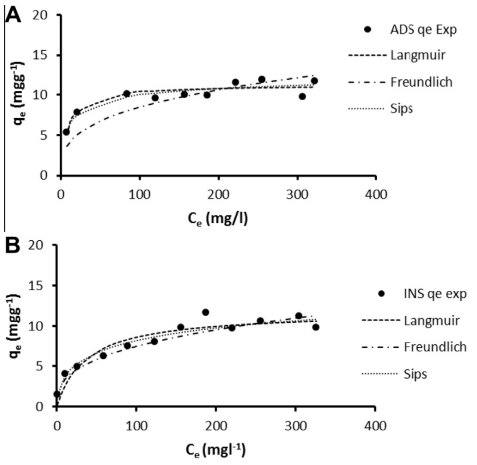

Fig. 3. Adsorption equilibrium curves and adsorption isotherms of Pb(II) adsorption of (A) ADS and (B) INS. Adsorbent dosage was 50 mg and Pb(II) solution amount was 25 ml. Agitation time 24 h and rotation 300 rpm.

Author's personal copy

Table 2
Langmuir, Freundlich and Sips adsorption isotherm parameters for Pb(II) adsorption of ADS and INS.

Langmuir				
Material	K_L (L mg^{-1})	q_m (mg g^{-1})	R^2	σ
ADS	0.112	11.27	0.839	1.87
INS	0.027	11.78	0.902	3.20
Freundlich				
Material	K_F (L mg^{-1})	n_F (mg g^{-1})	R^2	σ
ADS	7.219	3.1	0.052	2.45
INS	3.131	2.9	0.896	3.15
Sips				
Material	K_S (L mg^{-1})	q_m (mg g^{-1})	n_S (mg g^{-1})	R^2	σ
ADS	0.081	12.97	0.57	0.858	1.86
INS	0.007	17.66	0.51	0.931	3.04

(R^2) better approximation can be received for Sips. Sips adsorption isotherm was found to be the most representative in the modeling of INS adsorption properties. This was supported by the high correlation coefficient and lower standard deviation values. Deviation between theoretical maximum adsorption capacity (q_m) and experimental maximum adsorption capacity (q_e) is probably related to the heterogeneity of the adsorbent. Heterogeneity factors (n_S) in Sips isotherm in the case of both hydrochars differ from unity supporting the thought of somewhat heterogeneous nature of both ADS and INS. More homogeneous hydrochars may be achieved by modification of operation parameters, prolonging the reaction time and/or increasing reaction temperature. This may also increase the specific surface area and the pore volume, which could increase the adsorption efficiency as well. However, large surface area and well developed porosity does not always indicate efficient adsorption capacity. Surface functional groups perform essential role in the adsorption process besides to the structural morphology. Especially, in the removal of metal compounds amount of surface functional groups seems to be closely related to adsorption capacity (Repo et al., 2010).

Metal removal by hydrochars is not widely studied, making comparison to the literature challenging. One research group has studied Pb(II) removal by HTC treated pinewood and rice husk (Ahn et al., 2009). Removal efficiencies towards Pb(II) were q_e = 4.25 mg g^{-1} and q_e = 2.40 mg g^{-1} respectively. In our study removal of Pb(II) by both INS and ADS was around q_e = 11 mg g^{-1}. Removal of other pollutants such as Cu(II) and phenol has been studied by HTC treated pinewood sawdust and rice husk. Adsorption efficiency for phenol was found to be 83.88 mg g^{-1} and 39.30 mg g^{-1} and for Cu(II) 25.18 mg g^{-1} and 22.62 mg g^{-1} respectively of pinewood and rice husk. However, temperature in the hydrothermal carbonization was relatively high (300 °C) in this study (Liu and Zhang, 2009). Although adsorptive performance of hydrochars remains lower compared to that of activated carbon (Liu and Zhang, 2011), the promising properties of hydrochars indicate their potential in the adsorption applications in the future. HTC process allows utilization of lower process temperatures and wider range of feedstocks. Mild process conditions and simple one-step process scheme indicate significant cost-efficiency in the production of adsorbents via HTC method. Nevertheless more investigation is needed in order to extent understanding about the possibilities and restrictions of the method in adsorption processes.

3.2.2. Modeling of adsorption kinetics

In the modeling of adsorption kinetics for metal uptake by hydrochars, three kinetic models (pseudo-first-order, pseudo-second-order and intraparticle diffusion) were used to simulate the experimental data. Both, ADS and INS were found to follow better the pseudo-second-order model than the pseudo-first-order model (Fig. 4 and Table 3). This is according to Azizian's theory (Wilson et al., 2006) conventional when the initial concentration is not excessively high as in this study. q_t Values determined from the pseudo-second-order model were close to the experimental values whereas correlation coefficients (R^2) were rather low. This may be due to the influence of diffusion on the rate of the reaction (see below). The values of pseudo-second-order rate constants showed faster adsorption

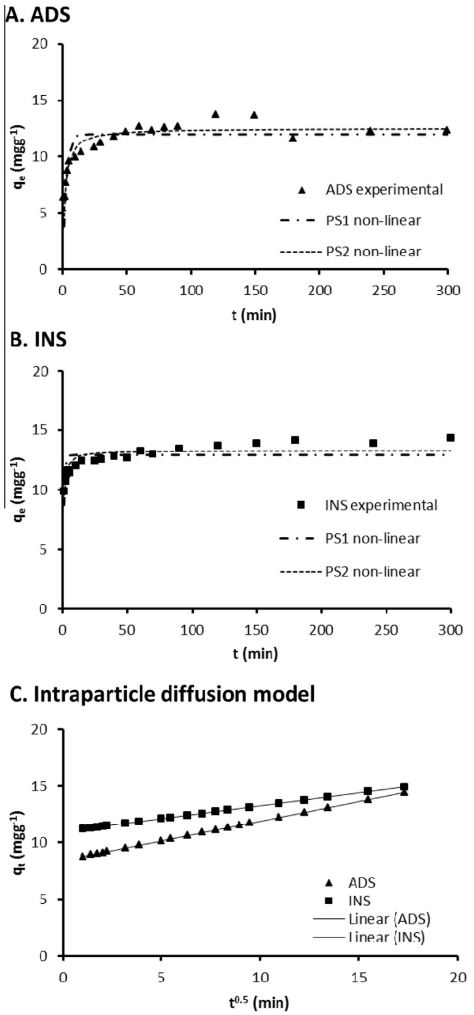

Fig. 4. Kinetic modeling of (A) ADS and (B) INS (PS1 = pseudo-first-order model, PS2 = pseudo-second-order model). (C) Intraparticle diffusion model of Pb(II) adsorption (ADS and INS). pH 5, dose 2 gl^{-1} and agitation speed: 100 rpm.

Author's personal copy

Table 3
Pseudo-first-order and pseudo-second-order non-linear models and intraparticle diffusion model parameters of Pb(II) adsorption by hydrochars ADS and INS.

Pseudo-first-order model (non-linear)					
Adsorbent	C_0 (mgl^{-1})	$q_{e,exp}$ ($mg\,g^{-1}$)	q_t ($mg\,g^{-1}$)	k_1 (min^{-1})	R^2
ADS	52.2	12.60	11.99	0.382	0.747
INS	51.0	13.69	12.89	1.122	0.440
Pseudo-second-order model (non-linear)					
Adsorbent	C_0 (mgl^{-1})	$q_{e,exp}$ ($mg\,g^{-1}$)	q_t ($mg\,g^{-1}$)	k_2 ($g\,mg\,min^{-1}$)	R^2
ADS	52.2	12.60	12.54	0.049	0.885
INS	51.0	13.69	13.27	0.160	0.766
Intraparticle diffusion model					
Adsorbent	C_0 (mgl^{-1})	k_{id} ($mg\,g^{-1}min^{-1/2}$)		C ($mg\,g^{-1}$)	
ADS	52.2	0.346		8.46	
INS	51.0	0.227		10.97	

kinetics for ADS compared to INS. Probably adsorption sites are better available in the case of ADS, which is consistent with the findings discussed earlier (surface area and porosity of ADS was greater compared to INS, Table 1). Part of the surface functionalities may be in unfavorable form for the adsorption of Pb(II). Then actual amount of surface functionalities available for adsorption process may be lower. Furthermore, to investigate if pore diffusion was the controlling step in the adsorption, intraparticle diffusion model was tested. q_t plotted against $t^{1/2}$ resulted straight lines not passing through the origin for both hydrochars (Fig. 4 and Table 3). This indicates that intraparticle diffusion was important but not the only rate determining step in the adsorption process. C values revealed some extent of boundary layer control, which seemed to be more evident for INS compared to ADS (Ayoob and Gupta, 2007; Azizian, 2004). Intercepts of ADS and INS were positive indicating rapid adsorption in a short period of time. Rate constants (k_{id}) of both hydrochars suggested rapid diffusion process (Wu et al., 2009).

4. Conclusion

Hydrochars prepared from anaerobically digested sludge (ADS) and industrial sludge (INS) via hydrothermal carbonization indicated significant adsorption efficiency towards Pb(II). ADS removed small amounts of Cr(VI), As(V) and As(III) as well. Adsorption of INS towards anionic compounds was low. Pb(II) adsorption (q_m = 11 mg g^{-1}) by ADS and INS was comparable, however, adsorption capacity of INS was slightly higher. Both hydrochars followed the Sips adsorption isotherm model, which allowed the best approximation of experimental data. Intraparticle diffusion seemed to be partly involved in adsorption processes. Hydrochars produced via HTC method indicated great potential as alternative low-cost adsorbents for the metal removal.

Acknowledgements

Authors are grateful to Finnish Funding Agency for Technology and Innovation (TEKES) for financial support. Emmanuelle Castagnoli is thanked for her valuable contribution to the experiments.

References

Ahn, C.K., Kim, Y.M., Woo, S.H., Park, J.M., 2009. Removal of cadmium using acid-treated activated carbon in the presence of nonionic and/or anionic surfactants. Hydrometallurgy 99, 209–213.
Allen, S.J., Mckay, G., Porter, J.F., 2004. Adsorption isotherm models for basic dye adsorption by peat in single and binary component systems. J. Colloid Interface Sci. 280, 322–333.
Ayoob, S., Gupta, A.K., 2007. Sorptive response profile of an adsorbent in the defluoridation of drinking water. Chem. Eng. J. 133, 273–281.
Azizian, A., 2004. Kinetic models of sorption: a theoretical analysis. J. Colloid Interface Sci. 276, 47–52.
Babel, S., Kurniawan, T.A., 2003. Low-cost adsorbents for heavy metal uptake from contaminated water – review. J. Hazard. Mater. 97, 219–243.
Bansal, R.C., Goyal, M., 2005. Activated Carbon Adsorption. Taylor & Francis Group, CRC Press, United States of America.
Bhatnagar, A., Sillanpää, M., 2010. Utilization of agro-industrial and municipal waste materials as potential adsorbents for water treatment – a review. Chem. Eng. J. 157, 277–296.
Bhatnagar, A., Hogland, W., Marques, M., Sillanpää, M., 2012. An overview of the modification methods of activated carbon for its water treatment applications. Chem. Eng. J. 219, 499–511.
Dias, J.M., Alvim-Ferraz, M.C.M., Almeida, M.F., Rivera-Utrilla, J., Sánchez-Polo, M., 2007. Waste materials for activated carbon preparation and its use in aqueous-phase treatment – review. J. Environ. Manage. 85, 833–846.
Do, D.D., 1998. Adsorption Analysis: Equilibria and Kinetics. Imperial College Press, London.
Funke, A., Ziegler, F., 2010. Hydrothermal carbonization of biomass: a summary and discussion of chemical mechanisms for process engineering. Biofuels, Bioprod. Biorefin. 4, 160–177.
Gu, L., Zhu, N., Zhou, P., 2012. Preparation of sludge derived magnetic porous carbon and their application in Fenton-like degradation of 1-diazo-2-naphthol-4-sulfonic acid. Bioresour. Technol. 118, 638–642.
Gupta, V.K., Carrott, P.J.M., Ribeiro, C., Suhas, M.M.L., 2009. Low-cost adsorbents: growing adsorbents to waste water treatment – a review. Environ. Sci. Technol. 39, 783–842.
Ho, Y.S., Porter, J.F., McKay, G., 2002. Equilibrium isotherm studies for the sorption of divalent metal ions onto peat: copper, nickel and lead single component systems. Water Air Soil Pollut. 141, 1–33.
Kadirvelu, K., Thamaraiselvi, K., Namasivayam, C., 2001. Adsorption of nickel(II) from aqueous solution onto activated carbon prepared from coir pith. Sep. Purif. Technol. 24, 497–505.
Kula, L., Ugurlu, M., Karaoglu, H., Celik, A., 2008. Adsorption of Cd(II) ions from aqueous solutions using activated carbon prepared from olive stone by $ZnCl_2$ activation. Bioresour. Technol. 99, 492–501.
Kumar, S., Loganathan, V.A., Gupta, R.B., Barnett, M.O., 2011. An assessment of U(VI) removal from groundwater using biochar produced from hydrothermal carbonization. J. Environ. Manage. 92, 2504–2512.
Li, Y.-H., Wang, S., Zhang, X., Wei, J., Xu, C., Luan, Z., Wu, D., 2003. Adsorption of fluoride from water by aligned carbon nanotubes. Mater. Res. Bull. 38, 469–476.
Libra, J.A., Ro, K.S., Kammann, C., Funke, A., Berge, N.B., Neubauer, Y., Titirici, M.M., Fühner, C., Bens, O., Kern, J., Emmerich, K.H., 2011. Hydrothermal carbonization of biomass residuals: a comparative review of the chemistry, processes and applications of wet and dry pyrolysis. Biofuels 2, 89–124.
Liu, Z., Zhang, F.S., 2009. Removal of lead from water using biochars prepared from hydrothermal liquefaction of biomass. J. Hazard. Mater. 167, 933–939.
Liu, Z., Zhang, F.S., 2011. Removal of copper(II) and phenol from aqueous solution using porous carbons derived from hydrothermal chars. Desalination 267, 101–106.
Park, S.-W., Jang, C.-H., 2011. Effects of carbonization and solvent-extraction on change in fuel characteristics of sewage sludge. Bioresour. Technol. 102, 8205–8210.
Repo, E., Warchol, J.K., Kurniawan, T.A., Sillanpää, M., 2010. Adsorption of Co(II) and Ni(II) by EDTA- and/or DTPA-modified chitosan: kinetic and equilibrium modeling. Chem. Eng. J. 161, 73–82.
Román, S., Valente Nabais, J.M., Ledesma, B., González, J.F., Laginhas, C., Titirici, M.M., 2013. Production of low-cost adsorbents with tunable surface chemistry by conjunction of hydrothermal carbonization and activation processes. Microporous Mesoporous Mater. 165, 127–133.
Singha, B., Kumar Das, S., 2012. Removal of Pb(II) ions from aqueous solution and industrial effluent using natural biosorbents. Environ. Sci. Pollut. Res. 19, 2212–2226.
Titirici, M.M., Antonietti, M., 2010. Chemistry and materials options of sustainable carbons materials made by hydrothermal carbonization. Chem. Soc. Rev. 39, 103–116.
Titirici, M.M., White, R.J., Falco, C., Sevilla, M., 2012. Black perspectives for a green future: hydrothermal carbons for environment protection and energy storage. Energy Environ. Sci. 5, 6796–6822.
Wilson, K., Yang, H., Seo, C.W., Marshall, W.E., 2006. Select metal adsorption by activated carbon made from peanut shells. Bioresour. Technol. 97, 2266–2270.
Wu, F.-C., Tseng, R.-L., Juang, R.-S., 2009. Initial behavior of intraparticle diffusion model used in the description of adsorption kinetics. Chem. Eng. J. 153, 1–8.

Publication II

S-M, Alatalo, E., Repo, E., Mäkilä, J., Salonen, M., Sillanpää.

Hydrothermal conversion of sludge into effective adsorbents for the removal of lead from aqueous media. Submitted.

Hydrothermal conversion of sludge into effective adsorbents for the removal of lead from aqueous media

Sara-Maaria Alatalo[1*]. Eveliina Repo[1]. Ermei Mäkilä[2], Jarno Salonen[2] and Mika Sillanpää[1]

[1] Laboratory of Green Chemistry. Department of Chemistry. Faculty of Technology. Lappeenranta University of Technology. Sammonkatu 12. FI-50130 Mikkeli. Finland

[2] Laboratory of Industrial Physics. Department of Physics and Astronomy. University of Turku. FI-20014 Turku University. Finland

[*]E-mail: sara-maaria.alatalo@lut.fi, Tel.: +358406843958(Corresponding author)

ABSTRACT

Hydrothermal carbonization is a beneficial waste conversion technique for the generation of novel, more value-added products for various industrial and environmental applications. In this study hydrothermally treated pulp and paper industry sludge (INS) and anaerobically digested sludge (ADS) prepared at different reaction temperatures were shown to adsorb heavy metal Pb(II) effectively. The maximum adsorption efficiency for INS and ADS based adsorbents was 15-40 mg/g and 12–27 mg/g respectively. Additionally, materials were found to follow Sips adsorption isotherm supporting idea of heterogeneous nature of adsorbent surface. Kinetics studies showed that equilibrium state was reached rapidly, within 100–150 min and adsorbents were found to follow the non-linear pseudo-second-order kinetic model indicating adsorption via chemical interaction.

KEY WORDS: Lead, Hydrochar, Low-cost Adsorbent, Hydrothermal carbonization, Adsorption

1. INTRODUCTION

Hydrothermal carbonization (HTC) has several advantages in environmental applications as a waste conversion technique. Reaction takes place in aqueous media under autogenous pressure (mild reaction temperatures 150-250 ˚C) allowing use of wider range of feedstock such as agricultural wastes (e.g. animal wastes), human wastes (e.g. waste water) and industrial by-products. Reason for restricted utilization of these materials in other more traditional techniques like pyrolysis is related to higher water content which many times require pre-treatment in order to reduce amount of water in the starting material [Titirici, 2013]. The use of HTC for waste conversion may significantly result reduce greenhouse gas emissions from sources such as landfills, composting facilities and waste water treatment plants by promoting carbon integration within hydrochars. Many countries are increasing the reuse and recycling of wastes to produce new value-added products, for which the HTC method may be advantageous [Titirici, 2013]. Moreover, this inexpensive environmentally friendly way to produce carbon based materials can be easily scaled up for industrial water treatment applications.

Quality of global water resources has declined in recent years and therefore water purification and water pollution issues are becoming ever more significant. In the purification of polluted water sources adsorption is one of the most widely used processes and activated carbon is commonly used adsorbent [Gupta et al., 2013]. However, besides adsorption numerous other techniques have been introduced for water purification and recycling purposes including screening, centrifugation, sedimentation, crystallization and gravity separation, precipitation, flotation, oxidation, evaporation, coagulation, solvent extraction, distillation, ion exchange, reverse osmosis, electrolysis and electrodialysis [Kurniawan et al., 2006; Fu et al, 2011; Rozada et al, 2008]. HTC-derived materials rich in surface functional groups are promising sources of

cheap, sustainable, and effective sorption materials for the removal of metal ions or organic pollutants. Water pollution by metal ions (e.g. chromium, zinc, nickel cadmium and arsenic) is known to be a serious worldwide environmental problem with significant impact on living organisms and the environment due to their high toxicity, non-biodegradability, and tendency to bioaccumulate through the food chain. The applicability of HTC-derived materials for metal ion removal from aqueous media has been studied for metal ions such as Pb(II), Cd(II), Cu(II), CrO_4(II) and Fe(III) [Titirici, 2013]. In these investigations carbohydrates were used as a starting material and the material properties were improved with additives [Demir-Cakan et al, 2010; Demir-Cakan et al., 2009] or post treatment at higher temperature [Chen et al., 2011]. However, there are only a few publications about the use of waste materials such as switchgrass [Regmi et al., 2012], pinewood and rice husks [Liu et al., 2009; Liu et al., 2010] as feedstock. The use of wastes as feedstock is beneficial from the point of view of recycling and the reduction of landfill, which is expected to be subject to strict legislative control in future. This creates a clear demand for alternative waste management techniques [Sitra, 2007; Chen et al., 2002].

The aim of this research was to clarify the effect of reaction temperature on the properties of HTC treated pulp and paper industry sludge and anaerobically digested sludge carbonaceous materials and to study the performance for Pb(II) removal from aqueous media. The effects of pertinent factors such as pH, adsorbent dosage and contact time on metal removal were examined. The Langmuir, Freundlich and Sips models were employed to simulate the adsorption equilibrium and the pseudo-first-order, pseudo-second-order and intraparticle diffusion models to investigate the adsorption kinetics.

2. MATERIALS AND METHODS

2.1 Carbonaceous material preparation

Pulp and paper industry sludge (total solids 38 wt.%, total N 17000 mg/kg, Phosphorus 2000 mg/kg)) and anaerobically digested sludge (total solids 27 wt.%, total N 42000 mg/kg, Phosphorus 34000 mg/Kg) were used as received. HTC treated carbonaceous materials were produced in a stainless steel high-pressure reactor (Mini bench top reactor 4560, Parr Instrument Company). The mini bench top reactor was composed of a reactor (volume 160 ml), thermocouple, manometer, stirrer and controller. This reactor was loaded with 70 wt.% of sludge and 30 wt.% of deionized water to a total sludge and water mixture load of 120 g. Reaction temperatures were 160 ºC, 200 ºC and 240 ºC and the reaction time was 12 h. The stirring speed was 60 rpm. The reactor was allowed to cool down after the reaction. The reaction mixture was vacuum filtrated and the solid carbonaceous material washed repeatedly with deionized water. Eventually, the carbonaceous material was dried at 80 ºC overnight and ground to finer powder for the further experiments. Carbonaceous materials were named as follows: INS = pulp and paper industry sludge, ADS = anaerobically digested sludge. The subscript refers to the operating temperature when the carbonaceous material was produced: 1= 160 ºC, 2= 200 ºC and 3= 240 ºC. For example INS_1 = pulp and paper industry sludge prepared at 160 ºC.

2.2 Characterization

The surface chemistry of the HTC treated carbonaceous materials were analyzed with Fourier transform infrared spectroscopy (FTIR Vertex 70 Bruker Corp.) with an integrated Diffuse

Reflectance Acessory EasiDiff^{TM} unit. Surface charge and isoelectric point (IEP) charge were determined by pH titration utilizing the Zetasizer Nano ZS (Malvern Instruments Ltd.). C, H, N and O elemental composition was determined with the Organic Elemental Analyzer Flash 2000 (Thermo Scientific). Ash content was defined by applying SFS-standard 3008. Field-Emission scanning electron microscopy (FE-SEM, Hitachi S-4800) was used for surface morphology examination.

Nitrogen adsorption isotherms at -196 ^{0}C were determined with TriStar 3000 (Micromeritics Inc.). The specific surface area was calculated from the adsorption branch of the isotherm using Brunauer-Emmett-Teller theory, and the total pore volume was taken from the adsorbed amount at a relative pressure of p/p_0=0.97. Metal content after adsorption was analyzed with the inductively coupled plasma optical emission spectrometry (ICP-OES) model iCAP 6300 (Thermo Electron Corporation, USA).

2.3 Batch Experiments

The applicability of HTC treated carbonaceous material for lead Pb(II) removal was determined using batch experiments. The effect of pH was studied in the pH range 3-6 at a metal concentration of 50 mg/l, diluted from 1000 mg/l stock solution which was prepared from the corresponding analytical grade salt $Pb(NO_3)_2$ (Merck). The metal solution pH was adjusted with 0.1 M NaOH or 0.1 M HNO_3 solutions. The adsorption dosage was 20 mg and the metal solution volume 10 ml. Agitation (200 rpm) was conducted during adsorption experiments using a rotary shaker (Ika KS 4000i). At the designated contact time (24 h), the carbonaceous material was separated from the solution using a 0.45 µm polypropylene syringe filter. The influence of adsorption dosage was tested with adsorbent amounts of 10, 20, 30 and 50 mg. The Pb(II) metal ion concentration was kept constant at 50 mg/l and the solution pH was adjusted to 5. Adsorption equilibrium studies were performed with varying metal concentrations: 5, 20, 40, 120, 160, 200, 240, 280, 320, 340 and 400 mg/l. In this experiment the amount of adsorbent was kept constant.

Pb(II) metal concentrations was analyzed at a wavelength of 220.353 nm by ICP-OES. The amount of metal ions adsorbed on hydrochars was calculated as follows:

$$q_e = \frac{(C_i - C_e)}{m} V \qquad (1)$$

Where q_e (mg/g) is equilibrium adsorption capacity, C_i and C_e (mg/l) are the initial and equilibrium ion concentrations, respectively, m (g) is the weight of the adsorbent, and V (l) is the volume of the solution.

Adsorption equilibrium isotherms were calculated according to the following equations:

Langmuir isotherm non-linear form:

$$q_e = q_m \frac{K_L C_e}{1+K_L C_e} \quad (2)$$

Where q_e is the equilibrium adsorption capacity, q_m is the theoretical maximum adsorption capacity and K_L is the affinity constant.

Freundlich isotherm equation non-linear form:

$$q_e = k_F C_e^{\frac{1}{n_F}} \quad (3)$$

In which k_F (Lmg/g) and n_F (mg/g) are Freundlich adsorption constants. The Freundlich adsorption isotherm is an empirical model which can be used for heterogeneous surface and multilayer adsorption [Liu et al., 2010].

Sips isotherm (Langmuir-Freundlich) equation:

$$q_e = q_m \frac{(K_S C_e)^{n_S}}{1+(K_S C_e)^{n_S}} \quad (4)$$

In which K_S (Lmg/g) is the affinity constant and n_S describes surface heterogeneity. When n_s equals unity, the Sips isotherm returns to the Langmuir isotherm and predicts homogeneous adsorption whereas at lower concentrations it reduces to Freundlich isotherm. Deviation of n_s from unity indicates a heterogeneous surface.

Adsorption kinetics were investigated with pseudo-first-order and pseudo-second-order models.

The non-linear pseudo-first-order model is expressed as:

$$q_t = q_e(1 - exp^{-kt}) \quad (5)$$

The pseudo-second-order model equation is:

$$q_t = \frac{q_e^2 k_2 t}{1+q_e k_2 t} \quad (6)$$

Where q_t and q_e (mg/g) are the adsorption capacity at time t (min) and at equilibrium, respectively, while k_1 (1/min) and k_2 (mg/gmin) are the pseudo-first-order and pseudo-second-order rate constants. Furthermore, importance of pore diffusion as a rate determining step in the adsorption was tested by the intraparticle diffusion model as follows:

$$q = k_{dif} t^{\frac{1}{2}} (+C) \quad (7)$$

Where k_{dif} (mg/gmin$^{1/2}$) is the rate constant of intraparticle diffusion and C represents the thickness of the boundary layer.

3. RESULTS AND DISCUSSION

3.1 Characterization

The characteristics of carbonaceous materials were investigated in order to understand more comprehensively their potential as adsorbents in water purification applications. Hydrothermal treatment of INS and ADS materials resulted fine light brown powderous material (Table 1). SEM imaging of prepared carbon materials revealed large micrometer sized particles with some surface roughness (Figure 1.).

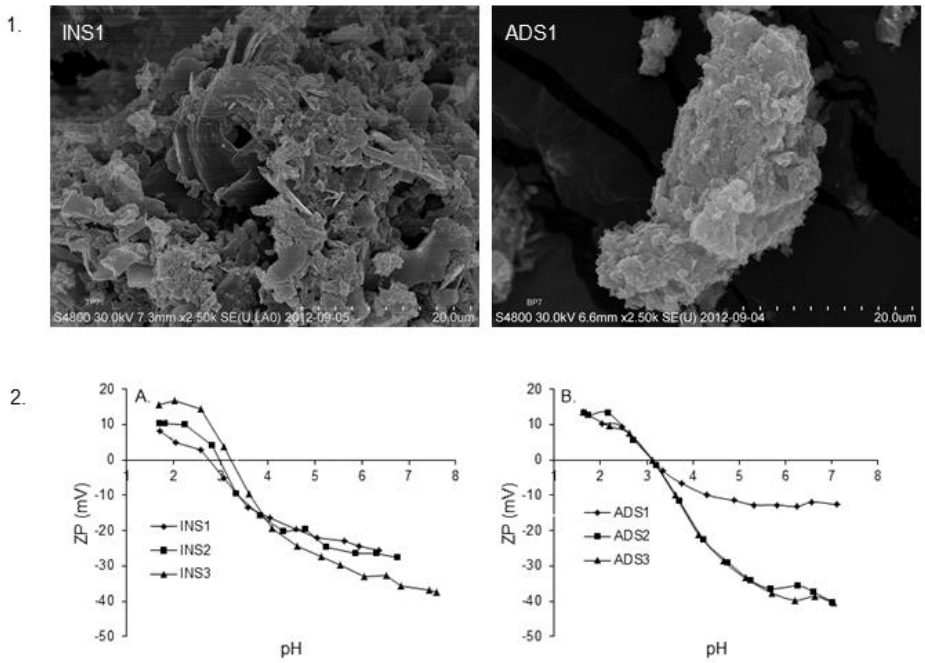

Figure 1. SEM images of 1. INS_1 and ADS_1 with 2.5k magnification and 2. pH_{IEP} titration curves of A. INS_1, INS_2 INS_3 and ADS_1, ADS_2, ADS_3 as a function of pH.

Surface morphology of ADS based adsorbents was relatively uniform whereas INS based adsorbents were clearly more heterogeneous in which morphological composition varied from spongy like spherical motifs to sheet like and fibrous structural motifs. Operational conditions did not indicate to have clear effect on the composition of surface morphology. Table 1 presents the elemental C, H, N and O compositions, ash contents, pH_{IEP}, surface area and pore volume of INS_1, INS_2, INS_3, ADS_1, ADS_2 and ADS_3. A determination of elemental composition revealed that carbon content did not change significantly when the pulp and paper industry sludge was treated at different temperatures (INS_1, INS_2 and INS_3).

Table 1. Elemental analysis data, pH_{IEP}, surface area and pore volume data of INS_1, INS_2, INS_3, ADS_1, ADS_2 and ADS_3. Image of ADS and INS adsorbents.

Sample	C (wt.%)	H (wt.%)	N (wt.%)	O (wt.%)	Ash (mg/g)	pH_{IEP}	Surface Area (m^2/g)	Pore Volume (cm^3/g)
INS_1	31.0	3.9	1.7	22.9	451.4	2.8	12.0	0.06
INS_2	33.9	3.7	1.7	17.3	452.8	3.0	15.9	0.07
INS_3	32.8	3.3	1.7	13.3	534.0	3.3	14.0	0.06
ADS_1	21.9	2.9	1.0	20.1	587.2	3.2	22.5	0.10
ADS_2	22.5	2.6	0.8	21.6	631.9	3.1	26.8	0.13
ADS_3	21.7	2.5	0.8	20.5	672.4	3.1	25.0	0.12

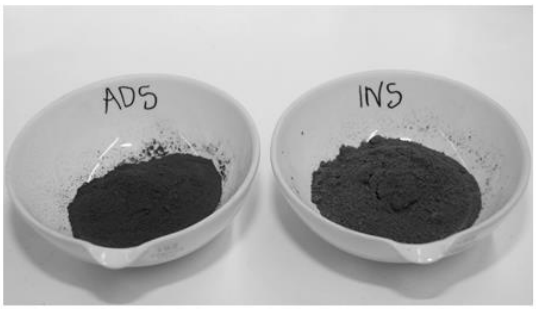

This differs from the earlier reported results in which HTC treated lignocellulosic biomass from an industrial palm oil process was used as feedstock by Parshetti *et al*: They detected a significant increase in carbon content when the operating temperature in the preparation of carbon material was increased from 150, to 250 and 350 ºC [Parshetti et al, 2013]. However, similarly to our research these authors also observed decrease in hydrogen and oxygen contents with increasing reaction temperature. This finding also supports the results from the determination of surface charge showing increase of pH_{IEP} values in order of $INS_1 < INS_2 < INS_3$ (Table 1. and Figure 1). Thus, treatment at higher temperatures makes adsorbent surfaces less acidic. Furthermore, the highest pH_{IEP} values obtained for INS_3 indicated its highest stability. Generally, increased operating temperature appears to result in higher ash content in the final product [Regmi et al.,

2012, Chen et al., 2002], which was also observed for INS based HTC treated carbonaceous materials. For ADS_1, ADS_2 and ADS_3 the elemental C, H, N and O composition remained rather same independently on the operating temperature during HTC. This may be related to the nature of the ADS (municipal anaerobically digested sludge) as a starting material. Anaerobic digestion of material involves the breakdown of organic wastes in the absence of oxygen leading to the release of gases and residual inorganic solid material. Unchanged pH_{IEP} also supported the constant amount of oxygen surface functional groups (Figure 1) although ADS_1 showed clearly lowest stability at neutral conditions. Notably, we obtained INS and ADS based carbonaceous materials with high amount of negative surface functional groups without any activation procedure, which is usually included in the preparation of activated carbon [Parshetti et al., 2013]. As is the case for INS based carbonaceous materials, the ash content of ADS based materials was observed to increase along with operation temperature, but the overall ash content was higher in ADS based carbonaceous materials.

Surface area and pore volume are shown to play a significant role in the adsorption processes together with surface functional groups [Moreno-Castilla et al., 2000]. The surface area of INS and ADS based carbonaceous materials was found 12-16 m^2/g and 22–27 m^2/g respectively, whereas pore volume was 0.06-0.07 cm^3/g and 0.10–0.13 cm^3/g, respectively. These quite low surface areas and pore volumes are peculiar for HTC treated materials. This may be due to the rather mild operating conditions, which are not drastic enough to improve surface properties. Additionally, pore blockage due to the presence of volatile matter not transferred into the liquid phase during HTC treatment or organic compounds from the liquid phase that migrate to the hydrochar surface may have an effect on the decreased surface area and pore volume [Chingombe et al., 2005, Ho et al., 2002]. Even though HCT treated carbonaceous materials tend to have lower

surface areas and pore volumes, it can be counterbalanced by greater surface functionality such as a presence of oxygen surface functional groups [Roman et al., 2013].

Surface functional groups were investigated by FTIR. The FTIR-spectra of INS based carbonaceous materials (INS_1, INS_2 and INS_3) showed a wide and strong intense peak at wavenumber 3400 cm^{-1} which is peculiar for O-H stretching. C=O stretch occurs at wavenumbers of 1800-1600 cm^{-1} where strong intense peaks were found with partial superimposing. It is probable that aromatics are present in the INS based carbonaceous materials. Peaks at wavenumbers 1650-1500 cm^{-1} indicated the presence of aromaticity in the material structure. Eventually aliphatic C-H bond stretching was found at wavenumbers of 3000-2800 cm^{-1} [Tascon, 2012]. Similar peaks were identified in the FTIR-spectra of ADS based carbonaceous materials (ADS_1, ADS_2 and ADS_3). A change in reaction temperature during material preparation was not observed to alter the peak positions between INS_1, INS_2 and INS_3 or ADS_1, ADS_2 and ADS_3. Yet, FTIR studies supported the theory that highly oxidized carbons were present in both prepared carbonaceous material types, although superimposing peaks made exact peak determination challenging.

3.2 Adsorption

3.2.1 Effect of pH

In adsorption, pH effects on the protonation of surface groups and the speciation of metal ions in the solution. Therefore optimal pH needs to be determined to maximize the removal of

target compounds. The adsorption performance of INS and ADS based carbonaceous materials as a function of pH is presented in Figure 2. Metal removal was found to increase along the pH (3-6). Maximum Pb(II) removal among examined carbonaceous materials was achieved at pH 5 or 6, which is in a good agreement with earlier studies [Chen et al., 2002]. With increasing pH, deprotonation of functional groups enabled co-ordination with Pb(II) resulting higher removal rate (see also Figure 1). Correspondingly the weaker adsorption of Pb(II) at lower pH is most probably related to the presence of H_3O^+ ions, which competed with Pb(II) ions for available adsorption sites [Kumar et al., 2011]. For later adsorption experiments conducted in this research an initial pH of 5 was chosen in order to achieve maximum Pb(II) removal capacity.

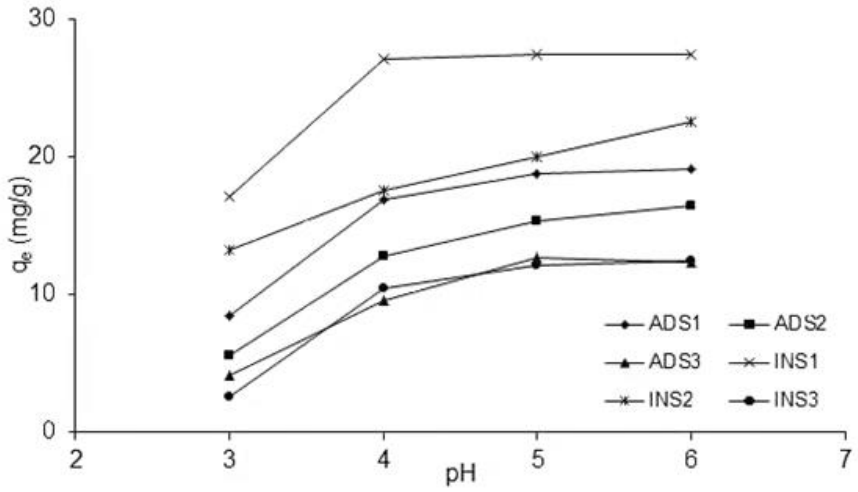

Figure 2. Effect of pH on the adsorption of Pb(II) by INS and ADS based carbonaceous materials INS_1, INS_2, INS_3, ADS_1, ADS_2 and ADS_3.

3.2.2 Effect of adsorbent dose on metal ion removal

The total Pb(II) removal capability of INS and ADS based adsorbents was examined with different adsorbent dosages (Figure 3). A constant increase in the percentage removal of Pb(II) ions was observed with increasing adsorbent dosage. INS_1 presented over 50 % Pb(II) removal efficiency when only 10 mg of adsorbent was used, while over 90 % removal was achieved with a dosage of 20 mg. Complete metal ion removal was reached when the adsorbent dosage was further increased. INS_2 presented over 50 % Pb(II) removal with 20 mg of adsorbent but removal efficiency was lower than for INS_1. ADS_1 and ADS_2 presented somewhat similar Pb(II) removal capability with increasing adsorbent dosage: Over 50 % Pb(II) metal removal when 20 mg of adsorbent was used and over 90 % Pb(II) removal when the adsorbent dosage was increased to 50 mg.

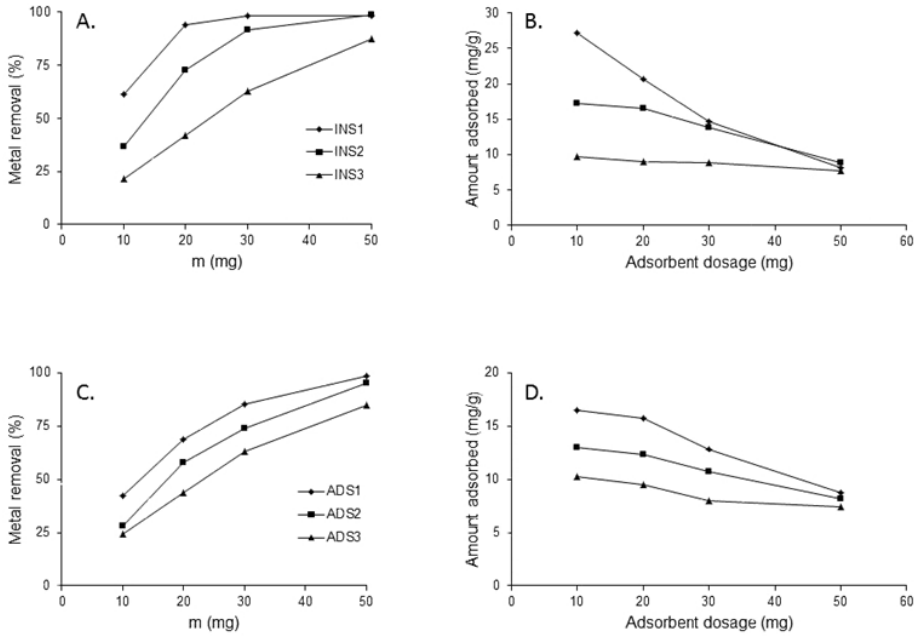

Figure 3. Effect of adsorbent dosage on the extent of Pb(II) removal by INS_1, INS_2 and INS_3 are presented in plots A. and B. and removal rates by ADS_1, ADS_2, ADS_3 are presented in plots C. and D. (The explanation of symbols in figures A. and C. is the same for plots B. and D.)

Higher metal removal levels with greater adsorbent dosage are related to an increased number of available adsorption sites. In contrast, a higher adsorbent dose will lead to a lower adsorption capacity when the Pb(II) concentration is kept constant. At lower adsorbent dosages, all types of available adsorption sites are entirely exposed and the surface is saturated faster, resulting higher maximum adsorption capacity (q_e) whereas at higher adsorbent dosages the availability of higher energy sites decreases as a larger fraction of lower energy sites become occupied, resulting in a lower q_e value [Kumar et al., 2011]. In addition, closer consideration of

the behavior of the adsorbents revealed that an increase in adsorption dosage changed the adsorption capacity of INS based carbonaceous materials more significantly than that of ADS based materials. Moreover there is more notable change in the adsorption capacity of INS_1 compared to those of INS_2 or INS_3 (Figure 3B). ADS based carbonaceous materials showed similar behavior but to a lesser extent (Figure 3D).

3.2.3 Modelling adsorption isotherms for one-component systems

The interaction between adsorbate and adsorbent can be analysed by adsorption isotherms, which define the relationship between the amount of adsorbate adsorbed per unit mass of adsorbent and adsorbate concentration in the solution phase at equilibrium conditions and constant temperature. The Langmuir, Freundlich, and Sips adsorption isotherms were used in this research to simulate the metal uptake of the adsorbents. The Langmuir and Freundlich isotherms are the most frequently used models to represent the equilibrium data of adsorption from aqueous solution. The Langmuir isotherm assumes that adsorption occurs at specific homogenous sites within the adsorbent without any interactions between the adsorbed substances [Gupta et al., 2008]. In contrast the Freundlich and Sips isotherms can be used for the modelling of heterogeneous adsorption processes.

Experimental adsorption equilibrium data and theoretical modelling of INS_1 and ADS_1 are presented in Figure 4. Data related to INS_2, INS_3 and ADS_2, ADS_3 can be found from the supporting information while experimental adsorption equilibrium data and theoretical modelling are presented in Figure S1. INS_1 appeared to be the most efficient for Pb(II) removal. The

experimental maximum adsorption capacity (q_e) was found to be circa 40 mg/g whereas the adsorption efficiencies of INS_2 and INS_3 were approximately 22 mg/g and 15 mg/g respectively.

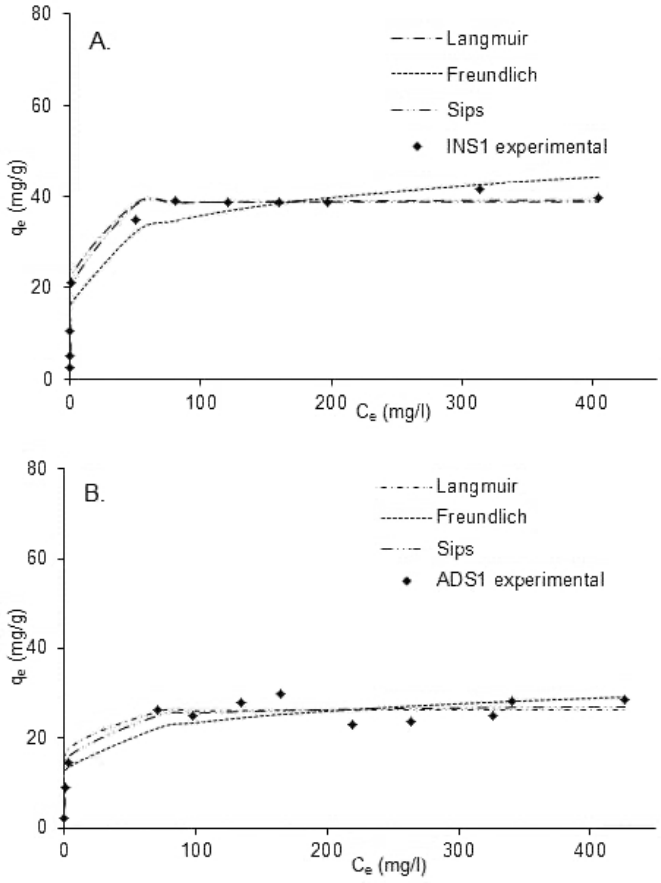

Figure 4. Adsorption equilibrium studies of A. INS_1 and B. ADS_1 for Pb(II) removal and modeling of the adsorption isotherms Langmuir, Freundlich and Sips. Adsorption equilibrium studies were performed at pH 5 and ambient temperature. The adsorbent dosage was 20 mg.

Changes in adsorption efficiency may be related to existence of oxygen surface functionalities, which enhance the cation exchange properties of the adsorbent. Both the adsorption efficiency and content of oxygen surface functional groups followed the order of INS_1>INS_2>INS_3. This supports the idea of surface functionalities may playing important role in adsorption compared to specific surface area, which in this case increased with temperature (INS_1<INS_2<INS_3). Theoretical modelling of the experimental adsorption equilibrium data of INS_1 indicated a rather good correlation with the Sips adsorption isotherm; its theoretical maximum adsorption capacity (q_m) corresponded well with experimental q_m. Furthermore the correlation coefficient (R^2) value shows that the Sips isotherm model can describe the adsorption data well (Table 2). The heterogeneity factor (n_s) differed slightly from unity, suggesting that INS_1 is rather homogeneous. Similarly to INS_1, data obtained with INS_2 and INS_3 also followed the Sips adsorption isotherm.

Table 2. Adsorption isotherm modeling parameters of Langmuir, Freundlich and Sips for Pb(II) removal of INS_1, INS_2, INS_3, ADS_1, ADS_2 and ADS_3.

	Langmuir			Freundlich			Sips			
Adsorbent	q_m (mg/g)	K_L (l/mg)	R^2	K_F (l/mg)	n_F	R^2	q_m (mg/g)	n_s	K_S (l/mg)	R^2
INS_1	38.9	2.16	0.982	17.8	6.58	0.922	39.4	0.77	1.77	0.985
INS_2	20.9	2.06	0.930	10.8	7.92	0.956	21.2	0.84	1.79	0.933
INS_3	14.0	0.49	0.806	6.6	7.04	0.782	15.5	0.49	0.44	0.838
ADS_1	26.4	0.76	0.928	11.7	6.62	0.936	28.4	0.53	0.61	0.965
ADS_2	14.6	0.45	0.839	7.1	7.38	0.777	15.5	0.58	0.51	0.857
ADS_3	11.9	0.56	0.844	5.8	7.31	0.892	14.9	0.35	0.26	0.928

ADS_1 removed Pb(II) most efficiently from the ADS based adsorbents, with an experimental adsorption capacity 27 mg/g, whereas the maximum adsorptions of ADS_2 and ADS_3 were 15 mg/g and 12 mg/g respectively. The weaker adsorption performance of ADS based compared to INS based carbonaceous materials was unexpected due to their higher pore volume, larger surface area and higher number of oxygen functional groups. Yet, inorganic matter content was significantly higher in ADS based carbonaceous materials than in the corresponding INS materials, which may partly explain their weaker adsorption performance. The Sips adsorption isotherm appeared to give the best correlation to the experimental adsorption data of ADS_1, ADS_2 and ADS_3. Theoretical q_m values matched rather well with those obtained experimentally, despite the minor scattering of data points indicated by the lower R^2 values. It should be noted, that n_s values obtained for ADS based materials deviated more from unity than those for INS based materials. This indicates that the adsorption took place on more heterogeneous surface, which is supported by the higher inorganic matter content of the ADS based adsorbents.

3.2.4 Adsorption Kinetics

Several steps occur in the adsorption process before the equilibrium state [Figueiredo et al., 1999; Plazinski et al, 2009]. At first, the adsorbate needs to travel closer to the adsorbent surface which can be enhanced by effective mixing. Secondly, adsorbates must diffuse through a layer around adsorbent before reaching the adsorbent surface. This is related to phenomenon in which solution properties around adsorbent differ from bulk phase solution. This stage is known as film or boundary diffusion. Thirdly, many adsorbents are porous therefore diffusion of the adsorbates in pores can have a major impact on the rate of adsorption. Finally, after reaching the

active site on the adsorbent, the adsorbate is bound to it via chemical or physical surface reaction. Normally the effect of bulk diffusion is eliminated by vigorous stirring, but the contribution of all the other stages should be investigated. Therefore different pseudo kinetic- and diffusion based models have been developed to evaluate the rate determining step of the adsorption [Plazinski et al., 2009]. Similarly to adsorption isotherms, adsorption kinetics have most often been fitted by the two simplest models: Pseudo-first (PS1) and pseudo-second-order (PS2). PS1 is associated with one-site adsorption governed by the rate of the surface reaction whereas PS2 represents two-site occupancy adsorption. The experimental adsorption kinetic data obtained for INS and ADS based materials as well as modelling results are presented in Figures 5, 2S and 3S.

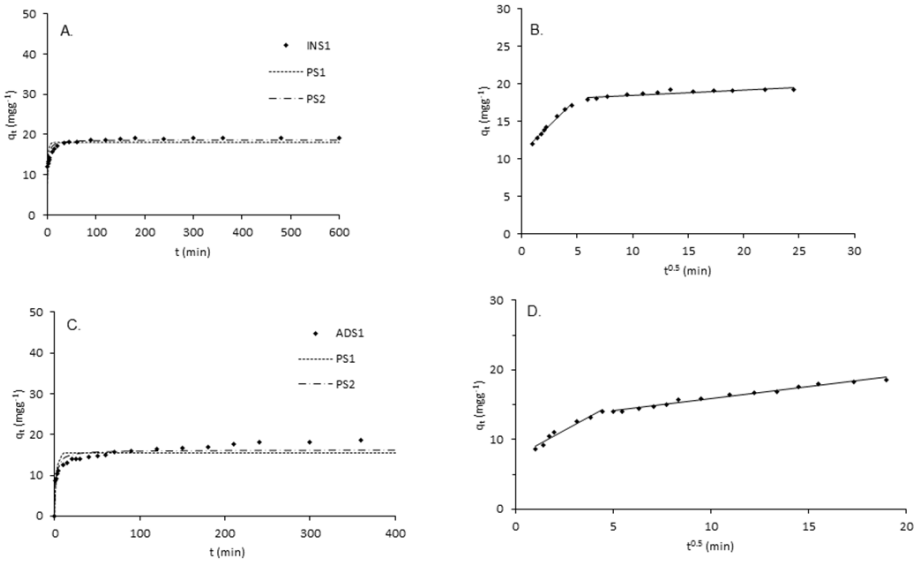

Figure 5. Pseudo-first-order non-linear (PS1), pseudo-second-order non-linear (PS2) kinetic intraparticle diffusion model for Pb(II) adsorption of: A. Experimental kinetic data, PS1 and PS2 models INS_1; B. Intraparticle diffusion model INS_1; C. Experimental kinetic data, PS1 and PS2 models ADS_1; D. Intraparticle diffusion model ADS_1.

The PS2 model has been reported to fit better to experimental data more often than the PS1 model. It has also been shown that PS2 can estimate experimental q_e values relatively well and is not very sensitive to arbitrary errors [Figueiredo *et al.*, 1999]. Accordingly, the reaction kinetics of INS_1, INS_2 and INS_3 were observed to follow the non-linear PS2 model rather than non-linear PS1, indicating that the adsorption process was governed by the surface reaction (Table 3). Data obtained for INS_1 fitted the PS2 model especially well, with a correlation coefficient (R^2) close to unity. INS_2 and INS_3 also appeared to favor the PS2 model but their R^2 values were rather low.

Adsorption capacity (q_e) decreased in the order of INS_1>INS_2>INS_3 as seen also from the adsorption equilibrium results. Similarly, ADS_1, ADS_2 and ADS_3 appeared to follow the PS2 model rather than the PS1 model. INS and ADS based adsorbents reached reaction equilibrium relatively rapidly within 100-150 min [Ho *et al.* 2000]. Grinding of the carbonaceous material may also increase the adsorption rate but this does not impact on the adsorption capacity [Eckenfelder, 2000]. Percentual removal rate of Pb(II) decreased in order INS_1>INS_2>INS_3 (4S.). INS_1 reached 99.9 % removal Pb(II) whereas corresponding ADS_1 reached only 70 % removal rate. In general Pb(II) removal efficiency of ADS based adsorbents was weaker compared to INS based adsorbents. Decreasing trend in adsorption efficiency between ADS_1, ADS_2 and ADS_3 was steadier than in case of INS based adsorbents.

Table 3. Pseudo-First-Order (PS1) and Pseudo-second-order (PS2) non-linear models and intraparticle diffusion model parameters of Pb(II) adsorption by hydrochars INS_1, INS_2, INS_3, ADS_1, ADS_2 and ADS_3.

	PS1 non-linear			PS2 non-linear			Intraparticle diffusion model	
	q_e (mg/g)	k (1/min)	R^2	q_e (mg/g)	k (g/mgmin)	R^2	K_{dif1} (mg/gmin$^{1/2}$)	K_{dif2} (mg/gmin$^{1/2}$)
INS_1	18.0	0.57	0.876	18.6	0.06	0.962	1.50	0.07
INS_2	18.6	0.82	0.923	19.01	0.08	0.952	0.56	0.25
INS_3	11.6	0.70	0.899	11.8	0.13	0.933	0.78	0.22
ADS_1	15.6	0.42	0.818	16.12	0.04	0.934	1.50	0.34
ADS_2	12.6	0.28	0.829	13.26	0.03	0.907	1.47	0.29
ADS_3	11.6	0.47	0.774	12.01	0.06	0.860	0.99	0.33

Intraparticle diffusion was used to examine importance of different diffusion stages on the adsorption process [Eckenfelder, 2000]. Modelling of intraparticle diffusion showed two step adsorption for both adsorbent types INS and ADS in which first step indicates external surface adsorption or boundary layer diffusion of solute molecules followed by gradual adsorption to

pores. Significance of diffusion rate K_{diff1} appear to decrease along with adsorbent type in order INS_1>INS_2>INS_3 and ADS_1>ADS_2>ADS_3 (Table 3.). Additionally, positive intercepts obtained for the studied adsorbents indicated rapid adsorption in a short period of time [Saadat et al., 2014; Alatalo et al., 2013].

4. CONCLUSION

It has been demonstrated that HTC is an economical and straightforward technique for converting inexpensive and easily available starting materials to carbonaceous adsorbents with potential water treatment properties. In this study, promising results were obtained with the maximum adsorption efficiency for INS based carbonaceous materials 15-40 mg/g and for ADS based materials 12–27 mg/g. The Sips adsorption isotherm fitted greatly to the experimental equilibrium data corresponding to heterogeneous adsorption. Study of the reaction kinetics revealed that Pb(II) adsorption of the both INS and ADS materials followed quite closely pseudo-second-order non-linear model suggesting chemical reaction being the rate determining step. Overall, in the present study, novel low-cost adsorbents for water treatment purposes were successfully produced and they could find a place in practical applications.

ACKNOWLEDGEMENTS

The authors are grateful to the Finnish Funding Agency for Technology and Innovation (TEKES) for their financial support.

REFERENCES

Alatalo, S-M, Repo, E., Mäkilä, E., Salonen, J., Vakkilainen, E., Sillanpää, M. (2013). Adsorption behaviour of hydrothermally treated municipal sludge & pulp and paper industry sludge. Bioresour. Technol. 147, 71-76.

Chen, Z., Ma, L., Li, S., Geng, J., Song, Q., Liu, J., Wang, C., Wang, H., Li, J., Li, Z. Q. S. (2011). Simple approach to carboxyl-rich materials through low-temperature heat treatment of hydrothermal carbon in air. Appl. Surf. Sci. 257, 8686-8691.

Chen, X., Jeyaseelan, S., Graham, N. (2002). Physical and chemical properties of the study of activated carbon made from sewage sludge. Waste Manage. 22, 755-760.

Demir-Cakan, R., Makowski, P., Antonietti, M., Goettmann, F., Titirici, M-M. (2010). Hydrothermal Synthesis of Imidazole Functionalized Carbon Spheres and their Application in catalysis. Catalysis today 150,115-118.

Demir–Cakan, R., Baccile N., Antonietti M., Titirici M-M. (2009). Carboxylate-rich carbonaceous materials via one-step hydrothermal carbonization of glucose in the presence of acrylic acid. Chem. Mater. 21, 484-490.

Chingombe, P., Saha, B., Wakeman, R.J. (2005). Surface modification and characterization of a coal-based activated carbon. Carbon 43, 3132-3143.

Eckenfelder, W.W. (2000). Industrial water pollution control 3rd edition, McGraw-Hill, p. 422

Figueiredo, J.L., Pereira, M.F.R., Freitas, M. M. A., Orfao, J. J. M. (1999). Modification of the surface chemistry of activated carbons. Carbon 37, 1379-1389.

Fu, F., Wang, Q. (2011) Removal of heavy metal ions from wastewaters: A review. J. Environ. Manag. 92, 407-418.

Gupta, V.K., Ali, I. (2013). Environmental water: Advances in treatment, remediation and recycling, Elsevier, p. 30.

Gupta, V.K., Rastogi, A. (2008). Biosorption of lead from aqueous solutions by green algae *Spirogyra* species: Kinetics and equilibrium studies. J. Hazard. Mater. 152, 407-414.

Ho, Y.S., Porter, J.F., McKay G. (2002). Equilibrium Isotherm Studies for the Sorption of Divalent Metal Ions Onto Peat: Copper, Nickel and Lead Single Component Systems. Water Air Soil Pollut. 141, 1-33.

Kumar, S., Loganathan V.A., Gupta, R.B., Barnett, M.O. (2011). An Assessment of U(VI) Removal from Groundwater Using Biochar Produced from Hydrothermal Carbonization. J. Environ. Manage. 92, 2504-2512.

Kurniawan, T.A., Chan, G. Y. S., Lo, W-H., Babel, S. (2006). Physico-Chemical treatment techniques for wastewater laden with heavy metals. Chem. Eng. J. 118, 83-98.

Liu Z., Zhang, F.S. (2009). Removal of lead from water using biochars prepared from hydrothermal liquefaction of biomass. J. Hazard. Mater. 167, 933-939.

Liu Z., Zhang F.S., Wu J. (2010). Characterization and application of chars produced from pinewood pyrolysis and hydrothermal treatment. Fuel 89, 510-514.

Moreno-Castilla C., López-Ramón M.V., Carrasco-Marín F. (2000). Changes in surface chemistry of activated carbons by wet oxidation. Carbon 38, 1995-2001.

Regmi P., Moscoso J.L.G., Kumar S., Cao X., Mao J., Schafran G. (2012). Removal of copper and cadmium from aqueous solution using switchgrass biochar produced via hydrothermal carbonization process. J. Environ. Manage. 109, 61-69.

Roman, S., Valente Nabais, J.M., Ledesma, B., Gonzáles, J.F., Laginhas C., Titirici MM. (2013). Production of low-cost adsorbents with tunable surface chemistry by conjuction of HTC and activation processes. Micropor. and Mesopor. Mat. 165, 127-133.

Rozada, F., Otero, M., Moran, A., García, I. (2008). Adsorption of heavy metals onto sewage sludge-derived materials. Bioresour. Technol. 99, 6332-6338.

Saadat, S., Karimi-Jashni, A., Doroodmand, M.M. (2014). Synthesis and characterization of novel single-walled carbon nanotubes- doped walnut shell composite and its adsorption performance for lead in aqueous solutions. J. Environ. Chem. Eng. 2, 2059-2067.

Sitra (2007). Lietteen käsittely Suomessa ja käsittelymenetelmien kilpailukyky selvitys, Helsinki.

Tascon J.M.D. (2012). Novel carbon adsorbents Elsevier, p. 376.

Titirici, M-M. (2013). Sustainable Carbon materials from hydrothermal processes. Wiley, p. 295-297.

Parshetti GK., Hoekman SK., Balasubramanian R. (2013). Chemical, structural and combustion characteristics of carbonaceous products obtained by hydrothermal carbonization of palm empty fruit bunches. Bioresour. Technol. 135, 683-689.

Plazinski, W., Rudzinski, W., Plazinska, A. (2009). Theoretical models of sorption kinetics including a surface reaction mechanism: A review. Adv. Colloid Interface Sci. 152, 2-13.

Publication III

S-M. Alatalo, F. Pileidis, E. Mäkilä, M. Sevilla, E. Repo, J. Salonen, M. Sillanpää and M-M. Titirici

Versatile cellulose based carbon aerogels for the removal of both cationic and anionic metal contaminants from water

Reprinted with permission from
Journal applied materials and interfaces
Vol. 7, 2015
© 2015, American Chemical Society

ACS APPLIED MATERIALS & INTERFACES

Research Article

www.acsami.org

Versatile Cellulose-Based Carbon Aerogel for the Removal of Both Cationic and Anionic Metal Contaminants from Water

Sara-Maaria Alatalo,[*,†] Filoklis Pileidis,[‡,§] Ermei Mäkilä,[∥] Marta Sevilla,[⊥] Eveliina Repo,[†] Jarno Salonen,[∥] Mika Sillanpää,[†] and Maria-Magdalena Titirici[*,‡,§]

[†]Laboratory of Green Chemistry, Department of Chemistry, Lappeenranta University of Technology, Sammonkatu 12, FI-50130 Mikkeli, Finland

[‡]School of Materials Science and Engineering, Queen Mary University of London, Mile End Road, E1 4NS, London, United Kingdom

[§]Materials Research Institute, Queen Mary University of London, Mile End Road, E1 4NS, London, United Kingdom

[∥]Laboratory of Industrial Physics, Department of Physics and Astronomy, University of Turku, FI-20014 Turku, Finland

[⊥]Instituto Nacional del Carbón (CSIC), P.O. Box 73, 33080 OVIEDO, Spain

Supporting Information

ABSTRACT: Hydrothermal carbonization of cellulose in the presence of the globular protein ovalbumin leads to the formation of nitrogen-doped carbon aerogel with a fibrillar continuous carbon network. The protein plays here a double role: (i) a natural source of nitrogen functionalities (2.1 wt %) and (ii) structural directing agent (S_{BET} = 38 m^2/g). The applicability in wastewater treatment, namely, for heavy metal removal, was examined through adsorption of Cr(VI) and Pb(II) ion solely and in a mixed bicomponent aqueous solutions. This cellulose-based carbogel shows an enhanced ability to remove both Cr(VI) (~68 mg/g) and Pb(II) (~240 mg/g) from the targeted solutions in comparison to other carbon materials reported in the literature. The presence of competing ions showed little effect on the adsorption efficiency toward Cr(VI) and Pb(II).

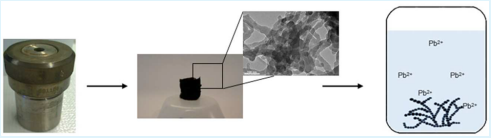

KEYWORDS: *adsorption, hydrothermal carbonization, carbon aerogel, heavy metals removal, water purification*

1. INTRODUCTION

A rapid industrialization, population expansion, and unplanned urbanization have caused a severe worldwide pollution of water and the surrounding soils. The main sources of freshwater pollution can be attributed to discharge of untreated sanitary and toxic industrial wastes, dumping of industrial effluents, and runoff from agricultural fields.[1] Heavy metals are one of the most significant groups of pollutants causing severe environmental (e.g., aquatic life) and public health problems because of their stability, persistency, and therefore, accumulation tendency.[2]

Metal pollution in the environment is the result of the direct or indirect release of metal containing waste waters especially in developing countries from industries such as metal plating facilities, mining operations, fertilizer and pesticide production, tanneries, and battery and paper industries.[3] The origin of heavy metals in natural waters is frequently attributed to improper disposal of industrial wastes. Because of mobility and toxicity, they have been classified as priority pollutants. For example, lead (Pb(II)) is known to cause encephalopathy, cognitive impairment, behavioral disturbances, kidney damage, anemia, and toxicity to the reproductive system for humans,[4] whereas chromium, particularly Cr(VI), is known to be carcinogenic and mutagenic.[5]

There are several techniques available for metal removal from waste effluents with varying degree of efficiency. These include adsorption, coagulation, foam flotation, filtration, ion exchange, aerobic and anaerobic treatment, advanced oxidation process (AOP), solvent extraction, electrolysis, and microbial reduction.[1,6] Compared to other processes, the adsorption process is considered to be better because of its convenience, ease of operation, and simple design. Activated carbons have been one of the most popular and widely used adsorbents in wastewater treatment, with good performance for the removal of organic pollutants, whereas their applicability for the removal of inorganics is limited.[7] Notably, the production conditions of activated carbons are rather harsh, including multistep processes and low product yields.[3,8−11] Because of drawbacks related to the production and use of activated carbons, alternative materials from readily available, renewable sources and softer condensation/production routes are required.[12] In this regard, hydrothermal carbonization provides an interesting approach toward the synthesis of sustainable functional carbons.[13] Hydrothermal carbonization (HTC) takes place in water at moderate temperatures between 180 and 250 °C under self-generated pressure, leading to carbonaceous materials with different shapes and sizes.[14,15] These carbonaceous materials are typically rich in oxygenated surface functional groups

Received: September 4, 2015
Accepted: November 5, 2015
Published: November 5, 2015

ACS Publications © 2015 American Chemical Society

DOI: 10.1021/acsami.5b08287
ACS Appl. Mater. Interfaces 2015, 7, 25875−25883

originating from gentle reaction conditions in which precursors like carbohydrates decompose to hydroxymethylfurfural (HMF) followed by reaction cascade comprising ring-opening reactions, substitutions, cycloadditions, and polycondensation to form final hydrophilic carbon.[16] Additionally, when globular proteins such as ovalbumin are used during HTC, nitrogen functionalities can be introduced into the carbonaceous network. These proteins form thermally induced aqueous gels when heated above the denaturation temperature. Furthermore, such proteins undergo Maillard reactions via co-condensation with the cellulose decomposition products leading to the formation of nitrogen-doped carbon scaffolds.[17] Their surface chemistry can be further modified by thermal treatment or post functionalization.[18,19] This in situ "one-step" functionalization is a readily practical solution, just implying the use of precursors or coreactants containing the desired functionalities.[20]

In this study, we present the hydrothermal synthesis of nitrogen-rich carbon materials from a sustainable, readily available, and inexpensive precursor cellulose. Ovalbumin from chicken egg white was used as a natural nitrogen source and structure directing agent in the formation of final carbon material. Pollutant removal from aqueous media is a potential application for this produced carbon material. Thereby, its ability to remove cationic and anionic metal pollutants from the aqueous media was studied. Lead, Pb(II), and chromium, Cr(VI), were selected as model pollutants. Adsorption behavior was studied with one-component and two-component solutions. Competing pollutants for Pb(II) and Cr(VI) in two-component solutions were Cu(II) and As(V), respectively. In addition kinetic studies were performed and modeled.

2. EXPERIMENTAL PROCEDURE

2.1. Synthesis. Carbogels were produced from microcrystalline cellulose (Sigma-Aldrich). Cellulose was mixed with ovalbumin (from chicken egg white, grade II, supplier Sigma-Aldrich) and water at the ratio of 1:0.5:9 (w/w/w), respectively.[17] Concentrated H_2SO_4 (Sigma-Aldrich) was added to the reaction mixture to catalyze degradation of cellulose.[21] With this aim, H_2SO_4 and H_2O were first mixed and the solution was allowed to cool down before addition of cellulose and ovalbumin. Then, the reaction mixture was placed in a glass inlet, sealed in a Teflon-lined autoclave and placed in the oven, which was preheated to 180 °C. The autoclave was kept in the oven for 5.5 h. After the reaction, the autoclave was allowed to cool down naturally. Carbonaceous products were removed from the glass inlet, washed extensively with deionized water, and finally freeze-dried.

2.2. Characterization. Determination of the surface area and pore volume was performed via N_2 sorption analysis at −196 °C with TriStar 3000 (Micromeritics Inc.). Apparent surface area was calculated by the BET method and the micropore surface area was evaluated by t-plot method. The total pore volume was determined from the amount of nitrogen adsorbed at p/p_o = 0.97. The pore size distribution was calculated with nonlocal density functional theory (NLDFT) assuming slit-shaped pores. Functional groups were analyzed through Fourier transform infrared spectroscopy (FTIR) performed on a Tensor 27 Bruker with attenuated total reflectance unit (ATR). Surface morphology was studied with FEI Quanta 3D environmental scanning electron microscope (ESEM) and JEOL JEM-2010 transmission electron microscopy (TEM) operating at 200 kV. Total acidity of the carbon materials was estimated mixing 50 mg of each carbon materials with 20 mL of 0.01 M NaOH. The suspension was mixed 1 h at room temperature. Then, it was filtrated and remaining NaOH solution was titrated with 0.01 M HCl solution in which phenolphthalein was used as indicator.[22,23] Total basicity was determined with a similar procedure in which 0.01 M HCl solution was mixed with carbon material and finally titrated with 0.01 M NaOH using methyl orange as indicator. Elemental composition of carbon materials was determined with Vario EL elemental analyzer and types of surface functional groups were analyzed by X-ray photoelectron spectroscopy (XPS) performed on a Specs spectrometer using Mg Kα (1253.6 eV) radiation from a double anode at 150 W. Binding energies for the high-resolution spectra were calibrated by setting C 1s at 284.6 eV. A nonlinear least-squares curve fit with a Gaussian−Lorentzian mix function and Shirley background subtraction, was used to deconvolute the XPS spectra. ^{13}C solid-state magic angle spinning (MAS) nuclear magnetic resonance spectra (NMR) have been acquired on Bruker Avance 300 MHz (7T) spectrometer using 4 mm zirconia rotors sipping at a MAS frequency of vMAS= 14 kHz. Chemical shifts were referenced relative to tetramethylsilane (TMS; δ= 0 ppm). Surface charge and zeta potential were determined by pH titration utilizing the Zetasizer Nano ZS (Malvern Instruments Ltd.)

2.3. Adsorption. Batch experiments were performed to study adsorption behavior of hydrothermal carbons/hydrochars toward Cr(VI) and Pb(II). The effect of pH was studied in the range of 3−6 at 50 mg/L metal concentration. Metal solutions were diluted from the corresponding 1000 mg/L stock solutions. Metal salts used in the adsorption studies were of analytical grade: $K_2Cr_2O_7$ (Sigma-Aldrich), $Pb(NO_3)_2$ (Merck), As_2O_5 (Alfa Aesar), and $Cu(NO_3)_2{\cdot}3H_2O$. The pH of the solutions was adjusted with 0.1 M HNO_3 or 0.1 M NaOH. The amount of adsorbent in the adsorption studies was 20 mg, and it was mixed with 10 mL of metal solution. This suspension was agitated (200 rpm) at ambient temperature by a rotary shaker (Ika KS 4000i) for 24 h. After agitation, the carbonaceous material was separated from the solution using a 0.45 μm polypropylene syringe filter before further analysis.

Adsorption equilibrium studies of one-component tests were performed with varying metal ion concentrations in the 5−1500 mg/L range. Bicomponent tests were conducted from metal solutions containing between 0.5 and 3.0 mmol/L Cr(VI)/As(V) and Pb(II)/Cu(II). These solutions were diluted from the 5 mmol/L stock solutions (5 mmol/L = 260 mg/L Cr(VI)/375 mg/L As(V) and 1036 mg/L Pb(II)/318 mg/L Cu(II)).

The metal concentrations of the filtrated solutions after adsorption were analyzed at a wavelength of 283.5 nm (Cr), 220.353 nm (Pb), 189.042 (As), and 324.7 nm (Cu) with inductively coupled plasma optical emission spectrometry (ICP-OES). The amount of metal ions adsorbed per unit mass of hydrochars was calculated as

$$q_e = \frac{(C_i - C_e)}{m} V \tag{1}$$

where q_e (mg/g) is equilibrium adsorption capacity, C_i and C_e (mg/L) are the initial and equilibrium ion concentrations, respectively, m (g) represents the weight of the adsorbent, and V (L) is the volume of the solution.

Sips adsorption isotherm was used to model the experimental data obtained in one-component systems. Equation for Sips isotherm is

$$q_e = \frac{q_m (K_S C_e)^{n_S}}{1 + (K_S C_e)^{n_S}} \tag{2}$$

in which K_S (L/mg) is the affinity constant and n_S describes the surface heterogeneity, which can arise from the solid or adsorbate or a combination of both. When n_s equals unity, the Sips isotherm transforms into the Langmuir isotherm and predicts homogeneous adsorption. Alternatively the deviation of n_s from unity indicates a heterogeneous surface; the larger the parameter, the more heterogeneous is the system. At high concentrations, Sips approaches a constant value and at low concentrations, a Freundlich-type equation.

In the modeling of two-component system, extended Sips isotherm was used to evaluate the adsorption performance

$$q_{e1} = \frac{q_{m1} (K_{S1} C_{e1})^{n_{S1}}}{1 + (K_{S1} C_{e1})^{n_{S1}} + (K_{S2} C_{e2})^{n_{S2}}} \tag{3}$$

DOI: 10.1021/acsami.5b08287
ACS Appl. Mater. Interfaces 2015, 7, 25875−25883

$$q_{e2} = \frac{q_{m2}(K_{S2}C_{e2})^{n_{S2}}}{1 + (K_{S1}C_{e1})^{n_{S1}} + (K_{S2}C_{e2})^{n_{S2}}} \quad (4)$$

where K_{S1} and K_{S2} (L/mmol) are similar to the Langmuir affinity constant and n_{S1} and n_{S2} are the heterogeneity constants. Similarly to the case of one-component Sips model, deviation of n_{S1}/n_{S2} from the unity indicates heterogeneous adsorption.

Modeling of adsorption kinetics was conducted by using pseudo-second-order model. The nonlinear pseudo-second-order model is expressed as

$$q_t = \frac{q_e^2 k_2 t}{1 + q_e k_2 t} \quad (5)$$

where q_t and q_e (mg/g) are the adsorption capacity at time t (min) and at equilibrium respectively, while k_2 (g/mg min) is the pseudo-second-order rate constant. Furthermore, pore diffusion as a controlling step in the adsorption was considered by intraparticle diffusion model as

$$q_t = k_{dif} t^{1/2} (+C) \quad (6)$$

where k_{dif} (mg/g min$^{1/2}$) is the rate constant of intraparticle diffusion and C represents the thickness of the boundary layer.

3. RESULTS AND DISCUSSION

3.1. Characterization of Hydrothermal Carbons.

Cellulose-based carbogel (CeOvaS) were produced via hydrothermal carbonization using microcrystalline cellulose as a starting material. The reaction was performed in a closed batch reactor, which was placed into the preheated oven (180 °C) and kept there for 5.5 h. Cellulose is a polymer formed by single glucose units linked together with $\beta(1\rightarrow4)$-glycosidic bonds and intermolecular hydrogen bonding.[24] These structural features make the hydrolysis of cellulose into glucose and further dehydration to hydroxymethylfurfural (HMF) difficult; however, dehydration can be catalyzed at lower pH.[25] With this aim, H_2SO_4 was added to the reaction mixture. On the other hand, ovalbumin had in this case a dual role, that is, structure directing agent and natural nitrogen source.[17,26] Indeed, globular proteins, such as ovalbumin, form thermally induced aqueous gels by heating above the denaturation temperature, while Maillard reactions allow its co-condensation with HMF at the initial state of development of the carbonaceous network.[27]

After the HTC process, firm/stable, dark brown colored monolith was obtained, as shown in Figure 1a corresponding to a wet carbogel. SEM and TEM images of CeOvaS are presented in Figures 1b and 1c, respectively. CeOvaS shows greatly branched long interconnected fibrous spacious network, in which the average diameter for single fiber is ≤50 nm. Fiber-like long filaments appear to be formed from single spherical particles, which may be due to the tendency of globular proteins to grow from single monomers to longer chains.[28−31] Morphological features of CeOvaS were found different from glucose-based carbon aerogels (sponge-like structure formed of nanosized primary particles) synthesized with a similar approach. The difference may be related to solution pH which determines the type of aggregates in the gelation of ovalbumin. It has been noticed that in near neutral or slightly acidic pH solutions, formation of random aggregates dominates, whereas at lower pH far from the isoelectric point (pI) formation of fibrous aggregates takes place.[31]

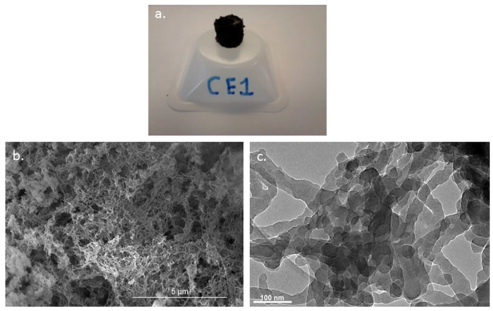

Figure 1. (a) Wet carbon aerogel after HTC synthesis, (b) SEM 20k magnification, and (c) TEM 40k magnification.

N_2 physisorption isotherms allow evaluating the nature of the interstitial porous system of the materials under study. As can be seen in Figure 2a, N_2 sorption isotherms of the studied

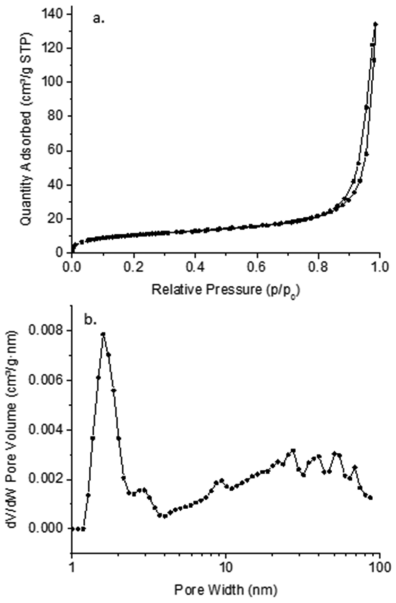

Figure 2. (a) N_2 sorption isotherms and (b) pore size distribution determined through NLDFT assuming slit-shaped pores.

carbon materials are type IV with H3 reversible sorption, indicative of a mesoporous network. This is confirmed by the pore size distribution shown in Figure 2b, which additionally shows the presence of some microporosity. The BET surface area of the carbogel is 38 m^2/g with some microporosity (13 m^2/g) evaluated with t-plot technique, as indicated in Table 1. Overall, the surface area of CeOvaS is higher than that of hydrothermal carbons in general, but lower than that of protein-controlled carbogels reported earlier. The difference is most probably related to the drying technique: freeze versus supercritical CO_2 drying.[17,32] In general, freeze-drying results in lower surface area than supercritical CO_2 drying, which may be due to crossing of liquid−gas boundary layer in the heterogeneous environment and surface tension of liquid

DOI: 10.1021/acsami.5b08287
ACS Appl. Mater. Interfaces 2015, 7, 25875−25883

Table 1. Characterization Results of CeOvaS

		N_2 physisorption			chemical composition						
sample	T_p (°C)	S_{BET} (m^2/g)	S_{micro} [a] (m^2/g)	V_R [b] (cm^3/g)	N	H	C	O	pH_{iep}	acidity (mmol/g)	basicity (mmol/g)
CeOvaS	180	38	13	0.18	2.1[c]/2.6[d]	4.8[c]	61.0[c]/60.9[d]	32.1[c]/27.9[d]	3.0	0.7	

[a]Evaluated by the *t*-plot method. [b]Total pore volume at $p/p_o \approx 0.97$. [c]Determined through elemental analysis. [d]Determined through XPS

phase pulling against the solid structure it is in contact with. Some materials are disrupted by it, unlike supercritical CO_2 drying, where any phase boundary is crossed.[33]

Results from bulk elemental analysis are summarized in Table 1, which show the typical elemental composition for hydrothermal carbon obtained in the presence of ovalbumin.[34] A bulk nitrogen content of 2.1 wt % is registered in the CeOvaS sample. The types of surface functionalities and carbon structure were estimated using FTIR, XPS and NMR techniques. FTIR spectrum and spectroscopical assignments are presented respectively in Figure S1 and Table 2. FTIR analysis indicates carboxylic/carbonyl features (~1700 cm^{-1}) together with oxygen and nitrogen-containing structures (1360–1020 cm^{-1}).[26,35] On the other hand, intense peaks at 2980–2890 cm^{-1} show the presence of aliphatic features[36] mixed with aromatic features, including furan-type motifs (~1620 and 1520 cm^{-1}).[17] The broad band at 3700–3100 cm^{-1} corresponds to the stretching vibration band of both hydroxyl ν(O–H) and amine ν(N–H) groups suggesting occurrence of hydroxyl and maybe amine groups.

Table 2. Assignments for Characteristic Vibrations for Surface Functional Groups Found in CeOvaS

wave number (cm^{-1})	functionality/characteristic vibration
3700–3100	hydroxyl ν(O–H) and amine ν(N–H)
2980–2890	aliphatic features ν(C–H)
1701	carboxylic/carbonyl ν(C═O)
1162	ν(C–NH_2) or ν(C–O)
1046	ν(C–NH–) or ν(C–O)
1616 and 1516	benzene- and furan-type structures ν(C═C and C═C–O)

The high-resolution C 1(s) XPS spectrum in Figure 3a shows three distinct binding energies for 284.6 eV (sp^2 C═C; 80.2% area), 286.6 eV (C–O–H/C–O–C; 12.9% area), and 288.8 eV (N–C═O; 6.9% area). N 1(s) envelope analysis reveals as well three different binding energies, showing a high amount of quaternary nitrogen (401.8 eV; 52.8% area), pyrrole (400.9 eV; 24.8% area), and pyrrolidonic/amide/lactam structural motifs (399.8 eV; 22.4% area). Composition of nitrogen functionalities in cellulose-based carbogels seems to differ from glucose-based carbogels, which have been reported to exhibit a high content of pyrrolic structures and some amine contribution.[17] XPS analysis is in a good agreement with FTIR studies. On the other hand, ^{13}C CP MAS NMR analysis indicates existence of delocalized aromatic sp^2-carbons (δ = 90–160 ppm), aliphatic sp^3-carbons (δ = 0–60 ppm) and carbonyl structural motifs in the carbonaceous material (Figure 3b). Distinct resonances at ~30 and ~55 ppm region correspond, respectively, to methylene- and methoxy-ester groups, whereas resonances at ~60 ppm refer to quaternary nitrogen.[37,38] Within the aromatic carbon region, a strong resonance is identified at ~130 ppm, indicating a high abundance of all-carbon aromatic structures, accompanied by a smaller proportion of furan-type structural

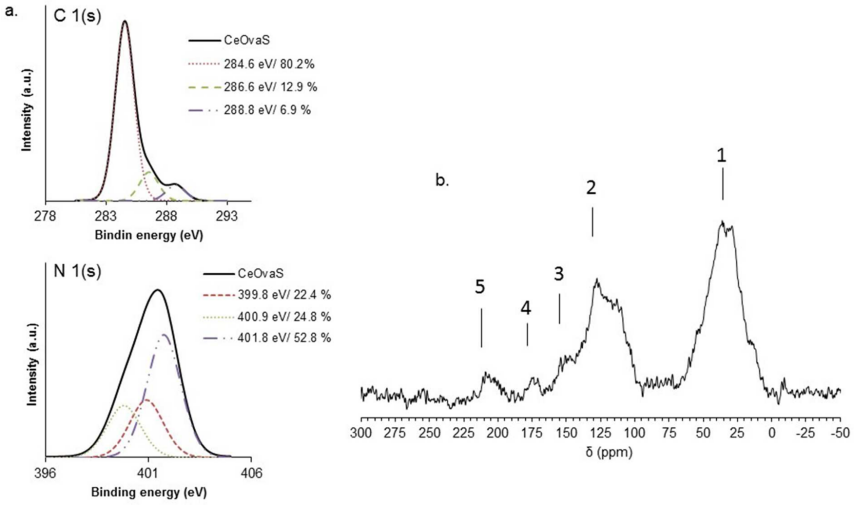

Figure 3. (a) High-resolution C 1(s) and N 1(s) XPS deconvoluted spectra and (b)^{13}C CP MAS NMR spectra: 1, aliphatic sp^3 carbon; 2, delocalized sp^2 carbon; 3, furan-type motif; 4, carboxylic acids; and 5, ketones/aldehydes.

DOI: 10.1021/acsami.5b08287
ACS Appl. Mater. Interfaces 2015, 7, 25875–25883

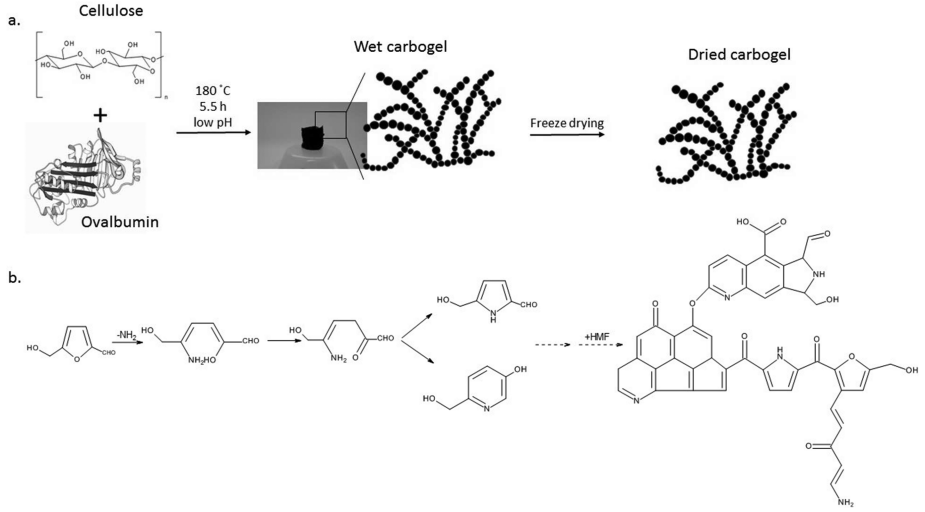

Figure 4. (a) Schematic illustration of the gelation process during hydrothermal carbonization (HTC) of cellulose and ovalbumin and (b) formation of pyridinic and pyrrolic structures during HTC via intramolecular condensation. These compounds further on take part in the formation of final N-enriched carbon network.

motifs (~150 ppm and ~110 ppm). Carboxylate/amide structural motifs are responsible for the resonance at ~175 ppm and further on resonance at ~210 ppm is indicative for ketone/aldehyde-type of groups.[17] Schematic presentation of the formation of carbogel CeOvaS and the reaction mechanism representing the structure of the final N-enriched carbon network supported by findings from FTIR, XPS, and NMR studies is presented in the Figure 4.

The protonation and deprotonation of surface functional groups creates net charge, forming an electrical double layer in the solution around the carbon surface. Determination of pH_{IEP} gives an indication of at which pH value the total surface charge is zero. Figure 5 depicts the change in zeta potential as a function of solution pH. Pure hydrothermal carbons show negative zeta potential values over the whole range of pH due to the high number of acidic oxygenated groups on the surface.[34] However, CeOvaS shows positive zeta potential at pH lower than 3.0, indicating coexistence of positively charged

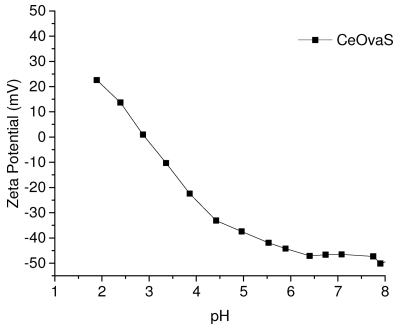

Figure 5. Change in zeta potential as a function of pH.

nitrogen groups in the carbon material with negatively charged oxygen moieties. The type of nitrogen and its chemical environment together with relative abundance play an important role in the acid–base properties of carbon materials. The acid/base properties were determined by titration and the results are shown in Table 1, which indicate strong acidity. Even though zeta potential analysis indicates the presence of basic surface functional groups on CeOvaS, basicity was not observed with titration analysis. This may be related to the small amount of nitrogen present in the material, as revealed by elemental analysis, or to the type of nitrogen functionalities.[39] Electron donor/acceptor features depend on nitrogen types and their chemical environment. XPS studies suggest that CeOvaS would consist mainly of sp^2-hybridized nitrogen functionalities, that is, quaternary nitrogen and pyrrole/pyrrolidonic resulting in delocalized electrons of the nitrogen in the carbon network. Removal of electron pair or protonation of nitrogen would be energetically unfavorable therefore these nitrogen may have rather acidic than basic character.[40] However, it should be noted that overall basicity covers impact from delocalized π-electron of the basal plane and from oxygen containing functional groups besides influencing on the acid–base distribution on the carbon material besides potential basic contribution of nitrogen functionalities.[41,42]

3.2. Adsorption Studies. *3.2.1. Effect of pH.* One of the main factors affecting the metal adsorption process is the solution pH, especially when electrostatic interactions are main driving force in the process. Because of the amphoteric character of the developed hydrothermal carbons, they may show sensitivity to changes in solution pH, which determines protonation of surface groups and the speciation of metal ions in the solution. In this study, acidic pH in the range of 3–6 was chosen because of the general properties of industrial waste waters and in order to prevent hydroxyl formation of Pb(II). Adsorption performance of CeOvaS shows to be independent

DOI: 10.1021/acsami.5b08287
ACS Appl. Mater. Interfaces 2015, 7, 25875–25883

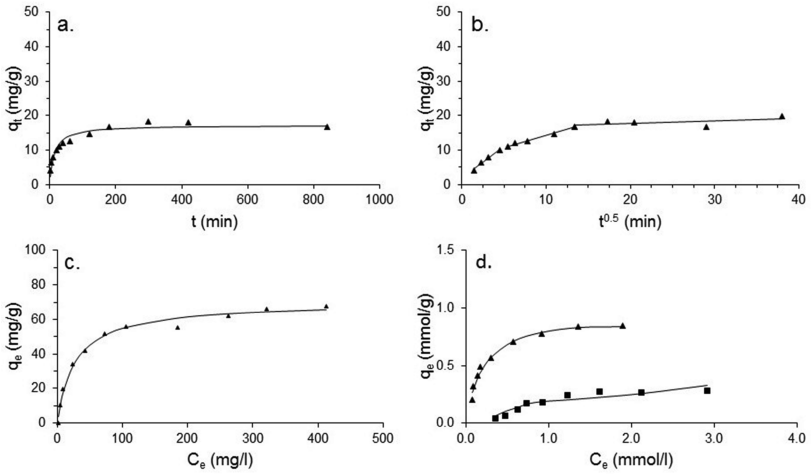

Figure 6. (a) Cr(VI) kinetic studies PS2, (b) intraparticle diffusion model Cr(VI) removal (▲), (c) one-component equilibrium studies and Sips adsorption isotherm for the removal of Cr(VI) (▲), and (d) bicomponent equilibrium studies Cr(VI) (▲) and As(V) (■).

Table 3. Nonlinear PS2 Kinetic Modeling Parameters and Intraparticle Diffusion Model Parameters of CeOvaS

		PS2 nonlinear				intraparticle diffusion		
adsorbent	metal	q_t (mg/g)	K_2 (g/mg min)	r^2	STDEV	k_{dif1} (mg/g min$^{1/2}$)	k_{dif2} (mg/g min$^{1/2}$)	k_{dif3} (mg/g min$^{1/2}$)
CeOvaS	Pb(II)	16.0	1.7	0.973	0.6	0.03		
	Cr(VI)	17.4	0.004	0.924	4.8	1.88	0.69	0.08

of the solution pH for both of the metal ions studied (see Figure S2). This may be related to cation exchange in the interlayers as a result of electrostatic interaction between the ions and the permanent charge.[43] Also, pH independent adsorption may be related to same charge on both the adsorbent and adsorbate.[44] Additionally, Cr(VI) can be reduced to Cr(III) at low pH, especially if negative surface functional groups are present.[20] pH independent adsorption would be a beneficial feature for real systems, allowing changes in acidity without a change in adsorption efficiency. For further studies, the solution pH for Cr(VI) removal was adjusted to pH 3 and for Pb(II) removal to pH 5.

3.2.2. Kinetics. When considering industrial applications, it is important to investigate the rate of adsorbate removal from the aqueous phase. Several steps affect this process before the equilibrium state is reached. Typically, the effect of bulk diffusion is eliminated by vigorous stirring, but the contribution of all of the other stages needs to be investigated. Different pseudo-kinetic models and diffusion-based models have been developed to predict the rate determining adsorption step.[45] In this study, nonlinear pseudo-second-order model (PS2)[46] and intraparticle diffusion model[47] (IPD) have been applied to evaluate kinetic aspects. In the nonlinear PS2 model, it is assumed that the rate of chemical reaction on the carbon surface is responsible for the rate of adsorption and the kinetic order of this reaction is two with respect to the number of adsorption sites available for the ion exchange. The IPD model can be applied to predict the importance of diffusion at different stages on the rate of adsorption.

Removal of Cr(VI) and Pb(II) as a function of time (t) and the corresponding nonlinear PS2 models are presented respectively in Figures 6a and S3a. According to the experimental kinetic data, the adsorption of Pb(II) is extremely fast (k = 1.7). Adsorption equilibrium is reached within a few minutes, which may be related to the immediate use of the readily available adsorption sites on the carbon surface. On the contrary, the adsorption of Cr(VI) is slower (k = 0.004), with two phase adsorption and fast linear phase followed by quasi-stationary phase. The second phase takes place after 150 min, during which the amount of Cr(VI) was constant. The maximum percentual removal rate for both metal ions was 70%. The PS2 model correlates reasonably well to all the experimental data with theoretical q_t (adsorption capacity) values being very close to the experimentally determined values ($r^2 \geq 0.924$, STDEV 0.6–4.8) (Table 3). The results received from intraparticle diffusion modeling are presented in Table 3 and Figures 6b and S3b. Adsorption of Pb(II) follows a very fast one-step adsorption process, resulting in a small diffusion rate constant (K_{dif} = 0.03) and suggesting that pore diffusion does not control Pb(II) adsorption to the same extent as does chemical reaction according to nonlinear PS2 model. The IPD modeling for Cr(VI) appears to follow three-step adsorption involving fast transport of sorbate on to the surface of the adsorbent, followed by mitigation of sorbate and finally equilibrium state.[47] Cr(VI) removal may be controlled by both pore diffusion and chemical reaction. Similar findings related to reaction kinetics of Cr(VI) and Pb(II) have also been reported by other authors.[48−50]

3.2.3. Cr(VI) and Pb(II) Removal from One-Component and Bicomponent Solutions. The adsorption of metal species is not a straightforward process. Metallic species are small in size and charged in solution. Adsorption of metal ions on

DOI: 10.1021/acsami.5b08287
ACS Appl. Mater. Interfaces 2015, 7, 25875−25883

Table 4. Adsorption Equilibrium Results for Single Metal Ion (One-Component) Removal[a]

adsorbent	metal	$q_{e,exp}$ (mg/g)	q_e (mg/g)	K_S (L/mg)	n_S	r^2	STDEV
CeOvaS	Cr(VI)	68.0	70.3	0.04	0.9	0.989	0.12
	Pb(II)	240.0	236.7	0.14	10.4	0.975	1.41

[a]Sips adsorption isotherm modeling parameters of studied carbon materials.

Table 5. Metal Adsorption Capacities of Different Hydrothermal Carbons and Carbon Composite Materials Towards Cr(VI) and Pb(II)

material/adsorbent	surface area (m^2/g)	acidity (mmol/g)	pH	q_e Cr(VI) (mg/g)	q_e Pb(II) (mg/g)	ref
leonardite	20	5.19	5−6		250.7	58
poly(4-vinylpyridine) coated AC	68		2.25	53.7		56
AC produced from apricot stone	393	0.78	6		21.4	59
mature tea leaves derived AC	1313		4.5	30.8		49
palm shell activated carbon	957	4.14	5		95.2	55
PAN based activated carbon fibers	12.2		3	140		57
CeOvaS carbogel N-enriched	38	0.7	3	68		this study
			5		240	

Table 6. Parameters of the Extended Sips Study for Cr(VI)/As(V) and Pb(II)/Cu(II) Two-Component Studies

adsorbent	metal	$q_{e,exp}$ (mmol/g)	q_e (mmol/g)	$k_{S(L/mmol)}$	n_S	r^2	STDEV
CeOvaS	Cr(VI)	0.9	1.1	4.48	1.0	0.983	0.20
	As(V)	0.3	2.6	0.41	1.8	0.880	0.10
	Pb(II)	1.0	1.0	5.17	2.2	0.971	0.27
	Cu(II)	0.02	n.e.	n.e.	0.5	n.e.	0.007

carbon materials is controlled by several factors such as surface functionality, chemistry of metal ions/complexes, solution pH, surface area and pore distribution.[7] Hydrothermal carbons contain a large amount of polar oxygen surface functional groups. These groups can be involved in the adsorption process by chemical bonding and are contributing to the cation exchange capacity of carbon materials. The contribution of nitrogen functionalities, basic/acid character depends on the type of nitrogen in carbon materials. The presence of acidic and basic functionalities would enable simultaneous removal of the positively and negatively charged metal ions and enable a wider applicability of the adsorbent itself. However, as discussed above, the presence of basic nitrogen functionalities was not confirmed. Experimental adsorption equilibrium studies of CeOvaS shows great performance toward removal of Pb(II) and Cr(VI) (Table 4 and Figures6c and S4). Experimental maximum adsorption capacity is estimated as 68 mg/g (1.3 mmol/g) for Cr(VI) and 240 mg/g (1.2 mmol/g) for Pb(II). In this case, both anionic and cationic species were adsorbed nearly in the same extent. Strong surface acidity of CeOvaS enhances Pb(II) adsorption via electrostatic interactions which is aligned with previous studies in the removal of Pb(II) by carbon based materials.[51] The adsorption mechanism under acidic conditions for Cr(VI) is adsorption-coupled reduction, which is mainly caused by the strong reduction potential of Cr(VI) and interaction which may be enhanced by nitrogen functionalities.[7,52−54]

The Sips model was used to estimate adsorption behavior of CeOvaS toward Pb(II) and Cr(VI). Sips model takes into account heterogeneity aspects of the studied adsorbent. Indeed, the Sips model appears to fit very well with the experimental data (Table 4 and Figures 6c and S4). Calculated q_e values are very close to those estimated experimentally and the obtained n_S values differ from the unity suggesting heterogeneous adsorption ($r^2 \geq 0.975$, STDEV ≤ 1.4). Clearly, higher affinities (K_S values) are seen between metals and CeOvaS. Table 5 provides a comparison between the Cr(VI) and Pb(II) adsorption capacity of activated carbons with different textural and physicochemical properties and that of the carbon aerogels fabricated in this work.[49,55−59] Overall, the adsorption capacity for both metals is higher for the materials here developed, proving their excellent performance in metal removal. The maximum adsorption capacity (q_e) in one-component systems is related only to a given cation/anion adsorbed from the liquid phase, without any competition, interaction, or displacement effects.[60] Many of the one-component isotherms (e.g., Sips) have been extended to be applicable for the simultaneous adsorption of more than one adsorbate.[61] Extended model of Sips isotherm was applied in order to evaluate the adsorption performance (Figures 6d and S5). The effect of the coexisting ion on the adsorption performance of Cr(VI) was studied with As(V) and the competing ion selected for Pb(II) was Cu(II). The presence of another species with a similar charge shows a minor to moderate interfering effect on the targeted metal adsorption, causing lower maximum adsorption capacities for aimed metals compared with one-component systems. Especially, Pb(II) has a much higher attraction toward CeOvaS compared to Cu(II). On the whole, some competition for the available adsorption sites was observed.[62] Finally, the extended Sips isotherm was applied to model two-component adsorption. This extended model provides a reasonable fit to most of the experimental data, but in both cases it tends to overestimate the maximum adsorption capacity (Table 6).

4. CONCLUSIONS

We have presented a simple, sustainable, and environmentally friendly one-step synthesis process for the production of nitrogen-rich carbogels from complex polysaccharide cellulose in the presence of glycoprotein ovalbumin. The role of ovalbumin was not only to provide nitrogen functionalities to

DOI: 10.1021/acsami.5b08287
ACS Appl. Mater. Interfaces 2015, 7, 25875−25883

the carbon network, but mainly to act as a structure directing agent in the formation of the final carbonaceous material, avoiding thereby the use of templates and template removal steps. The nitrogen heteroatom appeared to exist mainly in the quaternary form. In addition to the nitrogen functionalities, CeOvaS had increased number of oxygen functionalities with acidic character. Furthermore, CeOvaS showed a mesoporous network with moderate surface area. In spite of the moderate porosity of CeOvaS, it presented a great removal capacity toward Pb(II) and Cr(VI)metal ions, which may be due to the acidic character enhancing Pb(II) removal by electrostatic interaction and Cr(VI) removal through reduction. Adsorption of Pb(II) was found to be fast, indicating that the chemical reactivity takes control over the reaction kinetics, as suggested in the PS2 model. Cr(VI) removal, however, was slower, which may be controlled by pore diffusion and chemical reaction on adsorbent surface However, in general, both metal ions reached equilibrium state rather fast.

Competing ions had no significant effect on the removal of Pb(II) and Cr(VI). The presence of competing ions decreased the removal efficiency by approximately 20%, indicating a strong affinity toward Pb(II) and Cr(VI). The Sips model fitted well to the experimental data obtained from the one-component systems, but its extended version for two-component data form gave only approximate results. This excellent performance together with a simple and fast preparation technique reflects the great potential of these materials for adsorption applications.

■ ASSOCIATED CONTENT

Supporting Information

The Supporting Information is available free of charge on the ACS Publications website at DOI: 10.1021/acsami.5b08287.

FT-IR spectrum of CeOvaS, effect of pH on the removal of Pb(II) and Cr(VI), adsorption kinetic studies of CeOvaS, and experimental adsorption equilibrium studies and Sips modeling of Pb(II) (PDF)

■ AUTHOR INFORMATION

Corresponding Authors

*E-mail: sara-maaria.alatalo@lut.fi.
*E-mail: m.m.titirici@qmul.ac.uk.

Notes

The authors declare no competing financial interest.

■ ACKNOWLEDGMENTS

The authors are grateful to the Finnish Funding Agency for Technology and Innovation (TEKES) and Tekniikan edistämissäätiö, TES (31066) for financial support. M.S. acknowledges the Spanish Ministerio de Economia y Competitividad, MINECO (MAT2012-31651), and Fondo Europeo de Desarrollo Regional (FEDER) for financial support.

■ REFERENCES

(1) Bhatnagar, A.; Sillanpää, M. Utilization of Agro-Industrial and Municipal Waste Materials as Potential Adsorbents for Water Treatment—A Review. *Chem. Eng. J.* **2010**, *157* (2−3), 277−296.

(2) Demirbas, A. Heavy Metal Adsorption onto Agro-based Waste Materials: A Review. *J. Hazard. Mater.* **2008**, *157* (2−3), 220−229.

(3) Fu, F.; Wang, Q. Removal of Heavy Metal Ions from Wastewaters: A Review. *J. Environ. Manage.* **2011**, *92* (3), 407−418.

(4) O'Connell, D. W.; Birkinshaw, C.; O'Dwyer, T. F. Heavy Metal Adsorbents Prepared from the Modification of Cellulose: A Review. *Bioresour. Technol.* **2008**, *99* (15), 6709−6724.

(5) Singh, K. K.; Rastogi, R.; Hasan, S. H. Removal of Cr(VI) from Wastewater Using Rice Bran. *J. Colloid Interface Sci.* **2005**, *290* (1), 61−68.

(6) Kurniawan, T. A.; Chan, G. Y. S.; Lo, W.-h.; Babel, S. Comparisons of Low-Cost Adsorbents for Treating Wastewaters Laden with Heavy Metals. *Sci. Total Environ.* **2006**, *366* (2−3), 409−426.

(7) Dias, J. M.; Alvim-Ferraz, M. C. M.; Almeida, M. F.; Rivera-Utrilla, J.; Sánchez-Polo, M. Waste Materials for Activated Carbon Preparation and Its Use in Aqueous-Phase Treatment: A Review. *J. Environ. Manage.* **2007**, *85* (4), 833−846.

(8) Babel, S.; Kurniawan, T. A. Low-Cost Adsorbents for Heavy Metals Uptake from Contaminated Water: A Review. *J. Hazard. Mater.* **2003**, *97* (1−3), 219−243.

(9) Demir-Cakan, R.; Baccile, N.; Antonietti, M.; Titirici, M. M. Carboxylate-Rich Carbonaceous Materials via One-Step Hydrothermal Carbonization of Glucose in the Presence of Acrylic Acid. *Chem. Mater.* **2009**, *21* (3), 484−490.

(10) Nxumalo, E. N.; Nyamori, V. O.; Coville, N. J. CVD Synthesis of Nitrogen Doped Carbon Nanotubes Using Ferrocene/Aniline Mixtures. *J. Organomet. Chem.* **2008**, *693* (17), 2942−2948.

(11) Evans, M. J. B.; Halliop, E.; MacDonald, J. A. F. The Production of Chemically-Activated Carbon. *Carbon* **1999**, *37* (2), 269−274.

(12) Titirici, M.-M.; White, R. J.; Brun, N.; Budarin, V. L.; Su, D. S.; del Monte, F.; Clark, J. H.; MacLachlan, M. J. Sustainable Carbon Materials. *Chem. Soc. Rev.* **2015**, *44* (1), 250−290.

(13) White, R. J.; Brun, N.; Budarin, V. L.; Clark, J. H.; Titirici, M.-M. Always Look on the "Light" Side of Life: Sustainable Carbon Aerogels. *ChemSusChem* **2014**, *7* (3), 670−689.

(14) Brun, N.; Sakaushi, K.; Yu, L.; Giebeler, L.; Eckert, J.; Titirici, M. M. Hydrothermal Carbon-Based Nanostructured Hollow Spheres as Electrode Materials for High-Power Lithium-Sulfur Batteries. *Phys. Chem. Chem. Phys.* **2013**, *15* (16), 6080−6087.

(15) Ryu, J.; Suh, Y.-W.; Suh, D. J.; Ahn, D. J. Hydrothermal Preparation of Carbon Microspheres from Mono-Saccharides and Phenolic Compounds. *Carbon* **2010**, *48* (7), 1990−1998.

(16) Yu, L.; Falco, C.; Weber, J.; White, R. J.; Howe, J. Y.; Titirici, M.-M. Carbohydrate-Derived Hydrothermal Carbons: A Through Characterization Study. *Langmuir* **2012**, *28* (33), 12373−12383.

(17) White, R. J.; Yoshizawa, N.; Antonietti, M.; Titirici, M.-M. A Sustainable Synthesis of Nitrogen-Doped Carbon Aerogels. *Green Chem.* **2011**, *13* (9), 2428−2434.

(18) Titirici, M.-M. *Sustainable Carbon Materials from Hydrothermal Processes*; Wiley: Chichester, U.K., 2013.

(19) Titirici, M.-M.; Antonietti, M. Chemistry and Materials Options of Sustainable Carbon Materials Made by Hydrothermal Carbonization. *Chem. Soc. Rev.* **2010**, *39* (1), 103−116.

(20) Tascon, J. M. D. *Novel Carbon Adsorbents* **2012**, vii.

(21) Falco, C.; Baccile, N.; Titirici, M.-M. Morphological and Structural Differences Between Glucose, Cellulose and Lignocellulosic Biomass Derived Hydrothermal Carbons. *Green Chem.* **2011**, *13* (11), 3273−3281.

(22) Faria, P. C. C.; Órfão, J. J. M.; Pereira, M. F. R. Adsorption of Anionic and Cationic Dyes on Activated Carbons with Different Surface Chemistries. *Water Res.* **2004**, *38* (8), 2043−2052.

(23) Moreno-Castilla, C.; Carrasco-Marin, F.; Utrera-Hidalgo, E.; Rivera-Utrilla, J. Activated Carbons as Adsorbents of Sulfur Dioxide in Flowing Air. Effect of Their Pore Texture and Surface Basicity. *Langmuir* **1993**, *9* (5), 1378−1383.

(24) Sevilla, M.; Fuertes, A. B. The Production of Carbon Materials by Hydrothermal Carbonization of Cellulose. *Carbon* **2009**, *47* (9), 2281−2289.

(25) Saka, S.; Ueno, T. Chemical Conversion of Various Celluloses to Glucose and Its Derivatives in Supercritical Water. *Cellulose* **1999**, *6* (3), 177−191.

DOI: 10.1021/acsami.5b08287
ACS Appl. Mater. Interfaces 2015, 7, 25875−25883

(26) Baccile, N.; Antonietti, M.; Titirici, M. M. One-Step Hydrothermal Synthesis of Nitrogen-Doped Nanocarbons: Albumine Directing the Carbonization of Glucose. *ChemSusChem* **2010**, *3* (2), 246−253.
(27) Tressl, R.; Wondrak, G. T.; Krüger, R.-P.; Rewicki, D. New Melanoidin-like Maillard Polymers from 2-Deoxypentoses. *J. Agric. Food Chem.* **1998**, *46* (1), 104−110.
(28) Clark, A. H.; Kavanagh, G. M.; Ross-Murphy, S. B. Globular Protein Gelation—Theory and Experiment. *Food Hydrocolloids* **2001**, *15* (4−6), 383−400.
(29) Gosal, W. S.; Ross-Murphy, S. B. Globular Protein Gelation. *Curr. Opin. Colloid Interface Sci.* **2000**, *5* (3−4), 188−194.
(30) Kavanagh, G. M.; Clark, A. H.; Ross-Murphy, S. B. Heat-Induced Gelation of Globular Proteins: Part 3. Molecular Studies on Low pH β-lactoglobulin Gels. *Int. J. Biol. Macromol.* **2000**, *28* (1), 41−50.
(31) Weijers, M.; Sagis, L. M. C.; Veerman, C.; Sperber, B.; van der Linden, E. Rheology and Structure of Ovalbumin Gels at Low pH and Low Ionic Strength. *Food Hydrocolloids* **2002**, *16* (3), 269−276.
(32) Wohlgemuth, S.-A.; White, R. J.; Willinger, M.-G.; Titirici, M.-M.; Antonietti, M. A One-Pot Hydrothermal Synthesis of Sulfur and Nitrogen Doped Carbon Aerogels with Enhanced Electrocatalytic Activity in the Oxygen Reduction Reaction. *Green Chem.* **2012**, *14* (5), 1515−1523.
(33) Finka, M. E. S. E. H. Critical Point Drying of Soft Biological Material for the Scanning Electron Microscope. *Investigative Ophthalmology* **1972**, *11*, 127−131.
(34) Baccile, N.; Antonietti, M.; Titirici, M.-M. One-Step Hydrothermal Synthesis of Nitrogen-Doped Nanocarbons: Albumine Directing the Carbonization of Glucose. *ChemSusChem* **2010**, *3*, 246−253.
(35) Lua, A. C.; Yang, T. Effect of Activation Temperature on the Textural and Chemical Properties of Potassium Hydroxide Activated Carbon Prepared from Pistachio-Nut Shell. *J. Colloid Interface Sci.* **2004**, *274* (2), 594−601.
(36) Coates, J. Interpretation of Infrared Spectra: A Practical Approach. In *Encyclopedia of Analytical Chemistry*; Meyers, R. A., Ed.; John Wiley & Sons, Ltd: Hoboken, NJ, 2006.
(37) Liu, S.; Tian, J.; Wang, L.; Zhang, Y.; Qin, X.; Luo, Y.; Asiri, A. M.; Al-Youbi, A. O.; Sun, X. Hydrothermal Treatment of Grass: A Low-Cost, Green Route to Nitrogen-Doped, Carbon-Rich, Photoluminescent Polymer Nanodots as an Effective Fluorescent Sensing Platform for Label-Free Detection of Cu(II) Ions. *Adv. Mater.* **2012**, *24* (15), 2037−2041.
(38) Perinu, C.; Arstad, B.; Bouzga, A. M.; Jens, K.-J. 13C and 15N NMR Characterization of Amine Reactivity and Solvent Effects in CO2 Capture. *J. Phys. Chem. B* **2014**, *118* (34), 10167−10174.
(39) Hulicova-Jurcakova, D.; Seredych, M.; Lu, G. Q.; Bandosz, T. J. Combined Effect of Nitrogen- and Oxygen-Containing Functional Groups of Microporous Activated Carbon on its Electrochemical Performance in Supercapacitors. *Adv. Funct. Mater.* **2009**, *19* (3), 438−447.
(40) Bitter, J. H.; van Dommele, S.; de Jong, K. P. On the Virtue of Acid−Base Titrations for the Determination of Basic Sites in Nitrogen Doped Carbon Nanotubes. *Catal. Today* **2010**, *150* (1−2), 61−66.
(41) Arrigo, R.; Hävecker, M.; Wrabetz, S.; Blume, R.; Lerch, M.; McGregor, J.; Parrott, E. P. J.; Zeitler, J. A.; Gladden, L. F.; Knop-Gericke, A.; Schlögl, R.; Su, D. S. Tuning the Acid/Base Properties of Nanocarbons by Functionalization via Amination. *J. Am. Chem. Soc.* **2010**, *132* (28), 9616−9630.
(42) Radovic, L. R.; Moreno-Castilla, C.; Rivera-Utrilla, J. Carbon Materials as Adsorbents in Aqueous Solutions. *Chemistry and Physics of Carbon* **2000**, *27*, 227−405.
(43) Kraepiel, A. M. L.; Keller, K.; Morel, F. M. M. A Model for Metal Adsorption on Montmorillonite. *J. Colloid Interface Sci.* **1999**, *210* (1), 43−54.
(44) Rivera-Utrilla, J.; Sánchez-Polo, M. Adsorption of Cr(III) on Ozonised Activated Carbon. Importance of Cπ—Cation Interactions. *Water Res.* **2003**, *37* (14), 3335−3340.
(45) Ho, Y. S.; Ng, J. C. Y.; McKay, G. Kinetics of Pollutant Sorption by Biosorbents: Review. *Sep. Purif. Rev.* **2000**, *29* (2), 189−232.
(46) Plazinski, W.; Rudzinski, W.; Plazinska, A. Theoretical Models of Sorption Kinetics Including a Surface Reaction Mechanism: A review. *Adv. Colloid Interface Sci.* **2009**, *152* (1−2), 2−13.
(47) Cheung, W. H.; Szeto, Y. S.; McKay, G. Intraparticle Diffusion Processes During Acid Dye Adsorption onto Chitosan. *Bioresour. Technol.* **2007**, *98* (15), 2897−2904.
(48) Oliveira, E. A.; Montanher, S. F.; Andrade, A. D.; Nóbrega, J. A.; Rollemberg, M. C. Equilibrium Studies for the Sorption of Chromium and Nickel from Aqueous Solutions Using Raw Rice Bran. *Process Biochem.* **2005**, *40* (11), 3485−3490.
(49) Goswami, M.; Borah, L.; Mahanta, D.; Phukan, P. Equilibrium Modeling, Kinetic and Thermodynamic Studies on the Adsorption of Cr(VI) Using Activated Carbon Derived from Matured Tea Leaves. *J. Porous Mater.* **2014**, *21* (6), 1025−1034.
(50) Saadat, S.; Karimi-Jashni, A.; Doroodmand, M. M. Synthesis and Characterization of Novel Single-Walled Carbon Nanotubes- Doped Walnut Shell Composite and Its Adsorption Performance for Lead in Aqueous Solutions. *J. Environ. Chem. Eng.* **2014**, *2* (4), 2059−2067.
(51) Qiu, Y.; Cheng, H.; Xu, C.; Sheng, G. D. Surface Characteristics of Crop-Residue-Derived Black Carbon and Lead(II) Adsorption. *Water Res.* **2008**, *42* (3), 567−574.
(52) Valix, M.; Cheung, W. H.; Zhang, K. Role of Heteroatoms in Activated Carbon for Removal of Hexavalent Chromium from Wastewaters. *J. Hazard. Mater.* **2006**, *135* (1−3), 395−405.
(53) Miretzky, P.; Cirelli, A. F. Cr (VI) and Cr (III) Removal From Aqueous Solution by Raw and Modified Lignocellulosic Materials: A Review. *J. Hazard. Mater.* **2010**, *180* (1), 1−19.
(54) Reddad, Z.; Gerente, C.; Andres, Y.; Cloirec, P. L. Mechanisms of Cr (III) and Cr (VI) Removal from Aqueous Solutions by Sugar Beet Pulp. *Environ. Technol.* **2003**, *24* (2), 257−264.
(55) Issabayeva, G.; Aroua, M. K.; Sulaiman, N. M. N. Removal of Lead from Aqueous Solutions on Palm Shell Activated Carbon. *Bioresour. Technol.* **2006**, *97* (18), 2350−2355.
(56) Fang, J.; Gu, Z.; Gang, D.; Liu, C.; Ilton, E. S.; Deng, B. Cr(VI) Removal from Aqueous Solution by Activated Carbon Coated with Quaternized Poly(4-vinylpyridine). *Environ. Sci. Technol.* **2007**, *41* (13), 4748−4753.
(57) Jiang, Z.; Liu, Y.; Zeng, G.; Xu, W.; Zheng, B.; Tan, X.; Wang, S. Adsorption of Hexavalent Chromium by Polyacrylonitrile (PAN)-Based Activated Carbon Fibers from Aqueous Solution. *RSC Adv.* **2015**, *5* (32), 25389−25397.
(58) Lao, C.; Zeledón, Z.; Gamisans, X.; Solé, M. Sorption of Cd(II) and Pb(II) from Aqueous Solutions by a Low-Rank Coal (Leonardite). *Sep. Purif. Technol.* **2005**, *45* (2), 79−85.
(59) Mouni, L.; Merabet, D.; Bouzaza, A.; Belkhiri, L. Adsorption of Pb(II) from Aqueous Solutions Using Activated Carbon Developed from Apricot Stone. *Desalination* **2011**, *276* (1−3), 148−153.
(60) Papageorgiou, S. K.; Katsaros, F. K.; Kouvelos, E. P.; Kanellopoulos, N. K. Prediction of Binary Adsorption Isotherms of Cu2+, Cd2+ and Pb2+ on Calcium Alginate Beads from Single Adsorption Data. *J. Hazard. Mater.* **2009**, *162* (2−3), 1347−1354.
(61) Repo, E. EDTA- and DTPA-Functionalized Silica Gel and Chitosan Adsorbents for the Removal of Heavy Metals from Aqueous Solutions. Thesis for the degree of Doctor of Science. Lappenranta University of Technology, Lappeenranta, Finland, 2011.
(62) Repo, E.; Petrus, R.; Sillanpää, M.; Warchoł, J. K. Equilibrium Studies on the Adsorption of Co(II) and Ni(II) by Modified Silica Gels: One-Component and Binary Systems. *Chem. Eng. J.* **2011**, *172* (1), 376−385.

DOI: 10.1021/acsami.5b08287
ACS Appl. Mater. Interfaces 2015, 7, 25875−25883

Publication IV

S-M. Alatalo, E. Mäkilä, E. Repo, M. Heinonen, J. Salonen, E. Kukk, M. Sillanpää and M-M. Titirici

Meso- and microporous soft templated hydrothermal carbons for dye removal from water

Reprinted with permission from
Journal of Green Chemistry
Vol. 18, 2015
© 2015, Royal Society of Chemistry

Published on 05 October 2015. Downloaded by Lappeenranta University of Technology on 09/10/2015 13:59:44.

Green Chemistry

PAPER

View Article Online
View Journal

Cite this: DOI: 10.1039/c5gc01796c

Meso- and microporous soft templated hydrothermal carbons for dye removal from water†

Sara-Maaria Alatalo,*[a] Ermei Mäkilä,[b] Eveliina Repo,[a] Markku Heinonen,[c] Jarno Salonen,[b] Edwin Kukk,[c] Mika Sillanpää[a] and Maria-Magdalena Titirici*[d]

Received 4th August 2015,
Accepted 2nd October 2015
DOI: 10.1039/c5gc01796c

www.rsc.org/greenchem

The hydrothermal carbonization (HTC) technique has shown a great ability in the synthesis of carbon materials with special properties for a wide range of different applications. Here, a hypersaline salt mixture ($LiCl–ZnCl_2$) combined with hydrothermal carbonization was applied in order to obtain sulfur containing micro- and mesoporous (0.3–40 nm) monolithic carbons with high surface areas (400–550 $m^2\ g^{-1}$) and well developed porosity (0.4–1.2 $cm^3\ g^{-1}$). Fructose was used as a carbon source and sulfur was introduced in an aromatic configuration as 2-thiophenecarboxaldehyde. The resulting carbon materials showed a promising removal capacity (q_e = 0.3 mmol g^{-1}) towards methylene blue and the adsorption followed the Sips isotherm independent of the pH. Intraparticle diffusion appeared to control the adsorption kinetics. Carbon materials could be easily regenerated with simple ethanol washing. The dye pollutant could be completely desorbed from the adsorbent's surface, while the adsorbent still maintained removal efficiency of above 90% during three cycles.

1. Introduction

Porous carbon materials are still among the best material choices compared to other classes of porous materials such as zeolites, porous silica, and MOFs. This is due to their diverse properties, extraordinary chemical, mechanical and thermal stability, and the tunable electrical properties for a wide range of applications: catalysis, adsorption, batteries, supercapacitors, and fuel cells.[1–3] In recent years, hydrothermal carbonization (HTC) has confirmed its place, as a gentle alternative technique, among the other more classical carbonization techniques. In brief, HTC takes place at low temperatures under autogeneous pressures in aqueous media.[4–6] The reaction mechanism includes several simultaneous and consecutive reactions resulting in an amorphous polyfuranic carbon network.[7] Hydrothermal carbons tend to possess a limited porosity, which however, can be improved *via* various methodologies, such as soft-[8] and hard[9] templating techniques. These techniques include some drawbacks *i.e.* introduction of hazardous chemicals for the removal of hard templates, restriction to low temperature treatment or requirement for an additional post-activation step.[1] In the context of sustainability, green chemistry and industrial scale-up utilization of low-cost, benign and recyclable templates in the production of porous monolithic materials with polar surface functionalities would be beneficial.[10]

$ZnCl_2$ based salt mixtures (*e.g.* NaCl, KCl and LiCl) have been found to regulate the formation of pore diameters and stabilize the surface of the forming primary particles and at the same time prevent Ostwald ripening.[11,12] Additionally, the salt mixture acts as a molecular template, either forming ion pairs or little salt clusters.[13,14] These type of binary salt systems are known as low melting eutectics.[15,16] The introduction of these very hydrophilic ions in to the reaction media lowers the partial pressure of water and changes its structure so that reactions can be performed under hypersaline but otherwise less extreme conditions.[17,18] Due to the environmentally friendly and green sustainable approach, salt mixture could be removed from the carbon matrix simply by washing with water whereas carbon matrix would not be affected, opposite to other techniques.[19] Further on salt mixture could be removed from the water and reused. Additionally, the resulting carbon materials can be dried *via* ordinary drying techniques without the danger of collapsing the porous network due to capillary forces.

With the growth of standard of living, environmental pollution has increased significantly. Heavy metals and organic dyes are complicated pollutants in waste waters due to their

[a]*Laboratory of Green Chemistry, School of Engineering Science, Lappeenranta University of Technology, Sammonkatu 12, FI-50130 Mikkeli, Finland. E-mail: sara-maaria.alatalo@lut.fi*
[b]*Laboratory of Industrial Physics, Department of Physics and Astronomy, University of Turku, FI-20014 Turku, Finland*
[c]*Materials Research Laboratory, Department of Physics and Astronomy, University of Turku, FI-20014 Turku, Finland*
[d]*School of Materials Science and Engineering, Queen Mary University of London, Mile End Road, E1 4NS London, UK. E-mail: m.m.titirici@qmul.ac.uk*
†Electronic supplementary information (ESI) available. See DOI: 10.1039/c5gc01796c

Published on 05 October 2015. Downloaded by Lappeenranta University of Technology on 09/10/2015 13:59:44.

non-biodegradability and toxicity to plants, animals and humans.[20] The greatest environmental concern with dyes is their absorption and reflection of sunlight entering the water, which interferes with the growth of bacteria, limiting it to levels insufficient to biologically degrade impurities in the water. Dyes in waste water can cause acute and/or chronic effects on exposed organisms depending on the exposure time and dye concentration. Additionally, dyes are visible already at very low concentrations (~0.005 ppm).[21,22] Many dyes are also toxic having carcinogenic and mutagenic effects on humans. Various techniques are available for dye containing wastewater treatment, but conventionally no single process is capable of sufficient treatment and most likely a combination of different techniques is required.[23] The removal of dyestuff requires a combination of biological and physical processes and often this is not enough to remove dyes completely. In this context, adsorption would be a potential alternative.[24] Adsorption mechanism of organic compounds such as methylene blue are considered to happen mainly *via* electrostatic interactions and π–π dispersion interaction.[20,25–27] Various organic and inorganic adsorbents including modified graphite powder and the emerging carbon graphitic nanostructures have been tested for the removal of organic dyes from waste waters. Some of them have indicated a rather good dye removal efficiency, however low-cost, easily obtainable and regenerable adsorbents are still rare especially for field applications.[28–31]

Herein we have synthesized meso-/microporous carbon materials *via* hydrothermal carbonization and exploiting salt templating technique. Two different classes of materials have been produced. One from pure fructose containing polar oxygenated functionalities on the surface and another from fructose and 2-thiophenecarboxyaldehyde (TCA) resulting thiophenic sulfur doped within the final carbon network. The development of porosity and the formation of the carbon network was controlled by the presence of $LiCl–ZnCl_2$ salt-mixture. The as synthesized carbon monoliths, with abundant and versatile surface functionality together with well-developed porosity were tested for the removal of methylene blue from aqueous media.

2. Results and discussion

2.1. Synthesis and characterization

The monosaccharide fructose was used as a carbon source for the production of carbon materials in the presence of a $LiCl–ZnCl_2$ salt mixture *via* HTC at 180 °C in a closed batch reactor, resulting in a monolithic carbon structure shown in Fig. 1. The carbon monoliths were dark brown in color and structurally rigid. Scanning electron (SEM) (Fig. 1b and S1a†) and transmission electron microscopy studies (TEM) (Fig. 1c, d and S1b†) showed spherically shaped carbon aggre-

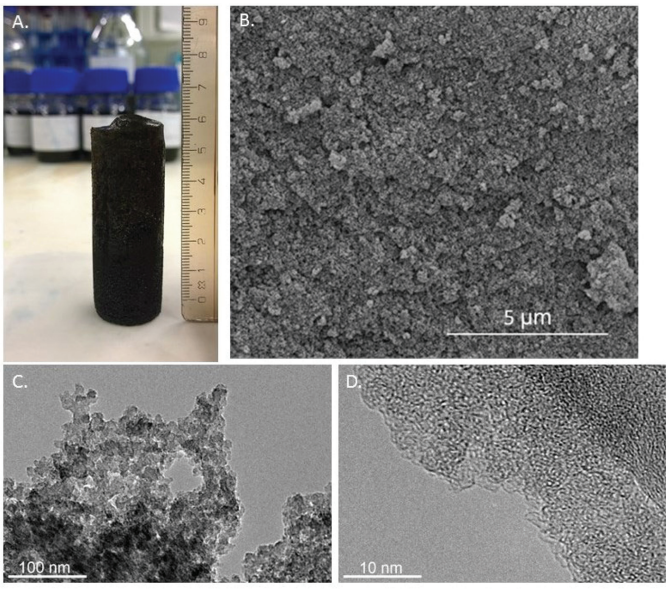

Fig. 1 A. Monolithic carbon structure (fructose based, FruLi) after synthesis, B. SEM image 20k magnification, C. and D. TEM images with 60k and 600k magnifications respectively.

 This journal is © The Royal Society of Chemistry 2015

Published on 05 October 2015. Downloaded by Lappeenranta University of Technology on 09/10/2015 13:59:44.

gates in which the diameters of individual particles were determined about ~20 nm attached together forming a continuous amorphous carbon network.[4] N_2 sorption data was in good agreement with SEM and TEM image analysis, indicating high surface area and pore volume for the produced carbon materials (Table 1, Fig. 2 and S2†). FruLi and FruLi + TCA carbons indicated type IV/H2 and IV/H3 N_2 adsorption isotherms with hysteresis loops indicative to mesoporous structure respectively, which is in a good agreement with the SEM images formed by agglomerated carbon nanoparticles of various sizes.[32] The presence of mesopores is further supported by the pore size distribution obtained from N_2 adsorption experiments (Fig. S2a and c†). Pore size distributions (PSD) were plotted using the non-local density functional theory (NLDFT) and assuming slit-shaped pores. The PSD appeared to concentrate on the lower mesoporous range in which pore sizes of FruLi were mainly less than 10 nm whereas FruLi + TCA indicated broader PSD ranging from 1–40 nm. The steep curve at the beginning of the N_2 adsorption isotherm (P/P_0 0.002–0.3) indicated the presence of microporosity in the network structure, which was confirmed with CO_2 sorption analysis at 0 °C (Table 1, Fig. 2b, d and S2b, d†). Micropores at widths of 0.3–0.8 nm were found in both types of carbon materials with similar V_{total} values. This is in good agreement with the TEM micrographs. Well pronounced microporosity is unusual to hydrothermal carbons, which clearly indicates the imprinting of $ZnCl_2$–LiCl salt mixture in the particles *via* an activation effect, similar to chemical activation.[11]

The introduction of heteroatoms has been shown to improve the performance of carbon materials in many applications. Sulfur doped carbons have received an increased attention due to their potential in the field of adsorption for *e.g.* metal removal and desulfurylation of crude oil. Elemental compositions of carbon materials are summarized in Table 1. S-doping resulted in 7.2 wt% of total sulphur content. FTIR, XPS and NMR analysis demonstrate the structural composition of produced carbon monoliths. FTIR analysis of FruLi and

Table 1 Characterization results for elemental analysis N_2- and CO_2 sorption analysis and total acidity determination by titration

Material	H[a] [%]	C[a] [%]	S[a] [%]	O[a] [%]	S_{N_2}[b] ($m^2\ g^{-1}$)	V_{N_2}[c] ($cm^3\ g^{-1}$)	S_{CO_2}[d] ($m^2\ g^{-1}$)	V_{CO_2}[d] ($cm^3\ g^{-1}$)	Total acidity (mmol g^{-1})
Fruli	4.7	70.2		25.1	431	0.4	415	0.14	0.87
Fruli + TCA	4.3	66.6	7.2	21.9	554	1.2	441	0.15	0.77

[a] Weight percent. [b] Surface area calculated by BET. [c] Total pore volume at $P/P_0 = 0.97$. [d] Surface area and pore volume calculated by NLDFT from CO_2 adsorption data at 0 °C.

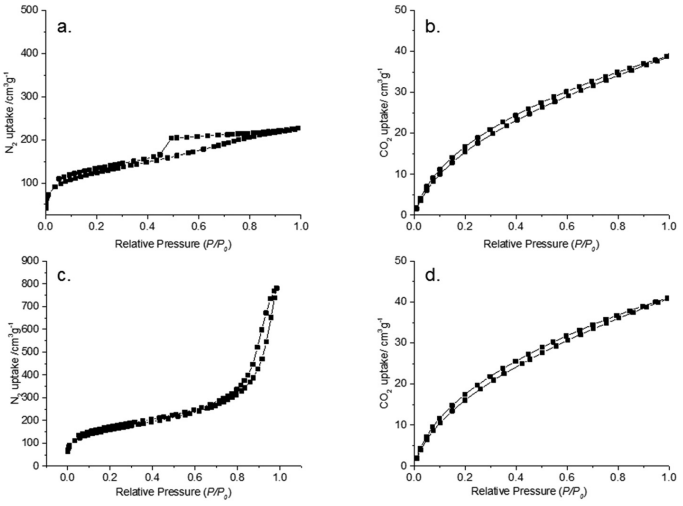

Fig. 2 Fruli A. N_2 adsorption–desorption isotherm, B. CO_2 adsorption–desorption isotherm analyzed at 0 °C. Fruli + TCA C. N_2 adsorption–desorption isotherm and D. CO_2 sorption isotherm analyzed at 0 °C.

Published on 05 October 2015. Downloaded by Lappeenranta University of Technology on 09/10/2015 13:59:44.

FruLi + TCA (Fig. 3) presented typical structural properties for hydrothermal carbons such as the vibration bands related to aromatic features at wavenumbers of 1615–1450 cm^{-1} and carbonyl/carboxylic (C═O) functionalities at 1850–1650 cm^{-1}. The band at wavenumber ~1396 cm^{-1} relate to carboxylate groups in the materials (C–O). The bands at 3000–2800 cm^{-1} can be assigned to aliphatic carbon (C–H) stretching vibrations.[5] Similar structural features compared to FruLi were also observed in FruLi + TCA. However, the weak band found at ~696 cm^{-1} indicates C–S stretching of thiophene ring.[33,34] Observed structural features of FruLi and Fruli + TCA are align with FTIR studies of hydrochars.[4] Further investigation of atomic binding states was conducted by XPS (Fig. 4). High resolution C(1s) analysis indicated four chemical states for FruLi at 285 eV (C═C/C–C/C–H 81.2% area), 286.4 eV (C–O; 11.4% area), 288.1 eV (C═O; 5.6% area) and 289.9 eV (O–C═O; 1.8% area). The C(1s) spectra of Fruli + TCA resulted in four distinct binding energies 285 eV (C═C/C–C/C–H, 80.9% area), 286.4 eV (C–O/C–S; 11.3% area), 288.1 eV (C═O; 3.7% area) and 289.9 eV (O–C═O; 2.2% area) indicating similar structural features as FruLi.[35,36] Due to the close binding energies between different bonding types (*e.g.* C–S and C–O) presence of thiophene type of sulphur in the carbon network was confirmed by S(2p) spectra of the Fruli + TCA.[37] The doublet peak at ~163.9–165 eV corresponds to neutral, thiophene type sulfur, while no oxidized sulfur was detected (165.3–168.6 eV).[34]

For deeper understanding of the chemical environment, solid-state ^{13}C CP NMR was conducted (Fig. 5). The ss-NMR spectrum indicates resonances in the δ = 0–70 ppm region

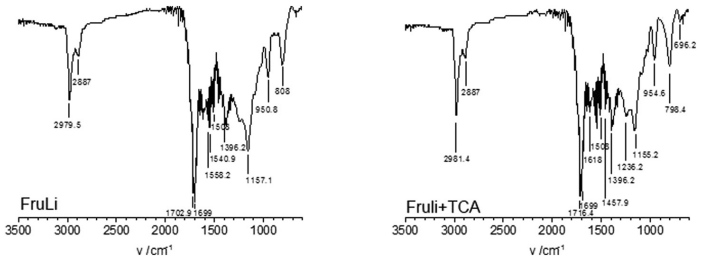

Fig. 3 FTIR spectras of FruLi and Fruli + TCA.

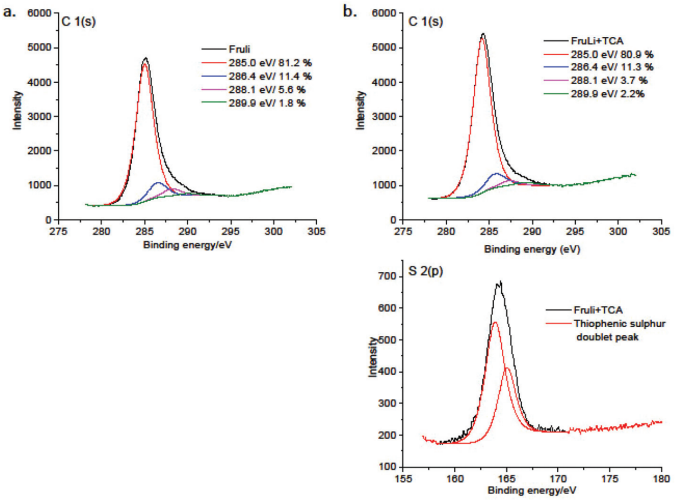

Fig. 4 XPS C 1(s) deconvolution spectra of A. FruLi and B. Fruli + TCA C 1(s) and S 2(p) deconvolution spectras.

Published on 05 October 2015. Downloaded by Lappeenranta University of Technology on 09/10/2015 13:59:44.

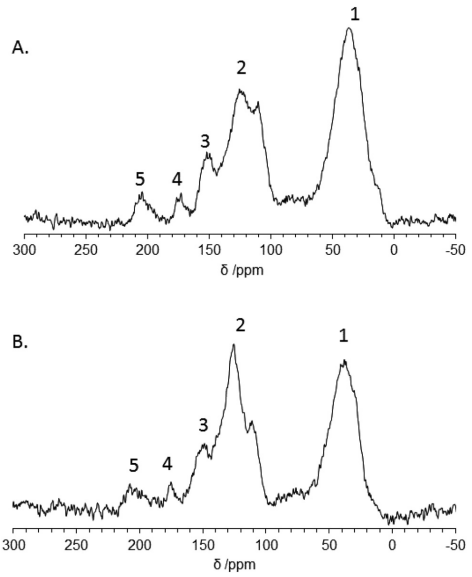

Fig. 5 ^{13}C CP MAS NMR spectras of A. FruLi and B. Fruli + TCA in which 1. Aliphatic sp^3 carbon, 2. sp^2 carbon related structures, 3. Furan type structure, 4. Carboxylate and 5. Ketone/aldehyde.

representative for aliphatic sp^3 hybridized carbon, whilst resonances at δ = 90–160 ppm are characteristic to sp^2 carbon structures. FruLi showed three distinct peaks in this area where δ = 110.7 ppm and δ = 149.5 ppm refer to furan type structures and the peak at δ = 125.2 ppm is characteristic to sp^2 aromatic bound carbon.[38] Further on, the bands at δ = 172.6 ppm and 204.2 ppm refer to carboxylate groups and ketone/aldehyde functionalities, respectively. FruLi + TCA showed similar structural properties to FruLi. However, a slight variation in the relative peak intensities between different structural groups was observed. The intensity of the peak related to sp^3 carbons was found weaker, whilst the peak related to the aromatic structure at δ = 124.8 ppm proved more intense in FruLi + TCA compared to FruLi. Additionally, the peak at 207.5 ppm referring to ketone/aldehyde functionalities was weaker than in FruLi. The contribution of thiophene ring in sulfur doped carbon structure (Fruli + TCA) can be seen as a weak shoulder at ~154.7 ppm.[39]

The change in the surface charge of the carbon materials was studied by determining the pH$_{IEP}$. The experiments were conducted as a function of pH, determining the changes in zeta potential (Fig. 6). The fructose based carbon materials were found to have negative surface zeta potentials over the studied pH range (1–8). The presence of thiophenic sulfur did not have a clear effect on the zeta potential of the carbon material, which may be related to electronegativity of sulfur

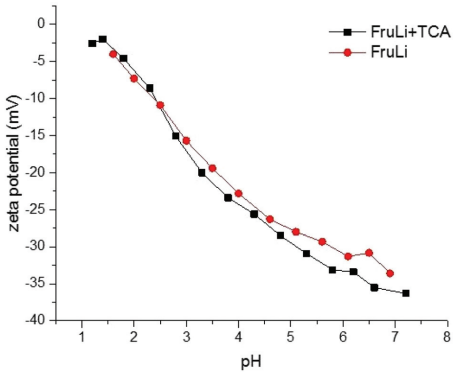

Fig. 6 Development of the surface charge of Fruli and Fruli + TCA as a function of pH.

(2.58 Pauling scale) being very close to electronegativity of carbon (2.55 Pauling scale).[40] The amount of acidic surface functional groups caused by the oxygen functional groups were determined with a simple back titration method. The results are shown in Table 1. Both carbon materials indicated a strong acidity. However, the sulfur doped carbon material (FruLi + TCA) indicated a slightly lower total acidity (mmol g^{-1}) value compared to FruLi. This is in a good agreement with XPS studies suggesting a lower abundance of the oxidized surface functional groups.

2.2. Adsorption

In adsorption applications related to water purification, activated carbon is traditionally used for the removal of pollutants from aqueous media. Its advantages are well developed textural properties (high internal surface area and porosity as well as surface chemical properties).[41] However, the production of activated carbon includes rather harsh and multistep preparation procedures and low yields. Additionally it has very high initial and regeneration costs. In this study, carbon materials with well-developed surface area, pore volume, and abundant surface functionality produced *via* one-pot hydrothermal carbonization technique were tested for the removal of methylene blue. Methylene blue is a basic polyaromatic dye with positively charged nitrogen and sulfur atom in its structure. Positive charge is delocalized through chromophoric system.[42] Structure of the methylene blue and molecule dimensions has been presented in the Table 2.[43]

Typically, the role of pH is considered crucial in the adsorption process. Carbon materials have an amphoteric character and therefore the charge on the surface may change depending on the solution pH. This has a considerable effect on the pollutant removal efficiency of the adsorbent in general.[44] This is crucial when electrostatic interactions are main attractive forces between the adsorbent and the adsorbate.[23] The initial

Published on 05 October 2015. Downloaded by Lappeenranta University of Technology on 09/10/2015 13:59:44.

Table 2 Composition details and properties of Synthetic sewage prepared following OECD guidelines. Molecular structure of Methylene Blue and compound details

	Methylene Blue/Basic Blue 9			
Synthetic sewage	C [mg l^{-1}]	M_w [g mol^{-1}]	pK_a	Dimensions [nm]
Peptone 160		373.9	0.61	1.43 × 0.61 × 0.4
Meat extract 110				
Urea 30				
K_2HPO_4 28				
$MgSO_4{\cdot}2H_2O$ 2				
$CaCl_2{\cdot}2H_2O$ 4				
Nacl 7				
TOC 111				
COD 312				
pH 7.3				

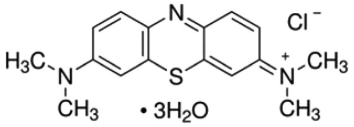

solution pH was observed to have a minor effect on the adsorption efficiency of Methylene blue for both carbon materials FruLi and Fruli + TCA (S3†) over the tested pH range (3–8). Adsorption irrespective of solution pH refers to dispersive interactions between delocalized π electrons in the carbon materials and free electrons in dye molecules responsible for the adsorption mechanism.[44] Similar observations have been reported for charcoal and mesoporous silica templated sucrose adsorbents for example.[41,45]

The experiments related to the effect of temperature on Methylene blue adsorption were conducted at 20, 40 and 60 °C degrees (S4†). The adsorption efficiency increased slightly when temperature increased from 20 to 40 °C. However, the change in the adsorption efficiency of the studied carbon materials was insignificant. Presumably, increased adsorption efficiency at higher temperatures may be due to decreased solution viscosity leading to an enhanced diffusion rate of adsorptive molecules across the external boundary layer and in the internal pores.[46] From an environmental and practical point of view, adsorption at ambient temperature and near neutral pH are highly beneficial in the field of water purification.

The experimental adsorption equilibrium tests were conducted at pH 6 at 20 °C with 24 h contact time. Experimentally determined maximum adsorption capacity of Methylene blue $q_{e,exp}$ was determined 0.3 mmol g^{-1} for Fruli and 0.2 mmol g^{-1} for Fruli + TCA (Table 3, Fig. 7a and S5a†). A successful representation of the dynamic adsorptive separation of solute from a solution onto an adsorbent is dependent upon a good description of the equilibrium separation between two phases. An equilibrium state is reached when the amount of adsorbate being adsorbed onto the adsorbent is equal to amount being desorbed. Sips adsorption isotherm is applicable for heterogeneous surfaces, and therefore applied in this study. Sips is a combination of Langmuir and Freundlich adsorption isotherms. At high concentrations, the Sips isotherm approaches a constant value, and, at low concentrations a Freundlich type equation.[47] The experimental adsorption maximum capacities $q_{e,exp}$, (obtained for both adsorbent types) fit well with the theoretically predicted q_e values which can be seen as a rather good correlation coefficients and standard deviations in the case of both carbon materials (*e.g.* Fruli r^2 = 0.962 and STDEV = 0.11) as well. The heterogeneous factors (n_S) differed from unity, as an indication of heterogeneous adsorption. The adsorption behavior of carbon materials in the pH studied, indicated that the adsorption takes place *via* dispersive interaction, as discussed earlier. However, the contribution of oxygen-containing functional groups cannot be excluded.[23] Besides oxygen functionalities, FruLi + TCA contains sulfur and as a large size atom (70 ppm) it disrupts connection pattern in the carbon network causing charge localization.[36] Sulfur was not found to alter surface acidity as pH_{IEP} remained similar to sulfur-free FruLi. However, the total acidity of Fruli + TCA was slightly lower, indicating a lower amount of oxygen functionalities, as also supported by XPS. A lower amount of oxygen functionalities as well as introduction of sulfur may have indeed an inhibiting effect on the adsorption performance of Fruli + TCA.

Besides the typical single solution experiments performed above, the adsorption capacity of the studied carbon materials towards methylene blue was also tested with synthetic sewage, prepared by following the standard procedure of Organization

Table 3 Experimental maximum adsorption capacity ($q_{e,exp}$) and Sips adsorption isotherm parameters for studied carbon materials and intraparticle diffusion constants for each step

	Sips						Intraparticle diffusion		
Material	$q_{e,exp}$ (mmol g^{-1})	q_e (mmol g^{-1})	K_S (l $mmol^{-1}$)	n_S	r^2	STDEV	k_{dif1} (mmol(g $min^{1/2}$)$^{-1}$)	k_{dif2} (mmol(g $min^{1/2}$)$^{-1}$)	k_{dif3} (mmol(g $min^{1/2}$)$^{-1}$)
FruLi	0.3	0.30	327.4	0.8	0.962	0.11	0.03	0.01	0.0002
Fruli + TCA	0.2	0.24	552.8	0.7	0.970	0.09	0.03	0.006	0.0001

 This journal is © The Royal Society of Chemistry 2015

Published on 05 October 2015. Downloaded by Lappeenranta University of Technology on 09/10/2015 13:59:44.

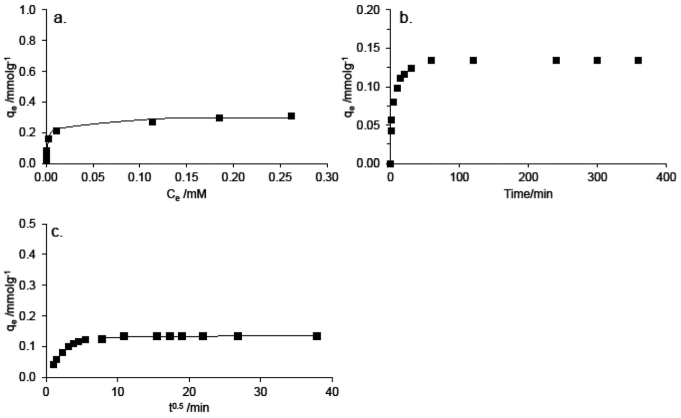

Fig. 7 A. Experimental adsorption equilibrium Fruli Methylene Blue (■) results and Sips adsorption isotherm (—) B. Experimental kinetic data and C. Intraparticle diffusion modeling.

for Economic Cooperation and Development (OECD) guidelines for chemical testing. The composition of this synthetic sewage is presented in Table 2. Interestingly, the Methylene blue adsorption was found to increase with more than 30% from the one-component solution test, for both carbon materials. A maximum adsorption capacity for the removal of methylene blue from the synthetic sewage was determined 0.3 mmol g^{-1} and 0.42 mmol g^{-1} for Fruli + TCA and FruLi respectively. Increase in the adsorption capacities are probably related to the fact that the combination of salts in the synthetic sewage is changing the strength of the repulsion between the adjacently adsorbed dye molecules. Therefore, a greater packing density of the adsorbed organic ions on the carbon surface can be achieved.[48]

The effect of contact time on the adsorption of methylene blue are presented in the Fig. 7b and S5b.† The experimental kinetic data, indicated that over 90% removal rate of methylene blue was reached during the first 30 min. This is due to a fast external diffusion. At the equilibrium state, 99.9% of the maximum removal of methylene blue was reached. The role of diffusion in the speed of the adsorption can be further examined using the so called intraparticle diffusion model, in order to separate different diffusion stages during the adsorption. From the plots of q_t *versus* $t^{0.5}$ of methylene blue, a multilinearity was observed, indicating a three step adsorption process (Fig. 7c, Table 3 and S5c†). The first, sharp step is attributed to the diffusion of the dye through the solution to the external surface of the adsorbent, or the boundary layer diffusion of solute molecules. The second step relates to a gradual adsorption stage, where the intraparticle diffusion was rate limiting. The third step is the final equilibrium step where intraparticle diffusion has started to decrease due to a low dye concentration left in the solution.[49] If the intraparticle diffusion was the only rate controlling step, the plot should pass through the origin, which is not the case in here. Presumably, film diffusion or chemical reaction controls the adsorption rate.[50]

The regeneration of adsorbent would extend the lifetime of the adsorbent and make it ecologically and economically feasible. The desorption technique, *i.e.* physical- or chemical (*e.g.* gas phase, extraction and pH shift desorption) depends on the type of adsorbent, the nature of wastewater and also on further treatments. Chemical extraction using solvents can be applied (KOH,[46] acetonitrile,[46] HNO_3, methanol/acetic acid (10 : 1)[26] and ethanol[51] in different H_2O/ethanol ratios) if the affinity of the adsorbate towards H_2O is low. Here, ethanol was chosen for the removal of Methylene blue, allowing an easy evaporation at room temperatures. However, it is applicable only if further reactivation of adsorbent is unnecessary. This is not the case for activated carbons, which often require an additional reactivation step at higher temperatures, after regeneration. This has been found to cause a decrease in the adsorption capacity.[52] Ethanol was found efficient in desorption of methylene blue from our carbon adsorbents (FruLi and FruLi + TCA). FruLi was found to maintain its adsorption capacity well over 99% through all three adsorption cycles, whereas the adsorption efficiency of FruLi + TCA decreased after regeneration and was found to be 90% after the third cycle (S6†).

In the Table 4 are presented activated carbons,[53,54] carbon composites[55] and other carbonaceous materials[56] with different production conditions, textural and surface properties. Carbon materials presented in this study have indicated benefits in both sides production and application. The clear advantage in production of carbon materials for adsorption application is the utilization of hydrothermal carbonization which is straightforward synthesis with reduced synthesis steps and still get materials with good textural and surface properties. From the sustainability and circular

Published on 05 October 2015. Downloaded by Lappeenranta University of Technology on 09/10/2015 13:59:44.

Table 4 Process conditions, structural properties and adsorption performance towards Methylene blue of different carbon materials

Adsorbent	Synthesis	S_{BET} (mg g^{-1})	V_p (cm^3 g^{-1})	Acidity (mmol g^{-1})	$pH_{optimal}$	q_e (mg g^{-1})	Ref.
Alginic acid derived Starbon (A300)	Retrogradion 5 °C, HT[a]-treatment 300 °C	280	1.41	n.a	n.a	186	56
Norit (commercial)	n.a	798	0.57	n.a	n.a	42	
Clay@Carbon composite	Pyrolysis in the presence of H_2SO_4 500 °C	1290	1.5	n.a	n.a	260	55
Activated carbon (Coconut)	Dried 110 °C, HT-treatment 500 °C, dried 130 °C and HT treatment 700 °C	2825	1.5	1.8	n.a	900	53
Activated carbon (Hazelnut shell)	Dried 110 °C, dehydration 103 °C and $ZnCl_2$ activated 850 °C	793	n.a	0	n.a	8.8	54
Fruli	HTC 180 °C in the presence eutectic salt mixture	431	0.4	0.87	6	83	This study

[a] High temperature.

economy point of view it would be advantageous if process can be kept circular as indicated in the reuse of reaction components (salt mixture) as well as high complete removal percentages and regeneration ability of the carbon materials itself.

3. Experimental section

3.1. Synthesis of carbon materials

The carbon materials were synthesized from D-Fructose (Alfa Aesar) *via* hydrothermal carbonization. 2-Thiophenecarboxyaldehyde (TCA) (Sigma-Aldrich) was added as a sulfur source. LiCl–$ZnCl_2$ eutectic salt mixture was used as soft template in which eutectic salt ratio was 23 mol% of lithium chloride. In a typical synthesis, the saccharide (Fructose, 6 g) was mixed with water (3 g), TCA (1 g) and LiCl–$ZnCl_2$ salt mixture (9 g). The reaction mixture was placed in glass inlet, sealed in a Teflon lined autoclave and placed in an oven, which was preheated to 180 °C. The autoclave was kept in the oven for 16 h. The obtained carbon material was removed from the glass inlet, placed in water (1 l) and stirred overnight in order to remove the salt from the carbon material. Finally, the carbon material was vacuum filtrated, washed extensively with water and dried in the oven under vacuum at 80 °C overnight. Complete salt removal was confirmed by thermogravimetric (TG) analysis under air (S7†).

3.2. Characterization

Nitrogen adsorption isotherms at −196 °C were determined with TriStar 3000 (Micromeritics Inc.). The specific surface area was calculated from the adsorption branch of the isotherm using Brunauer–Emmett–Teller theory (BET) and pore size distribution (PSD) was determined with non-local density functional theory (NLDFT) assuming slit shaped pores. CO_2 sorption isotherms were performed at 0 °C with Quantachrome autosorb-iQ C automated gas sorption analyzer. The surface area of the carbon materials were calculated by applying the BET model. Pore size distribution and pore volume were determined using NLDFT, similar to N_2 sorption studies. Before sorption the samples were degasses under vacuum at 150 °C for 20 h. Thermogravimetric analysis was performed with TA instruments Q500 under air up to 1000 °C. Fourier transform infrared spectroscopy (FTIR) was done with Bruker Tensor 27 equipped with an attenuated total reflectance unit for the analysis of the surface functionalities. Samples were dried under vacuum at 80 °C before analysis. The surface morphology was surveyed with FEI Quanta 3D environmental scanning electron microscope (ESEM) and JEOL JEM-2010 transmission electron microscope (TEM) operating at 200 kV. Elemental amounts of C, H, N and S present in the carbon materials composition were determined with Vario EL elemental analyzer. X-ray photoelectron spectroscopy (XPS) analysis was performed with PHI 5400 ESCA spectrometer (PerkinElmer Co.,) using a Mg Kα X-ray source ($h\nu$ = 1253.6 eV). The background pressure during the measurements was $<10^{-8}$ mbar. The peak fitting process was done with Casa XPS (Casa Software Ltd). Shirley-type background was subtracted from the spectra and the binding energy values were referenced to the hydrocarbon C(1s) peak at 285 eV. ^{13}C solid-state magic angle spinning (MAS) nuclear magnetic resonance studies (NMR) were acquired on Bruker Advance 300 MHz (7 T) spectrometer using 4 mm zirconia rotors sipping at a MAS frequency of vMAS = 14 kHz. Chemical shifts were referenced relative to tetramethylsilane (TMS; δ = 0 ppm). Zeta potential was determined by pH titration utilizing Zetasizer Nano ZS (Malvern Instruments Ltd) in which measurement was repeated three times and average of them presented in the plot. The total acidity of the carbon materials was estimated by mixing 50 mg of each carbon material with 30 ml of 0.1 M NaOH. The suspension was mixed for one hour at ambient temperature and separated using a 0.45 μm polypropylene syringe filter. The supernatant was titrated with 0.1 M HCl solution. The solution was sparged with N_2 for 10 min before titration and continued throughout titration in order to prevent interfering effect of dissolved CO_2.[23,57] The equivalent point was observed by color change using phenolphthalein indicator.

3.3. Adsorption

Dye removal efficiency of carbon materials was tested with basic blue 9 (methylene blue) (Sigma-Aldrich). The concentrations in the aqueous solution were determined spectro-

 This journal is © The Royal Society of Chemistry 2015

Published on 05 October 2015. Downloaded by Lappeenranta University of Technology on 09/10/2015 13:59:44.

photometrically in the visible range of the spectrum. Maximum wavelength (λ_{max}) was 664 nm for methylene blue. Methylene blue solutions for adsorption studies were diluted from 1 mM stock solution.

In the study of the pH effect (tested pH range 3–8), the amount of adsorbent was 20.0 mg and the volume of dye solution 10 ml. These amounts were used throughout all the adsorption experiments. Dye concentration was 0.4 mM, reaction temperature 20 °C, and stirring speed 200 rpm. The suspensions were agitated with a rotary shaker (Ika KS 4000i). The solution pH was adjusted with 0.1 M NaOH or 0.1 M HNO_3. The effect of the reaction temperature was carried out at temperatures of 20, 40 and 60 °C. The dye concentration and speed were the same as in the study of pH effect. The adsorption equilibrium studies were conducted at 20 °C, pH 6, and 24 h with 200 rpm stirring speed. The dye concentrations varied between 0.05–0.8 mM. The kinetic studies were conducted at ambient temperature and pH 6 under a constant stirring using a 0.2 mM Methylene Blue solution in which the "slurry batch reactor" method was applied as an experimental setup.[58]

The amount of Methylene Blue adsorbed per unit mass of adsorbent was calculated as follows:

$$q_e = (C_i - C_e)V/m \quad (1)$$

where q_e (mmol g^{-1}) is equilibrium adsorption capacity, C_i and C_e (mmol l^{-1}) are the initial and equilibrium dye concentrations, respectively, m (g) represents the weight of the adsorbent, and V (l) is the volume of the solution.

Sips adsorption isotherm was used to model the experimental data obtained in one-component systems. Equation for Sips isotherm is presented as follows:

$$q_e = q_m[(K_S C_e)^{n_S}/(1 + (K_S C_e)^{n_S}] \quad (2)$$

In which K_S (L $mmol^{-1}$) is the affinity constant, C_e (mmol l^{-1}) is the dye concentration at the equilibrium state and n_S describes the surface heterogeneity.

Pore diffusion as a controlling step in the adsorption was considered by intraparticle diffusion model as follows:

$$q_e = k_{dif} t^{1/2} + (C) \quad (3)$$

where k_{dif} (mmol (g $min^{1/2})^{-1}$) is the rate constant of intraparticle diffusion and C represents the thickness of the boundary layer.

Synthetic sewage was prepared according OECD guideline for the testing of chemicals.[45] The solution was prepared in tap water containing peptone 160 mg, meat extract 110 mg, urea 30 mg, anhydrous K_2HPO_4 28 mg, NaCl 7 mg $CaCl_2{\cdot}2H_2O$ 4 mg and $Mg_2SO_4{\cdot}7H_2O$ 2 mg. Synthetic sewage was used as solvent when preparing methylene blue solutions in varying concentrations (0.05 mM–0.9 mM). The Methylene blue addition did not change the solution pH significantly. The solution was prepared prior use and stored in the fridge for no more than one week.

In the regeneration studies, 0.4 mM Methylene blue solution was in contact with adsorbent under reaction conditions similar to the adsorption equilibrium studies. The desorption was performed with excess amount of Ethanol (denaturated). The dye containing EtOH adsorbent mixture was centrifuged at 10 000 rpm for 10 min (Centrifuge 5810R, Eppendorf) and the supernatant was carefully removed. The carbon materials were dried in the oven at 80 °C.

4. Conclusion

Porous carbonaceous materials were successfully synthesized from fructose in the presence of an eutectic salt mixture (LiCl–$ZnCl_2$) *via* hydrothermal carbonization technique (HTC) at low temperatures. Sulfur was successfully doped in the carbon network *via* 2-thiophenecarboxaldehyde. Among the several potential applications, the applicability of the produced carbon materials in water treatment for dye removal was tested. The carbon materials showed a great ability for the removal of methylene blue. Interestingly, the adsorption capacity improved significantly when synthetic sewage was used. The adsorption process was found to be fast and controlled by intraparticle diffusion. Furthermore, the carbon materials were successfully regenerated by liquid extraction using EtOH.

Acknowledgements

Finnish Funding Agency for Technology and Innovation (TEKES), Tekniikan edistämissäätiö (TES) and Maa-ja Vesitekniikan tuki (MVTT) are thanked for the financial support. Sakari Modig and Anna Timofeeva are thanked for their valuable contribution to the adsorption experiments, Dr Bingjun Zhu for the CO_2 sorption analysis and Dr Zhang is thanked for the scientifical discussions. Furthermore, Dr Niki Baccile and Guillaume Laurent from the Chimie de la Matière Condensée de Paris are thanked for their contribution with the NMR analysis.

References

1 N. Fechler, T.-P. Fellinger and M. Antonietti, *Adv. Mater.*, 2013, **25**, 75–79.
2 D.-W. Wang, Q. Zeng, G. Zhou, L. Yin, F. Li, H.-M. Cheng, I. R. Gentle and G. Q. M. Lu, *J. Mater. Chem. A*, 2013, **1**, 9382–9394.
3 J. Chen, X. Wang, X. Cui, G. Yang and W. Zheng, *Chem. Commun.*, 2014, **50**, 557–559.
4 L. Yu, C. Falco, J. Weber, R. J. White, J. Y. Howe and M.-M. Titirici, *Langmuir*, 2012, **28**, 12373–12383.
5 A. C. Lua and T. Yang, *J. Colloid Interface Sci.*, 2004, **274**, 594–601.
6 M. M. Titirici, A. Thomas and M. Antonietti, *Adv. Funct. Mater.*, 2007, **17**, 1010–1018.
7 M. M. Titirici, M. Antonietti and N. Baccile, *Green Chem.*, 2008, **10**, 1204–1212.

Published on 05 October 2015. Downloaded by Lappeenranta University of Technology on 09/10/2015 13:59:44.

8 R. J. White, K. Tauer, M. Antonietti and M.-M. Titirici, *J. Am. Chem. Soc.*, 2010, **132**, 17360–17363.
9 N. Brun, K. Sakaushi, L. Yu, L. Giebeler, J. Eckert and M. M. Titirici, *Phys. Chem. Chem. Phys.*, 2013, **15**, 6080–6087.
10 R. J. White, *Porous Carbon Materials from Sustainable Precursors*, Royal Society of Chemistry, 2015.
11 N. Fechler, S.-A. Wohlgemuth, P. Jaker and M. Antonietti, *J. Mater. Chem. A*, 2013, **1**, 9418–9421.
12 W. L. Queen, S.-J. Hwu and S. Reighard, *Inorg. Chem.*, 2010, **49**, 1316–1318.
13 N. Fechler, T. P. Fellinger and M. Antonietti, *Adv. Mater.*, 2013, **25**, 75–79.
14 C. J. Liao, C. F. Chen, J. H. Chen, S. F. Chiang, Y. J. Lin and K. Y. Chang, *J. Biomed. Mater. Res.*, 2002, **59**, 676–681.
15 G. Imperato, S. Hoger, D. Lenoir and B. Konig, *Green Chem.*, 2006, **8**, 1051–1055.
16 G. Janz, *Thermodynamic and Transport Properties for Molten Salts: Correlation Equations for Critically Evaluated Density, Surface Tension, Electrical Conductance and Viscosity Data*, American Chemical Society, 1988.
17 N. F. S.-A. W. P. J. a. M. Antonietti, *J. Mater. Chem. A*, 2013, 9418–9421.
18 X. Liu, N. Fechler and M. Antonietti, *Chem. Soc. Rev.*, 2013, **42**, 8237–8265.
19 N. F. T.-M. F. M. Antonietti, *Mater. Views*, 2012, **25**, 75–79.
20 Y. Yang, Y. Xie, L. Pang, M. Li, X. Song, J. Wen and H. Zhao, *Langmuir*, 2013, **29**, 10727–10736.
21 S. J. A. G. M. J. F. Porter, *J. Colloid Interface Sci.*, 2004, 322–333.
22 S. J. Allen, G. McKay and J. F. Porter, *J. Colloid Interface Sci.*, 2004, **280**, 322–333.
23 P. C. C. Faria, J. J. M. Órfão and M. F. R. Pereira, *Water Res.*, 2004, **38**, 2043–2052.
24 J. L. Figueiredo, J. P. S. Sousa, C. A. Orge, M. F. R. Pereira and J. J. M. Órfão, *Adsorption*, 2011, **17**, 431–441.
25 Y. Yan, M. Zhang, K. Gong, L. Su, Z. Guo and L. Mao, *Chem. Mater.*, 2005, **17**, 3457–3463.
26 Z. Wu, H. Zhong, X. Yuan, H. Wang, L. Wang, X. Chen, G. Zeng and Y. Wu, *Water Res.*, 2014, **67**, 330–344.
27 M. F. R. Pereira, S. F. Soares, J. J. M. Órfão and J. L. Figueiredo, *Carbon*, 2003, **41**, 811–821.
28 D. Liu, W. Yuan, P. Yuan, W. Yu, D. Tan, H. Liu and H. He, *Appl. Surf. Sci.*, 2013, **282**, 838–843.
29 L. Fan, C. Luo, X. Li, F. Lu, H. Qiu and M. Sun, *J. Hazard. Mater.*, 2012, **215–216**, 272–279.
30 L. Fan, Y. Zhang, C. Luo, F. Lu, H. Qiu and M. Sun, *Int. J. Biol. Macromol.*, 2012, **50**, 444–450.
31 K. A. G. Gusmão, L. V. A. Gurgel, T. M. S. Melo and L. F. Gil, *J. Environ. Manage.*, 2013, **118**, 135–143.
32 K. S. W. Sing, *Pure Appl. Chem.*, 1982, **54**, 2201–2218.
33 J. Coates, in *Encyclopedia of Analytical Chemistry*, John Wiley & Sons, Ltd, 2006.
34 H. Seema, K. C. Kemp, N. H. Le, S.-W. Park, V. Chandra, J. W. Lee and K. S. Kim, *Carbon*, 2014, **66**, 320–326.
35 Z. Liu, H. Nie, Z. Yang, J. Zhang, Z. Jin, Y. Lu, Z. Xiao and S. Huang, *Nanoscale*, 2013, **5**, 3283–3288.
36 S.-A. Wohlgemuth, R. J. White, M.-G. Willinger, M.-M. Titirici and M. Antonietti, *Green Chem.*, 2012, **14**, 1515–1523.
37 M. Sevilla and A. B. Fuertes, *Microporous Mesoporous Mater.*, 2012, **158**, 318–323.
38 S.-A. Wohlgemuth, F. Vilela, M.-M. Titirici and M. Antonietti, *Green Chem.*, 2012, **14**, 741–749.
39 T. Narasimhaswamy, N. Somanathan, D. K. Lee and A. Ramamoorthy, *Chem. Mater.*, 2005, **17**, 2013–2018.
40 J. M. D. Tascon, *Novel carbon adsorbents*, 2012.
41 J. Galán, A. Rodríguez, J. M. Gómez, S. J. Allen and G. M. Walker, *Chem. Eng. J.*, 2013, **219**, 62–68.
42 E. N. El Qada, S. J. Allen and G. M. Walker, *Chem. Eng. J.*, 2006, **124**, 103–110.
43 S. Lei, J.-i. Miyamoto, H. Kanoh, Y. Nakahigashi and K. Kaneko, *Carbon*, 2006, **44**, 1884–1890.
44 J. J. M. Órfão, A. I. M. Silva, J. C. V. Pereira, S. A. Barata, I. M. Fonseca, P. C. C. Faria and M. F. R. Pereira, *J. Colloid Interface Sci.*, 2006, **296**, 480–489.
45 M. J. Iqbal and M. N. Ashiq, *J. Hazard. Mater.*, 2007, **139**, 57–66.
46 X. He, K. B. Male, P. N. Nesterenko, D. Brabazon, B. Paull and J. H. T. Luong, *ACS Appl. Mater. Interfaces*, 2013, **5**, 8796–8804.
47 K. Foo and B. Hameed, *Chem. Eng. J.*, 2010, **156**, 2–10.
48 D. O. Cooney, *Adsorption design for wastewater treatment*, Lewis Publishers, 1999.
49 W. H. Cheung, Y. S. Szeto and G. McKay, *Bioresour. Technol.*, 2007, **98**, 2897–2904.
50 Z. Tian, B. Yang, G. Cui, L. Zhang, Y. Guo and S. Yan, *RSC Adv.*, 2015, **5**, 2266–2275.
51 J.-M. Chern and C.-Y. Wu, *Water Res.*, 2001, **35**, 4159–4165.
52 R. Berenguer, J. P. Marco-Lozar, C. Quijada, D. Cazorla-Amorós and E. Morallón, *Energy Fuels*, 2010, **24**, 3366–3372.
53 A. L. Cazetta, A. M. Vargas, E. M. Nogami, M. H. Kunita, M. R. Guilherme, A. C. Martins, T. L. Silva, J. C. Moraes and V. C. Almeida, *Chem. Eng. J.*, 2011, **174**, 117–125.
54 A. Aygün, S. Yenisoy-Karakaş and I. Duman, *Microporous Mesoporous Mater.*, 2003, **66**, 189–195.
55 A. Bakandritsos, E. Kouvelos, T. Steriotis and D. Petridis, *Langmuir*, 2005, **21**, 2349–2355.
56 H. L. Parker, A. J. Hunt, V. L. Budarin, P. S. Shuttleworth, K. L. Miller and J. H. Clark, *RSC Adv.*, 2012, **2**, 8992–8997.
57 C. Moreno-Castilla, F. Carrasco-Marin, E. Utrera-Hidalgo and J. Rivera-Utrilla, *Langmuir*, 1993, **9**, 1378–1383.
58 E. Worch, *Adsorption technology in water treatment: fundamentals, processes, and modeling*, Walter de Gruyter, 2012.

 This journal is © The Royal Society of Chemistry 2015

Publication V

Name, S-M. Alatalo, K. Qiu, K. Preuss, A. Marinovic, M. Sevilla E. Mäkilä, M. Sillanpää, X. Guo and M-M. Titirici

Soy protein directed hydrothermal synthesis of porous carbon aerogels for electrocatalytic oxygen reduction

Reprinted with permission from
Carbon
Vol. 96, 2016,
© 2016, Elsevier

Carbon 96 (2016) 622–630

Contents lists available at ScienceDirect

Carbon

journal homepage: www.elsevier.com/locate/carbon

Soy protein directed hydrothermal synthesis of porous carbon aerogels for electrocatalytic oxygen reduction

Sara-Maaria Alatalo [a, *], Kaipei Qiu [b], Kathrin Preuss [c, d], Adam Marinovic [c, d], Marta Sevilla [e], Mika Sillanpää [a], Xiao Guo [b], Maria-Magdalena Titirici [c, d, **]

[a] Laboratory of Green Chemistry, Department of Chemistry, Lappeenranta University of Technology, Sammonkatu 12, FI-50130 Mikkeli, Finland
[b] Department of Chemistry, University College London, 20 Gordon Street, WC1H 0AJ London, United Kingdom
[c] School of Materials Science and Engineering, Queen Mary University of London, Mile End Road, E1 4NS London, United Kingdom
[d] Materials Research Institute, Queen Mary University of London, Mile End Road, E1 4NS London, United Kingdom
[e] Instituto Nacional del Carbón (CSIC), P.O. Box 73, 33080 Oviedo, Spain

ARTICLE INFO

Article history:
Received 14 August 2015
Received in revised form
24 September 2015
Accepted 28 September 2015
Available online 1 October 2015

ABSTRACT

Herein we presented, for the first time, facile fabrication of nitrogen doped (0.5–4 wt.%) porous carbon aerogels using biomass derivatives (*i.e.* glucose or cellulose) as the carbon precursor and soy protein as both the nitrogen precursor and the structure directing agent. Through post thermal treatment to improve the electrical conductivity and porosity, the obtained materials showed excellent oxygen reduction reaction (ORR) catalytic activity. The electrochemical performance was further enhanced after platinum impregnation, combining the advantages of small over-potential from platinum catalyst and high limiting current density from the carbon substrate. Therefore, we demonstrated here not only a novel and low cost hydrothermal synthesis route to achieve high-performing metal-free ORR catalyst or carbon substrate for additional metal catalyst, but also a general principle on how to develop metal nanoparticles/carbon hybrids for ORR.

© 2015 Elsevier Ltd. All rights reserved.

1. Introduction

Carbon material technologies have made remarkable progress in recent years. Carbon have shown diverse physicochemical properties such as chemical and thermal stability, electrical conductivity and the ability to adopt a wide range of morphologies, making them very attractive in wide range of applications including sorption chromatography, energy storage and catalysis [1]. Among various carbon materials, carbon aerogels are of particular interest given that they can be easily synthesized towards uniform, low density lightweight and controllable structures (*i.e.* monolith, bead, powder or thin film) with excellent mass transfer properties, low thermal conductivity and dielectric permittivity [2,3]. Structural features such as micro-, meso- and macro-porosity, arrangement of carbon network and surface functionality are controlled by the employed drying technique (*i.e.* freeze drying, supercritical drying), carbonization temperature, or the selection of the gelation agent [4]. Depending on the choice of the precursors, these carbon aerogels may be engineered with oxygen and nitrogen functional groups which facilitate the anchoring of metal nanoparticles; the nitrogen functionalities after high temperature calcinations have shown to provide an enhanced electrical conductivity to the carbon materials and the protein acts as a porosity-directing agent. All these attributes (high surface area, electronic conductivities, active metal and non-metal catalytic sites) make them potentially attractive metal-free oxygen reduction reaction (ORR) electrocatalysts or heterogeneous catalysts in various chemical reactions [5].

During the hydrothermal carbonisation (HTC) process, cellulose is transformed in glucose which further degrades into furan-based intermediates before undergoing a complex series of reactions involving mainly polycondensations and Diels–Alder type reactions to form final spherical conjugated aromatic carbonaceous materials [4,6]. Hydrochars are typically rich in surface functional groups varying according to precursors used in the process. Nevertheless, without the use of any suitable soft- or hard

* Corresponding author. Laboratory of Green Chemistry, Department of Chemistry, Lappeenranta University of Technology, Sammonkatu 12, FI-50130 Mikkeli, Finland.
** Corresponding author. School of Materials Science and Engineering, Queen Mary University of London, Mile End Road, E1 4NS London, United Kingdom.
E-mail addresses: sara-maaria.alatalo@lut.fi (S.-M. Alatalo), m.m.titirici@qmul.ac.uk (M.-M. Titirici).

http://dx.doi.org/10.1016/j.carbon.2015.09.108
0008-6223/© 2015 Elsevier Ltd. All rights reserved.

templates, the obtained carbon materials are nonporous [7,8]. The use of additives offer control over particle size and porosity [9]. From this point of view, the introduction of secondary biomass precursor acting as a porosity directing agent is desired. At elevated temperatures, certain proteins such as soy protein form aqueous gels once denaturation point is crossed and therefore direct the development of a porous hydrothermal carbon network during HTC process while also introducing nitrogen heteroatom dopants via Maillard-type reactions [10].

Sluggish cathodic oxygen reduction reaction (ORR) is one of the key challenges for fuel cells or metal-air batteries [11]. Platinum based materials are efficient ORR catalysts but the large-scale commercial use is limited mainly due to its prohibitive cost and scarcity as well as the sensitivity to time dependent drift and CO deactivation [12–14]. Therefore increasing amount of efforts have been directed to develop cost-effective alternatives such as metal-free or non-precious metal based counterparts to replace commercial platinum catalysts. Heteroatom doped carbon has been demonstrated as not only the promising ORR catalysts itself, but the suitable substrates for additional metal catalysts as well, since the presence of heteroatoms can modify the electronic properties of the carbon material and influence its electrochemical performance [15,16].

Here, we present a straightforward and sustainable synthesis route of porous nitrogen doped carbon aerogels via hydrothermal carbonization of glucose and cellulose in presence of soy bean flour additive [17]. The advantages of using soy protein as a pore directing agent and nitrogen source are mainly related to the high abundance of soy proteins available form many soy plants along with its very low cost of about 7£/kg, which makes the large scale production of these materials of very low cost. To the best of our knowledge this is the first report using soy protein as a nitrogen source and pore directing agent for the production of carbon aerogels. The features of carbon materials were further improved with calcination under inert atmosphere. Electrocatalytic ORR activities of nitrogen rich calcined carbon materials were tested in alkaline electrolyte and their performance was compared to platinum impregnated carbon materials. It is shown the fabricated carbon aerogels can be adopted as both facile ORR catalysts themselves and ideal supporting materials for platinum catalyst as well. A generic strategy to achieve efficient metal/carbon hybrids for ORR has also been proposed.

2. Experimental

2.1. Synthesis of nitrogen rich carbon aerogels

In the synthesis of carbon aerogels two carbohydrates were introduced as main carbon source, *i.e.* D-Glucose (wasserfrei p.a., Carl Roth) and Cellulose (microcrystalline powder, Sigma–Aldrich), together with Soya bean flour (Sigma–Aldrich). In the synthesis of Glucose based carbon materials, 1 g of carbohydrate, 0.3 g Soy bean flour and 9 g of deionized H_2O was weighted in a 30 mL glass inlet and mixed well. Dry chemicals were well mixed followed by H_2O addition. When using cellulose as a starting material, acidic conditions were used in order to catalyse the reaction (concentrated H_2SO_4 1 mL) and the soy bean flour amount was 0.5 g. A glass inlet was introduced inside the PTFE-lined autoclave, sealed and placed into a preheated oven at 180 °C for 5.5 h. After allowing autoclaves to cool down, carbon materials were vacuum filtrated and washed extensively with deionized water and then freeze dried.

To prepare thermally treated carbon materials, the original freeze dried sample carbon material was placed in a crucible and introduced in a carbonization oven and then heated up to 1000 °C under inert atmosphere (N_2 flow of 25 mL/min) using a heating rate of 5.0 °C and 4 h dwell time. Samples were allowed to cool to ambient conditions and removed from the oven prior to further analysis.

Platinum impregnation was conducted for the HT-treated (1000 °C) carbon materials. Carbon material was suspended in 0.02 M H_2PtCl_6 (Sigma–Aldrich) solution and sonicated in ultrasonic water bath for 30 min [18]. An excess amount of 0.08 M $NaBH_4$ (Sigma–Aldrich) solution was prepared and poured quickly on the carbon suspension in order to reduce platinum on the carbon surface. The mixture was sonicated for 1 h. Carbon suspension was centrifuged and washed with water several times and dried under vacuum at 80 °C. Amount of platinum on the carbon surface was determined by inductively coupled plasma – optical emission spectrometer (ICP-OES) analysis at wavelength 224.5 nm. Carbon material was suspended in aqua regia and left over night. Suspension was filtrated and analysed with ICP-OES.

2.2. Characterization

Surface area and pore volume were analysed via N_2 sorption analysis at 77 K using a Quantachrome instrument consisting of high speed surface area and pore size analyser Nova 4000e. Micropore analysis was performed via CO_2 sorption at 273 K with Quantachrome autosorb-iQ C automated gas sorption analyzer. Before analysis samples were vacuum degassed at 150 °C for 20 h. Fourier transform infrared spectroscopy (FTIR) Tensor 27 Bruker with attenuated total reflectance unit (ATR) was performed to analyse the surface functionality. Particle morphology was surveyed with FEI Quanta 3D environment scanning electron microscope (ESEM) and JEOL JEM-2010 transmission electron microscopy (TEM) operating at 200 kV. Elemental composition of carbon materials was determined with Vario EL elemental analyzer. X-ray photoelectron spectroscopy (XPS) Specs spectrometer using Mg Kα (1253.6 eV) radiation from a double anode at 150 W. Binding energies for the high-resolution spectra were calibrated by setting C 1(s) at 284.6 eV. A nonlinear least-squares curve fit with a Gaussian–Lorentzian mix function and Shirley background subtraction was used to deconvolute the XPS spectra. ^{13}C solid-state magic angle spinning (MAS) nuclear magnetic resonance studies (NMR) have been acquired on Bruker Advance 300 MHz (7T) spectrometer using 4 mm zirconia rotors sipping at a MAS frequency of vMAS = 14 kHz. Chemical shifts were referenced relative to tetramethylsilane (TMS; $\delta = 0$ ppm). X-ray röntgen diffraction (XRD) patterns were recorded with a Panalytical Xpert Pro diffractometer over the 2 theta range of 10–70°, using Cu kα-radiation reflection mode, divergence slit and Ni-filter.

2.3. Oxygen reduction reaction

Electrocatalytic activities were measured in O_2- or N_2-saturated 0.1 M KOH. Oxygen or nitrogen was purged for 30 min before measurement, and continuously bubbled though the electrolyte during the tests, in order to ensure the saturation of the electrolyte with O_2 or N_2. Rotating ring disk electrode (Pt-ring/glassy carbon disk, Gamry) was used as working electrode, Ag/AgCl (sat. KCl, Sigma–Aldrich) as reference electrode and platinum sheet (Metrohm) as counter electrode. The scan rates for cyclic and rotating voltammetry were 100 mV/s and 10 mV/s respectively, and ring potential was constant at 0.4 V vs. Ag/AgCl for rotating voltammetry. All the results were recorded using Metrohm Autolab 302N.

For electrode preparation, 4 mg catalyst was added to a mixture of 100 μl nafion (5 wt.% in alcohol and water, Sigma–Aldrich), 150 μl ethanol absolute (VWR) and 750 μl distilled water, followed by ultrasonication for 30 min to achieve uniform dispersion of the sample in the solvent. 17.5 μl catalyst suspensions were then drop

casted on a rotating ring disk electrode (0.2475 cm^2) and dried at 60 °C.

The electron transfer number (n) and the ratio of peroxide formation (% HO_2^-) were determined by the followed equations respectively:

$$n = 4 \times \frac{I_d}{I_d + I_r/N} \quad (1)$$

$$\%\ HO_2^- = 200 \times \frac{I_r/N}{I_d + I_r/N} \quad (2)$$

where I_d is disk current, I_r is ring current and N is current collection efficiency of the Pt ring (0.37).

For Tafel plot, the kinetic current density (J_K) is calculated on the basis of Koutecky–Levich equation:

$$\frac{1}{J} = \frac{1}{J_L} + \frac{1}{J_K} = \frac{1}{B\omega^{1/2}} + \frac{1}{J_K} \qquad J_K = \frac{J \times J_L}{J_L - J} \quad (3)$$

$$B = 0.2nFC_0(D_0)^{2/3}v^{-1/6} \quad (4)$$

where J is the measured current density, J_K and J_L are the kinetic- and diffusion limiting current densities, ω is the angular velocity (in RPM), n is number of electron transfer, F is the Faraday constant (96485 s A/mol), C_0 is the bulk concentration of dissolved O_2 in 0.1 M KOH (1.2×10^{-3} mol/L), D_0 is the diffusion coefficient of O_2 in 0.1 M KOH (1.9×10^{-5} cm^2/s), and v is the kinematic viscosity of the electrolyte (0.01 m^2/s).

3. Results and discussion

3.1. Synthesis and characterization

In the present model system, glucose/cellulose, soya bean flour and H_2O were mixed and sealed in Teflon lined autoclave with glass inlet and heated at 180 °C for 5.5 h in order to produce nitrogen doped carbonaceous materials. The resulting solid materials were washed with an excess of H_2O followed by freeze drying. In the case of cellulose, its hydrolysis was promoted by acidic reaction solution (*i.e.* 2 M H_2SO_4). Protein acts as structure directing agent while reacting with glucose via Maillard [19] type of reactions when heated above denaturation temperature [20,21]. Soy bean contains proteins divided in albumins (10%), which can be extracted by water, and globulins (90%) extracted by dilute salt solutions. Globulins can further on be divided to glycinin and polymers of glycinin. Glycinin and β-conglycinin are the most important soy proteins. At similar conditions β-conglycinin has been observed less heat-stable than glycinin. Denaturation is a prerequisite for gel formation which depends strongly on solution pH and ionic strength [22]. Type of protein or protein mixture (soy protein isolate) has an effect on gel formation and properties (*e.g.* gel network). It has been observed that β-conglycinin forms gels at lower temperatures than glycinin [23]. Soy bean flour is rich in nitrogen and therefore offers natural addition of nitrogen into carbon network for which elemental analysis (EA) determined bulk nitrogen content 7.8 wt. % (Table 1). Carbon materials were named as GluSo referring to glucose based carbon material and CeSoS referring to cellulose based carbon material. These abbreviations will be used further in this study.

SEM and TEM imaging were used to investigate the morphology development of produced carbon materials (Fig. 1 and Fig. 2). GluSo carbon material is formed out of uniform homogeneous spongy-like aggregated clusters composed of single spherical particles.

Table 1
N_2 sorption and elemental composition data of Glucose-Soy (GluSo) and Cellulose-Soy (CeSoS) carbon materials and derivatives prepared at increasing thermal carbonization temperature (T_p = 1000 °C) and platinum impregnation.

Sample	N_2 sorption			Elemental composition		
	T_p (°C)	S_{BET} (m^2/g)	V_p (cm^3/g)[a]	N (%)	H (%)	C (%)
Soy bean flour				7.8	6.2	43.2
GluSo	180	22	0.14	3.7	5.2	63.0
GluSo_1000	1000	449	0.25	1.9	2.3	72.2
GluSo_1000_Pt	1000	294	0.19			
CeSoS	180	24	0.19	1.0	4.9	65.7
CeSoS_1000	1000	697	0.38	0.5	1.7	82.6
CeSoS_1000_Pt	1000	619	0.37			

[a] Total pore volume determined by density functional theory (DFT).

The primary spherical particles forming these clusters are approximately 100 nm in size. CeSoS carbon material is formed out of slightly larger fibrillar structures compared to GluSo. The formation of such fibrillar motifs can be related to the proteins tendency to form fibrillar structures in acidic condition, which was employed for cellulose [24]. Upon high temperature treatment under a nitrogen atmosphere (T_p = 1000 °C), the samples (GluSo_1000 and CeSoS_1000) maintained their morphology indicating that no morphological re-organisation occurs during high temperature carbonization [25].

The elemental composition and textural properties of the produced carbon materials determined by EA and N_2 sorption and are summarized in Table 1. The nitrogen contents vary between 1.0 and 3.7 wt.% for HTC produced carbons and 0.2–1.9 wt.% for the further calcined samples (GluSo_1000 and CeSoS_1000). This represents good nitrogen retention provided that the initial nitrogen content in the starting protein is 7.8 wt.%. The HTC materials produced (T_p = 180 °C, both GluSo and CeSoS) showed type IV/H3 reversible N_2 sorption isotherms with restricted hysteresis loop (S1a). The surface areas are low (around 40 m^2/g) presumably because of the freeze-drying technique used to maintain the porosity from the wet gel to the dry state. Cross of boundary layer taking place in freeze drying may disrupt the structure of the carbonaceous material [26,27]. Further carbonization of GluSo and CeSoS at higher temperatures (T_p = 1000 °C) lead to a loss of weakly bound polar groups and rearrangement of the framework into a more organized and condensed structure with a higher degree of aromaticity, improving material stability and conductivity and therefore increasing their applicability in electrochemical and energy storage applications [28]. N_2 sorption of calcined carbon materials exhibit similar IV/H3 type of isotherms to those of the HTC materials. The improved surface areas of the carbon materials upon calcination are related to loss of decomposition products. The surface area increases in this study from 22 m^2/g to 450 m^2/g in case of GluSo for example (Table 1) [1]. The porosity of both carbon materials was found to develop after high temperature treatment (S1b) [29]. In the case of CeSoS_1000, the pore diameter maximum shifts to the lower mesoporous range, ~5 nm. Calcination enhances the development of microporosity and therefore, CO_2 sorption analysis at 0 °C was applied [30]. Both HTT treated carbonaceous materials (GluSo_1000 and CeSoS_1000) indicated narrow micropores in a similar size range between 0.3 and 0.9 nm (S2).

The functional groups present on the carbonaceous materials were investigated by FTIR and XPS techniques. FTIR spectra and peak assignments of HTC GluSo and CeSoS carbon materials are presented in Fig. 3, Table 2 and S3. Spectral analysis of the initial HTC materials could indicate the presence of carbonyl/carboxylic

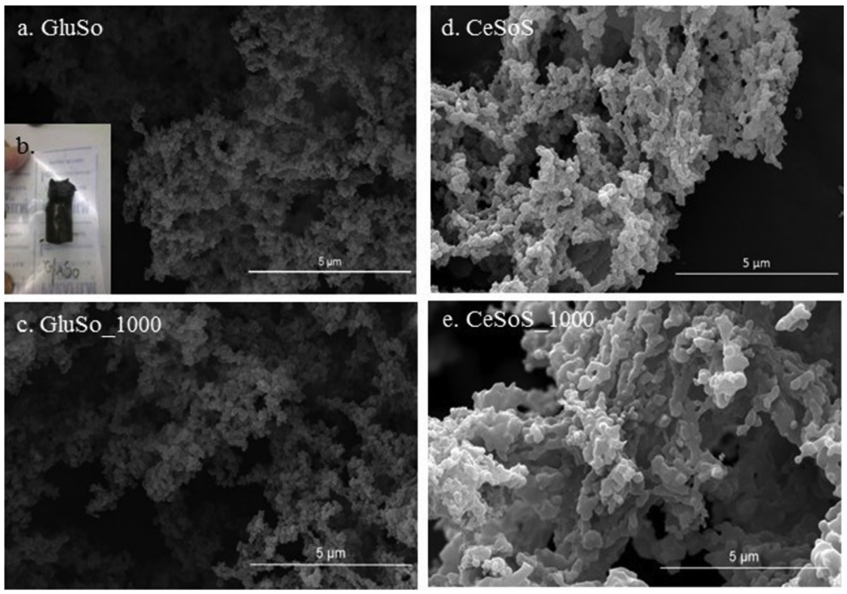

Fig. 1. Scanning electron microscopy (SEM) images of a. Glucose-soya (GluSo) carbonaceous material (T_p = 180 °C) b. GluSo wet carbogel after HTC synthesis and c. GluSo_1000 after calcination (T_p = 1000 °C). Images d. and e. present Cellulose-Soy carbonaceous materials after HTC (T_p = 180 °C) and after calcination at (T_p = 1000 °C) respectively. (A colour version of this figure can be viewed online.)

features (at 1800–1480 cm^{-1}) together with N-containing functional groups, such as amides (*e.g.* ~1670 cm^{-1}) and amines (*i.e* ~1022 cm^{-1}) [5,31]. Peaks at wavenumbers of 3000–2800 cm^{-1} indicate the presence of aliphatic C–H stretching and peaks/bands at 3700–3100 cm^{-1} may refer to v(O–H) and/or v(N–H) stretching. C 1(s) analysis of HTC (T_p = 180 °C) produced GluSo and CeSoS indicates/shows that they are composed mainly of sp^2 and sp^3 carbon (284.6 eV; 71.1%), hydroxyl/ether/amine (286.3 eV; 22.0%) and amide carbonyl (288.2 eV; 6.9%) type of structures (Table 3, Fig. 3 and S3). High temperature treatment of these HTC carbon materials changed the amount and type of surface species bringing two new binding energies referring to carbonyl (287.4 eV; 5.1%) and carboxyl/lactone/ester (289.3 eV; 5.6%) structural motifs, whereas amide type of structures were observed anymore.

N 1(s) analysis of the HTC GluSo (HTC T_p = 180 °C) reveals high amine (399.2 eV; 47.0%) and amide/lactam (399.9 eV; 40.4%) surface character, with minor contribution from imine (397.5 eV; 6.6%) and protonated/hydrogen bonded amines (401.6 eV; 6.0%), results which are consistent with findings from FTIR analysis. Further high temperature treatment of GluSo converts nitrogen to quaternary-N (400.9 eV; 55.4%), pyridinic-N (398.9 eV; 35.2%) and pyridine-N-oxide (402.9 eV; 9.3%) structural motifs (S4). The effect of temperature treatment on the surface species followed a similar pathway to that reported earlier in the literature, in which high temperature favoured formation of more stable N-moieties, *i.e.* quaternary nitrogen and pyridinic nitrogen type of functionalities [32,33]. In the HTC treated CeSoS sample nitrogen occurred mainly as amide/lactam (400.2 eV/54.0%), quaternary nitrogen (401.6 eV; 37.8%) and minority as pyridinic form (398.3 eV, 8.2%). Calcination of CeSoS results in increased amount of quaternary nitrogen (59.2%) and pyridinic nitrogen (34.1%). It has been observed that quaternary and pyridine-N-oxide nitrogen moieties have enhancing effect on the specific capacitance due to the positive charge and thus improved electron transfer at high current loadings [34]. Furthermore, nitrogen functionalities are responsible for an increase in the surface polarity and wettability of carbon. Besides, pyridinic nitrogen brings a lone electron pair into the carbon network. Thereby, it is assumed that pyridinic nitrogen can increase the electron-donating ability to promote the oxygen reduction reaction (ORR) electrocatalytic activity through a $4e^-$ pathway [35]. For further understanding of the chemical environment, solid-state ^{13}C CP NMR was performed (Fig. 3 and S3). GluSo (T_p = 180 °C) spectrum indicated strong aromatic furan-type of carbon network in the material at resonances ~109.5 ppm, ~128.3 ppm, ~149.5 ppm in typical sp^2 carbon region (δ = 100–160 ppm), confirming FTIR and XPS findings. Rather strong peaks at ~171.6 ppm refer to the presence of carboxylate and weaker wider peak at ~205.3 ppm is characteristic of ketone/aldehyde type of structures [25]. Presence of aliphatic sp^3 carbons is confirmed by resonances on 0–100 ppm region (~29.8 ppm and ~52.1 ppm are characteristic of methyl and/or methoxyester groups). Peak at 75 ppm refers to the presence of residual glucose in the solution phase [36]. Amine groups occur at resonances δ = 37–50 ppm typical for several aliphatic carbon structures [37]. There were a broad combination of peaks in this area and therefore it was difficult to confirm clear presence of amine from NMR spectra. CeSoS showed similar structural features to those of GluSo described above, yet abundance of aliphatic features was found somewhat higher than that of aromatic structures. Additionally, peak intensity reflecting presence of carboxylate groups (~174.7 ppm) was found to be slightly lower in the NMR

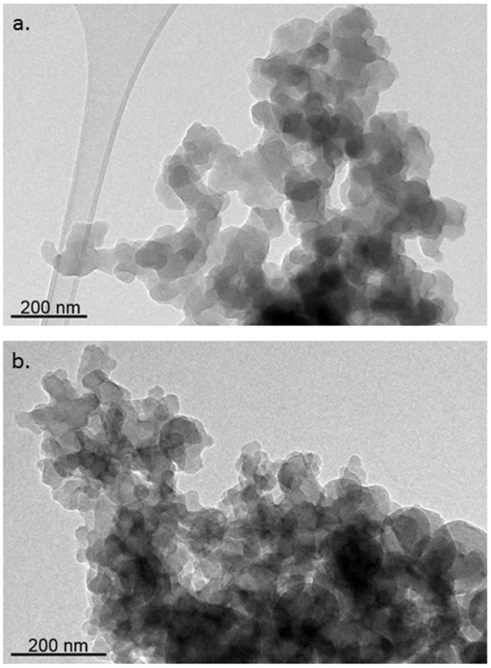

Fig. 2. Transmission electron images of a. Glucose-Soya (GluSo) (T_p = 180 °C) and b. Cellulose-Soya (CeSoS) (T_p = 180 °C) carbonaceous materials.

spectrum of CeSoS.

Platinum doping was conducted on the calcined (T_p = 1000 °C) GluSo (GluSo_1000_Pt) and CeSoS (CeSoS_1000_Pt). As can be seen from SEM and TEM analysis, the calcined carbon materials maintained the spongy-like morphology throughout the whole process from HTC the Pt-impregnation step (Fig. 4, S5 and Fig. 1). Furthermore, TEM imaging shows the presence of numerous highly dispersed Pt nanoparticles of about 5–10 nm in size (Pt loading of 17 wt. %) on the carbon material. This high dispersion may have been enhanced by interaction of Pt with nitrogen functional groups [38]. EDX mapping supports indication of fine dispersion of platinum on the carbon material observed from TEM images (S6). N_2 sorption isotherms remain similar to pristine carbonaceous materials however, platinum impregnation indicated to cause decrease in surface area and pore volume of the carbon materials after platinum impregnation *e.g.* when considering Gluso_1000 vs. GluSo_1000_Pt S_{BET} before impregnation was 449 m^2/g and after 294 m^2/g whereas change in the pore volume V_p was 0.25 cm^3/g to 0.19 cm^3/g before and after impregnation respectively. Changes in S_{BET} or V_p before and after impregnation in case of Cellulose were smaller (S7, Table 1) [39,40]. XRD analysis shows diffraction peaks at 40.0°, 46.6° and 68.0°, which are associated with the (111), (200) and (220) planes of the face-centered-cubic (fcc) structure of Pt, suggesting high crystallinity metallic state of the supported Pt nanoparticles on the carbon materials (Fig. 4 and S5) [41,42]. The diffraction peak at 22° corresponds to the (002) plane of graphite being obvious in the XRD spectrum corresponding to CeSoS_1000_Pt than in that of GluSo_1000_Pt [2].

3.2. Electrocatalytic activity for oxygen reduction reaction

Fig. 5 shows the cyclic voltammetry (CV) of GluSo_1000, CeSoS_1000, GluSo_1000_Pt and CeSoS_1000_Pt in O_2- and N_2-saturated 0.1 M KOH electrolytes. The current density presented here corresponds to the measured current divided by the geometric surface area of the glassy carbon electrode. GluSo_1000 and CeSoS_1000 show similar peak reduction potential (*ca.* −0.3 V vs. Ag/AgCl), but the peak current density of GluSo_1000 is much higher, in accordance with its higher nitrogen content compared to CeSoS_1000 [14]. After impregnation with Pt, both samples' onset reduction potential is significantly positively shifted due to the more active Pt catalytic sites. As shown by the CV plots measured in N_2-saturated electrolyte, the specific capacitance of GluSo_1000_Pt is reduced with respect to that of GluSo_1000, but that of CeSoS_1000_Pt does not change much compared to that of CeSoS_1000, which is probably because of the different changes of BET specific surface area before and after Pt impregnation (Table 1).

To analyse the oxygen reduction kinetics, rotating ring disk electrode (RRDE) measurements were adopted. It can be seen in the linear sweep voltammetry (LSV) plots at 1000 RPM (Fig. 6a) that the onset reduction potential for GluSo_1000 is more positive than for CeSoS_1000, and the reduction current under the same potential for GluSo_1000 is higher than for CeSoS_1000, which agrees well with the aforementioned CV results. The onset reduction potentials of two Pt-loaded samples are similar and more positive than those without platinum impregnation. Notably, GluSo_1000_Pt shows higher limiting current density than CeSoS_1000_Pt even though both samples have almost the same Pt loading and the BET specific surface area of CeSoS_1000_Pt is even higher than that of GluSo_1000_Pt. Since the limiting current densities of GluSo_1000_Pt and CeSoS_1000_Pt are both similar to their corresponding carbon substrate, it is likely that for the metal/carbon hybrid ORR catalysts, carbon substrate rather than the metal catalyst determines the limiting current density. The electron transfer number and the ratio of peroxide formation during oxygen reduction process (Fig. 6b.) were calculated based on the LSV results from RRDE [43]. The electron transfer number for GluSo_1000 (3.3–3.7) is constantly higher than that of CeSoS_1000 (3–3.2) within the potential range of −0.1 to −0.6 V vs. Ag/AgCl, in line with the lower peroxide formation ratio of 10–30% for Glucose_1000 than the 35–50% for CeSoS_1000. The electron transfer numbers for both Pt loaded samples are within 3.8–4, leading to a peroxide formation ratio below 10%. According to the Koutecky–Levich equation ($1/J = 1/J_L + 1/J_K$), the measured current density (J) is composed of diffusion limiting current density (J_L) and kinetic current density (J_K), where J_L only depends on two variables, electron transfer number and rotation speed (see the experimental section for details) [43]. Given that the electron transfer numbers for both Pt-loaded samples are almost the same, the variation in limiting current densities under the same rotation speed must be because of their different kinetic current densities, which is further demonstrated by Tafel plots (Fig. 6c.). Two distinct ranges of kinetic current density can be observed for Pt loaded samples: 1) when the potential is more positive than - 0.12 V, the kinetic current densities for the two Pt-loaded samples are almost the same and much higher than those without Pt; 2) when the potential is more negative than - 0.2 V, both J_K change little as potential is further reduced, but J_K for GluSo_1000_Pt is significantly greater than that of CeSoS_1000_Pt, and interestingly, the J_K for GluSo_1000_Pt and CeSoS_1000_Pt are close to their Pt-free counterparts. Besides, it is also shown in Fig. 6C that the Tafel slopes for both calcined carbon materials (84 and 75 mV/dec for GluSo_1000 and CeSoS_1000 respectively) are smaller than those of Pt-loaded carbon materials (101 and 99 mV/dec for GluSo_1000_Pt and CeSoS_1000_Pt respectively). Such

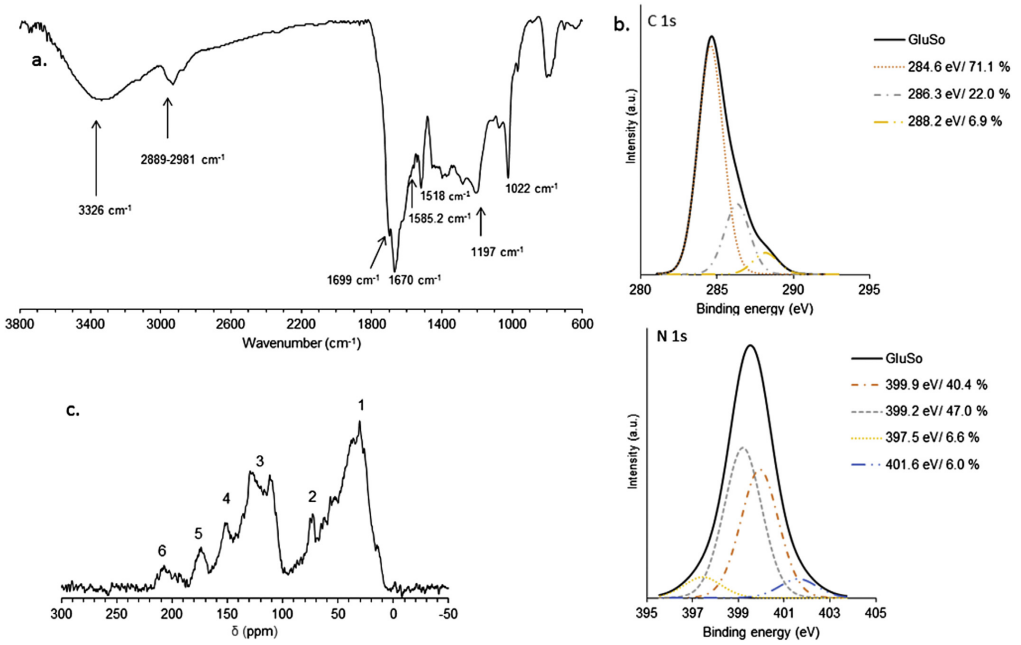

Fig. 3. GluSo HTC (T_p = 180 °C) a. FTIR spectra, b. High resolution XPS deconvolution spectras C 1(s) and N 1(s) photoelectron envelopes and c. ^{13}C CP MAS NMR spectra in which 1. Aliphatic sp^3 carbon, 2. Residual Glucose, 3. Delocalized sp^2 carbon, 4. Furan type, 5. Carboxylic acids and 6. Ketones/Aldehydes. (A colour version of this figure can be viewed online.)

Table 2
FTIR assignments for characteristic vibrations for surface functional groups found in GluSo and CeSoS carbonaceous materials after HTC (T_p = 180 °C).

GluSo	CeSoS	Functionality/characteristic vibration
Wave number (cm^{-1})	Wave number (cm^{-1})	
3326	3369, 3122	Hydroxyl ν(O–H) and Amine ν(N–H)
2996–2838.7	3000–2875	Aliphatic features ν(C–H)
1699	1699	Carbonyl ν(C–O)
1670	1683.6	Amide ν(N–C=O)
1197	1164	Amine ν(C–N)
1022	1047	Amine ν(C–N), ν(C=C–O)
1518	1519.7	Furan type of structure ν(C=C–O)
1585.2	1583.3	Pyridinic, pyridonic and pyrrolic

Table 3
Peak assignments for the C 1(s) and N 1(s) photoelectron envelopes for GluSo and CeSoS after HTC (T_p = 180 °C) and GluSo_1000 and CeSoS_1000 after calcination (T_p = 1000 °C).

Peak	Binding energy (eV)/Relative amount %				
	GluSo	GluSo_1000	CeSoS	CeSoS_1000	Assignment
C 1s	284.6/71.1	284.6/68.9	284.6/78.5	284.6/55.9	C=C/C–C/C–H, Sp^2 and Sp^3 C
	286.3/22.0	286.0/20.4	286.5/15.0	285.7/26.3	C–O–H/C–O–C/C–N
	–	287.4/5.1	–	287.0/9.1	–C=O
	–	289.3/5.6		289.2/8.8	COOH/COOR
	288.2/6.9	–	288.7/6.5	–	N–C=O
N 1s	397.5/6.6	–	–	–	–N=C–
	–	398.9/35.2	398.3/8.2	398.8/34.1	Pyridinic-N
	399.2/47.0	–	–	–	$–NH_2$
	399.9/40.4	–	400.2/54.0	–	–N–C=O
	–	400.9/55.4	401.6/37.8	401.0/59.2	Quaternary-N
	401.7/6.0	–	–	–	$H–NH_2/NH_3^+$
	–	402.9/9.3	–	403.2/6.7	Pyridine-N-oxide

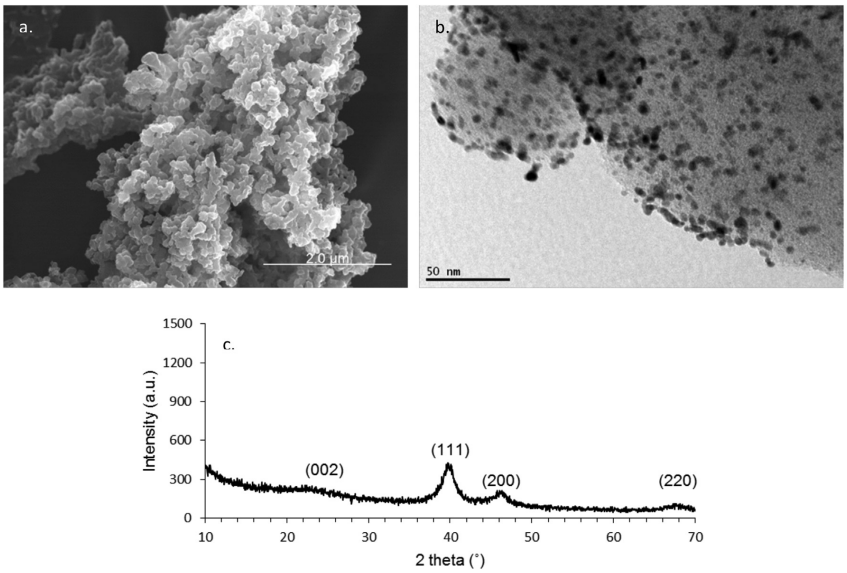

Fig. 4. Morphological, structural and crystal analysis of platinum impregnated GluSo_1000_Pt carbon material a. SEM image 20 k magnification, b. TEM image 80 k magnification revealing well dispersed platinum nanoparticles on the carbon material and c. XRD pattern indicating crystalline structure of Pt on GluSo_1000 carbon material.

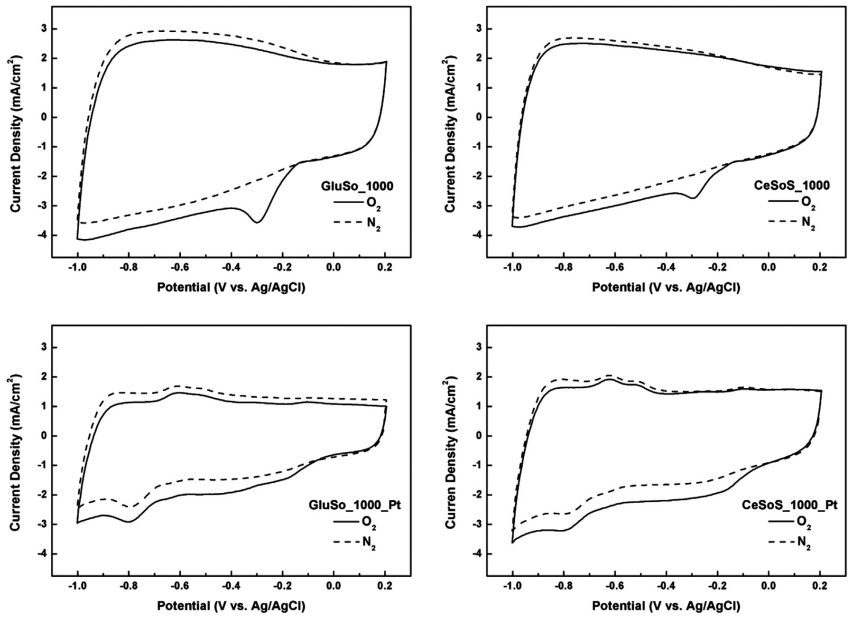

Fig. 5. Cyclic voltammetry of GluSo_1000, CeSoS_1000, GluSo_1000_Pt and CeSoS_1000_Pt in O_2-saturated (solid) and N_2-saturated (dash) 0.1 M KOH. Scan rate is 100 mV/s.

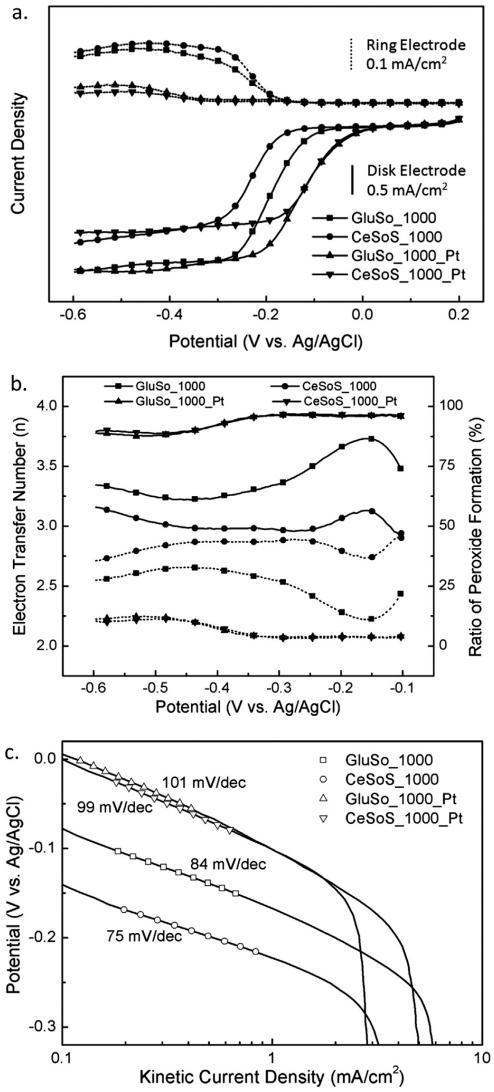

Fig. 6. Rotating ring disk electrode (RRDE) measurement for GluSo_1000, CeSoS_1000, GluSo_1000_Pt and CeSoS_1000_Pt. a. Linear sweep voltammetry (LSV) at 1000 RPM with scan rate of 10 mV/s b. Electron transfer number (solid) and ratio of peroxide (HO_2^-) formation (dash) and c. Tafel plots derived from the LSV results.

changes in Tafel slopes indicate the switch-over from Temkin conditions of adsorption (higher coverage of reaction intermediate) to Langmuir conditions (smaller coverage of reaction intermediate), assuming in both cases the first electron transfer is the rate determining step (RDS) [44–46].

In order to explain why carbon substrate could play a more important role to determine the kinetic current density of the metal/carbon hybrid catalysts when the limiting current density is achieved, the Koutecky–Levich equation is extended to the more general Tafel–Volmer equation (Equation (5).) [47–49]:

$$\frac{1}{J} = \frac{1}{J_L} + \frac{1}{J_K} = \frac{1}{J_L} + \frac{1}{J_0} \times \frac{1}{(\theta/\theta_0)\exp(|\eta|/b)} + \frac{1}{J_{Ads}} + \frac{1}{J_{Nafion}} \quad (5)$$

Here the kinetic current density J_K is determined by three factors: (1) the thermodynamic barrier $J_0 \times (\theta/\theta_0) \times \exp(|\eta|/b)$ where J_0 is exchange current density, θ and θ_0 are degrees of oxygen coverage at potential E and the equilibrium E_0, η is the over-potential, and b is tafel slope, (2) the oxygen adsorption process J_{Ads} and (3) the oxygen diffusion in Nafion J_{Nafion}. Since the effect of Nafion is sample-independent and can be eliminated, J_{Nafion} is ignored below for the convenience of discussion. It is well-known that as the over-potential increases, the thermodynamic barrier of each individual electron transfer step is reduced almost in proportion while the barrier of oxygen adsorption process changes little [50]. When the over-potential is small (*i.e.* $P > -0.12$ V vs. Ag/AgCl), the kinetic current density is dominated by the thermodynamic barrier and the very similar kinetic current densities for Pt loaded samples mainly represent the catalytic property of more active Pt sites. However when the over-potential is large (*i.e.* $P < -0.2$ V vs. Ag/AgCl), the thermo-dynamic barrier becomes negligible and the kinetic current density is now determined by the oxygen adsorption process. It might be possible for the hybrid catalysts in this work that the platinum sites less accessible to oxygen, particularly when the over-potential is large, and so the limiting current density is restricted by carbon substrate. Such phenomenon sheds light on the generic strategy to develop metal/carbon hybrids for ORR: the carbon substrates that can afford high limiting current density (*i.e.* to ensure sufficient mass transport and metal catalysts exposure) should be achieved first before the addition of extra metal catalysts.

4. Conclusions

Hydrothermal carbonization allowed the synthesis of carbon materials via one-pot technique at low reaction temperature (180 °C) under autogenous pressure in which glucose and cellulose were used as primary carbon source. Addition of soy bean flour as a source of globular proteins and (soy proteins) as a secondary precursor resulted in interconnected carbon network formed from single spherical primary particles and increased amount of nitrogen functional groups in the carbon network. HTT treatment as an additional post-synthesis step was applied to alter physico-chemical properties of amorphous HTC carbon to more crystalline graphitic structure. HTT treatment improved significantly the porosity development of as-synthesized HTC carbons and resulted in rearrangement of nitrogen functionalities to quaternary and pyridinic type of structures.

The porous carbon aerogels alone after HTT treatment displayed excellent ORR performance which was further improved after platinum impregnation. It was noticed that the platinum loaded carbon sample took the advantages of both fast electron-transfer capability of more active platinum catalysts and rapid mass-transfer capability from porous carbon aerogels substrate, which revealed the general guidance to optimise the electrocatalytic activity of metal/carbon hybrid materials.

The development of low cost and easy to manufacture carbon electrodes has an important impact on the fuel cell performance as it influences mass transport of educts and products as well as electron and conductive pathways.

Acknowledgements

S-M. Alatalo is grateful to Tekniikan edistämissäätiö (TES) and Maa-ja vesitekniikan tuki (MVTT) for financial support. Additionally Finnish Funding Agency for Technology and Innovation (TEKES) is thanked for their financial support. M. Sevilla thanks the Spanish Ministerio de Economía y Competitividad, MINECO (MAT2012-31651), and Fondo Europeo de Desarrollo Regional (FEDER) for their funding and the Spanish Ministerio de Ciencia e Innovación for her *Ramón y Cajal* contract.

Appendix A. Supplementary data

Supplementary data related to this article can be found at http://dx.doi.org/10.1016/j.carbon.2015.09.108.

References

[1] S.-A. Wohlgemuth, R.J. White, M.-G. Willinger, M.-M. Titirici, M. Antonietti, A one-pot hydrothermal synthesis of sulfur and nitrogen doped carbon aerogels with enhanced electrocatalytic activity in the oxygen reduction reaction, Green Chem. 14 (5) (2012) 1515–1523.
[2] H. Jin, H. Zhang, H. Zhong, J. Zhang, Nitrogen-doped carbon xerogel: A novel carbon-based electrocatalyst for oxygen reduction reaction in proton exchange membrane (PEM) fuel cells, Energy Environ. Sci. 4 (9) (2011) 3389–3394.
[3] C. Moreno-Castilla, F.J. Maldonado-Hódar, Carbon aerogels for catalysis applications: an overview, Carbon 43 (3) (2005) 455–465.
[4] R.J. White, N. Brun, V.L. Budarin, J.H. Clark, M.-M. Titirici, Always look on the "light" side of life: sustainable carbon aerogels, ChemSusChem 7 (3) (2014) 670–689.
[5] S.-A. Wohlgemuth, T.-P. Fellinger, P. Jaker, M. Antonietti, Tunable nitrogen-doped carbon aerogels as sustainable electrocatalysts in the oxygen reduction reaction, J. Mater. Chem. A 1 (12) (2013) 4002–4009.
[6] M. Antonietti, N. Fechler, T.-P. Fellinger, Carbon aerogels and monoliths: control of porosity and nanoarchitecture via sol–gel routes, Chem. Mater. 26 (1) (2014) 196–210.
[7] N. Brun, K. Sakaushi, L. Yu, L. Giebeler, J. Eckert, M.M. Titirici, Hydrothermal carbon-based nanostructured hollow spheres as electrode materials for high-power lithium-sulfur batteries, Phys. Chem. Chem. Phys. 15 (16) (2013) 6080–6087.
[8] S. Kubo, R.J. White, N. Yoshizawa, M. Antonietti, M.-M. Titirici, Ordered carbohydrate-derived porous carbons, Chem. Mater. 23 (22) (2011) 4882–4885.
[9] M.-M. Titirici, R.J. White, N. Brun, V.L. Budarin, D.S. Su, F. del Monte, et al., Sustainable carbon materials, Chem. Soc. Rev. 44 (1) (2015) 250–290.
[10] M.-M. Titirici, Sustainable Carbon Materials from Hydrothermal Processes, Wiley, 2013.
[11] M. Sevilla, L. Yu, T.P. Fellinger, A.B. Fuertes, M.-M. Titirici, Polypyrrole-derived mesoporous nitrogen-doped carbons with intrinsic catalytic activity in the oxygen reduction reaction, RSC Adv. 3 (25) (2013) 9904–9910.
[12] T.X. Wu, G.Z. Wang, X. Zhang, C. Chen, Y.X. Zhang, H.J. Zhao, Transforming chitosan into N-doped graphitic carbon electrocatalysts, Chem. Commun. 51 (7) (2015) 1334–1337.
[13] K. Gong, F. Du, Z. Xia, M. Durstock, L. Dai, Nitrogen-doped carbon nanotube arrays with high electrocatalytic activity for oxygen reduction, Science 323 (5915) (2009) 760–764.
[14] K. Qiu, Z.X. Guo, Hierarchically porous graphene sheets and graphitic carbon nitride intercalated composites for enhanced oxygen reduction reaction, J. Mater. Chem. A 2 (9) (2014) 3209–3215.
[15] E. Frackowiak, Carbon materials for supercapacitor application, Phys. Chem. Chem. Phys. 9 (15) (2007) 1774–1785.
[16] B. Zhu, K. Qiu, C. Shang, Z. Guo, Naturally derived porous carbon with selective metal- and/or nitrogen-doping for efficient CO_2 capture and oxygen reduction, J. Mater. Chem. A 3 (9) (2015) 5212–5222.
[17] R.J. White, N. Yoshizawa, M. Antonietti, M.-M. Titirici, A sustainable synthesis of nitrogen-doped carbon aerogels, Green Chem. 13 (9) (2011) 2428–2434.
[18] J. Marie, S. Berthon-Fabry, P. Achard, M. Chatenet, A. Pradourat, E. Chainet, Highly dispersed platinum on carbon aerogels as supported catalysts for PEM fuel cell-electrodes: comparison of two different synthesis paths, J. Non-Crystalline Solids 350 (0) (2004) 88–96.
[19] R. Tressl, G.T. Wondrak, R.-P. Krüger, D. Rewicki, New melanoidin-like Maillard polymers from 2-deoxypentoses, J. Agric. Food Chem. 46 (1) (1998) 104–110.
[20] J.M.D. Tascon, Novel carbon adsorbents, 2012.
[21] S. Petruccelli, M.C. Anon, Thermal aggregation of soy protein isolates, J. Agric. Food Chem. 43 (12) (1995) 3035–3041.
[22] J.M.S. Renkema, H. Gruppen, T. van Vliet, Influence of pH and ionic strength on heat-induced formation and rheological properties of soy protein gels in relation to denaturation and their protein compositions, J. Agric. Food Chem. 50 (21) (2002) 6064–6071.
[23] J.M.S. Renkema, J.H.M. Knabben, T. van Vliet, Gel formation by β-conglycinin and glycinin and their mixtures, Food Hydrocoll. 15 (4–6) (2001) 407–414.
[24] C.-H. Tang, C.-S. Wang, Formation and characterization of amyloid-like fibrils from soy β-conglycinin and glycinin, J. Agric. Food Chem. 58 (20) (2010) 11058–11066.
[25] N. Baccile, M. Antonietti, M.M. Titirici, One-step hydrothermal synthesis of nitrogen-doped nanocarbons: albumine directing the carbonization of glucose, Chemsuschem 3 (2) (2010) 246–253.
[26] M.E. SMITH, E.H. FINKE, Critical point drying of soft biological material for the scanning electron microscope, Invest. Ophthalmol. Vis. Sci. 11 (3) (1972) 127–132.
[27] A.C. Pierre, G.M. Pajonk, Chemistry of aerogels and their applications, Chem. Rev. 102 (11) (2002) 4243–4266.
[28] L. Zhao, N. Baccile, S. Gross, Y. Zhang, W. Wei, Y. Sun, et al., Sustainable nitrogen-doped carbonaceous materials from biomass derivatives, Carbon 48 (13) (2010) 3778–3787.
[29] L. Yu, C. Falco, J. Weber, R.J. White, J.Y. Howe, M.-M. Titirici, Carbohydrate-derived hydrothermal carbons: a thorough characterization study, Langmuir 28 (33) (2012) 12373–12383.
[30] D. Lozano-Castelló, D. Cazorla-Amorós, A. Linares-Solano, Usefulness of CO_2 adsorption at 273 K for the characterization of porous carbons, Carbon 42 (7) (2004) 1233–1242.
[31] J. Coates, Interpretation of Infrared Spectra, a Practical Approach. Encyclopedia of Analytical Chemistry, John Wiley & Sons, Ltd, 2006.
[32] H.F. Gorgulho, F. Gonçalves, M.F.R. Pereira, J.L. Figueiredo, Synthesis and characterization of nitrogen-doped carbon xerogels, Carbon 47 (8) (2009) 2032–2039.
[33] R. Arrigo, M. Hävecker, S. Wrabetz, R. Blume, M. Lerch, J. McGregor, et al., Tuning the acid/base properties of nanocarbons by functionalization via amination, J. Am. Chem. Soc. 132 (28) (2010) 9616–9630.
[34] D. Hulicova-Jurcakova, M. Seredych, G.Q. Lu, T.J. Bandosz, Combined effect of nitrogen- and oxygen-containing functional groups of microporous activated carbon on its electrochemical performance in supercapacitors, Adv. Funct. Mater. 19 (3) (2009) 438–447.
[35] J. Chen, X. Wang, X. Cui, G. Yang, W. Zheng, Amorphous carbon enriched with pyridinic nitrogen as an efficient metal-free electrocatalyst for oxygen reduction reaction, Chem. Commun. 50 (5) (2014) 557–559.
[36] N. Baccile, G. Laurent, F. Babonneau, F. Fayon, M.-M. Titirici, M. Antonietti, Structural characterization of hydrothermal carbon spheres by advanced solid-state MAS 13C NMR investigations, J. Phys. Chem. C 113 (22) (2009) 9644–9654.
[37] C. Perinu, B. Arstad, A.M. Bouzga, K.-J. Jens, 13C and 15N NMR characterization of amine reactivity and solvent effects in CO_2 capture, J. Phys. Chem. B 118 (34) (2014) 10167–10174.
[38] F. Su, Z. Tian, C.K. Poh, Z. Wang, S.H. Lim, Z. Liu, et al., Pt nanoparticles supported on nitrogen-doped porous carbon nanospheres as an electrocatalyst for fuel cells, Chem. Mater. 22 (3) (2010) 832–839.
[39] L. Zhao, Z.-B. Wang, X.-L. Sui, G.-P. Yin, Effect of multiwalled carbon nanotubes with different specific surface areas on the stability of supported Pt catalysts, J. Power Sources 245 (0) (2014) 637–643.
[40] N. Job, M.F.R. Pereira, S. Lambert, A. Cabiac, G. Delahay, J.-F. Colomer, et al., Highly dispersed platinum catalysts prepared by impregnation of texture-tailored carbon xerogels, J. Catal. 240 (2) (2006) 160–171.
[41] H. Huang, S. Yang, R. Vajtai, X. Wang, P.M. Ajayan, Pt-decorated 3D architectures built from graphene and graphitic carbon nitride nanosheets as efficient methanol oxidation catalysts, Adv. Mater. 26 (30) (2014) 5160–5165.
[42] B. Singh, E. Dempsey, Exceptional Pt nanoparticle decoration of functionalised carbon nanofibers: a strategy to improve the utility of Pt and support material for direct methanol fuel cell applications, RSC Adv. 3 (7) (2013) 2279–2287.
[43] X. Ge, A. Sumboja, D. Wuu, T. An, B. Li, F.W.T. Goh, et al., Oxygen reduction in alkaline media: from mechanisms to recent advances of catalysts, ACS Catal. 5 (8) (2015) 4643–4667.
[44] A. Damjanovic, M.A. Genshaw, Dependence of the kinetics of O_2 dissolution at Pt on the conditions for adsorption of reaction intermediates, Electrochim. Acta 15 (7) (1970) 1281–1283.
[45] A. Damjanovic, D.B. Sepa, An analysis of the pH dependence of enthalpies and Gibbs energies of activation for O_2 reduction at Pt electrodes in acid solutions, Electrochim. Acta 35 (7) (1990) 1157–1162.
[46] G. Ma, R. Jia, J. Zhao, Z. Wang, C. Song, S. Jia, et al., Nitrogen-doped hollow carbon nanoparticles with excellent oxygen reduction performances and their electrocatalytic kinetics, J. Phys. Chem. C 115 (50) (2011) 25148–25154.
[47] C. Coutanceau, M. Croissant, T. Napporn, C. Lamy, Electrocatalytic reduction of dioxygen at platinum particles dispersed in a polyaniline film, Electrochim. Acta 46 (4) (2000) 579–588.
[48] M.J. Croissant, T. Napporn, J.M. Léger, C. Lamy, Electrocatalytic oxidation of hydrogen at platinum-modified polyaniline electrodes, Electrochim. Acta 43 (16–17) (1998) 2447–2457.
[49] T.J. Schmidt, H.A. Gasteiger, R.J. Behm, Rotating disk electrode measurements on the CO tolerance of a high-surface area Pt/Vulcan carbon fuel cell catalyst, J. Electrochem. Soc. 146 (4) (1999) 1296–1304.
[50] G.-L. Chai, Z. Hou, D.-J. Shu, T. Ikeda, K. Terakura, Active sites and mechanisms for oxygen reduction reaction on nitrogen-doped carbon alloy catalysts: Stone–Wales defect and curvature effect, J. Am. Chem. Soc. 136 (39) (2014) 13629–13640.

ACTA UNIVERSITATIS LAPPEENRANTAENSIS

663. VÄNTSI, OLLI. Utilization of recycled mineral wool as filler in wood plastic composites. 2015. Diss.

664. KLEMOLA, KATJA. Tuottavuuden, vaikuttavuuden ja kustannusvaikuttavuuden arviointi alueellisesti integroiduissa sosiaali- ja terveyspalveluissa – palvelujen käyttöön perustuva malli ja esimerkkejä. 2015. Diss.

665. HEROLD, KRISTIINA. Impact of Word-of-Mouth on consumer decision-making: An information processing perspective in the context of a high-involvement service. 2015. Diss.

666. OLABODE, MUYIWA. Weldability of high strength aluminium alloys. 2015. Diss.

667. VANHALA, ERNO. The role of business model in computer game development organizations. 2015. Diss.

668. SALAMPASIS, DIMITRIOS. Trust-embedded open innovation: Towards a human-centric approach in the financial industry. 2015. Diss.

669. DE SMET, DIETER. Innovation ecosystem perspectives on financial services innovation. 2015. Diss.

670. PORRAS, PÄIVI. Utilising student profiles in mathematics course arrangements. 2015. Diss.

671. SALMINEN, JUHO. The role of collective intelligence in crowdsourcing innovations. 2015. Diss.

672. ROSAS, SAILA. Co-operative acquisitions – the contextual factors and challenges for co-operatives when acquiring an investor-owned firm. 2015. Diss.

673. SINKKONEN, TIINA. Item-level life-cycle model for maintenance networks – from cost to additional value. 2015. Diss.

674. TUUNANEN, JUSSI. Modelling of changes in electricity end-use and their impacts on electricity distribution. 2015. Diss.

675. MIELONEN, KATRIINA. The effect of cationic-anionic polyelectrolyte multilayer surface treatment on inkjet ink spreading and print quality. 2015. Diss.

676. OMAJENE, JOSHUA. Underwater remote welding technology for offshore structures. 2015. Diss.

677. NUUTINEN, PASI. Power electronic converters in low-voltage direct current distribution – analysis and implementation. 2015. Diss.

678. RUSATSI, DENIS. Bayesian analysis of SEIR epidemic models. 2015. Diss.

679. STRAND, ELSI. Enhancement of ultrafiltration process by pretreatment in recovery of hemicelluloses from wood extracts. 2016. Diss.

680. TANNINEN, PANU. Press forming of paperboard – advancement of converting tools and process control. 2015. Diss.

681. VALTONEN, PETRI. Distributed energy resources in an electricity retailer’s short-term profit optimization. 2015. Diss.

682. FORSSTROM-TUOMINEN, HEIDI. Collectiveness within start up-teams – leading the way to initiating and managing collective pursuit of opportunities in organizational contexts. 2015. Diss.

683. MAGUYA, ALMASI. Use of airborne laser scanner data in demanding forest conditions. 2015. Diss.

684. PEIPPO, JUHA. A modified nominal stress method for fatigue assessment of steel plates with thermally cut edges. 2015. Diss.

685. MURASHKO, KIRILL. Thermal modelling of commercial lithium-ion batteries. 2016. Diss.

686. KÄRKKÄINEN, TOMMI. Observations of acoustic emission in power semiconductors. 2016. Diss.

687. KURVINEN, EMIL. Design and simulation of high-speed rotating electrical machinery. 2016. Diss.

688. RANTAMÄKI, JUKKA. Utilization of statistical methods for management in the forest industry. 2016. Diss.

689. PANOVA, YULIA. Public-private partnership investments in dry ports – Russian logistics markets and risks. 2016. Diss.

690. BAHARUDIN, EZRAL. Real-time simulation of multibody systems with applications for working mobile vehicles. 2016. Diss.

691. MARTIKAINEN, SOILI. Development and effect analysis of the Asteri consultative auditing process – safety and security management in educational institutions. 2016. Diss.

692. TORVINEN, PEKKA. Catching up with competitiveness in emerging markets – An analysis of the role of the firm’s technology management strategies. 2016. Diss.

693. NORONTAUS, ANNUKKA. Oppisopimuskoulutus yritysten tuottamana koulutuspalveluna: tavoitteista vaikutuksiin. 2016. Diss.

694. HALMINEN, OSKARI. Multibody models for examination of touchdown bearing systems. 2016. Diss.

695. TALONPOIKA, ANNA-MARIA. Financial working capital – management and measurement. 2016. Diss.

696. INKINEN, HENRI. Intellectual capital, knowledge management practices and firm performance. 2016. Diss.

697. YANG, XIAOCHEN. Development of a welding production quality control and management system model for China. 2016. Diss.

698. LEMINEN, VILLE. Leak-proof heat sealing of press-formed paperboard trays. 2016. Diss.

699. LAAKSONEN, LAURI. Spectral retinal image processing and analysis for ophthalmology. 2016. Diss.

700. OINONEN, MINNA. Management of customer co-development in business-to-business markets. 2016. Diss.